The Dissertation Committee for Eulalio Fernandez Gomez Certifies that this is the approved version of the following dissertation:

Design Criteria for Strength and Serviceability of Inverted-T Straddle Bent Caps

Committee:

Wassim M. Ghannoum, Co-Supervisor

Oguzhan Bayrak, Co-Supervisor

James O. Jirsa

Sharon L. Wood

Ofodike A. Ezekoye

Design Criteria for Strength and Serviceability of Inverted-T Straddle Bent Caps

by

Eulalio Fernandez Gomez, I.C., M.S.E.

Dissertation

Presented to the Faculty of the Graduate School of

The University of Texas at Austin

in Partial Fulfillment

of the Requirements

for the Degree of

Doctor of Philosophy

The University of Texas at Austin

August 2012

Dedication

To my wife, Perla,

for all your love, support, and encouragement.

Acknowledgements

First and foremost, I would like to thank my advising professors, Dr. Wassim Ghannoum and Dr. Oguzhan Bayrak, for all your continuous guidance and constructive criticism. The many lessons I learned from you go far beyond engineering and research. Many thanks are also extended to Dr. James O. Jirsa, Dr. Sharon L. Wood, and Dr. Ofodike A. Ezekoye for serving in the doctoral committee, greatly improving the quality of this dissertation.

I owe huge thanks to my project team mates David Garber and Nancy Larson, whose dedication and determination made possible to accomplish as much as we did. It has been a great pleasure to work with you. Thanks also to all the helping hands who built those beams with us along these three years on the lab floor: Michelle Wilkinson, Laura Chimelski, Daniel Bejarano, Allison Lehman, Alexander Peña, Michael Weyenberg, and Michael Carrell. Also thanks to the many fellow students who helped us pouring concrete in multiple occasions.

This project was possible thanks to the financial support provided by the Texas Department of Transportation. I would like to thank our project director Jamie Farris and our monitoring committee: Dean Van Landuyt, Courtney Holle, Glenn Yowell, Mike Stroope, Nicholas Nemec, Roger Lopez, and Duncan Stewart, for all their valuable contributions.

Thanks are due to the staff of the Ferguson Laboratory: Blake Stasney, Dennis Fillip, Barbara Howard, Jessica Hanten, Scott Hammock, Eric Schell, and Mike Wason, who ensured that things run smoothly in the lab. Particularly, I would like to thank Andrew Valentine who put a lot of effort into these beams.

Finally, I would like to thank my parents and wife for your unconditional love, support, and example. This accomplishment is yours as much as it is mine.

Design Criteria for Strength and Serviceability of Inverted-T Straddle Bent Caps

Eulalio Fernandez Gomez, Ph.D.

The University of Texas at Austin, 2012

Supervisors: Wassim M. Ghannoum, Oguzhan Bayrak

Several recently built inverted-T bent caps in Texas have shown significant inclined cracking triggering concern about current design procedures for such structures. The repair of such structures is very costly and often requires lane closures. For these reasons TxDOT funded Project 0-6416 aimed at obtaining a better understanding of the structural behavior of inverted-T bent caps and developing new design criteria to minimize such cracking in the future. Several tasks of the aforementioned project are addressed in this dissertation with particular focus on developing design criteria for strength and serviceability of inverted-T bent caps.

Literature review revealed a scarcity of experimental investigation of inverted-T specimens. As part of this dissertation, an inverted-T database was assembled with experimental results from the literature and the current project. An extensive experimental program was completed to accomplish the objectives of the project with thirty one full-scale tests conducted on inverted-T beams. Experimental parameters varied in the study were: ledge length, ledge depth, web reinforcement, number of point loads, web depth, and shear span-to-depth ratio. The dissertation focuses on the effects of ledge length, ledge depth, number of point loads, and developing design criteria for strength and serviceability of inverted-T beams.

Most inverted-T bent caps in Texas are designed using the traditional empirical design procedures outlined in the TxDOT bridge design manual LRFD (2011 current version) that follows closely the AASHTO LRFD bridge design specifications (2012 current version). Given the observed cracking in inverted-T bent caps, the accuracy and conservatism of the traditional design methods were evaluated based on experimental results. The accuracy and conservatism of STM design provisions recently developed in a TxDOT study (TxDOT Project 0-5253, Strength and Serviceability Design of Reinforced Concrete Deep Beams) were also evaluated.

Table of Contents

List of Tables

List of Figures

CHAPTER 1
Introduction

1.1 OVERVIEW

Diagonal web cracking of recently built inverted-T straddle bent caps has been reported with increasing frequency in Texas, triggering concerns about current design procedures for such elements. To address the concerns, the Texas Department of Transportation (TxDOT) funded project 0-6416 with objectives of obtaining a better understanding of the behavior of inverted-T beams and developing strength and serviceability design criteria that will minimize such cracking in the future. This dissertation reports on part of the work that was done within project 0-6416.

Inverted-T straddle bent caps are beam elements to which loads are applied at ledges at the bottom of the section (bottom- or tension-chord loading). Loads need to be transferred in the transverse direction from the ledges to the web, then vertically to the compression chord, and finally in the longitudinal direction to the supports. This three-dimensional flow of forces in addition to the deep beam loading conditions commonly encountered in bent caps generates stress discontinuities that have been traditionally designed for using empirical equations and *rules of thumb*. In the past two decades, US structural design codes have adopted strut-and-tie modeling as a more rational option for the design of deep beams and other structures with discontinuities like the ones present in inverted-T bent caps.

Most inverted-T bent caps in Texas are designed using the traditional empirical design procedures outlined in the TxDOT bridge design manual LRFD (2011 current version) that follows closely the AASHTO LRFD bridge design specifications (2012 current version). Given the observed cracking in inverted-T bent caps, it was the intent of this work to investigate the accuracy and conservatism of the traditional design methods. It was also the intent of the work presented to investigate the accuracy and conservatism of STM procedures for inverted-T beams. Of particular interest were the STM design

provisions recently developed in a TxDOT study (TxDOT Project 0-5253, Strength and Serviceability Design of Reinforced Concrete Deep Beams). These provisions provided several improvements on the AASHTO (2012) STM procedures, but were developed using rectangular beam test data.

Due to scarcity of experimental investigations on inverted-T beams, a comprehensive experimental program was undertaken as part of project 0-6416 to assess the accuracy and validity of traditional design methods and the STM design guidelines of project 0-5253 when used for the design of inverted-T beams.

1.2 PROJECT SCOPE

In order to accomplish the objectives mentioned above, the following tasks are addressed in TxDOT project 0-6416:

1. Literature review
2. Inverted-T database
3. Examination of bent caps in the field
4. Experimental research on strength and serviceability of inverted-T beams.
   Experimental parameters include:
   i. Ledge length
   ii. Ledge depth
   iii. Web reinforcement ratio
   iv. Number of point loads
   v. Loaded chord
   vi. Web depth
5. Development of design recommendations
6. Proof testing of the proposed design recommendations

The scope of this dissertation includes the work done in the literature review, inverted-T database assembly, experimental research on ledge length, ledge depth, and number of point loads series, as well as the development of the design recommendations.

Assembly of the inverted-T database produced 128 tests from the literature. However, most of the tests were either not applicable to the inclined cracking focus of this project or conducted on beams drastically smaller than the bent caps in service in Texas. Moreover, very limited serviceability information regarding diagonal crack widths was available in the literature. It was therefore deemed necessary to conduct a comprehensive experimental program of full-scale inverted-T beam specimens to achieve project goals.

Thirty one full-scale tests were conducted with some of the specimens measuring among the largest reinforced concrete deep beams ever tested to determine shear capacity.

Based on the results of the experimental series treated in this dissertation, design recommendations for strength of inverted-T beams were developed and are presented in the dissertation. Serviceability criteria for minimizing diagonal cracking in inverted-T beams under service loads were developed based on test results of the series treated in this dissertation.

The accuracy of the inverted-T design provisions in AASHTO LRFD Bridge Design Specification (2012) and TxDOT Bridge Design Manual – LRFD (2011) is compared with that of the STM provisions of TxDOT project 5253.

Additional tasks and design series not covered in this dissertation will be presented in the final report of TxDOT project 0-6416 and another dissertation. Additional tasks not covered include the evaluation of distressed bents caps in service, and correlation of crack widths with beam residual capacity. Additional test series not discussed in this dissertation focus on the effects of web reinforcement ratios, web depth, and loaded chord on the behavior of inverted-T beams.

1.3 ORGANIZATION

Four topics are addressed in Chapter 2. First, a general description of the distressed bent caps in service is presented. Second, some background information on design and behavior of inverted-T bent caps is discussed. Third, current design provisions for inverted-T beams from AASHTO LRFD Code, TxDOT bridge design manual, and

TxDOT project 5253 are summarized. Fourth, the assembly of the inverted-T database from the literature is summarized.

In chapter 3, the experimental program is described in detail; an overview of the specimens is provided, a description of the six experimental series is provided, design and fabrication of the specimens is presented, the test setup and instrumentation is described, and finally the test procedure is outlined.

Experimental results are presented in chapter 4. Criteria for strength and serviceability evaluation are detailed. The design assumption for load spread under the loading plates is verified with measured strains of hanger reinforcements. Comparisons of strength, crack progression, and performance of STM provisions are presented for the three experimental series covered in this dissertation.

Analysis of the experimental results is provided in Chapter 5. Comparisons between traditional and STM design methods are made. An analysis of the failure modes is provided along with strength and serviceability design recommendations.

Findings from the experimental program are summarized in Chapter 6 and conclusions for each of the topics addressed in the dissertation are presented.

Appendix A presents the references from which the inverted-T database was compiled. Detailed drawings of the specimens fabricated in the experimental portion of this project are provided in Appendix B. Detailed designs for one of the experimental specimens is provided in Appendix C. A brief description of each test conducted within this project is provided in Appendix D along with some basic information and particularities of atypical tests.

CHAPTER 2
Background Information on Design and Behavior of Inverted-T Deep Beams

2.1 OVERVIEW

Four topics are addressed in this chapter. First, several cases of distressed inverted-T bent caps in service in Texas are presented. Next, background information on inverted-T beams behavior and strut-and-tie modeling for these members is provided. Then, design provisions for inverted-T beams from the AASHTO LRFD code, TxDOT bridge design manual, and TxDOT project 5253 are summarized. Finally, an inverted-T deep beam database is described; tests included in this database contain results from the literature review and from the experimental program of this study.

2.2 FIELD PROBLEMS

Several recently built inverted-T caps in Texas have shown significant inclined cracking triggering concern about current design procedures for such structures. For this reason TxDOT funded Project 0-6416 aimed at obtaining a better understanding of the structural behavior of inverted-T bent caps and developing new design criteria to minimize/eliminate such cracking in the future. As part of the aforementioned project, this dissertation focuses on the effects of ledge geometry and number of point loads on strength and serviceability of inverted-T beams.

One of the tasks of this project was to conduct a thorough inspection of the distressed bent caps in service. In general, the measured crack widths were small (≤ 0.016 in.) posing only aesthetic and durability concerns, but in some cases, like the bent in El Paso, diagonal crack widths measured up to 0.040 in. In all cases, observed cracking patterns on both faces of the distressed bent caps were symmetric about the longitudinal axis of the beams indicating web-shear deficiencies rather than torsional deficiencies. While cracking is expected in reinforced concrete, the crack widths observed in some

caps suggest structural deficiencies that must be investigated. It is therefore important to obtain a better understanding of the inverted-T bent cap behavior to determine the causes of cracking and to adequately evaluate the severity of the problem. A summary of the results from inspections of the bent caps is provided in Table 2-1. Maximum diagonal crack widths of the inspected bent caps varied between 0.010 and 0.040 in. Vertical reinforcement ratios ranged from 0.0043 to 0.0057 and horizontal reinforcement ratios from 0.0019 to 0.0037. Shear span-to-depth ratio is presented, defining the shear span as the distance between centers of the reaction and the concentrated load closest to that reaction (consistent with ACI 318-11).

Table 2-1: Crack width summary of bent caps in service

Bent	**Connection type**	ρ_v	ρ_h	**a/d**	**Max diagonal crack width(in)**
Austin IH-35 / TX-290 Bent 3M	Simply supported	0.0043	0.0037	1.40	0.020
Austin IH-35 / TX-290 Bent 6K	Simply supported	0.0043	0.0037	1.68	0.016
Austin IH-35 / TX-290 Bent 28K	Simply supported	0.0043	0.0037	1.40	0.030
San Antonio IH-35 S Exit 165	Fixed or Partial	Not available	Not available	1.76	0.015
El Paso IH-10 / Geronimo Bent 4	Partialy fixed	0.0057	0.0019	2.31	0.040
El Paso IH-10 / Geronimo Bent 5	Partialy fixed	0.0057	0.0019	3.98	0.020
Waco IH-35 / LP 340 Bent 17	Simply supported	0.0046	0.003	2.52	0.010
Waco IH-35 / LP 340 Bent 19	Simply supported	0.0046	0.003	2.52	0.015

According to AASHTO (2012) and TxDOT Bridge Design Manual (2011) strut-and-tie modeling should be considered for specimens in which the distance between the center of a support and the center of applied load, this could be interpreted as the location of the resultant force of all the applied loads, in this case all the bent caps presented above could not be classified as deep beams and sectional shear design could be used (although strut-and-tie modeling is also allowed). However, considering the *a/d* ratios with shear span measured to the first concentrated load, several of these specimens would be classified as deep beams and therefore strut-and-tie modeling would have to be considered for web-shear design. It is not clear which of the two definitions of *a/d* ratios is more representative of the actual behavior of inverted-T beams as most past tests were conducted with single point loads. The test series conducted in this project comparing one and three point loading will shed some light on this matter.

Figure 2-1 shows the conditions the inspected bent on exit 165 of IH-35 S just outside of San Antonio, TX. Some of these bents have simple support connections to the columns without moment transfer, like the bent located in IH-35 / LP 340 in Waco, TX, shown in Figure 2-2. In some other cases, the bent caps have partial or full moment connection with the columns, like the bent located in IH-35 / Geronimo in El Paso, TX, shown in Figure 2-3.

Figure 2-1: IH-35 S. Exit 165 / San Antonio, TX; left: north face, right: south face

Figure 2-2: Simply supported bent cap in IH-35 / LP 340, Waco, TX.

Figure 2-3: Partial moment connection bent cap in I-10/Geronimo, El Paso, TX.

A summary of the condition of the distressed bent caps was provided, however the evaluation of the distressed bent caps in the field is not within the scope of this dissertation; but will be included in the final report of TxDOT project 0-6416, along with detailed inspection reports for the distressed bents.

2.3 BACKGROUND ON INVERTED-T BENT CAPS

In this section, the behavior of inverted-T beams is described and compared with that of rectangular beams. Behavioral implications of tension-chord loading are discussed. The application of strut-and-tie modeling to inverted-T beams is also discussed.

2.3.1 Inverted-T Beams vs. Rectangular Beams

Inverted-T straddle bent caps are often used in bridge construction to reduce the elevation of bridges and/or to improve available clearance beneath the beams (Figure 2-4). The bridge-deck stringers are supported on ledges at the bottom of the inverted-T bent cap, effectively loading the caps along their tension chord. This arrangement generates a tension field in the web near loading points (Figure 2-5), as forces are "hung" from the compression chord at the top of the beam. In contrast, top- or compression-chord loading does not generate such tension field in the web.

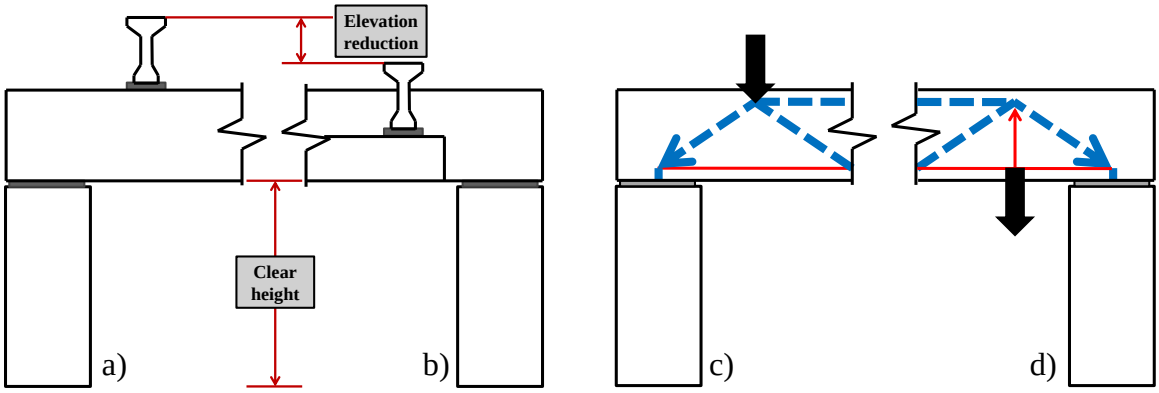

Figure 2-4: Left: (a) rectangular bent cap, (b) inverted-T bent cap; right: flow path of forces in strut-and-tie models: (c) compression-chord loaded beam, (d) tension-chord loaded beam

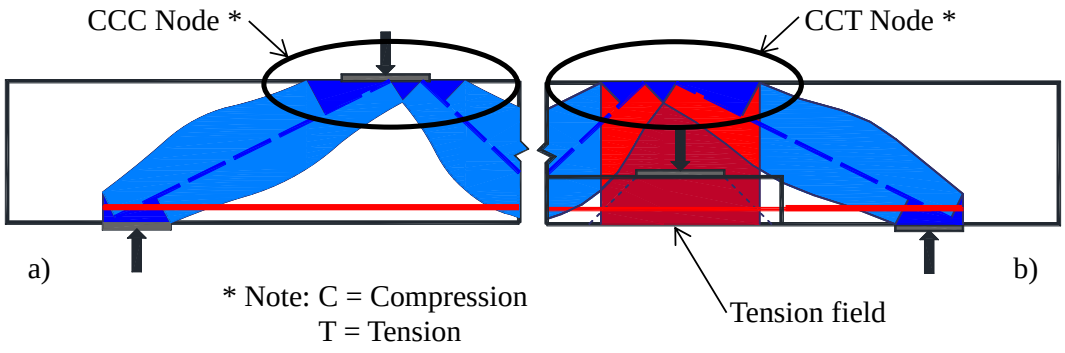

Figure 2-5: (a) CCC node in compression-chord loaded beam, (b) CCT node in tension-chord loaded beam

2.3.2 Components of an Inverted-T Beam

Inverted-T cross sections have two main components: (1) stem or web; this is the main component carrying the shear forces, and (2) ledges; these are the brackets at the bottom of the cross section where the loads are applied to the beam. These components are shown in Figure 2-6 along with the reinforcement terminology. Two additional types of reinforcement are required in an inverted-T beam compared to the typical reinforcement of a rectangular beam: (1) hanger reinforcement; these are the vertical stirrups engaged in transferring the loads applied at the bottom of the beam to the compression chord at the top of the beam (excess web-shear reinforcement can be used as hanger reinforcement), and (2) ledge reinforcement; the main function of this reinforcement is to resist flexural tension forces in the cantilevered ledge. Ledges may be continuous or discontinuous near the supports (Figure 2-7).

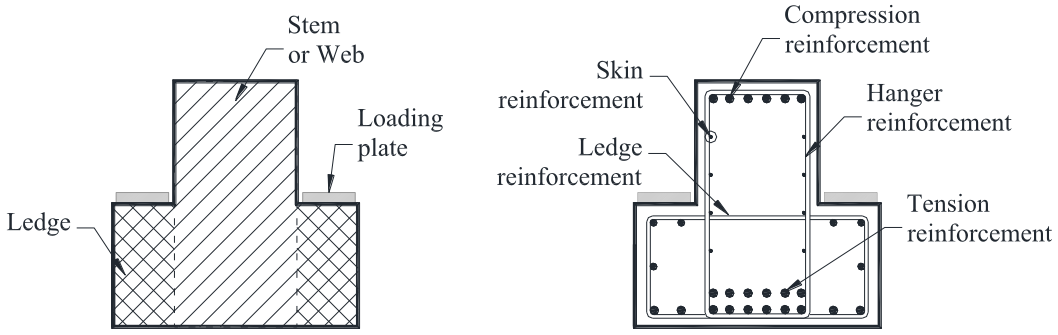

Figure 2-6: Inverted-T bent caps main components

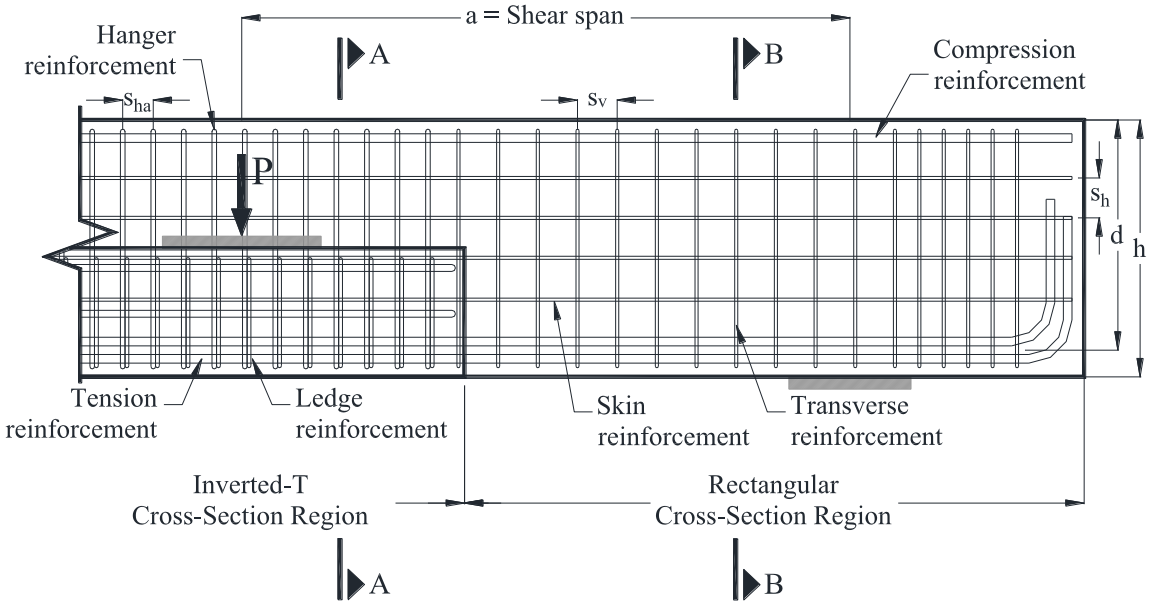

Figure 2-7: Longitudinal elevation of an inverted-T bent cap with discontinuous ledges

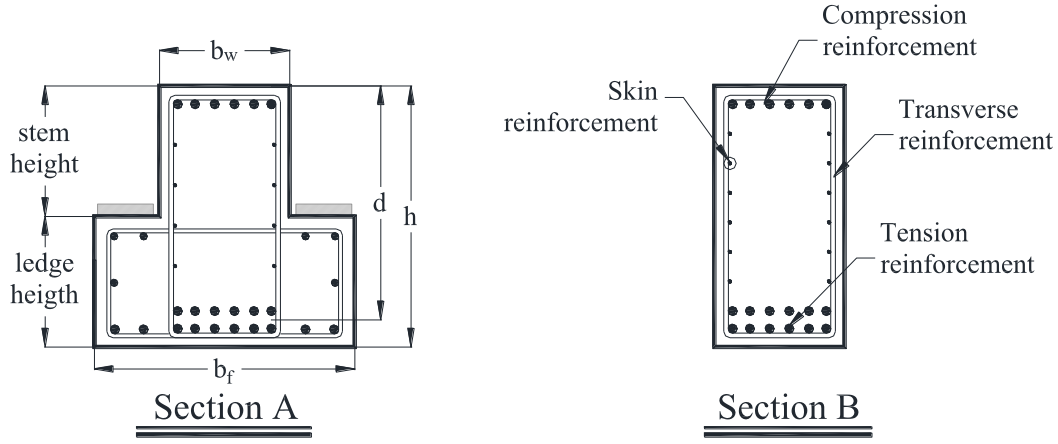

Figure 2-8: Inverted-T and rectangular cross sections

2.3.3 Strut-and-Tie Modeling of Inverted-T Bent Caps

Many inverted-T bent caps can be classified as deep beams when their shear span (*a*) is equal or less than 2.0 times their effective depth (*d*), as illustrated in Figure 2-9. For low shear span-to-depth ratios, the assumption that plain sections remain plain is not valid and sectional design approaches are not applicable. Several empirical methods and rules of thumb have been used to design deep beams due to the “disturbed” state of

stresses they exhibit, (see Figure 2-9). Such methods, however, lack transparency and versatility as they each target very specific elements and sections (e.g., rectangular deep beams, inverted-T beams, corbels, etc.).

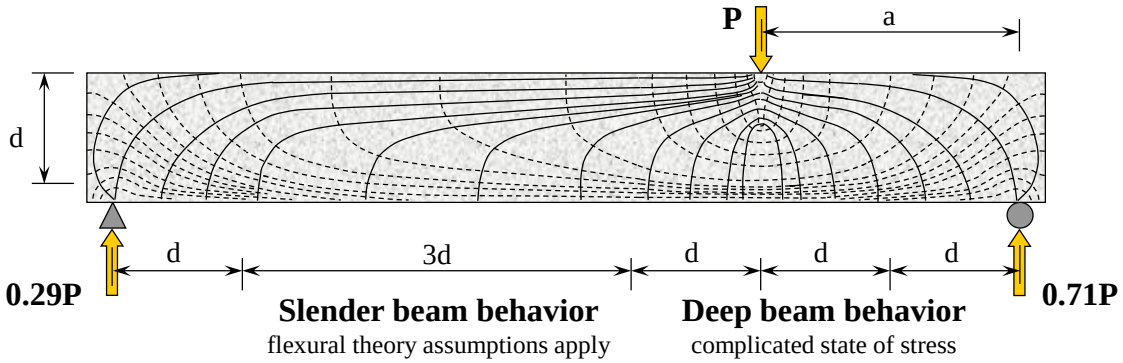

Figure 2-9: Stress trajectories in deep beams (Adapted from Birrcher, et al. 2009)

Strut-and-tie modeling (STM) is a relatively new design method that offers a rational approach for obtaining lower-bound solutions for the strength design of deep beams. In STM, the complex state of stresses in a member is idealized as a system of uniaxial force elements acting as a truss within the concrete member, as shown in Figure 2-10. Compression elements of the truss are called struts and are comprised of the concrete resisting the compression fields. Tension elements are called ties and are comprised of the reinforcement in the member. The regions where struts and ties intersect are called nodes. A more detailed explanation of the strut-and-tie method and its application to deep beams can be found in Birrcher, et al. (2009) and Williams (2011).

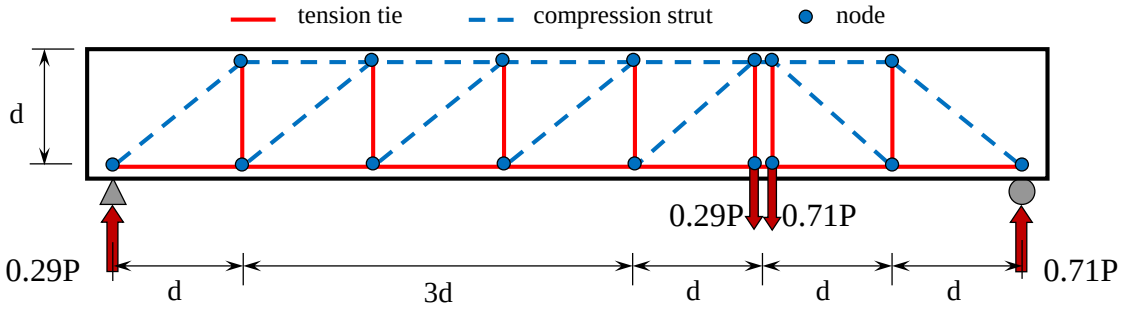

Figure 2-10: Idealized strut-and-tie model of an inverted-T deep beam

One important parameter influencing the behavior of inverted-T bent caps is the tension field induced in the web by the bottom- or tension-chord loading. At the loading points, the applied forces being "hung" from the compression chord add to the shear carried by the specimen. Illustrated in Figure 2-11 is the strut-and-tie model of a compression-chord loaded beam and the strut-and-tie model for the same beam loaded at the tension chord. The STM for both beams are identical except for the forces in the ties "hanging" the loads from the compression chord. The tie forces in the inverted-T beam are larger than the corresponding ties in the rectangular beam by the amount of the force being hung at that location (e.g., *+P* in Figure 2-11).

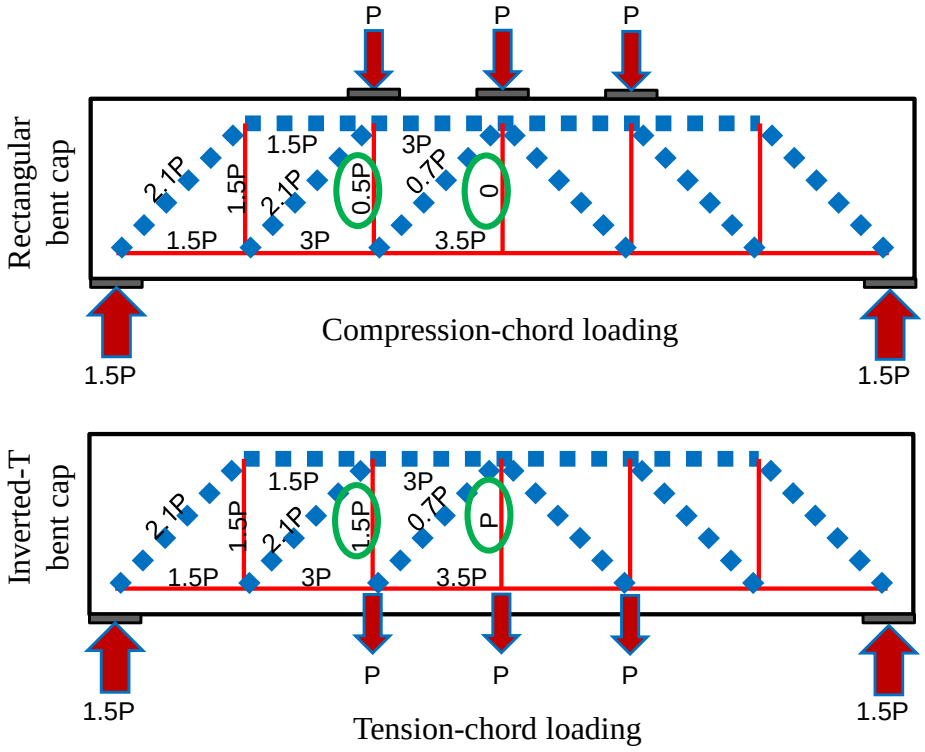

Figure 2-11: Addition of hanger forces to shear forces in inverted-T strut-and-tie models

Another important parameter influencing the inverted-T deep beam behavior is the shear span-to-depth (*a/d*) ratio. Specimens with shear span-to-depth ratios smaller than 2.0 present a direct strut from the loading point to the support. In this type of models, the shear capacity of the member is generally controlled by the strength of the

direct strut and nodes, which in turn depends of the concrete strength. Specimens with shear span-to-depth ratios larger than 2.5 transfer shear forces through a multi-panel model; the capacity of this type of members is generally controlled by the strength of the intermediate ties (vertical ties at mid shear span). Specimens with shear span-to-depth ratios between 2.0 and 2.5 (transition zone) generally resist shear through a combination of both load transfer mechanisms acting simultaneously. The three models are illustrated in Figure 2-12.

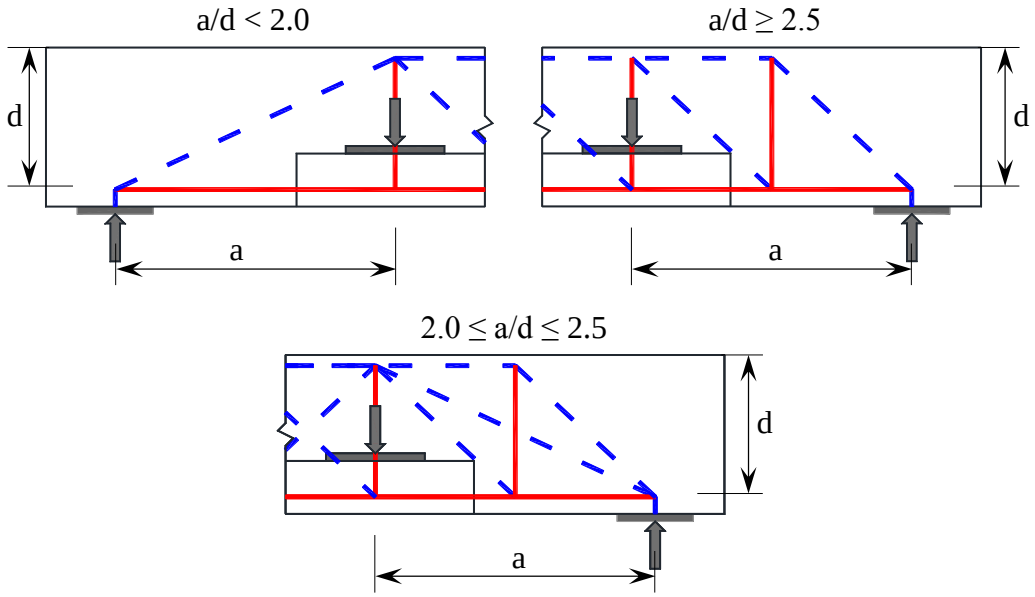

Figure 2-12: a/d influence on strut-and-tie models; left: direct strut model, right: multiple panel model, bottom: transition zone model

Inverted-T bent caps transfer the loads in multiple dimensions: from the ledges to the web, from the tension- to the compression-chord, and from the loading points to the supports. In order to properly model this behavior it is necessary to consider a three-dimensional strut-and-tie model, such as the one shown in Figure 2-13. The model can be divided into two two-dimensional models to simplify the analysis, provided that the interaction between them is considered as follows: first, the external loads are applied to the longitudinal model and forces are calculated for the hanger ties, then, these calculated hanger forces are applied to the cross-sectional models.

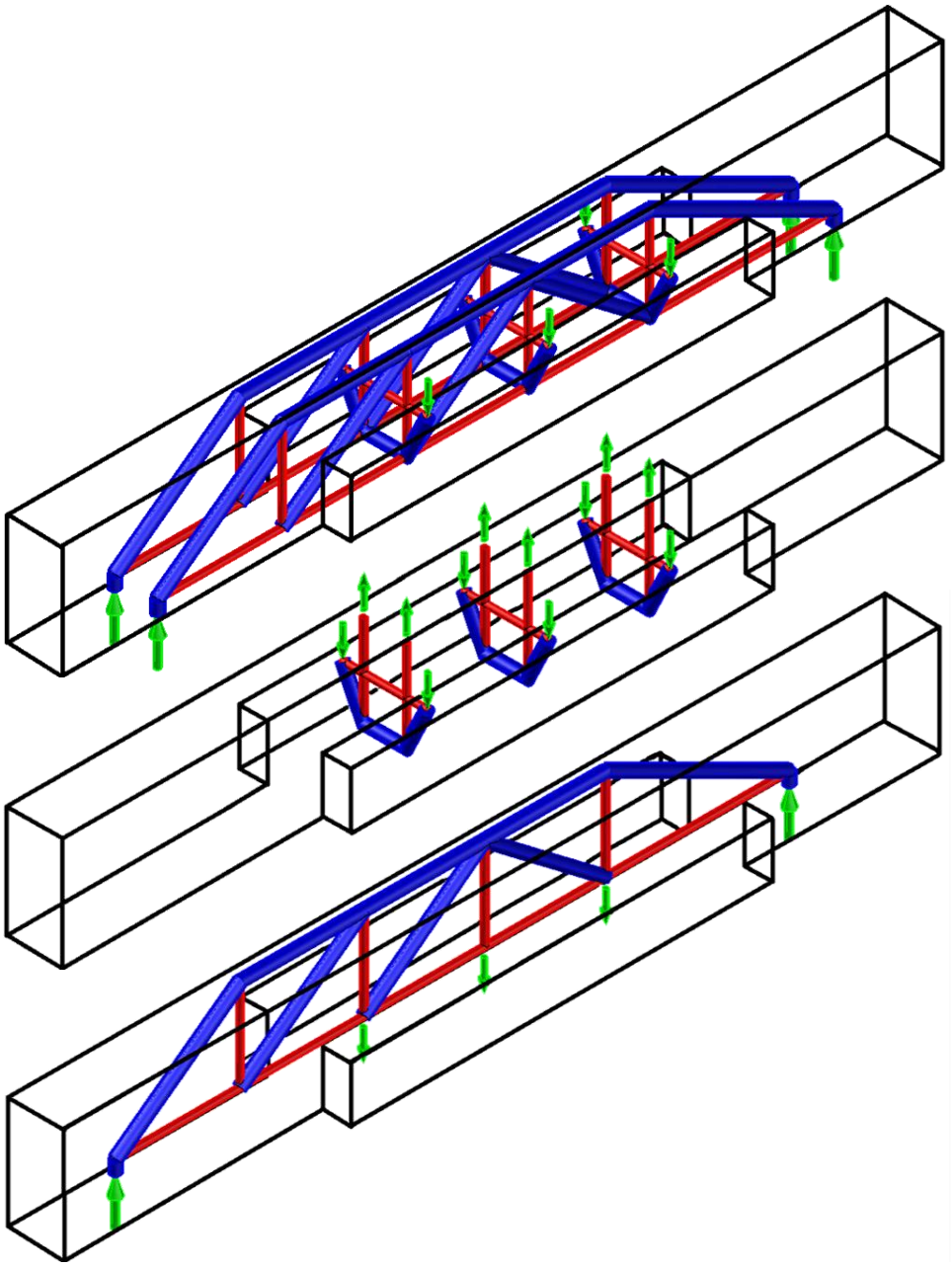

Figure 2-13: Strut-and-tie model of an inverted-T bent cap; top: tri-dimensional model, center: cross-sectional models, bottom: longitudinal model

2.4 INVERTED-T DESIGN PROVISIONS

In this section, design provisions for inverted-T beams of the following three codes are summarized:

- AASHTO LRFD Bridge Design Specifications, 2012
- TxDOT Bridge Design Manual – LRFD, 2011
- TxDOT Project 5253 Strut-and-Tie Modeling provisions

2.4.1 Inverted-T Beam Design Provisions of AASHTO LRFD Bridge Design Specifications, 2012

The AASHTO Code specifies separate design provisions for the web portion of an inverted-T and the ledge portion. For the web portion, rectangular-beam design provisions apply. If the shear span-to-depth ratio of a beam is less than about 2.0, the AASHTO Code specifies that strut-and-tie modeling should be considered. AASHTO (2012) Clause 5.6.3.1 specifies: *"The strut-and-tie model should be considered for the design of deep footings and pile caps or other situations in which the distance between the centers of applied load and the supporting reactions is less than about twice the member thickness."* A detailed overview of the rectangular beam provisions of AASHTO (2008) can be found in Birrcher (2008) and will not be covered here. Note that these provisions changed little in AASHTO (2012).

The AASHTO Code specifies that beam ledges in inverted-T specimens may be designed using the strut-and-tie model or the provisions of Articles 5.13.2.5.2 through 5.13.2.5.5; these provisions are summarized as follows:

"Beam ledges shall be designed to resist forces at the cracks shown in Figure 2-14:

- *Flexure, shear, and horizontal forces at the location of Crack 1*
- *Tension force in the supporting element at the location of Crack 2*
- *Punching shear at points of loading at the location of Crack 3*
- *Bearing force at the location of Crack 4"*

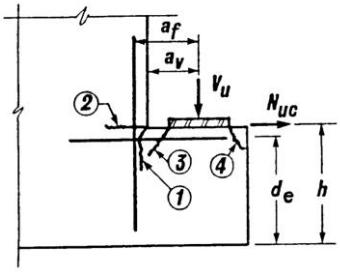

Figure 2-14: Notation and potential crack locations for ledge beams (AASHTO, 2012)

If the strut-and-tie approach is not used, the following design checks must be performed for ledge design.

1. Shear Friction

Shear friction shall be designed according to Article 5.8.4, which states that the nominal interface shear resistance must satisfy the following equations for normal weight concrete:

$$V_{ni} = cA_{cv} + \mu(A_{vf}f_y + P_c) \quad \text{(AASHTO Eq. 5.8.4.1-3)} \qquad \textbf{(2-1)}$$

but:

$$V_{ni} \leq K_1 f'_c A_{cv} \quad \text{(AASHTO Eq. 5.8.4.1-4)} \qquad \textbf{(2-2)}$$

$$V_{ni} \leq K_2 A_{cv} \quad \text{(AASHTO Eq. 5.8.4.1-5)} \qquad \textbf{(2-3)}$$

additionally:

$$V_{ni} = 0.2 f'_c A_{cv} \quad \text{(AASHTO Eq. 5.13.2.4.2-1)} \qquad \textbf{(2-4)}$$

$$V_{ni} = 0.8 A_{cv} \quad \text{(AASHTO Eq. 5.13.2.4.2-2)} \qquad \textbf{(2-5)}$$

where:

V_{ni} = nominal shear resistance of the interface plane (kips)

c = cohesion factor (c = 0 for ledges)

A_{cv} = area of concrete considered to be engaged in interface shear transfer (in.^{2}), see Figure 2-15
interior beams: minimum of ($W+4a_v$, S) times d_e
exterior beams: minimum of ($W+4a_v$, S, $2c$) times d_e

d_e = depth of ledge from bottom surface to center of gravity of top tension steel (in.), as shown in Figure 2-14

μ = friction factor = 1.4 for normal weight concrete placed monolithically

A_{vf} = Area of shear friction steel (in.^{2})

P_c = permanent net compressive force normal to the shear plane (kips)

K_1 = 0.25 for normal weight concrete placed monolithically

K_2 = 1.5 ksi for normal weight concrete placed monolithically

The provisions neglect any cohesion in the concrete area and consider only the friction shear strength provided by the prestressed and mild reinforcement at the ledge-web interface. The width of the interface area is considered equal to the width of the loading plate plus four times the distance from the face of the web to the center of the load (a_v). This value is consistent with the results of the experimental and analytical work of Ma (1971).

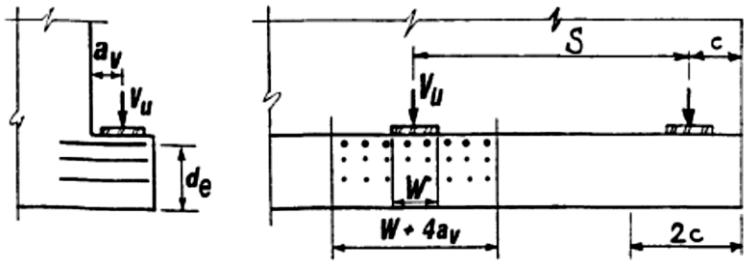

Figure 2-15: Design of beam ledges for shear (AASHTO, 2012)

2. Ledge Top Reinforcement

Primary tension reinforcement A_s (Figure 2-16), shall be determined as for ordinary members subjected to flexure and axial load, and shall satisfy:

$$A_s \geq \frac{2A_{vf}}{3} + A_n \qquad \text{(AASHTO Eq. 5.13.2.4.2-5)} \qquad \textbf{(2-6)}$$

where:

A_n = area of reinforcement in ledge resisting tensile force N_{uc} (in.^{2})

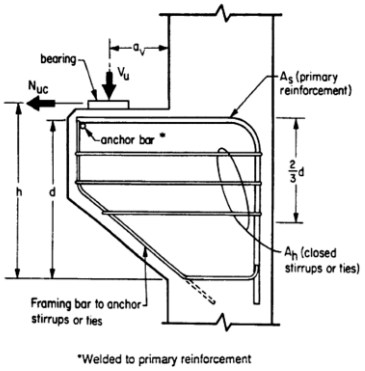

Figure 2-16: Notation (AASHTO, 2012)

The provisions here provide a minimum steel area to resist longitudinal forces perpendicular to the inverted-T beam axis generated by the beams supported on the ledge. These longitudinal forces must be taken at least as 20% of the vertical load applied on the ledge.

Primary tension reinforcement A_s shall be spaced uniformly within the region (W+5a_f) or 2c, as illustrated in Figure 2-17.

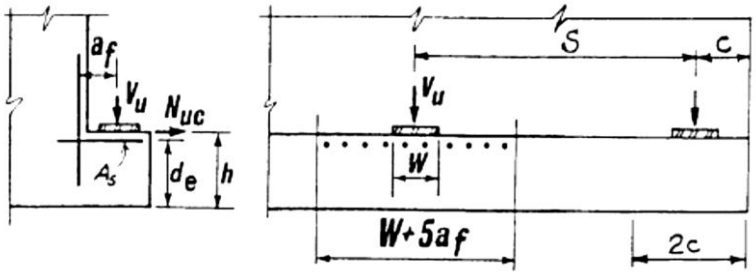

Figure 2-17: Design of beam ledges for flexure and horizontal force (AASHTO, 2012)

The area of closed stirrups A_h (Figure 2-16) or ties placed within 2d_e/3 from the primary reinforcement A_s shall satisfy:

$$A_h \geq 0.5(A_s - A_n) \qquad \text{(AASHTO Eq. 5.13.2.4.2-6)} \quad \textbf{(2-7)}$$

in which:

$$A_n \geq N_{uc}/\emptyset f_y \qquad \text{(AASHTO Eq. 5.13.2.4.2-7)} \quad \textbf{(2-8)}$$

where:

$$\emptyset = 0.90 \qquad \text{(AASHTO Art. 5.5.4.2.1)} \quad \textbf{(2-9)}$$

3. Hanger Reinforcement

Forces acting as hangers and forces acting as shear must be superimposed to design the vertical hanger reinforcement (A_{hr} in Figure 2-18) at the loading points, as stated in AASHTO Art. 5.13.2.5.5: *"The hanger reinforcement specified herein shall be provided in addition to the lesser shear reinforcement required on either side of the beam reaction being supported."*

Service Load Check

The hanger nominal shear resistance V_n for the service limit state in single-beam ledges shall be taken as:

$$V_n = \frac{A_{hr}(0.5f_y)}{s}(W + 3a_v) \qquad \text{(AASHTO Eq. 5.13.2.5.5-1)} \quad \textbf{(2-10)}$$

This section is limiting the shear stresses to half of the yield stress of the hanger reinforcement to reduce cracking under service loads, and conservatively distributing the stresses in a width of $W+3a_v$ instead of using $4a_v$.

Ultimate Load Check

The hanger nominal shear resistance V_n for the strength limit state in inverted T-beam ledges shall be taken as the lesser of:

$$V_n = \frac{A_{hr}f_y}{s}S \qquad \text{(AASHTO Eq. 5.13.2.5.5-2)} \quad \textbf{(2-11)}$$

and:

$$V_n = \left(0.063\sqrt{f'_c}b_f d_f\right) + \frac{A_{hr}f_y}{s}(W + 2d_f)$$

$$\text{(AASHTO Eq. 5.13.2.5.5-3)} \quad \textbf{(2-12)}$$

where:

A_{hr} = area of one leg of hanger reinforcement as illustrated in Figure 2-18 (in.^{2})

S	=	spacing of bearing places (in.)
s	=	spacing of hanger bars (in.)
d_f	=	distance from the top of ledge to compression reinforcement as illustrated in Figure 2-19 (in.)
b_f	=	full width of the flange as shown in Figure 2-19 (in.)

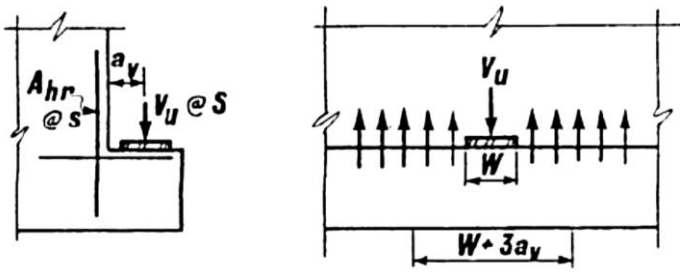

Figure 2-18: Single-ledge hanger reinforcement (AASHTO, 2012)

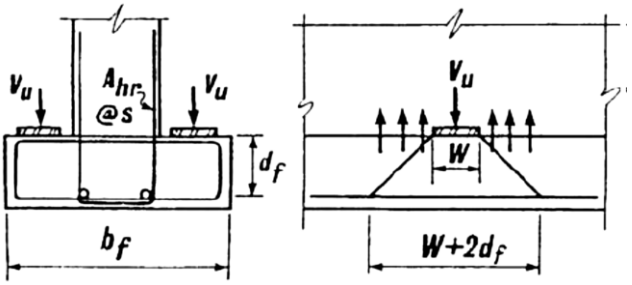

Figure 2-19: Inverted-T beam hanger reinforcement (AASHTO, 2012)

The second equation considers $V_n = V_c + V_s$, where the concrete contribution (V_c) is equal to two square roots of the compressive strength (in psi units, or 0.063 roots of the compressive strength in ksi units), and the steel contribution (V_s) is based on effective hanger bars encompassed in the area created by a 45-deg spreading of the loads under the bearing plate. The same width over which hanger bars are effective was suggested to be conservative by Garber (2011), and is evaluated in more depth in Chapter 4 of this dissertation.

Note that the area of hanger reinforcement at each beam reaction (A_{hr}) as determined by the above strength check must be added to the area of web shear

reinforcement required to resist the lesser shear force on either side of the beam reaction being supported.

4. Development of Reinforcement

Ledge and hanger reinforcement shall be properly developed in accordance with Article 5.11.1.1, which states that the basic tension development length, ℓ_{db} in in. for number 11 bars and smaller shall be taken as:

$$\ell_{db} = \frac{1.25 A_b f_y}{\sqrt{f'_c}} \qquad \text{(AASHTO 5.11.2.1.1)} \quad \textbf{(2-13)}$$

but not less than:

$$0.4\, d_b f_y \qquad \text{(AASHTO 5.11.2.1.1)} \quad \textbf{(2-14)}$$

where:

A_b = area of bar (in.^{2})

f_y = specified yield strength of reinforcing bars (ksi)

f'_c = specified compressive strength of concrete at 28 days (ksi)

d_b = diameter of bar (in.)

5. Punching Shear

The truncated pyramids assumed as failure surfaces for punching shear, as illustrated in Figure 2-20, shall not overlap.

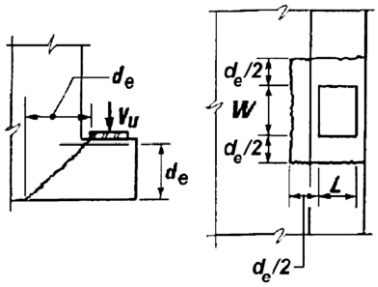

Figure 2-20: Design of beam ledges for punching shear (AASHTO, 2012)

Nominal punching shear resistance, *Vn*, in kips, shall be taken as:

i. At interior pads, or exterior pads where the end distance *c* is greater than *S*/2:

$$V_n = 0.125\sqrt{f'_c}(W + 2L + 2d_e)d_e$$

(AASHTO Eq. 5.13.2.5.4-1) ***(2-15)***

b. At exterior pads where the end distance *c* is less than *S*/2 but *c* - 0.5*W* is less than d_e:

$$V_n = 0.125\sqrt{f'_c}(W + L + d_e)d_e$$

(AASHTO Eq. 5.13.2.5.4-2) ***(2-16)***

c. At exterior pads where the end distance *c* is less than *S*/2 and *c* - 0.5*W* is greater than d_e:

$$V_n = 0.125\sqrt{f'_c}(0.5W + L + d_e + c)d_e$$

(AASHTO Eq. 5.13.2.5.4-3) ***(2-17)***

These equations require that the truncated pyramids of adjacent loads do not overlap. In cases where overlapping occurs the AASHTO Code requires an investigation of the combined surface areas to be conducted.

6. Bearing

Bearing resistance of ledges shall be taken as:

$$P_n = 0.85f'_cA_1m$$ (AASHTO Eq. 5.7.5-2) ***(2-18)***

where:

P_n = nominal bearing resistance (kip)

A_1 = area under bearing device (in.^{2})

m = modification factor

$$m = \sqrt{A_2/A_1} \leq 2.0$$ (AASHTO Eq. 5.7.5-3) ***(2-19)***

A_2 = a notational area defined as shown in Figure 2-21 (in.^{2})

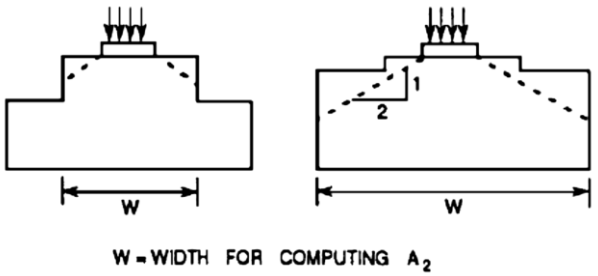

Figure 2-21: Determination of A_2 (AASHTO, 2012)

This provision recognizes that triaxial confinement provides additional bearing capacity thereby allowing beam specimens with less than full-width bearings to reach their full shear capacity.

2.4.2 Inverted-T Beam Design Provisions of TxDOT Bridge Design Manual – LRFD, 2011

The TxDOT Bridge Design Manual mandates designers to adhere to the AASHTO LRFD Bridge Design Specifications, 5th edition, with 2010 interim revision, unless directed otherwise. The AASHTO (2012) provisions for inverted-T beams summarized in section 2.4.1 are all applicable with the following modifications:

1. Use concrete TxDOT class C with $f'c$ = 3.6 ksi; higher strengths may be used in special cases
2. Use grade 60 reinforcing steel
3. Limit tensile stress in steel reinforcement, f_{ss} under Service I limit state to 0.6 f_y
4. Limit reinforcement steel to 22 ksi under Service I limit state with dead load only to minimize cracking
5. Use d_f, not d_e, in all ledge punching shear calculations
6. The truncated pyramids assumed as failure surfaces for punching shear (Figure 2-20 shall not overlap, therefore:

$$0.5b_w + a_v > 0.5L + d_f \quad \textbf{(2-20)}$$

$$S > 2d_f + W \quad \textbf{(2-21)}$$

7. Normal punching shear resistance, *Vn* (in kips), shall be taken as:

- At interior pads: $V_n = 0.125\sqrt{f'_c}(W + 2L + 2d_f)d_f$ ***(2-22)***
- At exterior pads: $V_n = 0.125\sqrt{f'_c}(0.5W + L + d_f + c)d_f$

  but not greater than V_n for interior pads ***(2-23)***

8. Replace AASHTO Equation 5.13.2.5.5-1 with the following:

$$V_n = \frac{A_{hr}\left(\frac{2}{3}f_y\right)}{s}(W + 3a_v) \qquad \textbf{(2-24)}$$

This section allows for higher stresses in the hanger reinforcement than those allowed in the AASHTO LRFD code. The limit is increased to 2/3 of f_y, instead of 1/2.

9. Replace the following sentence in AASHTO Art. 5.13.2.5.5: "The edge distance between the exterior bearing pad and the end of the inverted T-beam shall not be less than d_e" with the following: "The edge distance between the exterior bearing pad and the end of the inverted T-beam shall not be less than 12 in."
10. Replace the following sentence in AASHTO Art. 5.13.2.5.5: *"The hanger reinforcement specified herein shall be provided in addition to the lesser shear reinforcement required on either side of the beam reaction being supported"* with the following: *"Do not superimpose loads on stirrups acting has hangers and loads on stirrups acting as shear reinforcement. Proportion the web reinforcement in the stem of an invert T-beam based on required hanger reinforcement or required shear reinforcement, whichever is greater."* [sic]

This statement is consistent with the conclusions from Ma (1971). In that study, stresses due to hanging loads and web shear were found to be additive before yielding of the hanger bars. However, due to the conservative estimates of steel and concrete contributions, the study found that the stirrup design is safe without the need to superimpose shear and hanger forces at loading points.

11. Take the modulus of rupture, f_r, as $0.24\sqrt{f'_c}$, for all normal weight concrete (in ksi units).

12. Provide minimum stirrups and longitudinal side face reinforcing in the region between each face of column and first girder such that the following are satisfied:

$$\frac{A_v}{b_w s_v} \geq 0.003 \qquad \textbf{(2-25)}$$

and:

$$\frac{A_h}{b_w s_h} \geq 0.003 \qquad \textbf{(2-26)}$$

where:

A_v = Area of transverse reinforcement (in.^{2}); Figure 2-22

A_h = Area of skin reinforcement (in.^{2}); Figure 2-22

b_w = web width (in.); Figure 2-22

s_v = spacing of transverse reinforcement (in.); Figure 2-22

s_h = spacing of skin reinforcement (in.); Figure 2-22

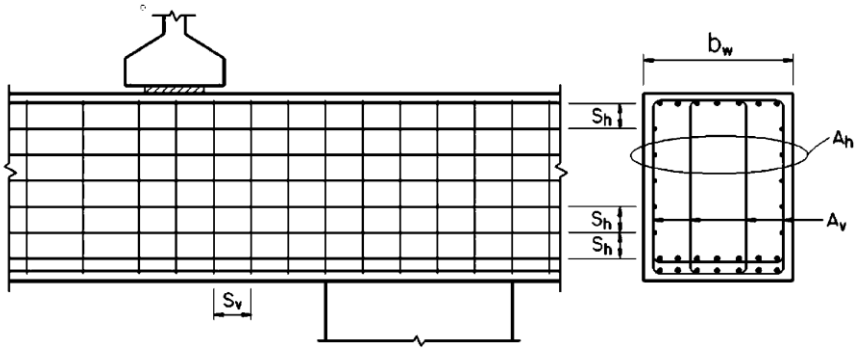

Figure 2-22: Clarification of terms A_v and A_h (TxDOT, 2001)

The minimum web and skin reinforcement requirement (numbered 12 above) was introduced in the 2011 manual revision along with a maximum spacing limitation of 12 in. or *d*/4, as mandated per AASHTO Art. 5.6.3.6. The recommendations are consistent with the findings of TxDOT Project 0-5253 that recommends a minimum reinforcement ratio of 0.3% in each orthogonal direction be used in deep beams to (1) adequately restrain the width of diagonal cracks at service loads, (2) distribute the diagonal cracks, and (3) allow for enough force redistributions to reach the full design strength of compression struts.

2.4.3 Strut-and-Tie Modeling Provisions of TxDOT Project 5253

TxDOT Project 0-5253 and 5-5253-01 developed new strut-and-tie (STM) modeling provisions and recommended modifications to both the ACI 318 and AASHTO LRFD codes; these provisions are presented by Birrcher, et al. (2009) and Williams (2011).

The most significant modifications proposed for AASHTO LRFD are:

- Concrete efficiency factors, ν, for the nodal faces are modified according to Table 2-2.

Table 2-2: TxDOT Project 5-5253-01 concrete efficiency factors, v

	Node Type		
Face	***CCC***	***CCT***	***CTT***
Bearing Face	0.85	0.70	$0.45 \le 0.85 - \frac{f'_c}{20} \le 0.65$
Back Face			
Strut-to-Node Interface*	$0.45 \le 0.85 - \frac{f'_c}{20} \le 0.65$	$0.45 \le 0.85 - \frac{f'_c}{20} \le 0.65$	

** If crack control reinforcement requirement of AASHTO Art. 5.6.3.5 is not satisfied, use v = 0.45 for the strut-to-node interfaces*

The concrete efficiency factors (ν) reduce the compressive strength of the concrete in the node depending on the type of node (CCC, CCT, or CTT) and face (bearing face, back face, strut-to-node interface) under consideration. The three types of nodes and their efficiency factors for each face are illustrated in Figure 2-23.

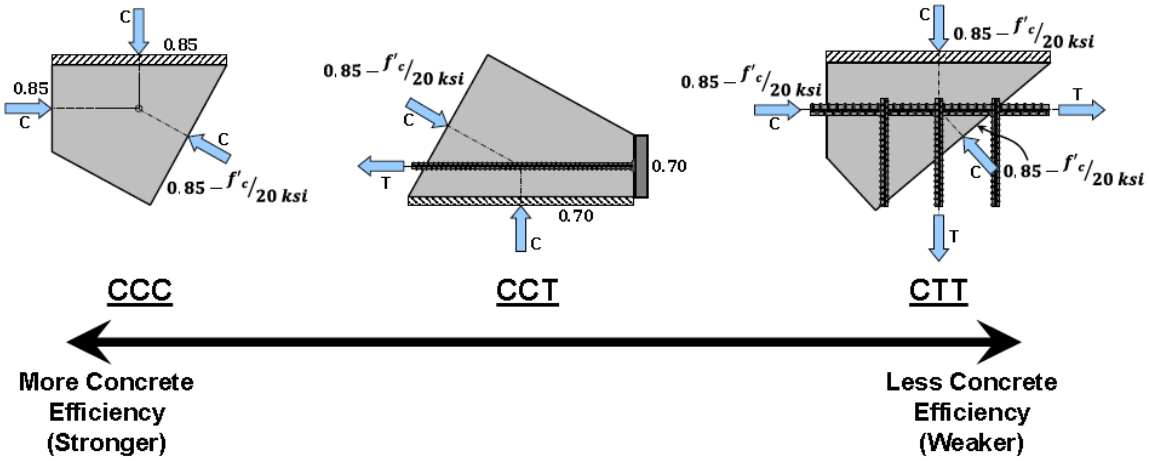

Figure 2-23: Node efficiency factors (Williams, 2011)

One can note from Table 2-2 that the efficiency factor at a strut-to-node interface is the same for both CCC and CCT nodes. Current recommendations therefore do not reduce the nodal strength due to the presence of a tension field in CCT nodes. In compression-chord loaded members, the node below the applied load is a CCC node. However, the same node in a tension-chord loaded inverted-T member is a CCT node (Figure 2-5). TxDOT project 0-6416 that includes the work presented in this dissertation aims to explore potential differences between tension- and compression-chord loaded members that may affect efficiency factors of CCT nodes.

- Design of struts is simplified by focusing on the design of the strut-to-node interfaces, which implicitly accounts for the strut capacity and eliminates trivial checks.
- The location of the critical point at which the yield strength of tie bars must be developed was revised according to Figure 2-24.

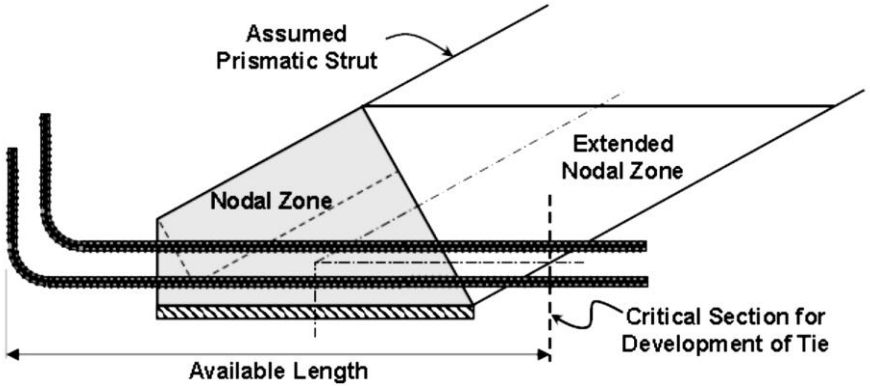

Figure 2-24: Available development length for ties (Williams, 2011)

- Strength provided by compression steel is included in the nominal resistance of the back face of the nodes, as follows:

$$P_n = f_{cu}A_{cn} + f_yA_{sn} \quad \textbf{(2-27)}$$

$$f_{cu} = mvf'_c \quad \textbf{(2-28)}$$

where:

f_{cu} = limiting compressive stress at the face of the node (ksi)

A_{cn} = effective cross-sectional area of the face of a node (in.^{2})

f_y = Yield strength of mild steel reinforcement (ksi)

A_{sn} = area of reinforcement entering the back face (in.^{2})

m = confinement modification factor, taken as $\sqrt{A_1/A_2}$ but not more than 2 as defined in AASHTO Art. 5.7.5, see Figure 2-21

v = concrete efficiency factor, as specified in Table 2-2

- Minimum bend radius of curved bars at nodes is specified to limit the radial compressive stress to a permissible level, see Figure 2-25.

$$r_b \geq A_sf_y/vbf'_c \quad \textbf{(2-29)}$$

where:

r_b = bend radius of a curved-bar node, measured to the inside of a bar (in.)

A_{st} = total area of longitudinal mild steel reinforcement in the ties ($in.^2$)

v = back face concrete efficiency factor as specified in Table 2-2

b = width of the strut transverse to the plane of the strut-and-tie model (in.)

f'_c = specified compressive strength of concrete (ksi)

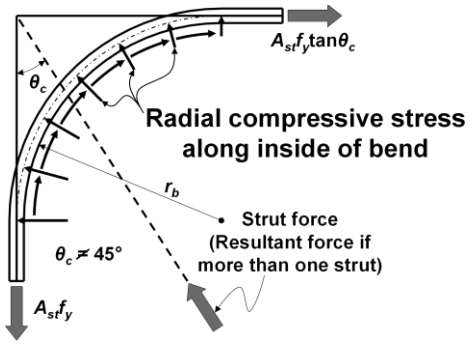

Figure 2-25: Bend radius for curved bars at nodes (Williams, 2011)

- To provide sufficient length along the bend of a curved bars at nodes required to develop differences in tie forces (see Figure 2-26), the following equation must be satisfied:

$$r_b \geq \frac{2l_d(1-tan\theta_c)}{\pi} - \frac{d_b}{2} \qquad \textbf{(2-30)}$$

where:

l_d = development length for straight bars (in.)

θ_c = smaller of the two angles between the strut and the ties that extend from the node

d_b = diameter of bar (in.)

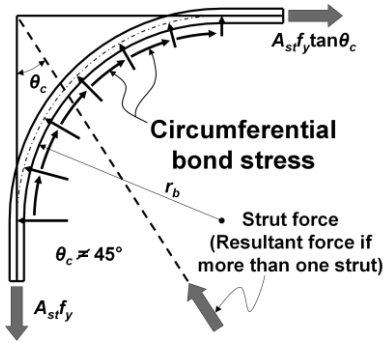

Figure 2-26: Length of bend of curved bars at nodes (Williams, 2011)

2.5 STRUT-AND-TIE MODELING OF INVERTED-T BEAMS ACCORDING TO TXDOT PROJECT 5253 PROVISIONS

TxDOT project 5253 demonstrated the effectiveness of the modifications proposed to the AASHTO LRFD STM design procedures. As such, the modified design procedures will be used when estimating the capacities of the inverted-T beams tested in this study. A detailed design example for one of the specimens of the experimental program is provided in Appendix C. More details on the use of TxDOT 5253 STM design can be found in Williams (2011). The STM design procedures as applied to inverted-T beams are summarized next. Validity of the proposed application of STM provisions of project 5253 will be investigated in subsequent chapters.

2.5.1 Outline of Strut-and-tie Modeling of Inverted-T Bent Caps

The design procedures for inverted-T bent caps are summarized as follows:

1. Define loads and solve statics (Figure 2-27).

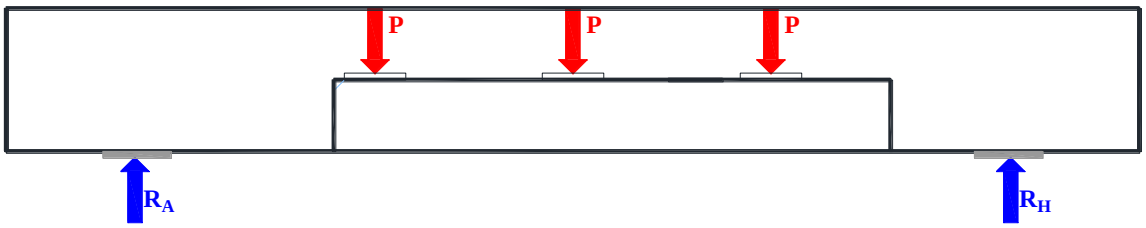

Figure 2-27: Loads and reactions acting on inverted-T bent cap

2. Define geometry of the longitudinal strut-and-tie model

a. Assume 45-degree spread of loads under the loading plates to define width of hanger ties, as shown in Figure 2-28

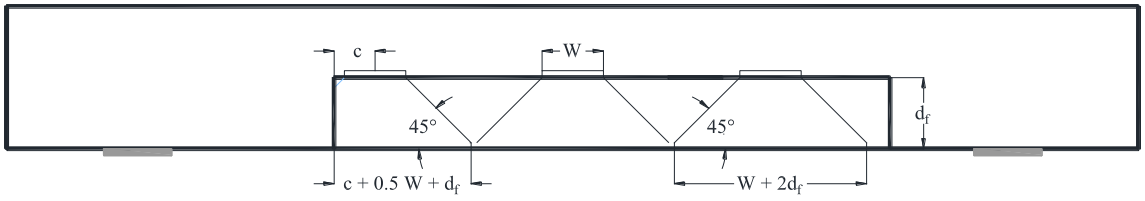

Figure 2-28: Hanger tie widths

b. Define depth of compression block using the following equation and assume prismatic strut in compression chord of depth a:

$$a = \frac{A_s f_y - A_s' f_y'}{0.85 b_w f_c'} \qquad \textbf{(2-31)}$$

where:

A_s = area of longitudinal tension steel (in.^{2})

f_y = yield strength longitudinal tension steel (psi)

A_s' = area of longitudinal compression steel (in.^{2})

f_y' = yield strength longitudinal compression steel (psi)

b_w = web width (in.)

f_c' = specified compressive strength of concrete (psi)

c. Define width of tension chord tie w_{AJ} as twice the distance from the extreme tension fiber to centroid of longitudinal steel reinforcement (Figure 2-29).

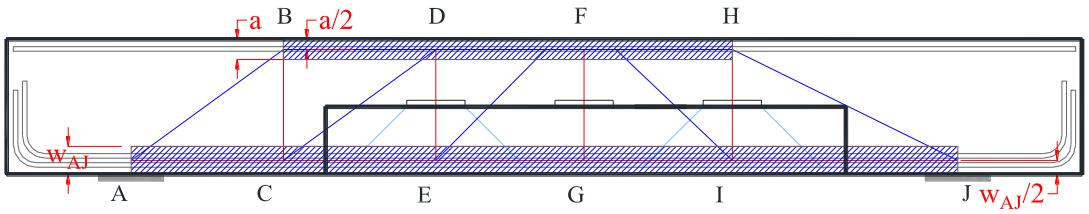

Figure 2-29: Widths of compression and tension chords

d. Define location of intermediate ties (BC) using the technique proposed by Wight and Parra-Montesinos (2003). Project a line at 25 degrees form the edge of the support plate at node A to the top of the beam to define the limit of tie BC; tie BC will be centered half way between the 45-degree projection from the loading plate at DE and the 25-degree projection from support plate at node A (see Figure 2-30).

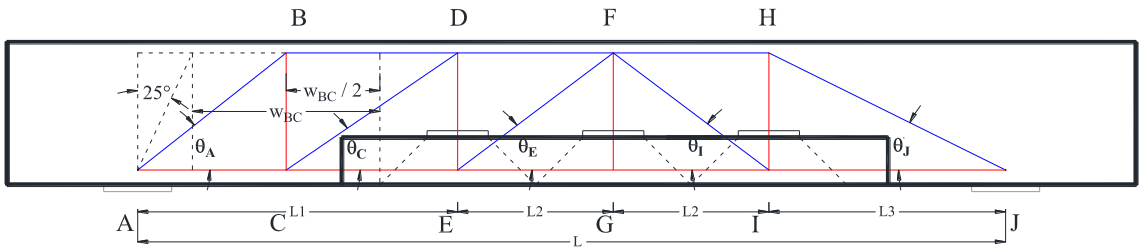

Figure 2-30: Development of strut and tie model

e. Check angles between strut and ties to be equal or greater than 25 deg.

3. Solve for truss forces in longitudinal model (Figure 2-31).

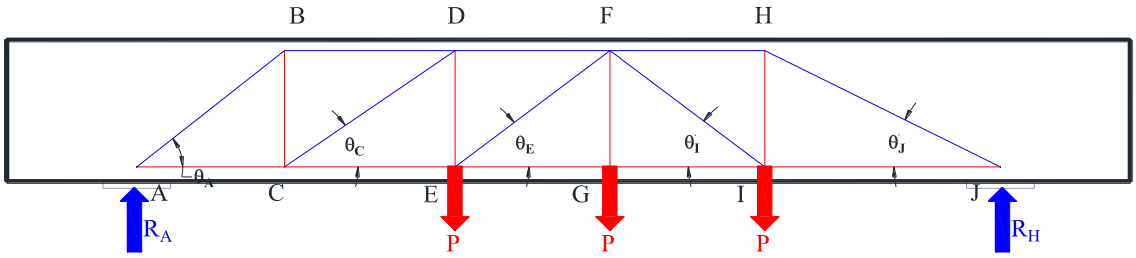

Figure 2-31: Truss forces in longitudinal model

4. Solve for truss forces in cross-sectional model using the hanger tie forces found in step 3 (Figure 2-32) and the external loads.

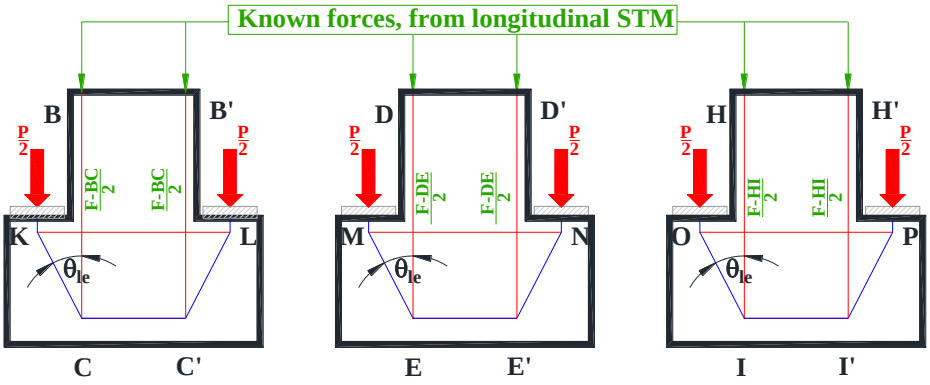

Figure 2-32: Forces in cross-sectional models

5. Calculate required steel area to satisfy calculated forces in tension chord with the following equation:

$$As_{AJ} = \frac{F_{AJ}}{\emptyset f_y} \qquad \textbf{(2-32)}$$

where:

As_{AJ} = required steel area for tie AJ (in.^{2})

F_{AJ} = calculated factored truss force in tie AJ (kip)

$\emptyset$ = 0.90; resistance factor for tension ties (AASHTO Art. 5.5.4.2.1)

f_y = yield strength of tie reinforcement (ksi)

6. Calculate required steel area to satisfy calculated forces in hanger ties using equation 2-32. Uniformly distribute required steel within load spreading area calculated in step 2a (Figure 2-33).
7. Calculate required steel area to satisfy calculated forces in intermediate ties using equation 2-32. Uniformly distribute required steel within tie width calculated in step 2d (Figure 2-33).

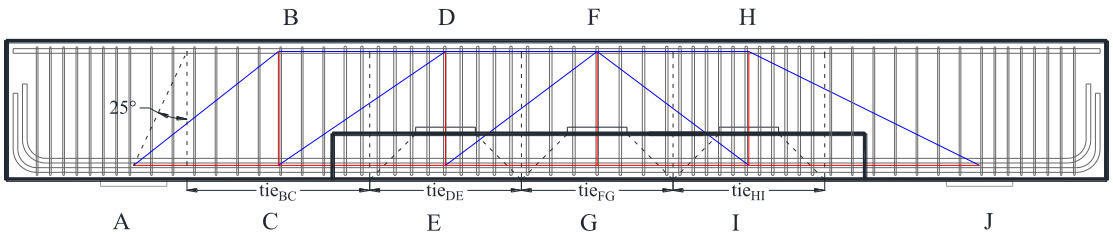

Figure 2-33: Proportion steel in ties to satisfy factored truss forces

8. Calculate required steel area to satisfy calculated forces in horizontal ties in cross-sectional models using equation 2-32. Uniformly distribute required steel within load spreading area the smaller of $W+5a_f$ or $2c$ as defined in AASHTO 5.13.2.5.3 (see Figure 2-34). AASHTO load spread recommendations for ledge reinforcement were used as the experimental program of this study did not investigate ledge strength and therefore did not provide information that would allow modifications to AASHTO.

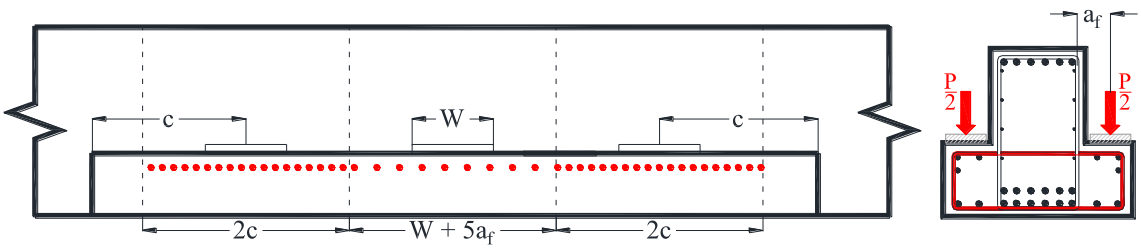

Figure 2-34: Load spread area for ledge reinforcement

9. Perform nodal strength checks following procedure for rectangular beams as indicated in Section 2.4.3. Detailed examples of STM for rectangular deep beams are provided in Birrcher, et al. (2009) and Williams (2011).
10. Proportion crack control reinforcement as specified in TxDOT project 5253: provide at least 0.3% distributed vertical and horizontal reinforcement ratios with maximum bar spacing of $d/4$ or 12 in.
11. Ensure proper anchorage for ties as specified in Section 2.4.1-4, see Figure 2-24 to Figure 2-26.
12. Perform shear serviceability check. Shear force at the critical section, defined as the midpoint between the center of the support and the first

concentrated load, under service loads must be less than the diagonal cracking load defined as:

$$V_{cr} = \left[6.5 - 3\left(\frac{a}{d}\right)\right]\sqrt{f_c'}\,b_w d \qquad \textbf{(2-33)}$$

where f_c' is the specified concrete strength in psi.

The empirical equation 2-33 was developed for rectangular deep beams. Applicability of this equation is evaluated in Section 5.3.

2.6 INVERTED-T DEEP BEAM DATABASE

This section documents the inverted-T deep beam database task of TxDOT Project 0-6416. The purpose of this database is to supplement the results of the experimental program in verifying the accuracy of proposed design provisions. The database assembly comprised three stages: (1) Collection database, (2) Filtered database, and (3) Evaluation database.

The majority of the specimens found in the literature are unrepresentative of the bent caps in service in Texas. Most of the inverted-T specimens found in the literature have shear areas of less than 200 in.^{2}. Texas bent caps typically have shear areas of 1,200 in.^{2} or greater. Also, a significant number of specimens in the literature review have an aspect ratio greater than 4; some have a depth over 12 times greater than their width (Figure 2-35). Such a high aspect ratio is unrealistic for inverted-T bent caps. Conventional beams have an aspect ratio of approximately one to three.

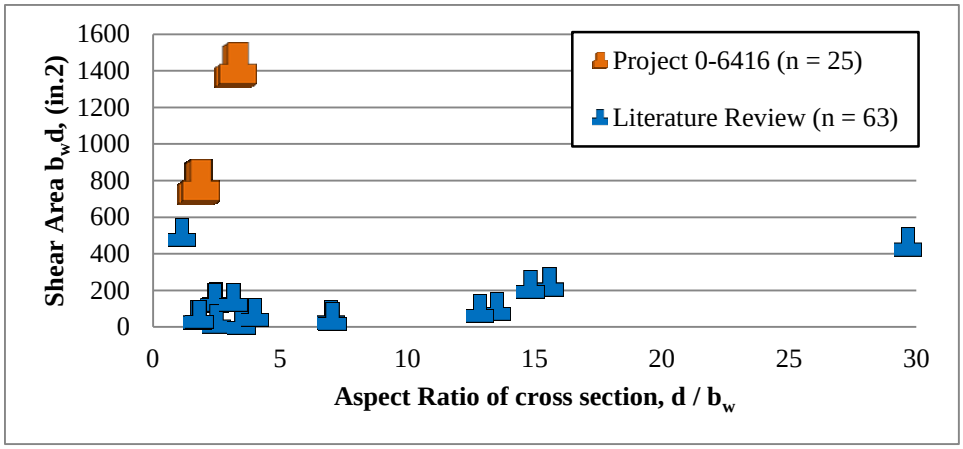

Figure 2-35: Summary of beam proportions for specimens with shear failures (n = 96); b_w = web width, d = effective web depth

2.6.1 Collection database

The first stage, collection database, consisted in gathering all the inverted-T specimens found in the literature and collecting all the pertaining information regarding geometry, reinforcement, boundary conditions, strength, and serviceability. A total of 128 specimens from 14 different sources compose the collection database; including 31 tests conducted within Project 0-6416. The collection database was compiled based on the research papers cited in Appendix A.

2.6.2 Filtered database

The second stage, filtered database, consisted in removing 41 specimens for the following reasons: (1) specimens did not fail; this information is essential to evaluate the performance of the specimens and calibrate the new design provisions for inverted-T beams, (2) specimens were lacking plate size information; this information is essential to generate strut-and-tie models to evaluate the performance of the specimens, (3) specimens had no shear reinforcement; this condition is unrealistic, as in-service beams generally have a minimum amount of transverse reinforcement, (4) specimens had complicated support conditions, complicated geometry, or complicated reinforcement details; these conditions hinder the generation of strut-and-tie models to evaluate their performance.

2.6.3 Evaluation database

The third stage, evaluation database, consisted in further refinement of the database removing specimens that were unrepresentative of the distressed field members. In this stage 56 test were filtered due to the following reasons: (1) specimens with a web depth-to-web width aspect ratio greater than four; specimens under this condition resemble walls and their behavior is different from that of bent caps that typically have an aspect ratio on the order of one to three, (2) specimens had web widths smaller than 4.5; this minimum limit was selected as the required width to accommodate two number five longitudinal bars with one in. of clear space between them, with a number three stirrup and a clear cover of ¾ in., (3) combined tension- and compression-chord loading, this condition is unrepresentative of the field specimens which do not present loads on both chords, and (4) specimens with torsional loads, these specimens were filtered out since the distressed field members showed no signs of torsional problems but only web shear deficiencies (in all cases the observed cracking pattern is consistent with web shear distress).

Filtering based on failure mode was not performed as it is the intent of the project to perform a comprehensive assessment of all design provisions for inverted-T beams (not just those applicable to web shear). As such some beams in the evaluation database had ledge or flexural failures.

2.6.4 Database summary

A total of one hundred twenty eight specimens from fourteen different sources are included in the collection database (Figure 2-36). A summary of the database filtering record is provided in Table 2-3. Thirty one specimens remained in the evaluation database, all of them conducted within project 0-6416. This fact highlights the importance of the experimental program and the need for a large number of test specimens to fully evaluate the strength and serviceability behavior of inverted-T bent caps.

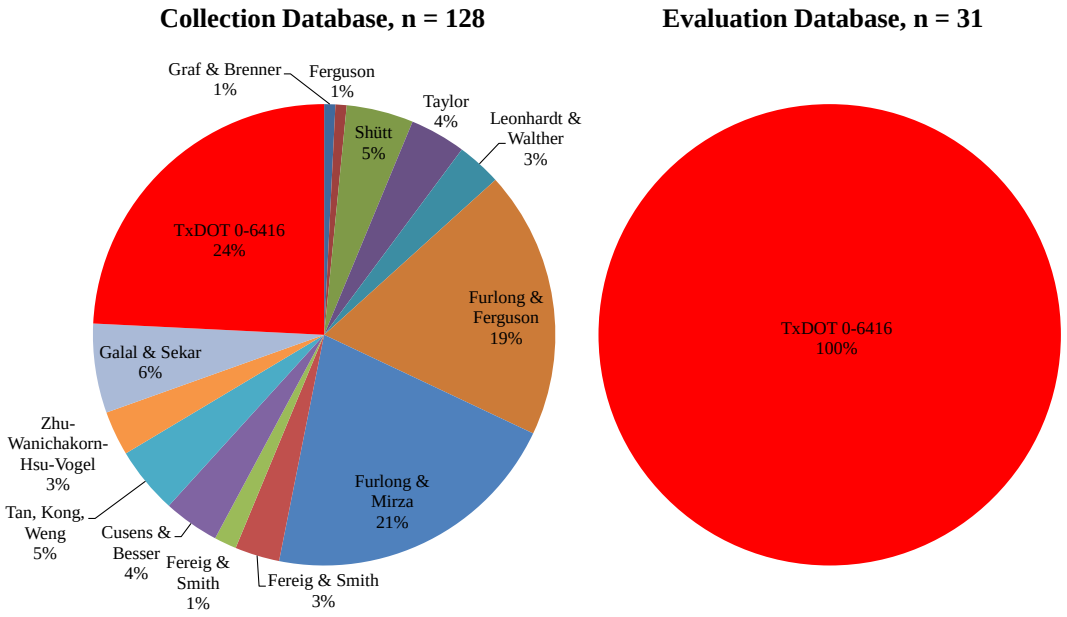

Figure 2-36: Sources of inverted-T database

Table 2-3: Database assembly

Collection Database		***128 tests***
Stage 1 filtering	specimen did not fail	- ***10 tests***
	incomplete plate size information	- ***10 tests***
	no shear reinforcement	- ***2 tests***
	complicated supports/geometry/reinforcement	- ***19 tests***
Filtered Database		***87 tests***
Stage 2 filtering	$h / b_w > 4$	- ***11 tests***
	$b_w < 4.5$in.	- ***9 tests***
	tension- and compression-chord loaded	- ***9 tests***
	torsional loads	- ***27 tests***
Evaluation Database		***31 tests***

2.7 SUMMARY

Four topics were reviewed in this chapter. First, several cases of distressed inverted-T bent caps in service in Texas were presented including diagonal crack width information. Next, background information on strut-and-tie modeling design and behavior of inverted-T beams was presented. Then, design provisions for inverted-T beams from the AASHTO LRFD code, TxDOT bridge design manual, and TxDOT project 5253 were summarized. Finally, assembly of the inverted-T deep beam database was presented.

CHAPTER 3
Experimental Program

3.1 OVERVIEW

Design, fabrication, and testing details of the 19 specimens on which 31 tests were conducted are discussed in this chapter. Additionally, material properties and instrumentation details are presented for each specimen.

The experimental program was designed to encompass the variables found in the beams exhibiting problems in the field and to investigate the influence of these variables in the strength and serviceability of inverted-T bent caps. Parameters varied in the tests were ledge length, ledge depth, shear reinforcement, web depth, shear span-to-depth ratio, loaded chord, and number of loading points.

3.2 TESTING PROGRAM

Literature review revealed the scarcity of research of tension-chord loaded specimens. Cross-sections of the specimens analyzed in this project are shown to scale in Figure 3-1 to highlight the significant differences between dimensions of the bent caps in service and the specimens found in the literature. In order to properly address the objectives of this study it was deemed necessary to fabricate full-scale specimens within the experimental program.

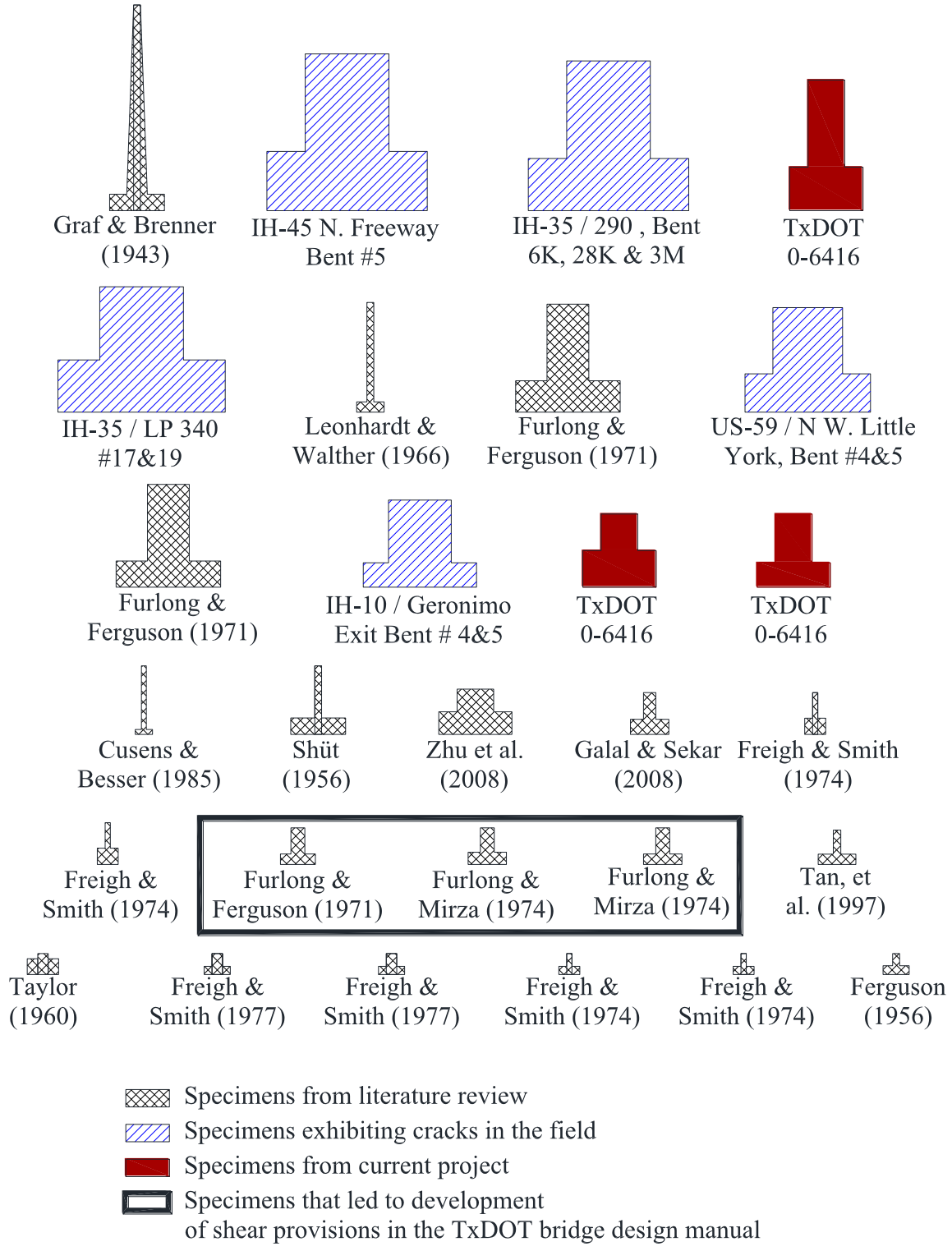

Figure 3-1: Specimen cross-sections to scale

The experimental program was divided into six series in order to isolate the effects on strength and serviceability of each one of the variables analyzed in this study. These series are presented as follows and detailed in sections 3.2.3.2 through 3.2.3.7.

Series I: Ledge length

Series II: Ledge depth

Series III: Web reinforcement

Series IV: Number of point loads

Series V: Loaded chord

Series VI: Web depth

This dissertation focuses on the effects of ledge geometry and number of point loads on strength and serviceability of inverted-T straddle bent caps (Series I, II, and IV).

3.2.1 Nomenclature

The specimen naming system used to identify the experimental variables studied in each specimen is described in this section. Details of each of the experimental variables are provided in sections 3.2.3.2 to 3.2.3.7. A typical specimen name is shown in Figure 3-2.

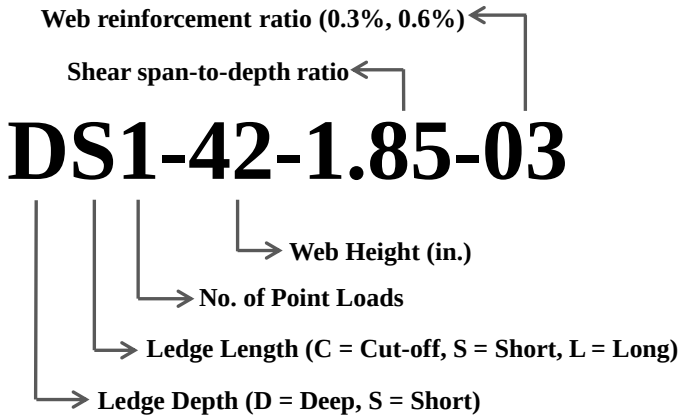

Figure 3-2: Specimen nomenclature

The first character (D or S) refers to the ledge depth, Deep or Shallow. Deep ledges have a height equal to half of the depth of the web, whereas shallow ledges have a

height equal to one third of the depth of the web. More details on ledge depths are provided in section 3.2.3.3.

The second character (C, S, or L) refers to the ledge length, Cut-off, Short, or Long. Cut-off ledges end at the edge of the outer most loading plate. Short ledges extend beyond the outer most loading plate a distance equal to the ledge height. Long ledges run continuously from support to support. More details on ledge lengths are provided in section 3.2.3.2.

The third character refers to the number of point loads applied to the specimen (1 or 3). Specimens with one point load were directly comparable with compression-chord loaded specimens from TxDOT Project 0-5253, whereas specimens with multiple point loads are more representative of field conditions. Spreading the load over multiple loading points also allowed the use of shallower ledges by helping avoid local failures in the ledges. More details on the number of point loads are provided in section 3.2.3.5.

The next two groups of characters indicate the web depth in in., and the shear span-to-depth (or *a/d*) ratio. More details on web height and a/d ratio are provided in sections 3.2.3.7 and 3.2.3.1 respectively.

The last group of characters refers to the web reinforcement ratio, as defined in Figure 3-3. “03” refers to specimens with $\rho_v = \rho_h = 0.3\%$, “06” refers to specimens with $\rho_v = \rho_h = 0.6\%$ and “06/03” refers to specimens with $\rho_v = 0.6\%$ and $\rho_h = 0.3\%$; More details on web reinforcement ratios are provided in section 3.2.3.4.

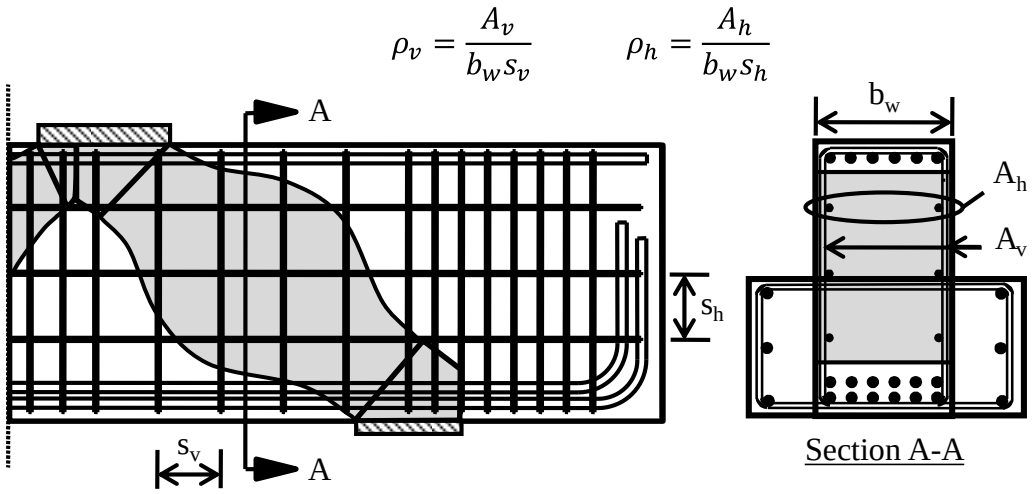

Figure 3-3: Definition for vertical and horizontal web reinforcement ratios

3.2.2 Overview of Test Specimens

An overview of the 31 test regions of 19 full-scale specimens are presented in this section. Tests were conducted as described in section 3.6. A summary of the experimental specimens is provided in Table 3-1. Typical specimen geometries and reinforcing details are shown in Figure 3-4 and Figure 3-5. One should note that for all specimens web width was 21 in., while ledge overhang was 10.5 in. Other dimensions varied between specimens. Details of geometry and reinforcing details of each specimen are provided in Appendix B.

Table 3-1: Testing program

Test	Specimen	Ledge Depth	Ledge Length	Loading Points	d (in)	a / d ratio	Support Plate	Loading Plate	ρ_v	ρ_h
01a	DS1-42-1.85-03	h/2	Short	1	37.6	1.96	16" x 20"	26" x 9"	0.003	0.003
01b	DS1-42-2.50-03	h/2	Short	1	37.6	2.65	16" x 20"	26" x 9"	0.003	0.003
02a	DS1-42-1.85-06	h/2	Short	1	37.6	1.85	16" x 20"	26" x 9"	0.006	0.006
02b	DS1-42-2.50-06	h/2	Short	1	37.6	2.50	16" x 20"	26" x 9"	0.006	0.006
03a	DL1-42-1.85-06	h/2	Long	1	37.6	1.85	16" x 20"	26" x 9"	0.006	0.006
03b	DL1-42-2.50-06	h/2	Long	1	37.6	2.50	16" x 20"	26" x 9"	0.006	0.006
04a	SS3-42-1.85-03	h/3	Short	3	37.6	1.85	16" x 20"	18" x 9"	0.003	0.003
04b	SS3-42-2.50-03	h/3	Short	3	37.6	2.50	16" x 20"	18" x 9"	0.003	0.003
05b	SS3-42-2.50-06	h/3	Short	3	37.6	2.50	16" x 20"	18" x 9"	0.006	0.006
06a	SC3-42-2.50-03	h/3	Cut-off	3	37.6	2.50	16" x 20"	18" x 9"	0.003	0.003
06b	SC3-42-1.85-03	h/3	Cut-off	3	37.6	1.85	16" x 20"	18" x 9"	0.003	0.003
07a	SS1-75-1.85-03	h/3	Short	1	68.2	1.87	16" x 20"	30" x 10"	0.003	0.003
08b	SS1-75-2.50-06	h/3	Short	1	68.2	2.53	16" x 20"	30" x 10"	0.006	0.006
09a	DS3-42-2.50-03	h/2	Short	3	37.6	2.50	16" x 20"	18" x 9"	0.003	0.003
10a	DL1-42-1.85-03	h/2	Long	1	37.6	1.85	16" x 20"	26" x 9"	0.003	0.003
10b	DL1-42-2.50-03	h/2	Long	1	37.6	2.50	16" x 20"	26" x 9"	0.003	0.003
11a	SL3-42-1.85-03	h/3	Long	3	37.6	1.85	16" x 20"	18" x 9"	0.003	0.003
12a	SL3-42-1.85-06	h/3	Long	3	37.6	1.85	16" x 20"	18" x 9"	0.006	0.006
14a	SS1-75-1.85-03b	h/3	Short	1	68.2	1.87	16" x 20"	30" x 10"	0.003	0.003
15a	DC3-42-1.85-03	h/2	Cut-off	3	37.6	1.85	16" x 20"	18" x 9"	0.003	0.003
15b	DS3-42-1.85-03	h/2	Short	3	37.6	1.85	16" x 20"	18" x 9"	0.003	0.003
16a	SS1-42-2.50-03	h/3	Short	1	37.6	2.50	16" x 20"	26" x 9"	0.003	0.003
16b	SS1-42-1.85-03	h/3	Short	1	37.6	1.85	16" x 20"	26" x 9"	0.003	0.003
17a	DC1-42-2.50-03	h/2	Cut-off	1	37.6	2.50	16" x 20"	18" x 9"	0.003	0.003
17b	DL3-42-1.85-03	h/2	Long	3	37.6	1.85	16" x 20"	18" x 9"	0.003	0.003
18a	SL1-42-2.50-03	h/3	Long	1	37.6	2.50	16" x 20"	26" x 9"	0.003	0.003
18b	SC1-42-2.50-03	h/3	Cut-off	1	37.6	2.50	16" x 20"	26" x 9"	0.003	0.003
19a	DS1-42-1.85-06/03	h/2	Short	1	37.6	1.85	16" x 20"	26" x 9"	0.006	0.003
19b	DS1-42-2.50-06/03	h/2	Short	1	37.6	2.50	16" x 20"	26" x 9"	0.006	0.003
20a	SC1-42-1.85-03	h/3	Cut-off	1	37.6	1.85	30" x 20"	26" x 9"	0.006	0.003
20b	DC1-42-1.85-03	h/2	Cut-off	1	37.6	1.85	30" x 20"	26" x 9"	0.006	0.003

Plate dimensions: [in direction of span] x [transverse to direction of span]

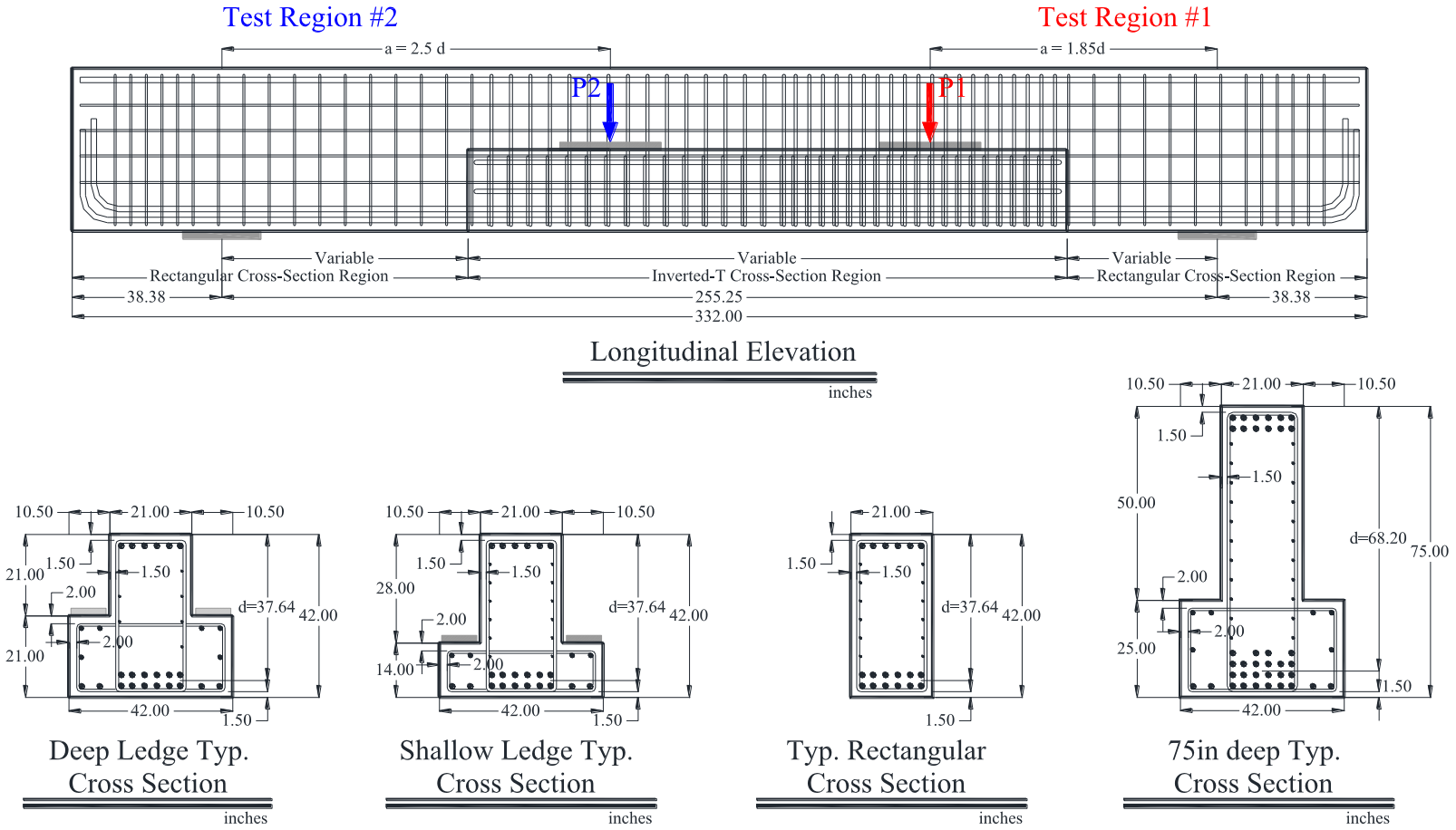

Figure 3-4: Typical specimen geometries

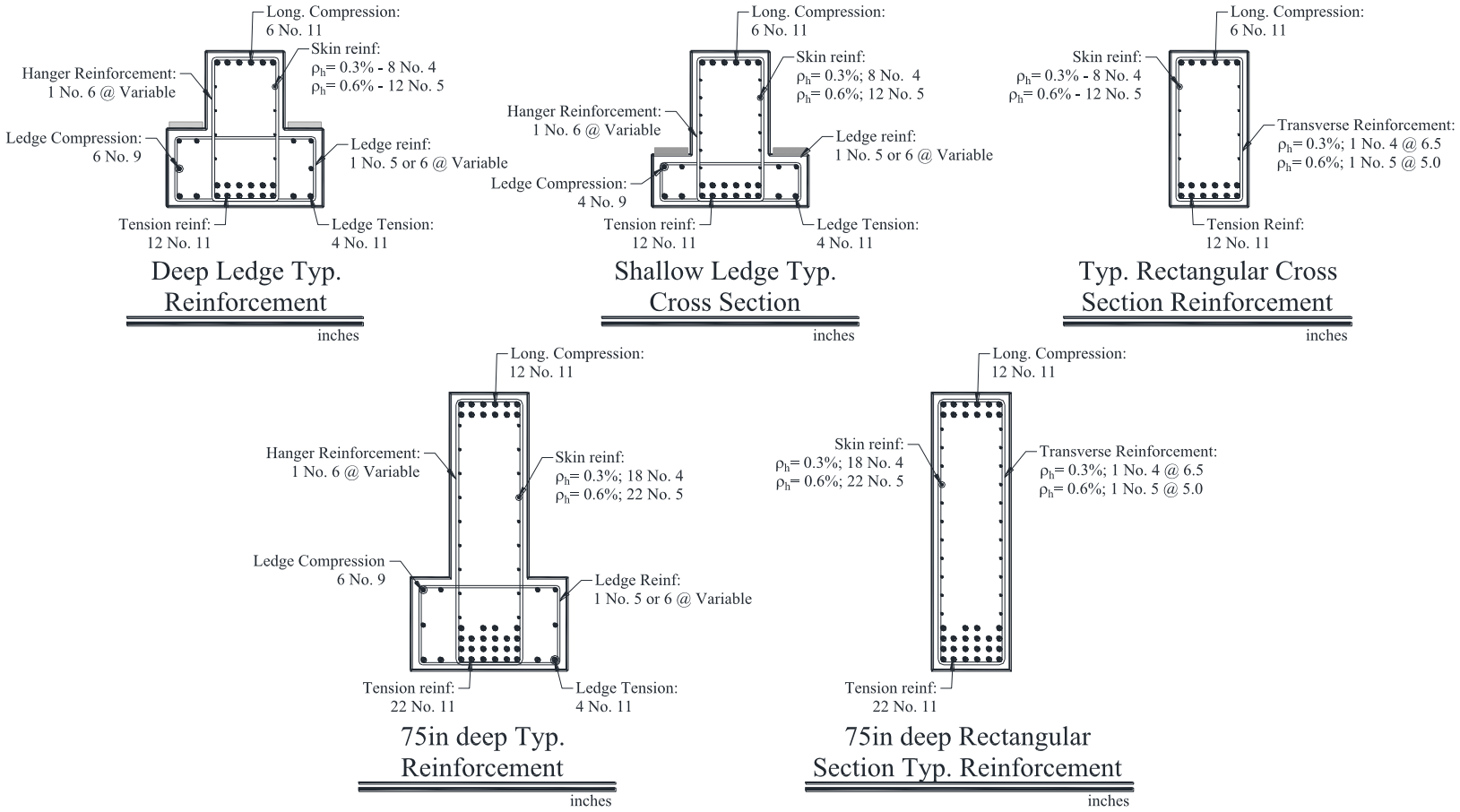

Figure 3-5: Typical reinforcement details

3.2.3 Test Series

3.2.3.1 Shear span-to-depth ratio

Shear span-to-depth (*a/d*) ratios equal to 2.50 and 1.85 were used throughout the test program and in all test series. Shear span-to-depth ratio is defined within the context of this document as the ratio of the distance from the center of the support to the center of the nearest loading point (*a*) with respect to the effective depth of the specimen (*d*) measured from the centroid of web longitudinal tension steel to the extreme compression fiber of the web; see Figure 3-6.

The *a/d* ratios used in this study were selected to be directly comparable with compression-chord loaded specimens of TxDOT Project 0-5253. Specimens with *a/d* ratios of 1.85 capture the deep beam behavior transferring shear through a direct compression strut. Specimens with *a/d* ratios of 2.50 transfer shear forces through a double strut (or double panel) system and are at the limit of sectional shear behavior (Birrcher, et al., 2009).

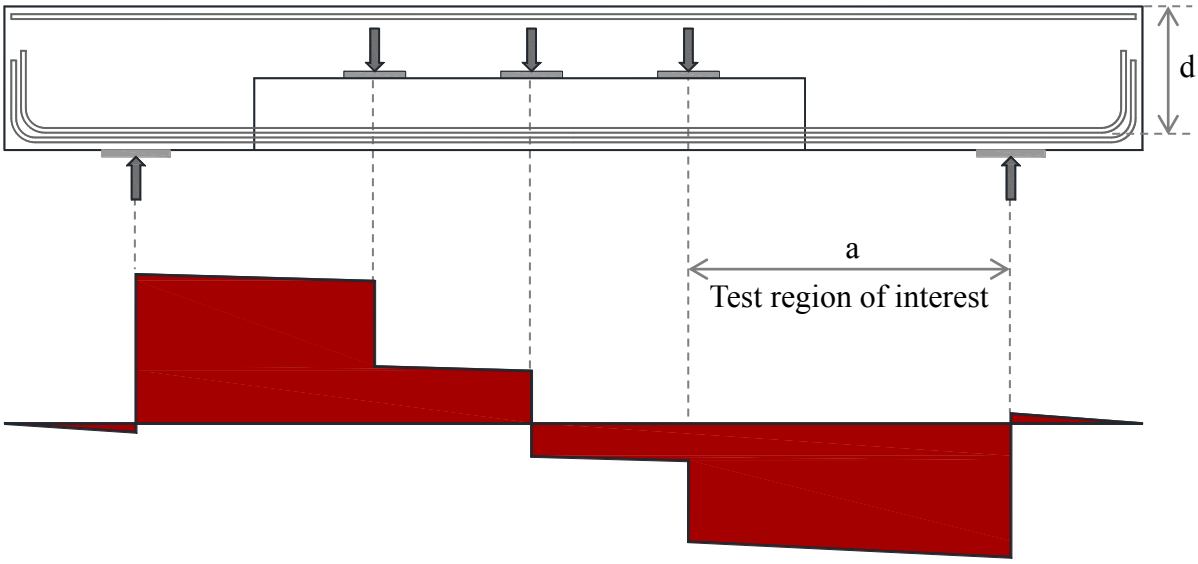

Figure 3-6: Free body and shear diagrams for a specimen subjected to three point loads

AASHTO bridge design specifications (2012) Art. 5.6.3.1 specifies that: *"The strut-and-tie model should be considered for the design of deep footings and pile caps or other situations in which the distance between the centers of applied load and the supporting reactions is less than about twice the member thickness."* The definition of the shear span in AASHTO may be interpreted in such way that all the specimens with three point loads in the experimental program can be designed using the sectional shear approach regardless of some of them having 33% of their total load concentrated at 1.85*d* from the center of the support. Experimental results of this project will be used to validate the applicability of sectional shear design for this type of members.

3.2.3.2 Series I: Ledge Length

The distressed bent caps in the field had several ledge length configurations. Some had ledges that were interrupted right next to the outer most stringer (cut-off ledge in Figure 3-7), whereas some had long ledges running continuously from support to support (long-ledge in Figure 3-7). In other cases the ledge ended in between these two extreme cases (short-ledge in Figure 3-7).

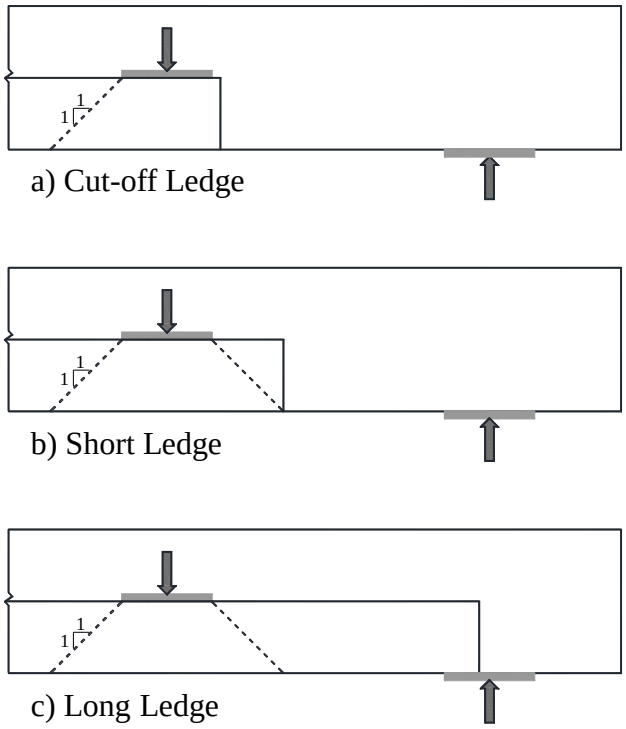

Figure 3-7: Ledge lengths

Inverted-T beams are tension-chord loaded specimens in which the forces have to be “hung” from the compression chord before being transferred to the support, as shown in Figure 3-8. This tension-chord loading induces a tension field in the web, highlighted in red in Figure 3-9, and changes the configuration of the node at the top of the beam at the loading point. In compression-chord loaded specimens, only compression forces converge at this node; whereas, in tension-chord loaded specimens an additional tension tie converges at this node.

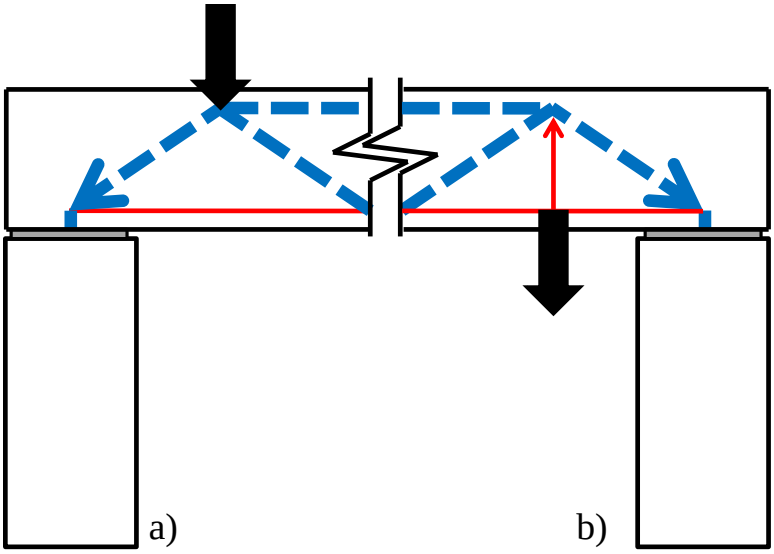

Figure 3-8: Flow path of forces in strut-and-tie models; (a) compression-chord loaded beam, (b) tension-chord loaded beam

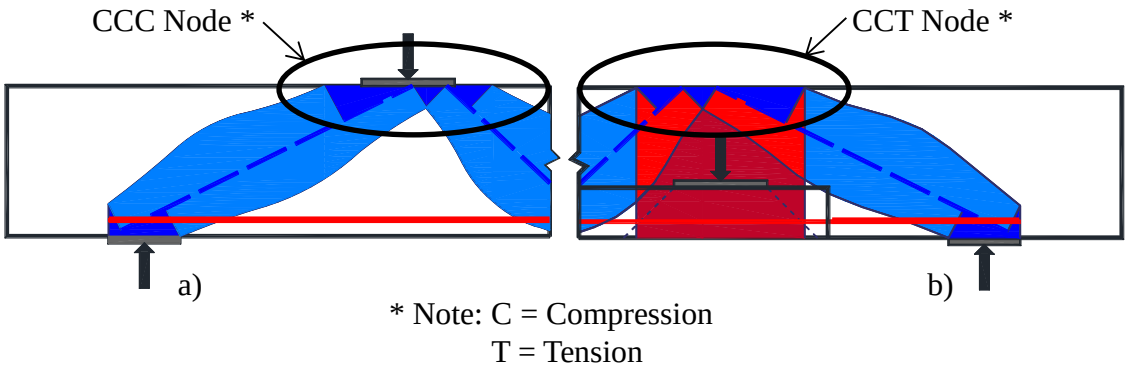

Figure 3-9: (a) Compression-chord loaded beam, (b) tension-chord loaded beam highlighting in red the tension field induced by the bottom loading

The ledge length has a direct effect on the area over which the tension field spreads, and consequently the width of the hanger tie; this effect is illustrated in Figure 3-10. In the cases of short and long ledges, this tension field has enough room to fully spread over a distance equal to the length of the bearing pad plus two times the ledge height. In the case of cut-off ledges, the force can only spread on one side of the bearing plate thereby reducing the width of the tension field and increasing tensile stresses.

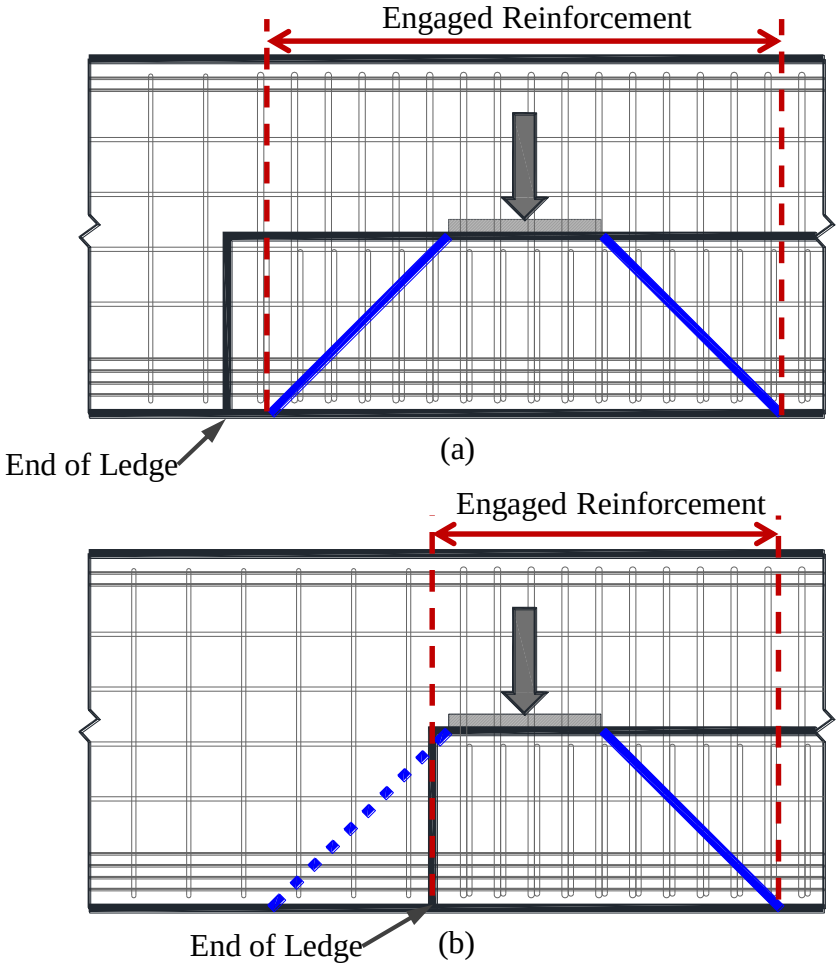

Figure 3-10: Effect of ledge length on tie width; (a) short ledge, (b) cut-off ledge

Long ledges may also affect the strength of the support region by: (1) increasing the confinement of the support nodal region, and (2) increasing the support bearing width compared with short and cut-off ledges (see Figure 3-11 for illustration).

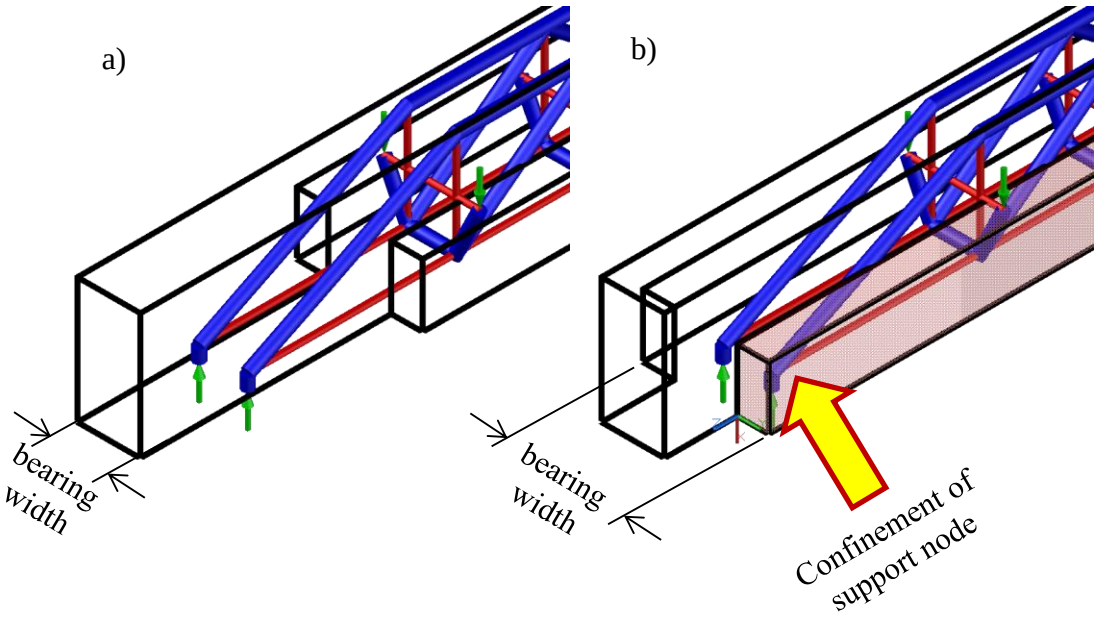

Figure 3-11: Ledge length effect on support region; (a) short ledge, (b) long ledge

Series I was designed to evaluate the influence of the ledge length on the strength and serviceability of the inverted-T specimens. Twenty tests were conducted in eight groups of two or three directly comparable specimens, in which every parameter was kept constant except the ledge length. The specimens evaluated in this series are outlined in Table 3-2.

Table 3-2: Series I: Ledge length

Test	Specimen	Ledge Depth	Ledge Length	Number of Loads	Web Depth (in.)	a/d	$\rho_v = \rho_h$
01a 10a	DS1-42-1.85-03 DL1-42-1.85-03	Deep	Short Long	1	42	1.85	0.003
15a 15b 17b	DC3-42-1.85-03 DS3-42-1.85-03 DL3-42-1.85-03	Deep	Cut-off Short Long	3	42	1.85	0.003
02a 03a	DS1-42-1.85-06 DL1-42-1.85-06	Deep	Short Long	1	42	1.85	0.006
17a 01b 10b	DC1-42-2.50-03 DS1-42-2.50-03 DL1-42-2.50-03	Deep	Cut-off Short Long	1	42	2.50	0.003
02b 03b	DS1-42-2.50-06 DL1-42-2.50-06	Deep	Short Long	1	42	2.50	0.006
06b 04a 11a	SC3-42-1.85-03 SS3-42-1.85-03 SL3-42-1.85-03	Shallow	Cut-off Short Long	3	42	1.85	0.003
18b 16a 18a	SC1-42-2.50-03 SS1-42-2.50-03 SL1-42-2.50-03	Shallow	Cut-off Short Long	1	42	2.50	0.003
06a 04b	SC3-42-2.50-03 SS3-42-2.50-03	Shallow	Cut-off Short	3	42	2.50	0.003

3.2.3.3 Series II: Ledge Depth

The purpose of the Series II specimens was to evaluate the effects on strength and serviceability of the ledge-depth to web-depth ratio (h_{le} / h). The inspected distressed bent caps had values of h_{le} / h between 0.28 and 0.42. Ledge-depth to web-depth ratios were selected as 0.5 and 0.33 in test specimens to be representative of the distressed beams in the field as can be seen in Figure 3-12. An attempt to design test specimens with a h_{le} / h ratio equal to 0.25 was made but was abandoned due to insufficient safety factors against local ledge failures.

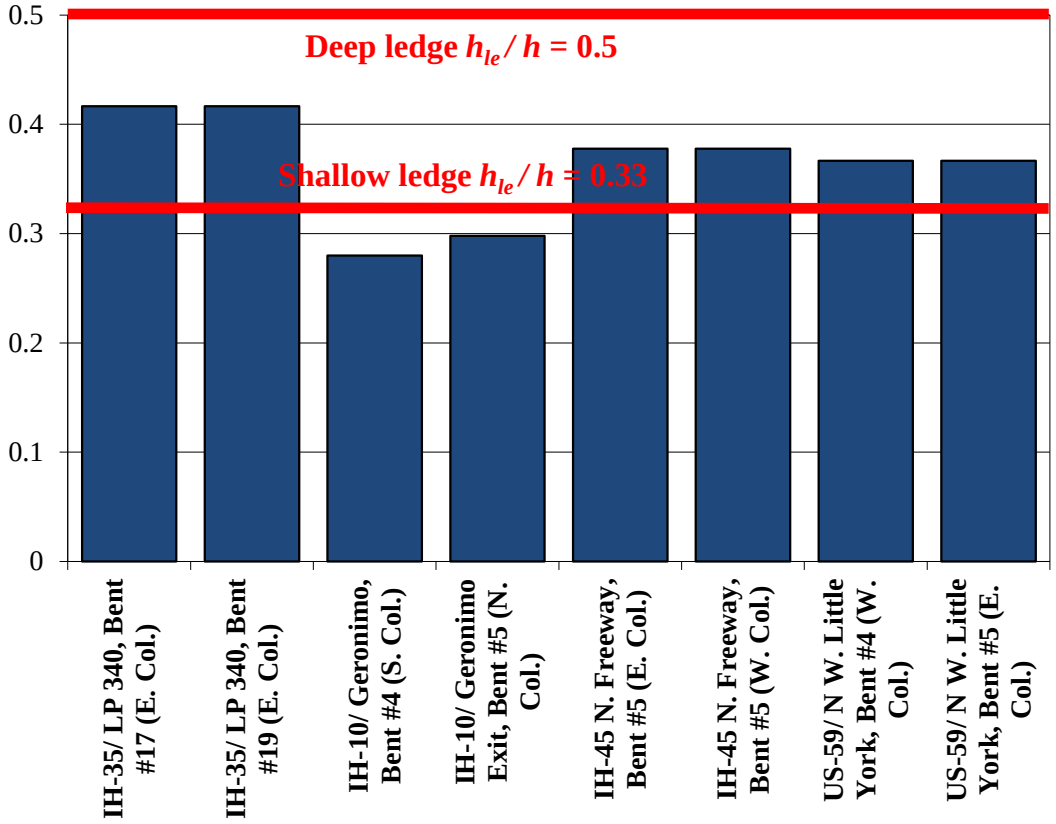

Figure 3-12: h_{le} / h ratios of distressed bent caps in service in Texas

As mentioned in section 3.2.3.2, tension-chord loading of the specimens induces a tension field in the web as the forces have to be "hung" to the compression chord. The ledge depth has a direct effect on the width of the area over which this tension field spreads. Deeper ledges allow applied forces to spread over a wider area and consequently can decrease the tensile stresses in the web. This effect is illustrated in Figure 3-13.

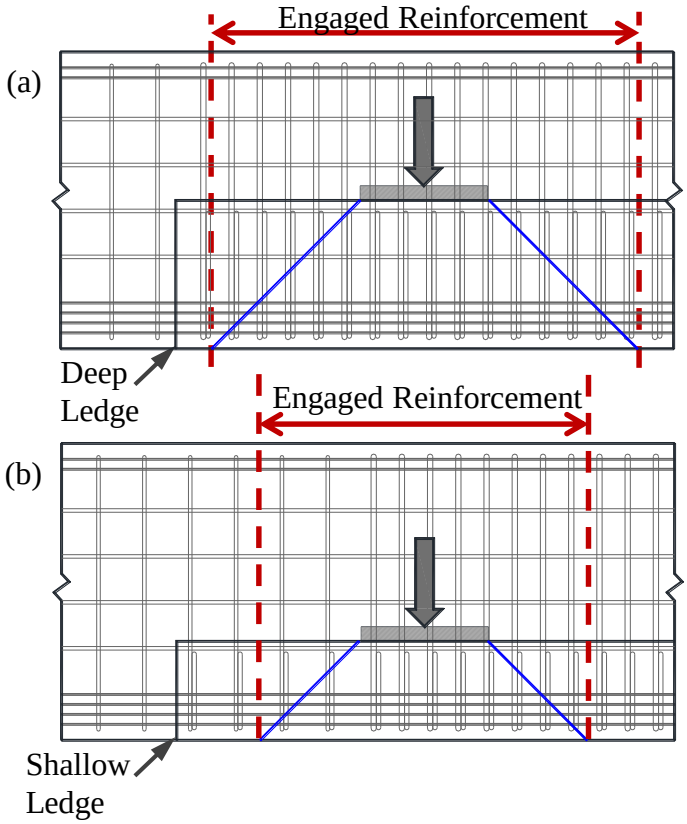

Figure 3-13: Load spreading in specimens with: (a) deep ledge and (b) shallow ledge

Additionally, the ledge depth will define the inclination of the ledge strut as shown in Figure 3-14. This inclination will impact the strength of the ledge and may lead to incompatibility of strains in the associated nodes particularly as the angle between the strut and tie reduces below 25 degrees.

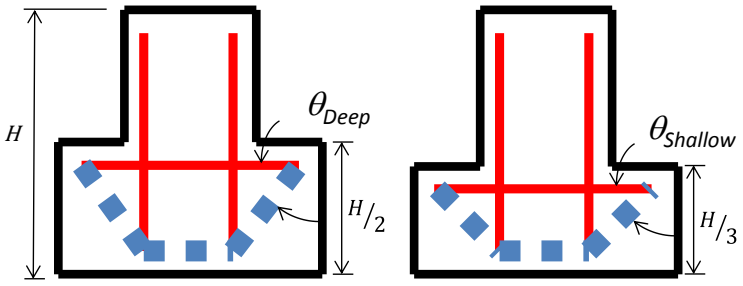

Figure 3-14: Inclination angle of ledge strut

The test specimens were constructed with h_{le} / h equal to 0.5 or 0.33 as illustrated in Figure 3-15. These h_{le} / h ratios are representative of the range of configurations used in practice. Eighteen tests are included in this series for a total of nine direct comparisons. The specimens evaluated in this series are outlined in Table 3-3.

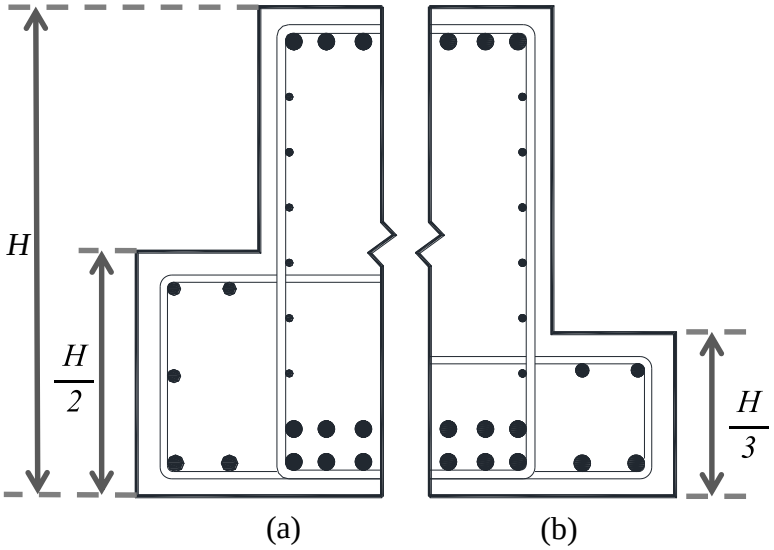

Figure 3-15: Ledge Depths; (a) Deep Ledge, (b) Shallow Ledge (Garber 2011)

Table 3-3: Series II: Ledge depth

Test	Specimen	Ledge Depth	Ledge Length	Number of Loads	Web Depth (in.)	a/d	$\rho_v = \rho_h$
16b	SS1-42-1.85-03	Shallow	Short	1	42	1.85	0.003
01a	DS1-42-1.85-03	Deep					
06b	SC3-42-1.85-03	Shallow	Cut-Off	3	42	1.85	0.003
15a	DC3-42-1.85-03	Deep					
04a	SS3-42-1.85-03	Shallow	Short	3	42	1.85	0.003
15b	DS3-42-1.85-03	Deep					
11a	SL3-42-1.85-03	Shallow	Long	3	42	1.85	0.003
17b	DL3-42-1.85-03	Deep					
20a	SC1-42-1.85-03	Shallow	Cut-Off	1	42	1.85	0.003
20b	DC1-42-1.85-03	Deep					
18b	SC1-42-2.50-03	Shallow	Cut-Off	1	42	2.50	0.003
17a	DC1-42-2.50-03	Deep					
16a	SS1-42-2.50-03	Shallow	Short	1	42	2.50	0.003
01b	DS1-42-2.50-03	Deep					
18a	SL1-42-2.50-03	Shallow	Long	1	42	2.50	0.003
10b	DL1-42-2.50-03	Deep					
04b	SS3-42-2.50-03	Shallow	Short	3	42	2.50	0.003
09a	DS3-42-2.50-03	Deep					

3.2.3.4 Series III: Web Reinforcement Ratio

This series was designed to evaluate the effects of web reinforcement on strength and serviceability of inverted-T specimens, considering direct strut or double panel failure modes. Two amounts of web reinforcement were used: 0.3% and 0.6% of the effective web area (Figure 3-16). In most tests, the vertical and horizontal web reinforcement ratios were equal. Two specimens had 0.3% horizontal and 0.6% vertical web reinforcement ratios. The lower limit of 0.3% was selected to match the minimum requirement of the TxDOT Bridge Design Manual – LRFD (2011), the AASHTO LRFD Bridge Design Specifications 2012, and the findings of TxDOT Research Project 0-5253. The maximum limit of 0.6% was selected to encompass the maximum reinforcement ratios found in the distressed bents in the field of 0.57%. Web reinforcements were

chosen such that bar spacing was small enough to ensure adequate crack control (see Figure 3-16). According to Project 0-5253, adequate crack control was ensured for web bar spacing less than 12 in. or *d*/4. Fourteen tests were conducted in six groups of two or three directly comparable specimens in which every parameter was kept constant except the web reinforcement ratio. The specimens evaluated in this series are outlined in Table 3-4.

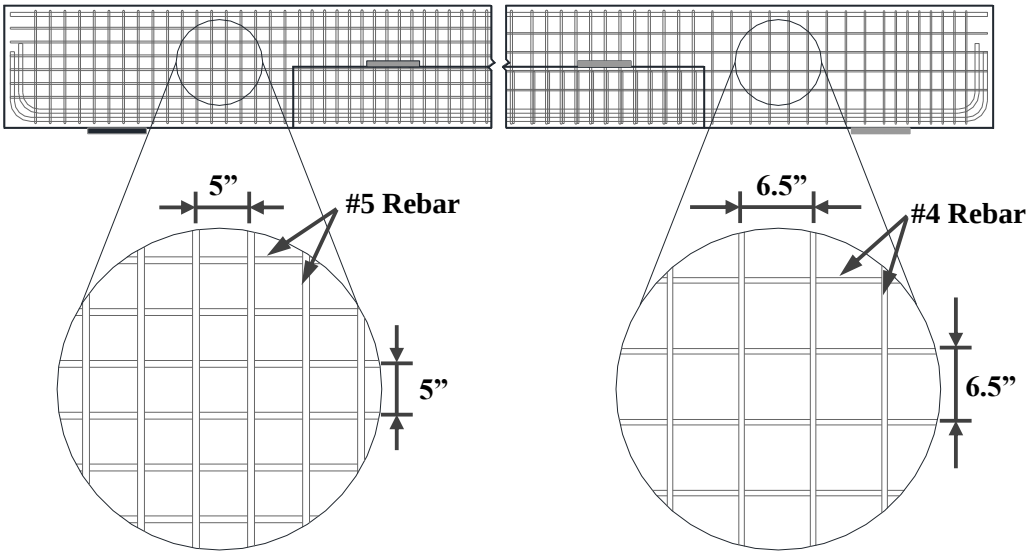

Figure 3-16: Web reinforcement ratios; (a) #5 @ 5” on center at each face with $\rho_v = \rho_h = 0.006$, (b) #4 @ 6.5” on center at each face with $\rho_v = \rho_h = 0.003$

Table 3-4: Series III: Web reinforcement ratio

Test	Specimen	Ledge Depth	Ledge Length	Number of Loads	Web Depth (in.)	a/d	ρ_v	ρ_h
01a	DS1-42-1.85-03	Deep	Short	3	42	1.85	0.003	
19a	DS1-42-1.85-06/03						0.006	0.003
02a	DS1-42-1.85-06						0.006	
10a	DL1-42-1.85-03	Deep	Long	1	42	1.85	0.003	
03a	DL1-42-1.85-06						0.006	
11a	SL3-42-1.85-03	Shallow	Long	1	42	2.50	0.003	
12a	SL3-42-1.85-06						0.006	
01b	DS1-42-2.50-03	Deep	Short	3	42	1.85	0.003	
19b	DS1-42-2.50-06/03						0.006	0.003
02b	DS1-42-2.50-06						0.006	
10b	DL1-42-2.50-03	Deep	Long	1	42	2.50	0.003	
03b	DL1-42-2.50-06						0.006	
04b	SS3-42-2.50-03	Shallow	Short	3	42	2.50	0.003	
05b	SS3-42-2.50-06						0.006	

3.2.3.5 Series IV: Number of Point Loads

This series was designed to evaluate the effects of single vs. multiple loading points on strength and serviceability of inverted-T specimens. The specimens in this series were loaded with one or three point loads (Figure 3-17). The specimens with a single loading point allowed for a direct comparison with compression-chord loaded specimens from TxDOT project 0-5253. The specimens with multiple loading points allowed the use of shallower ledges as distributing the applied force to multiple locations helped prevent local failure of the ledge and ensured web shear failure. Twelve tests were conducted in six groups of two directly comparable specimens in which every parameter was kept constant except the number of point loads. The specimens evaluated in this series are outlined in Table 3-5.

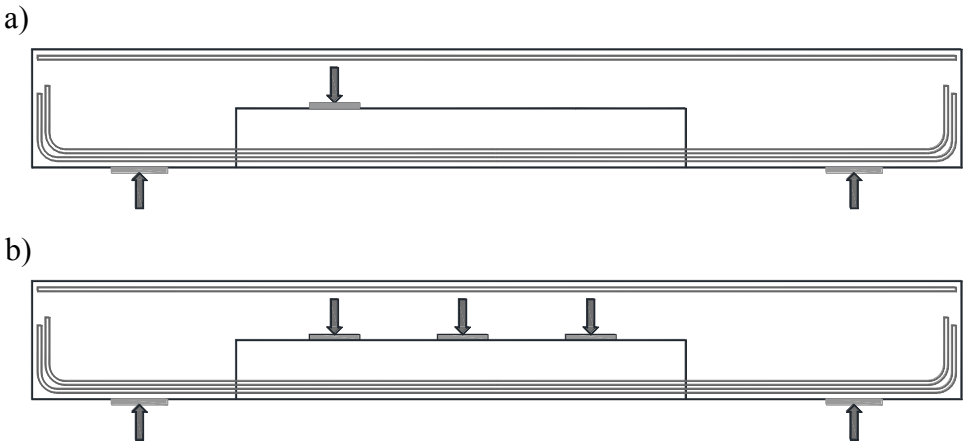

Figure 3-17: (a) One point load specimen, (b) three point load specimen

Table 3-5: Series IV: number of point loads

Test	Specimen	Ledge Depth	Ledge Length	Number of Loads	Web Depth (in.)	a/d	$\rho_v = \rho_h$
16b 04a	SS1-42-1.85-03 SS3-42-1.85-03	Shallow	Short	1 3	42	1.85	0.003
01a 15b	DS1-42-1.85-03 DS3-42-1.85-03	Deep	Short	1 3	42	1.85	0.003
10a 17b	DL1-42-1.85-03 DL3-42-1.85-03	Deep	Long	1 3	42	1.85	0.003
18b 06a	SC1-42-2.50-03 SC3-42-2.50-03	Shallow	Cut-Off	1 3	42	2.50	0.003
16a 04b	SS1-42-2.50-03 SS3-42-2.50-03	Shallow	Short	1 3	42	2.50	0.003
01b 09a	DS1-42-2.50-03 DS3-42-2.50-03	Deep	Short	1 3	42	2.50	0.003

3.2.3.6 Series V: Loaded Chord

The purpose of this series is to evaluate the differences between compression- and tension-chord loaded members. Strength and serviceability of tension-chord loaded specimens tested in this project will be compared with compression-chord loaded specimens from the previous TxDOT Project 0-5253. Twenty three tests were conducted

in four groups of directly comparable specimens, in which every parameter was kept constant except the loaded chord. The specimens evaluated in this series are outlined in Table 3-6.

Table 3-6: Series V: Loaded chord

Test	Specimen	Ledge Depth	Ledge Length	Loaded Chord	Number of Loads	Web Depth (in.)	a/d	$\rho_v = \rho_h$
01a	DS1-42-1.85-03	Deep	Short	Tension	1	42	1.85	0.003
10a	DL1-42-1.85-03	Deep	Long	Tension				
16b	SS1-42-1.85-03	Shallow	Short	Tension				
20b	SC1-42-1.85-03	Shallow	Cut-Off	Tension				
20a	DC1-42-1.85-03	Deep	Cut-Off	Tension				
5A	III-1.85-03 *	-	-	Compression				
9A	III-1.85-03b *			Compression				
7A	I-03-2 *			Compression		44		
7B	I-03-4 *			Compression				
14a	SS1-75-1.85-03b	Shallow	Short	Tension	1	75	1.85	0.003
7c	SS1-75-1.85-03(c)	-	-	Compression				
13B	IV-2175-1.85-03 *			Compression				
13a	DC1-42-1.85-06	Deep	Short	Tension	1	42	1.85	0.006
02a	DS1-42-1.85-06	Deep	Long	Tension				
03a	DL1-42-1.85-06	Shallow	Short	Tension				
13b	C1-42-1.85-06	-	-	Compression				
10b	DL1-42-2.50-03	Deep	Long	Tension	1	42	2.50	0.003
17a	DC1-42-2.50-03	Deep	Cut-Off	Tension				
18b	SC1-42-2.50-03	Shallow	Cut-Off	Tension				
16a	SS1-42-2.50-03	Shallow	Short	Tension				
18a	SL1-42-2.50-03	Shallow	Long	Tension				
18b	SC1-42-2.50-03 (c)	-	-	Compression				
11B	III-2.5-03 *			Compression				

* Specimen from previous TxDOT Project 0-5253

(c) Inverted-T specimen loaded at the compression chord

3.2.3.7 Series VI: Web Depth

This series was designed to evaluate the effects of web depth on strength and serviceability of inverted-T specimens. Literature review revealed a significant difference in size of the distressed bent caps in the field and the specimens used to calibrate the shear provisions in the current code (TxDOT Bridge Design Manual - 2011). Full-scale specimens with different web depths were constructed to evaluate the web depth effect.

Web depths of 42 and 75 in. were used in this series. This series contains four specimens in two pairs of directly comparable specimens, in which every parameter was kept constant except the web depth. The specimens evaluated in this series are outlined in Table 3-7. Test setup restrictions limited the number of specimens that could be successfully tested for this series.

Table 3-7: Series VI: Web depth

Test	Specimen	Ledge Depth	Ledge Length	Number of Loads	Web Depth (in.)	a/d	$\rho_v = \rho_h$
16b	SS1-42-1.85-03	Shallow	Short	1	42	1.85	0.003
14a	SS1-75-1.85-03b				75		
16a	SS1-42-2.50-03	Shallow	Short	1	42	1.85	0.003
22a	SS1-75-2.50-03				75		

3.3 SPECIMEN DESIGN

Specimens of the experimental program were designed using the Strut-and-Tie Modeling (STM) provisions of TxDOT Project 5253. Estimated capacities were also calculated using the AASHTO LRFD – 2012, and TxDOT LRFD – 2011 specifications.

Furlong, et al. (1974) identified six failure modes in inverted-T beams:

1. Flexure. Either controlled by yielding of the main reinforcement leading to excessive cracking or by concrete crushing in the compression block.
2. Torsion. Compression in top or compression in bottom.
3. Web Shear. This failure mode is the focus of the current project.
4. Yielding of hanger reinforcement.
5. Punching shear in ledge.
6. Shear friction in ledge.

Consistent with the objectives of the project, the specimens in this experimental program were designed to fail in web shear. STM inherently considers all failure modes. In order to ensure web shear failures, the strut-and-tie designs were adjusted such that specimen capacities are controlled by the elements carrying the web shear; i.e. direct strut

for beams with *a/d* = 1.85, and intermediate web tie for beams with *a/d* = 2.50 (see Figure 3-18).

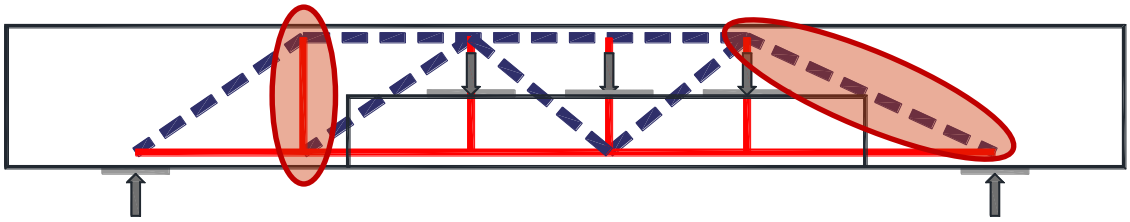

Figure 3-18: Strut-and-tie model, web-shear critical elements

According to STM procedures, elements governing the capacities of the inverted-T specimens are:

1. Strut-to-Node Interface (STNI) at the support
2. STNI at the compression chord
3. Intermediate tie
4. Hanger tie
5. Tension chord
6. Bearing at loads and support
7. Ledge tie
8. Ledge strut

When estimating specimen capacities using the TxDOT LRFD and AASHTO LRFD specifications the following elements need to be considered:

9. Bearing at loads and support
10. Stirrups for web shear
11. Hangers at service
12. Hangers at ultimate
13. Shear friction steel
14. Shear friction concrete
15. Ledge punching shear

16. Ledge reinforcement
17. Flexure

The location of the listed design elements is shown in Figure 3-19. Ratios of capacity to demand for each one of these elements are presented in Table 3-8 to Table 3-10 for all three design methods. The estimated nominal capacity (V_n) of each specimen is also presented in the tables and is taken as the shear at the critical section that causes the weakest element in each specimen to fail. In the tables, a value of 1.00 indicates the element governing the capacity of the specimen. Highlighted in the tables are values between 1.00 and 1.20 indicating potentially critical elements. The specified yield stress of steel was 60 ksi. The specified compressive strength of concrete was 3000, 3500, and 4000 psi for the various beams. Even though initial designs were made using specified material properties, results in Table 3-8 to Table 3-10 are based on measured material properties that are listed in sections 3.4.1and 3.4.2. Appendix C contains a detailed design example of one of the experimental specimens.

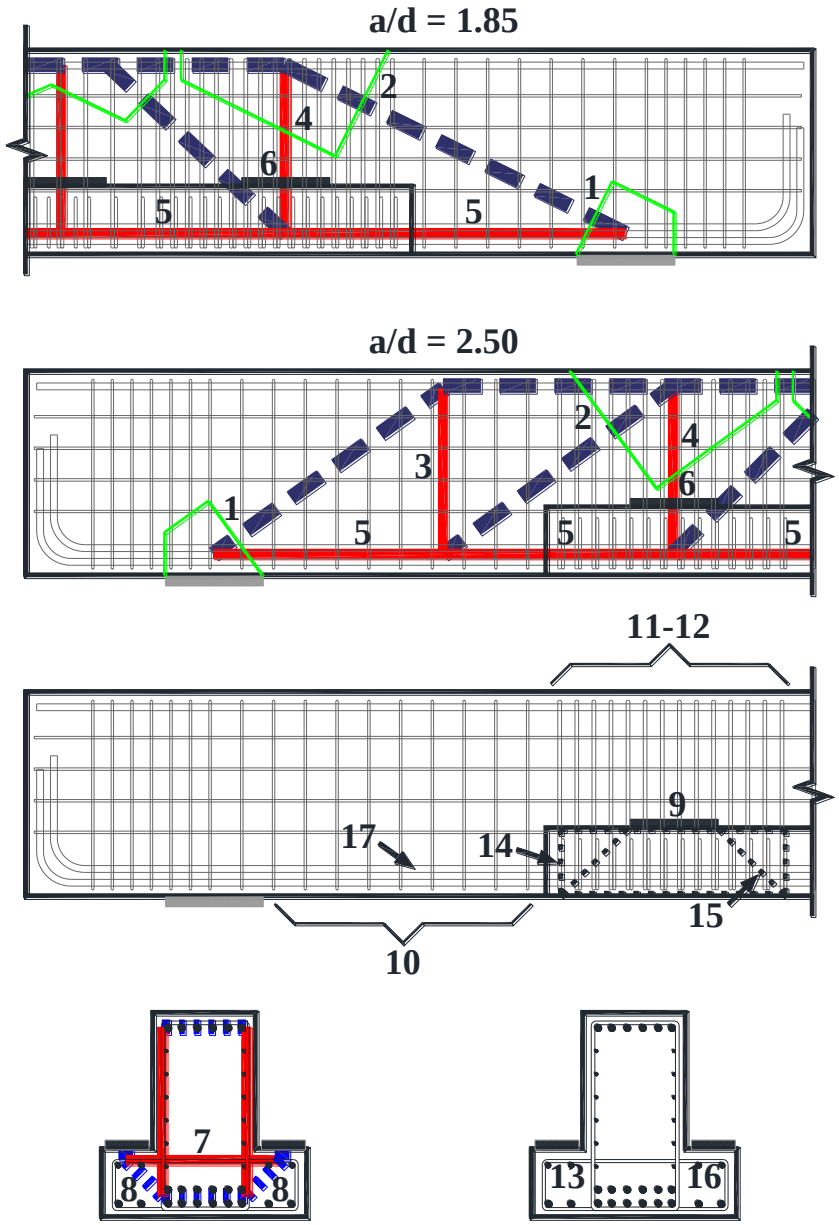

Figure 3-19: Location of critical elements for design

Table 3-8: Capacity / demand design ratios using the STM TxDOT 5253 provisions

		STM TxDOT 5253 (Capacity/Demand)								
Test	Specimen	Vn	STNI at support	STNI at compression chord	Intermediate tie	Hanger tie	Tension Chord	Bearing at loads	Ledge tie	Ledge strut
		kips	(1)	(2)	(3)	(4)	(5)	(6)	(7)	(8)
01a	DS1-42-1.85-03	463	1.00	1.81	N/A	1.64	1.49	2.65	1.75	2.22
01b	DS1-42-2.50-03	202	3.49	3.59	1.00	2.20	2.53	5.33	2.52	4.42
02a	DS1-42-1.85-06	479	1.00	1.86	N/A	1.53	1.41	2.50	1.66	2.14
02b	DS1-42-2.50-06	338	2.13	2.35	1.00	1.56	1.48	3.11	1.50	2.64
03a	DL1-42-1.85-06	464	1.00	1.90	N/A	1.58	1.53	2.48	1.72	2.16
03b	DL1-42-2.50-06	353	2.01	2.13	1.00	1.50	1.51	2.92	1.64	2.51
04a	SS3-42-1.85-03	456	1.00	1.63	N/A	1.75	1.14	4.81	1.25	2.88
04b	SS3-42-2.50-03	215	3.12	5.67	1.00	3.17	2.00	8.42	2.19	5.03
05b	SS3-42-2.50-06	415	1.67	3.01	1.00	1.83	1.06	4.63	1.35	2.68
06a	SC3-42-2.50-03	257	2.62	3.49	1.00	2.83	1.57	7.03	2.15	4.21
06b	SC3-42-1.85-03	427	1.00	1.32	N/A	1.70	1.24	5.13	1.57	3.07
07a	SS1-75-1.85-03	628	1.10	1.52	N/A	1.00	2.07	1.98	1.79	1.57
08b	SS1-75-2.50-06	474	1.00	2.02	1.61	1.00	2.26	1.84	1.52	1.39
09a	DS3-42-2.50-03	236	2.81	6.49	1.00	2.34	1.72	7.41	2.92	5.99
10a	DL1-42-1.85-03	468	1.00	1.91	N/A	1.19	1.58	2.51	1.20	2.16
10b	DL1-42-2.50-03	235	2.86	3.38	1.00	1.17	2.33	4.34	1.46	3.74
11a	SL3-42-1.85-03	409	1.00	1.72	N/A	1.83	1.36	4.59	2.20	2.96
12a	SL3-42-1.85-06	424	1.00	1.68	N/A	1.84	1.25	4.62	2.17	2.92
14a	SS1-75-1.85-03b	361	1.00	1.83	N/A	1.60	3.37	1.67	2.27	1.55
15a	DC3-42-1.85-03	370	1.00	1.33	N/A	1.41	1.27	4.20	4.01	3.73
15b	DS3-42-1.85-03	389	1.00	2.11	N/A	1.64	1.21	4.00	2.64	3.55
16a	SS1-42-2.50-03	213	3.11	4.18	1.00	3.08	2.35	5.53	3.06	3.36
16b	SS1-42-1.85-03	503	1.00	1.49	N/A	1.51	1.35	2.70	1.50	1.64
17a	DC1-42-2.50-03	250	2.10	1.32	1.00	2.00	1.89	3.31	3.61	3.07
17b	DL3-42-1.85-03	359	1.00	1.67	N/A	1.88	1.38	4.36	2.69	3.98
18a	SL1-42-2.50-03	269	2.20	1.71	1.00	2.51	1.88	3.29	1.76	2.25
18b	SC1-42-2.50-03	258	2.16	1.12	1.00	2.15	1.83	3.42	1.83	2.35
19a	DS1-42-1.85-06/03	361	1.00	1.94	N/A	2.07	1.63	2.39	2.05	2.19
19b	DS1-42-2.50-06/03	417	1.73	1.73	1.00	1.63	1.39	2.38	1.50	2.18
20a	SC1-42-1.85-03	444	1.18	1.00	N/A	1.20	1.35	1.61	1.10	1.10
20b	DC1-42-1.85-03	460	1.02	1.00	N/A	1.43	1.24	1.43	1.71	1.33

Table 3-9: Capacity / demand design ratios using the TxDOT LRFD provisions

		TxDOT LRFD - 2011 (Capacity/Demand)									
Test	Specimen	Vn	Bearing at loads	Shear stirrups	Hanger at service	Hanger at ultimate	Shear friction steel	Shear friction concrete	Punching shear	Ledge reinforcement	Flexure
		kips	(9)	(10)	(11)	(12)	(13)	(14)	(15)	(16)	(17)
01a	DS1-42-1.85-03	238	6.25	1.00	4.11	3.43	2.13	4.28	2.42	3.95	2.54
01b	DS1-42-2.50-03	240	5.44	1.00	2.44	2.13	1.27	3.64	2.08	2.35	1.87
02a	DS1-42-1.85-06	362	4.01	1.00	3.66	2.30	1.43	2.88	1.59	2.56	1.64
02b	DS1-42-2.50-06	363	3.52	1.00	2.55	1.67	1.02	2.50	1.39	1.83	1.21
03a	DL1-42-1.85-06	359	3.90	1.00	6.11	2.32	1.45	2.91	1.57	2.59	1.75
03b	DL1-42-2.50-06	316	3.97	1.14	5.23	1.67	1.00	2.87	1.58	1.86	1.47
04a	SS3-42-1.85-03	255	10.47	1.00	8.53	5.60	4.48	4.83	3.57	4.77	1.99
04b	SS3-42-2.50-03	255	8.63	1.00	6.03	3.96	3.17	3.98	2.95	3.39	1.64
05b	SS3-42-2.50-06	377	6.20	1.00	3.86	2.28	1.50	1.61	2.05	1.36	1.13
06a	SC3-42-2.50-03	249	8.85	1.00	7.22	4.26	2.73	2.45	1.93	2.45	1.63
06b	SC3-42-1.85-03	249	10.72	1.00	8.75	5.16	3.31	2.97	2.34	2.97	1.98
07a	SS1-75-1.85-03	387	3.90	1.20	1.89	1.61	1.00	2.44	1.33	2.38	1.61
08b	SS1-75-2.50-06	293	3.61	1.14	2.03	1.81	1.00	2.09	1.19	1.99	1.75
09a	DS3-42-2.50-03	248	8.56	1.00	4.20	2.76	2.28	6.54	4.33	3.45	1.57
10a	DL1-42-1.85-03	237	6.02	1.00	2.87	2.50	1.53	4.40	2.41	2.90	2.76
10b	DL1-42-2.50-03	197	6.29	1.20	1.87	1.77	1.00	4.60	2.51	1.90	2.46
11a	SL3-42-1.85-03	240	9.50	1.00	8.49	5.57	4.76	5.12	3.51	5.16	2.29
12a	SL3-42-1.85-06	381	6.23	1.00	5.57	3.66	2.99	3.22	2.25	3.31	1.36
14a	SS1-75-1.85-03b	358	2.04	1.07	2.03	1.80	1.53	1.88	1.00	3.06	1.73
15a	DC3-42-1.85-03	231	8.17	1.00	8.91	6.19	3.25	4.66	2.74	4.58	1.99
15b	DS3-42-1.85-03	231	8.17	1.00	5.26	4.37	2.71	7.77	4.61	4.22	1.99
16a	SS1-42-2.50-03	252	5.68	1.00	4.39	2.76	2.96	2.25	1.49	3.37	1.79
16b	SS1-42-1.85-03	252	6.55	1.00	5.06	3.19	3.42	2.59	1.71	3.89	2.42
17a	DC1-42-2.50-03	220	4.56	1.00	4.34	3.15	1.43	2.06	1.19	2.23	2.14
17b	DL3-42-1.85-03	223	8.51	1.00	7.23	4.75	3.83	8.79	5.01	6.06	2.28
18a	SL1-42-2.50-03	229	4.70	1.00	4.97	3.09	3.27	2.48	1.42	4.53	2.04
18b	SC1-42-2.50-03	229	4.70	1.00	4.35	2.56	2.18	1.65	1.21	2.32	2.04
19a	DS1-42-1.85-06/03	319	3.28	1.00	3.03	2.48	1.41	2.84	1.43	2.69	1.64
19b	DS1-42-2.50-06/03	422	2.86	1.00	2.17	1.81	1.01	2.47	1.24	1.93	1.43
20a	SC1-42-1.85-03	236	3.68	1.00	4.11	2.52	2.19	1.39	1.23	2.09	2.59
20b	DC1-42-1.85-03	231	3.46	1.00	4.19	3.17	2.23	2.26	1.69	3.19	2.62

Table 3-10: Capacity / demand design ratios using the AASHTO LRFD provisions

		AASHTO LRFD - 2012 (Capacity/Demand)									
Test	Specimen	Vn	Bearing at loads	Shear stirrups	Hanger at service	Hanger at ultimate	Shear friction steel	Shear friction concrete	Punching shear	Ledge reinforcement	Flexure
		kips	(9)	(10)	(11)	(12)	(13)	(14)	(15)	(16)	(17)
01a	DS1-42-1.85-03	238	6.25	1.00	3.08	3.43	2.13	4.28	2.42	3.95	2.54
01b	DS1-42-2.50-03	240	5.44	1.00	1.83	2.13	1.27	3.64	2.08	2.35	1.87
02a	DS1-42-1.85-06	362	4.01	1.00	2.07	2.30	1.43	2.88	1.59	2.56	1.64
02b	DS1-42-2.50-06	363	3.52	1.00	1.47	1.67	1.02	2.50	1.39	1.83	1.21
03a	DL1-42-1.85-06	359	3.90	1.00	2.09	2.32	1.45	2.91	1.57	2.59	1.75
03b	DL1-42-2.50-06	316	3.97	1.14	1.44	1.67	1.00	2.87	1.58	1.86	1.47
04a	SS3-42-1.85-03	255	10.47	1.00	6.40	5.60	4.48	4.83	3.57	4.77	1.99
04b	SS3-42-2.50-03	255	8.63	1.00	4.52	3.96	3.17	3.98	2.95	3.39	1.64
05b	SS3-42-2.50-06	377	6.20	1.00	2.89	2.28	1.50	1.61	2.05	1.36	1.13
06a	SC3-42-2.50-03	249	8.85	1.00	5.41	4.26	2.73	2.45	1.93	2.45	1.63
06b	SC3-42-1.85-03	249	10.72	1.00	6.56	5.16	3.31	2.97	2.34	2.97	1.98
07a	SS1-75-1.85-03	387	3.90	1.20	1.42	1.61	1.00	2.44	1.33	2.38	1.61
08b	SS1-75-2.50-06	293	3.61	1.14	1.52	1.81	1.00	2.09	1.19	1.99	1.75
09a	DS3-42-2.50-03	248	8.56	1.00	3.15	2.76	2.28	6.54	4.33	3.45	1.57
10a	DL1-42-1.85-03	237	6.02	1.00	2.15	2.50	1.53	4.40	2.41	2.90	2.76
10b	DL1-42-2.50-03	197	6.29	1.20	1.41	1.77	1.00	4.60	2.51	1.90	2.46
11a	SL3-42-1.85-03	240	9.50	1.00	6.37	5.57	4.76	5.12	3.51	5.16	2.29
12a	SL3-42-1.85-06	381	6.23	1.00	4.18	3.66	2.99	3.22	2.25	3.31	1.36
14a	SS1-75-1.85-03b	358	2.04	1.07	1.53	1.80	1.53	1.88	1.00	3.06	1.73
15a	DC3-42-1.85-03	231	8.17	1.00	6.69	6.19	3.25	4.66	2.74	4.58	1.99
15b	DS3-42-1.85-03	231	8.17	1.00	3.94	4.37	2.71	7.77	4.61	4.22	1.99
16a	SS1-42-2.50-03	252	5.68	1.00	3.29	2.76	2.96	2.25	1.49	3.37	1.79
16b	SS1-42-1.85-03	252	6.55	1.00	3.80	3.19	3.42	2.59	1.71	3.89	2.42
17a	DC1-42-2.50-03	220	4.56	1.00	3.26	3.15	1.43	2.06	1.19	2.23	2.14
17b	DL3-42-1.85-03	223	8.51	1.00	5.42	4.75	3.83	8.79	5.01	6.06	2.28
18a	SL1-42-2.50-03	229	4.70	1.00	3.73	3.09	3.27	2.48	1.42	4.53	2.04
18b	SC1-42-2.50-03	229	4.70	1.00	3.27	2.56	2.18	1.65	1.21	2.32	2.04
19a	DS1-42-1.85-06/03	319	3.28	1.00	2.27	2.48	1.41	2.84	1.43	2.69	1.64
19b	DS1-42-2.50-06/03	422	2.86	1.00	1.63	1.81	1.01	2.47	1.24	1.93	1.43
20a	SC1-42-1.85-03	236	3.68	1.00	3.08	2.52	2.19	1.39	1.23	2.09	2.59
20b	DC1-42-1.85-03	231	3.46	1.00	3.14	3.17	2.23	2.26	1.69	3.19	2.62

As can be seen from Table 3-8, all specimens were expected to fail by web shear or hanger ties according to STM provisions of TxDOT Project 5253. Only limited concerns of localized ledge failures and flexural failures arose at the design phase.

Capacity predictions shown in Table 3-9, using the TxDOT LRFD – 2011 specifications, and Table 3-10, using the AASHTO LRFD – 2012, indicate that most

specimens should fail by web shear with only a few showing other modes of failure as slightly more critical.

3.4 FABRICATION OF SPECIMENS

Test specimens were constructed using materials and methods typically used in practice. Steel formwork was used to expedite the fabrication process and ensure dimensional accuracy. Specimens were allowed to cure for at least 28 days prior to testing. The following sections describe in detail the construction process and materials used.

3.4.1 Steel Reinforcement Properties

Grade 60 deformed bars satisfying the requirements of ASTM A615 were used for all steel reinforcement. Each bar size for every beam was tested to determine actual yield strength in accordance with ASTM A370 testing procedures. Measured material properties of the reinforcements for each specimen are summarized in Table 3-11.

Table 3-11: Mean yield stress of reinforcement

Test	Specimen	# 11 Bars f_y (ksi)	# 6 Bars f_y (ksi)	# 5 Bars f_y (ksi)	# 4 Bars f_y (ksi)
01a	DS1-42-1.85-03	69.24	63.38	64.69	63.14
01b	DS1-42-2.50-03	69.24	63.38	64.69	63.14
02a	DS1-42-1.85-06	64.13	63.38	60.68	N/A
02b	DS1-42-2.50-06	64.13	63.38	60.68	N/A
03a	DL1-42-1.85-06	67.90	63.38	64.69	N/A
03b	DL1-42-2.50-06	67.90	63.38	64.69	N/A
04a	SS3-42-1.85-03	68.60	64.68	62.75	67.25
04b	SS3-42-2.50-03	68.60	64.68	62.75	67.25
05b	SS3-42-2.50-06	69.50	61.83	60.90	N/A
06a	SC3-42-2.50-03	66.20	63.50	60.25	64.27
06b	SC3-42-1.85-03	66.20	63.50	60.25	64.27
07a	SS1-75-1.85-03	64.95	62.03	73.15	65.73
08b	SS1-75-2.50-06	72.50	66.50	61.53	N/A
09a	DS3-42-2.50-03	63.60	62.63	60.22	64.58
10a	DL1-42-1.85-03	71.01	61.90	64.29	64.43
10b	DL1-42-2.50-03	71.01	61.90	64.29	64.43
11a	SL3-42-1.85-03	75.18	60.62	63.58	65.57
12a	SL3-42-1.85-06	70.38	63.26	64.80	62.62
14a	SS1-75-1.85-03b	66.10	61.97	64.69	65.08
15a	DC3-42-1.85-03	63.63	66.00	63.09	63.16
15b	DS3-42-1.85-03	63.63	66.00	63.09	63.16
16a	SS1-42-2.50-03	65.44	69.57	77.76	66.58
16b	SS1-42-1.85-03	65.44	69.57	77.76	66.58
17a	DC1-42-2.50-03	70.06	64.13	69.77	62.44
17b	DL3-42-1.85-03	70.06	64.13	69.77	62.44
18a	SL1-42-2.50-03	68.70	71.41	N/A	64.47
18b	SC1-42-2.50-03	68.70	71.41	N/A	64.47
19a	DS1-42-1.85-06/03	65.80	70.92	64.94	65.18
19b	DS1-42-2.50-06/03	65.80	70.92	64.94	65.18
20a	SC1-42-1.85-03	66.36	64.04	N/A	67.28
20b	DC1-42-1.85-03	66.36	64.04	N/A	67.28

3.4.2 Concrete Properties

TxDOT engineers typically specify concrete strengths ranging between 3600 and 5000 psi for inverted-T bent caps. Specimens were designed using specified compressive strengths of 3000, 3500, and 4000. The variations in specified compressive strengths were intended to ensure web shear failures. Mean compressive strength of three cylinders was measured the same day of testing for each specimen; actual strengths varied from 2870 to 6400 psi. For each specimen, standard 4" x 8" test cylinders were cast following ASTM C31 procedures and tested in accordance with ASTM C39. Typical proportions of the concrete mixture are presented in Table 3-12. A summary of all specimen concrete compressive strengths are presented in Table 3-13.

Table 3-12: Typical concrete mixture proportions for a specified 28-day compressive strength of 3000 psi

Material	**Quantity**
Type I Portland Cement	300 lb/cy
Flys Ash	79 lb/cy
CA: 3/4" River Rock	1846 lb/cy
FA: Sand	1554 lb/cy
Water	22 gallons/cy
HRWR Admixture	30 oz/cy
Set Retardant Admixture	5.6 oz/cy
Water/Cement Ratio	0.62
Slump	6 ± 2 inches

Table 3-13: Mean compressive strengths at testing day

Test	Specimen	f'_c (psi)
01a	DS1-42-1.85-03	5258
01b	DS1-42-2.50-03	5389
02a	DS1-42-1.85-06	5024
02b	DS1-42-2.50-06	5088
03a	DL1-42-1.85-06	4830
03b	DL1-42-2.50-06	4986
04a	SS3-42-1.85-03	5891
04b	SS3-42-2.50-03	5891
05b	SS3-42-2.50-06	6255
06a	SC3-42-2.50-03	5873
06b	SC3-42-1.85-03	5873
07a	SS1-75-1.85-03	5925
08b	SS1-75-2.50-06	6404
09a	DS3-42-2.50-03	5687
10a	DL1-42-1.85-03	4929
10b	DL1-42-2.50-03	4929
11a	SL3-42-1.85-03	5037
12a	SL3-42-1.85-06	5250
13a	DC1-42-1.85-06	3727
13b	C1-42-1.85-06	3727
14a	SS1-75-1.85-03b	2867
15a	DC3-42-1.85-03	4568
15b	DS3-42-1.85-03	4568
16a	SS1-42-2.50-03	5703
16b	SS1-42-1.85-03	5721
17a	DC1-42-2.50-03	4035
17b	DL3-42-1.85-03	4202
18a	SL1-42-2.50-03	4281
18b	SC1-42-2.50-03	4281
19a	DS1-42-1.85-06/03	4173
19b	DS1-42-2.50-06/03	4173
20a	SC1-42-1.85-03	4330
20b	DC1-42-1.85-03	4303

3.4.3 Construction of Specimens

Cage assembly, strain gage instrumentation, and casting took approximately two weeks per beam. Specimens were allowed to cure for at least 28 days before testing. Specimens were built and tested in an up-side down orientation (i.e., loaded from the bottom). Reinforcing steel was ordered from a local supplier; bars were cut and bent before being shipped to the Ferguson Laboratory. Upon assembling of the steel cages (Figure 3-20a), strain gauges were glued to the steel reinforcement as described in section 3.5.1. The specimens were then moved to the casting area (Figure 3-20b) and placed into the steel forms (Figure 3-20c). Two pre-mixed concrete trucks were ordered from a local supplier for each 75-in deep beam, and one truck per each 42-in deep beam. For each truck a slump tests was conducted according to ASTM C143. Within the limit of the water held back at the batch plant, water was added to each mix to adjust the slump to the target value of 6 ± 2 in. Concrete was placed using a one-cubic yard bucket lifted by an overhead crane as shown in Figure 3-20d. Internal and external vibrators were used to ensure proper consolidation (Figure 3-20e). After initial setting, the top surface was finished (Figure 3-20f-g) and covered with a plastic film to limit water evaporation. Seven days after casting, forms were striped, specimens were uncovered, and stored in the laboratory for at least 28 days before testing.

(a) (b)

(c) (d) (e)

(f) (g)

Figure 3-20: Fabrication of Specimens; (a) cage assembly and instrumentation, (b) cage being moved to casting area, (c) re-bar cage in the steel formwork, (d) placing of concrete (e) internal vibrators, (f) screeding, (g) top surface finishing (from Garber 2011)

3.5 TEST SETUP

Specimens were tested at the Ferguson Structural Engineering Laboratory of the University of Texas at Austin. The setup consists of an upside-down simply-supported beam test setup (Figure 3-21). U-shape loading frames were introduced to spread loads around the web and load the ledges evenly on both faces of the test specimens; as shown in Figure 3-21. More details on the loading "U" frame can be found in Garber (2011). The centerpiece of the setup is a 96,000-lb steel platen that serves as a rigid floor. Twelve 3-in diameter rods threaded into the strong floor reacted against two 7,000-lb transfer girders. More details are available in Huizinga (2007).

Loads were applied using a double-acting hydraulic ram with 6-million pound capacity for beams with a single loading point, and three 2-million pound capacity rams for the three point load tests.

Three-in. diameter rollers were placed between loading-point steel plates while two-in. diameter rollers were added at the supports; the rollers allowed for horizontal movement and bending at those locations. A ¼-in. reinforced neoprene bearing pad was placed between loading plates and the concrete to ensure a uniform load distribution avoiding stress concentrations. A thin layer of self-leveling gypsum cement was applied between the reaction plates and the concrete to ensure a smooth planar bearing surface.

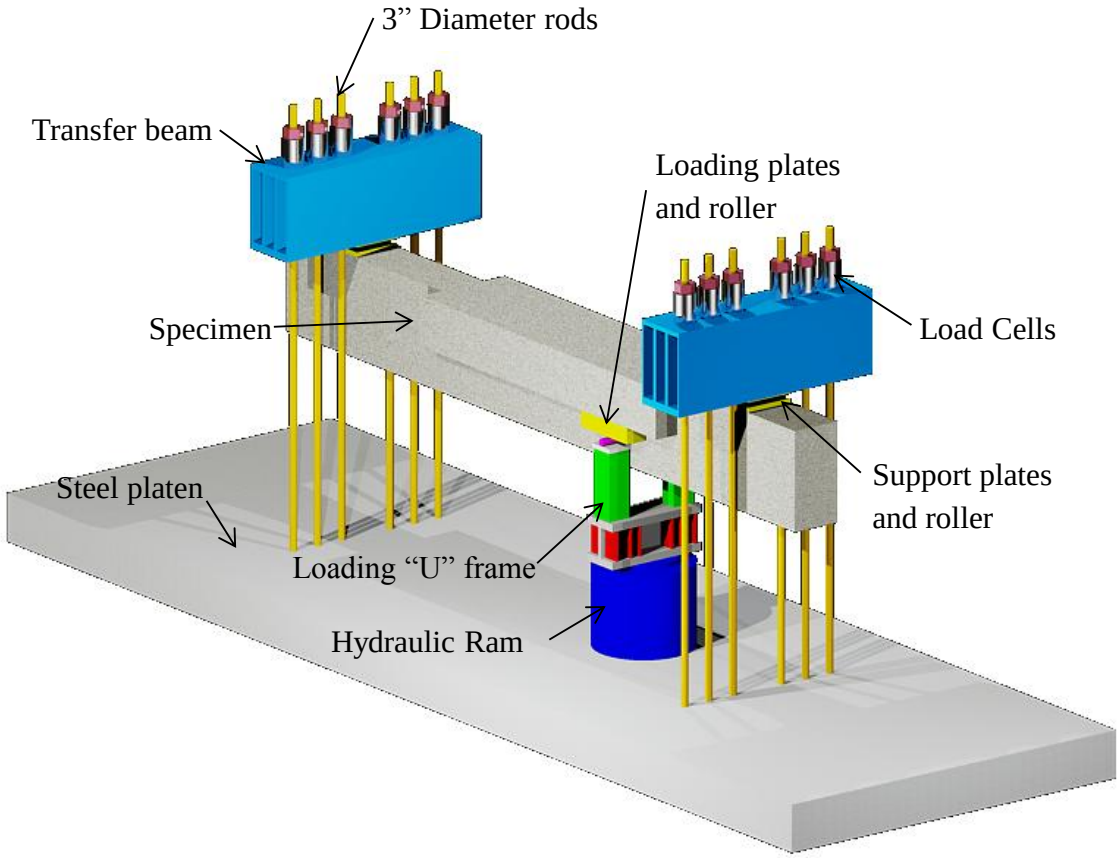

Figure 3-21: Test setup

Each test was monitored using several instruments to measure strains, loads, displacements, and crack widths. Instrumentation details are provided in the following sections.

3.5.1 Strain Measurements

Strain gauges model FLA-3-11-10LT manufactured by Tokyo Sokki Kenkyujo Co., Ltd. were affixed to the longitudinal, hanger, and ledge reinforcement at the locations of maximum expected strain. In the transverse reinforcement strain gauges were placed along the axis of the critical struts, as shown in Figure 3-22 and Figure 3-23. Specimens with a shear span-to-depth ratio of 1.85 were instrumented along the axis of the direct strut that spans from the support to the first loading point. Specimens with a shear span-to-depth ratios of 2.50 were instrumented with strain gauges along the axis of

the direct strut that spans form the support to the first loading point as well as along the first strut from the support of the multiple panel model (Figure 3-22a).

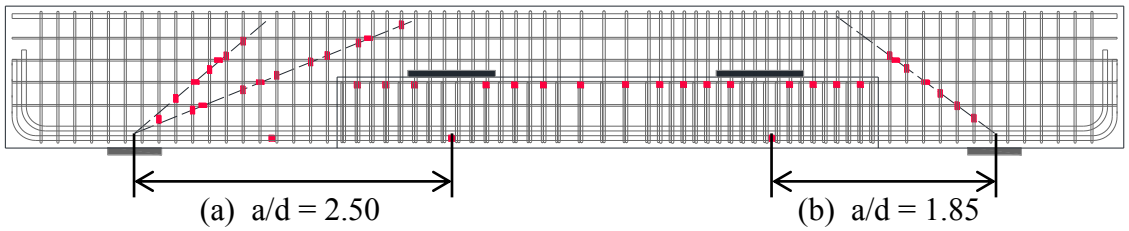

Figure 3-22: Typical location of strain gauges in longitudinal section;

(a) a/d = 2.50, (b) a/d = 1.85

The strain gauges were placed along the axes of the critical struts to measure steel strains at the expected locations of the primary splitting cracks. Strain measurements in the longitudinal steel were translated to stresses to calculate forces in the tension chord of the specimens. Strains measured on the hanger and ledge reinforcement were used to verify the assumed 45 degree load-spread (Figure 3-23) and the associated number of hanger bars that transfer applied loads to the compression chord.

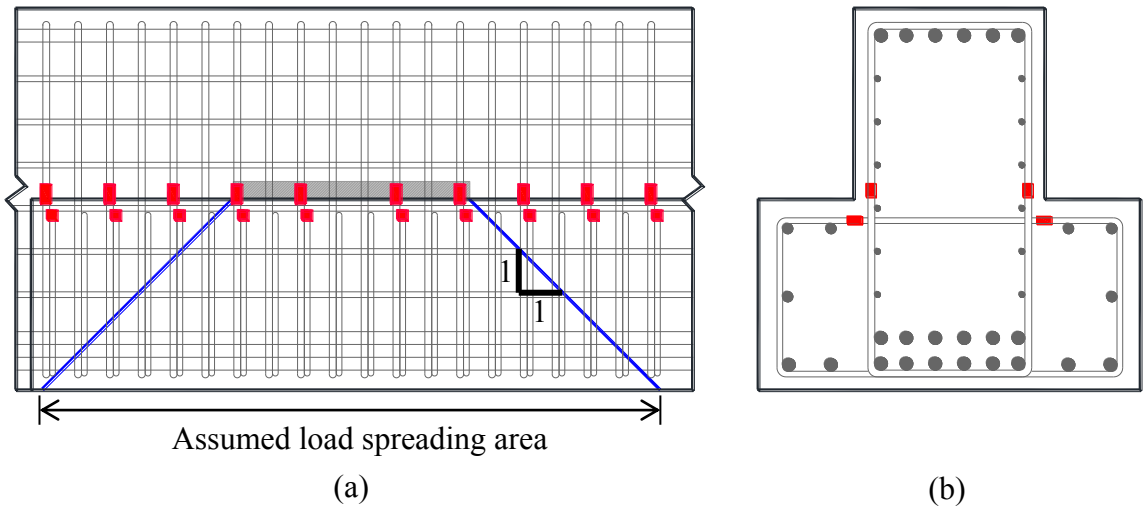

Figure 3-23: Strain gauges in hanger and ledge reinforcements;

(a) longitudinal section, (b) cross section

The installation procedure of the strain gauges is depicted in Figure 3-24. First the bar deformations were removed using a grinder, without significantly reducing the cross section of the bar. The cleared surface was polished to provide a smooth planar surface (Figure 3-24a) that was then cleaned using acetone. Strain gauges were glued to the cleaned surface (Figure 3-24b) and covered with a butyl rubber tape to water proof them. Finally the strain gauges were wrapped in foil tape (Figure 3-24c) to further isolate them and the ends were sealed with electrical tape (Figure 3-24d).

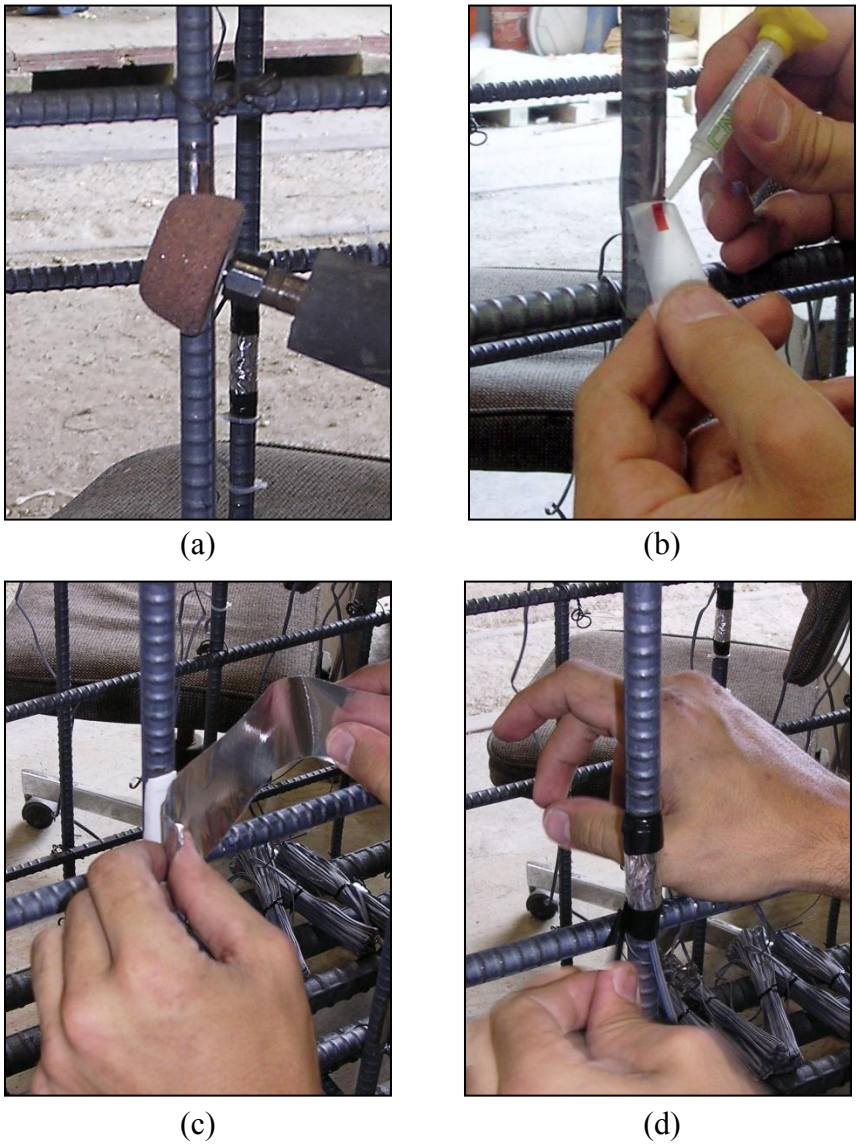

Figure 3-24: Strain gauge installation; (a) grind off bar deformations, (b) glue strain gauges to steel bar, (c) isolate with butyl tape and foil tape, (d) seal ends with electrical tape

3.5.2 Load and Displacement Measurements

A pressure gauge was placed at the hydraulic line feeding the loading rams. The pressure readings were used to confirm load cell readings. The applied forces were measured at the reaction supports using 500-kip capacity load cells placed at each of the twelve support rods; as shown in Figure 3-25. Care was taken to balance the reaction at each side of the supports to prevent torsion in the test specimens.

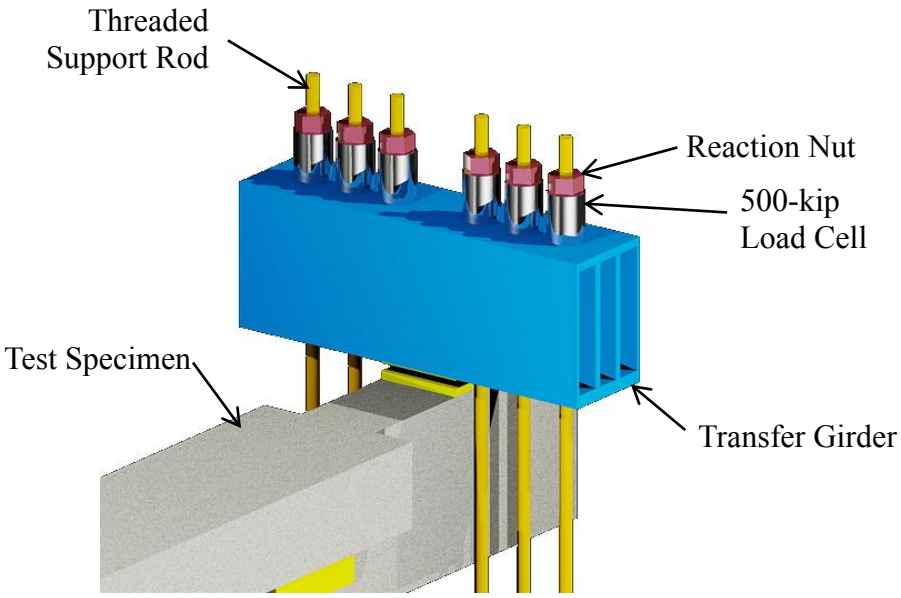

Figure 3-25: Load cell arrangement at supports

Beam deflections and rigid body motions were measured using an arrangement of five linear potentiometers located one at each support, one at mid-span, and two at the location of the loading point (Figure 3-26 and Figure 3-27). The two linear potentiometers at the location of the loading point allowed checking for rotation of the beam along the longitudinal axis.

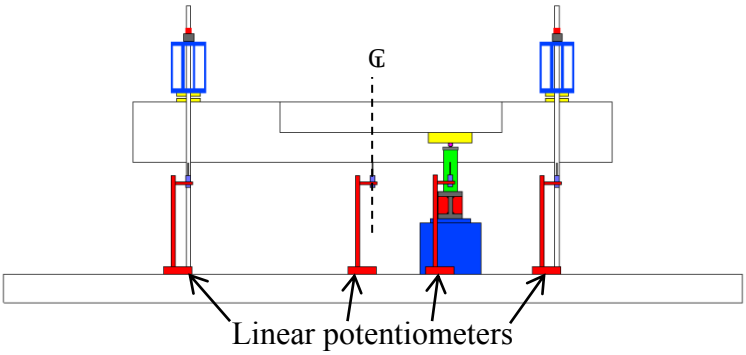

Figure 3-26: Location of linear potentiometers

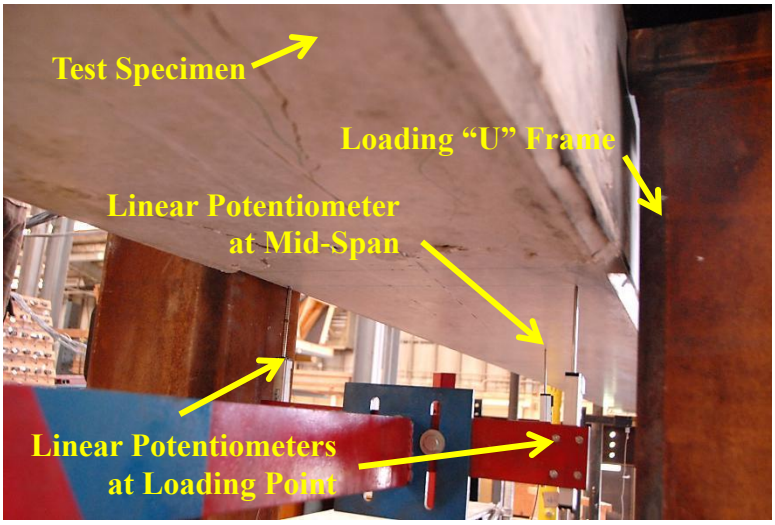

Figure 3-27: Linear potentiometers at the loading point and mid-span

3.5.3 Crack Width Measurements

Diagonal crack widths were measured on each face between each load increment using crack comparators as shown in Figure 3-28. Independent measurements were taken by two students and then averaged. Several cracks were selected arbitrarily to be monitored at the same location throughout the entire test. The maximum diagonal crack width on each face was recorded between each load increment; the location of the maximum diagonal crack width generally varied between each load increment.

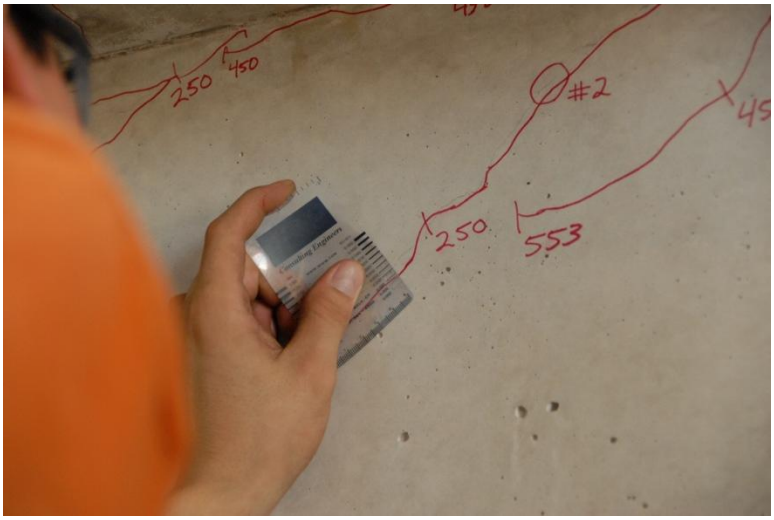

Figure 3-28: Crack width measurement

3.6 TESTS PROCEDURE

Test specimens were monotonically loaded in 50-kip increments up to the appearance of the first diagonal crack, then in 100-kip increments up to failure. Crack widths were measured between each load increment. Photographs of each face of the specimen were taken before each load increment. A video camera was used to record the failure of each test.

Specimens with only one point load were loaded at the appropriate location to get the desired a/d ratio. After reaching failure, the load was removed, and post-tensioning clamps were installed (Figure 3-29). The hydraulic ram was moved to the opposite end of the beam and the load was reapplied to fail the second test region. Both test regions cracked during the first test on each specimen. The cracking load was therefore not recorded for the second test region of specimens with only one loading point.

Specimens with three loading points were designed such that both ends were tested simultaneously. For those specimens, the cracking load was obtained for both test regions. After reaching first failure of one end of the beam, the load was removed, post-tensioning clamps were installed to strengthen the failed region, and the load was reapplied to fail the opposite end of the beam. This testing procedure is depicted in Figure 3-29.

a) Failure crack – Test # 1

b) External Post-tensioning clamps

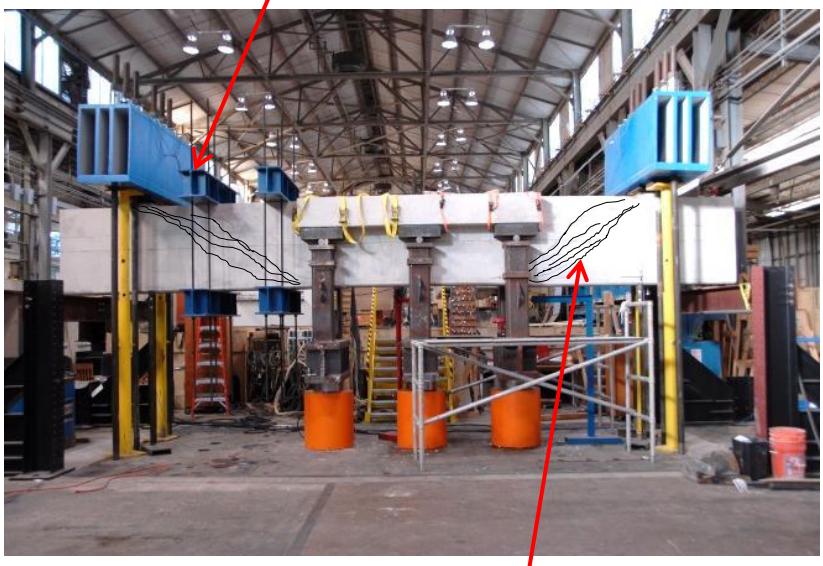

Failure Crack – Test # 2

Figure 3-29: Three point loads, testing procedure; (a) test # 1, (b) test #2 - after repair

3.7 SUMMARY

Details of the experimental program are provided in this chapter. Experimental variables studied in this project were: ledge length, ledge depth, web reinforcement, number of point loads, loaded chord, and web depth. The design procedure from which test specimen details were obtained is outlined. Fabrication of specimens, material properties, and construction details are also provided in this chapter.

The testing frame described in this section consisted in an upside-down simply-supported beam setup, whose centerpiece consisted in a 96,000-lb steel strong floor, with twelve 3-in diameter threaded rods reacting against two 7,000-lb transfer girders.

The testing procedure allowed for two tests to be performed on each beam; one test for each shear span. External post-tensioned clamps were used to strengthen the beam after the first shear span failure to get a second test out of the second shear span. Steel strains, applied loads, reaction forces, and beam deflections were monitored throughout the entire tests. Crack width measurements were taken between each load increment. Results of the experimental program are presented in Chapter 4.

CHAPTER 4
Experimental Results

4.1 OVERVIEW

Experimental results of strength and serviceability of the 31 tests conducted in 19 full-scale specimens as part of the TxDOT Project 0-6416 are summarized and discussed in this chapter. A brief report for each test is provided in Appendix D. Effects of the ledge length, ledge depth, and numbers of point loads are discussed in detail in Sections 4.4, 4.5, 4.6 respectively.

4.2 SUMMARY OF EXPERIMENTAL RESULTS

Strength and serviceability results of the 31 tests in the experimental program are summarized in Table 4-1. Fabrication details of the specimens are provided in Table 4-1 and Appendix B. The variables used in Table 4-1 are defined as follows:

b_w = web width, in.

d = distance from extreme compression fiber to centroid of tensile reinforcement of the web, in.

f_c' = compressive strength of concrete at the time of testing measured in accordance with ASTM C39, psi.

f_{yl} = yield strength of longitudinal reinforcement measured in accordance with ASTM A370, ksi.

f_{yv} = yield strength of transverse reinforcement measured in accordance with ASTM A370, ksi.

f_{yh} = yield strength of skin reinforcement measured in accordance with ASTM A370, ksi.

f_{yha} = yield strength of hanger reinforcement measured in accordance with ASTM A370, ksi.

***a/d* ratio** = shear span-to-depth ratio; with the shear span (a) measured from the center of the reaction plate to the center of closest loading plate

V_{crack} = shear carried in the critical section of the test region when the first diagonal crack formed, kips; the critical section is defined as the point halfway between the support and the nearest load.

Specific details regarding the determination of the diagonal cracking load are presented in Section 4.2.2

V_{test} = maximum shear carried in the critical section of the test region, including self-weight of the specimen and test setup

Specific details regarding the determination of the applied shear are presented in Section 4.2.1

Table 4-1: Summary of experimental results

Test	Specimen I.D.	b_w in	d in	f'c psi	f_{yl} ksi	f_{yv} ksi	f_{yh} ksi	f_{yha} ksi	a/d ratio	V_{crack} kip	$\frac{V_{crack}}{\sqrt{f'_c} b_w d}$	$\frac{V_{crack}}{V_{test}}$	V_{test} kip	$\frac{V_{test}}{f'_c b_w d}$	$\frac{V_{test}}{\sqrt{f'_c} b_w d}$
01a	DS1-42-1.85-03	21	37.64	5258	69	63	63	64	1.96	172	2.99	0.24	712	0.17	12.42
01b	DS1-42-2.50-03	21	37.64	5389	69	63	63	64	2.65	N/A	N/A	N/A	406	0.10	6.99
02a	DS1-42-1.85-06	21	37.64	5024	64	61	61	64	1.85	188	3.35	0.30	621	0.16	11.09
02b	DS1-42-2.50-06	21	37.64	5088	64	61	61	64	2.50	N/A	N/A	N/A	503	0.13	8.93
03a	DL1-42-1.85-06	21	37.64	4830	68	61	61	64	1.85	168	3.06	0.23	741	0.19	13.48
03b	DL1-42-2.50-06	21	37.64	4986	68	61	61	64	2.50	N/A	N/A	N/A	622	0.16	11.15
04a	SS3-42-1.85-03	21	37.64	5891	69	67	67	65	1.85	126	2.08	0.24	523	0.11	8.62
04b	SS3-42-2.50-03	21	37.64	5891	69	67	67	65	2.50	140	2.31	0.31	447	0.10	7.38
05b	SS3-42-2.50-06 (f)	21	37.64	6255	70	61	61	62	2.50	115	1.84	0.22	516	0.10	8.25
06a	SC3-42-2.50-03	21	37.64	5873	66	64	64	64	2.50	113	1.87	0.34	329	0.07	5.44
06b	SC3-42-1.85-03	21	37.64	5873	66	64	64	64	1.85	90	1.48	0.19	483	0.10	7.98
07a	SS1-75-1.85-03 (p)	21	68.2	5925	65	66	66	62	1.87	260	2.36	0.28	913	0.11	8.28
08b	SS1-75-2.50-06 (p)	21	68.2	6404	73	62	62	67	2.53	232	2.02	0.34	688	0.08	6.01
09a	DS3-42-2.50-03	21	37.64	5687	64	65	65	63	2.50	143	2.40	0.33	430	0.10	7.21
10a	DL1-42-1.85-03	21	37.64	4929	71	64	64	62	1.85	242	4.36	0.39	626	0.16	11.28
10b	DL1-42-2.50-03	21	37.64	4929	71	64	64	62	2.50	N/A	N/A	N/A	510	0.13	9.19

(f) Flexural failure
(p) Punching shear failure of the ledge

Table 4-1 (cont.'d): Summary of experimental results

Test	Specimen I.D.	b_w in	d in	f'c psi	f_{yl} ksi	f_{yv} ksi	f_{yh} ksi	f_{yha} ksi	a/d ratio	V_{crack} kip	$\frac{V_{crack}}{\sqrt{f'_c}b_w d}$	$\frac{V_{crack}}{V_{test}}$	V_{test} kip	$\frac{V_{test}}{f'_c b_w d}$	$\frac{V_{test}}{\sqrt{f'_c}b_w d}$
11a	SL3-42-1.85-03	21	37.64	5037	75	66	66	61	1.85	172	3.06	0.30	571	0.14	10.17
12a	SL3-42-1.85-06	21	37.64	5250	70	65	65	63	1.85	154	2.69	0.21	744	0.18	13.00
14a	SS1-75-1.85-03b	21	68.2	2867	66	65	65	62	1.87	346	4.51	0.46	745	0.18	9.72
15a	DC3-42-1.85-03	21	37.64	4568	64	63	63	66	1.85	152	2.84	0.38	395	0.11	7.39
15b	DS3-42-1.85-03	21	37.64	4568	64	63	63	66	1.85	164	3.07	0.36	454	0.13	8.49
16a	SS1-42-2.50-03	21	37.64	5703	65	67	67	70	2.50	157	2.63	0.39	398	0.09	6.67
16b	SS1-42-1.85-03	21	37.64	5721	65	67	67	70	1.85	N/A	N/A	N/A	583	0.13	9.75
17a	DC1-42-2.50-03	21	37.64	4035	70	62	62	64	2.50	70	1.40	0.19	365	0.11	7.28
17b	DL3-42-1.85-03 (f)	21	37.64	4202	70	62	62	64	1.85	276	5.39	0.44	629	0.19	12.27
18a	SL1-42-2.50-03	21	37.64	4281	69	64	64	71	2.50	167	3.24	0.34	498	0.15	9.62
18b	SC1-42-2.50-03 (r)	21	37.64	4281	69	64	64	71	2.50	N/A	N/A	N/A	319	0.09	6.18
19a	DS1-42-2.50-06/03	21	37.64	4173	66	65	65	71	2.50	115	2.25	0.21	539	0.16	10.56
19b	DS1-42-1.85-06/03	21	37.64	4173	66	65	65	71	1.85	N/A	N/A	N/A	739	0.22	14.47
20a	SC1-42-1.85-03 (le)	21	37.64	4330	66	67	67	64	1.85	N/A	N/A	N/A	451	0.13	8.67
20b	DC1-42-1.85-03	21	37.64	4303	66	67	67	64	1.85	127	2.44	0.24	517	0.15	9.98

(f) Flexural failure
(r) Shear friction failure of the web-ledge interface
(le) Horizontal ledge tie failure in cross section

It should be noted that the majority of the specimens sustained web shear failures, but in a few cases flexure, ledge punching shear, diagonal strut failure in the cross section or ledge-to-web shear friction failures were observed. The value reported for V_{test} is the maximum shear carried at the critical section at the onset of failure, regardless of the failure mode. A note was added in Table 4-1 to the specimens which experienced a failure mode different than web shear.

4.2.1 Evaluation of Strength Data

The shear strength of the specimens (V_{test}) was defined as the maximum shear carried at the critical section. The critical section was defined as the point halfway between the support and the nearest load. V_{test} was calculated considering the reactions measured by the load cells at the supports (R_A and R_B), the self-weight of the specimen (ω_{SW}) and of the transfer girders ($2P_{TR}$) as shown in Figure 4-1. The self-weight of the ledges was considered uniformly distributed along the entire length of the beam.

Strength results are normalized by both $\sqrt{f'_c}b_w d$ and $f'_c b_w d$ in Table 4-1. Specimens with *a/d* ratios of 1.85 behaved as deep beams and generally failed by crushing of the direct strut between the support and the loading point. Shear strength of these specimens is related to the concrete compressive strength and the size of the element, and therefore more appropriately normalized by $f'_c b_w d$. Specimens with *a/d* ratios of 2.50 typically experienced sectional shear failures whereby diagonal tension in the web influenced the shear capacity. It is therefore more appropriate to normalize them by $\sqrt{f'_c}b_w d$.

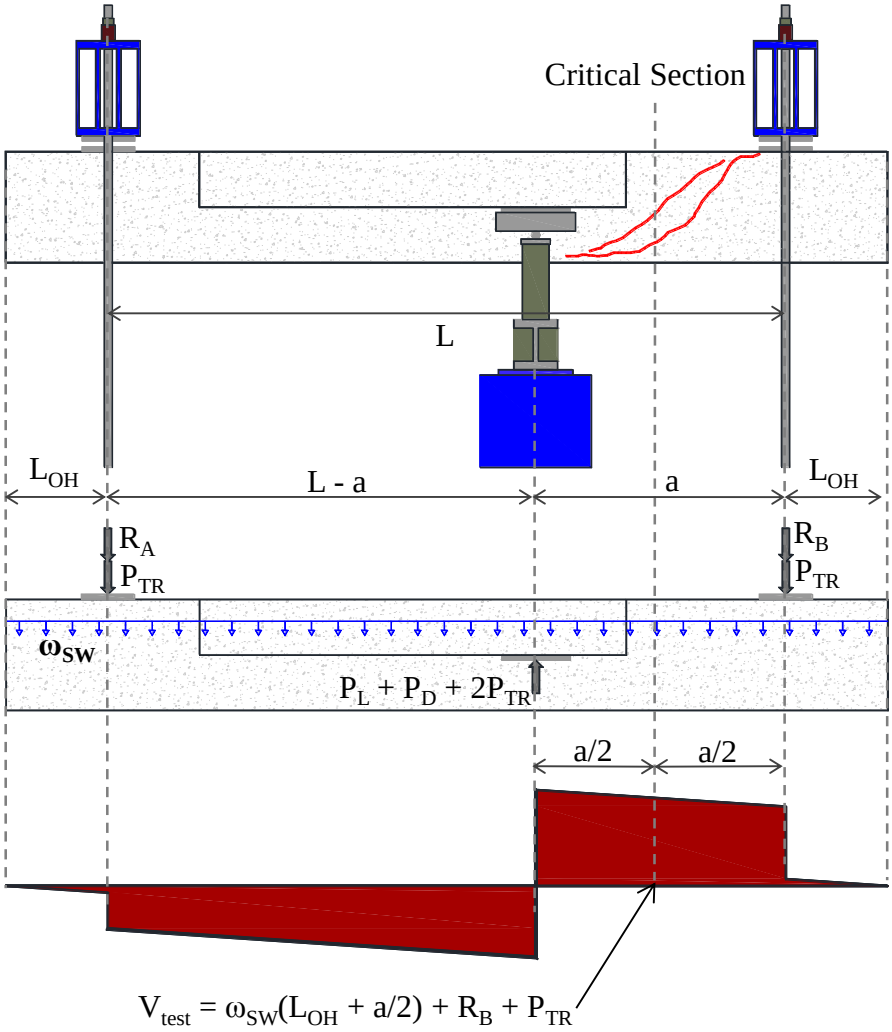

$V_{test} = \omega_{SW}(L_{OH} + a/2) + R_B + P_{TR}$

Where: $P_L = R_A + R_B$ L = 255.25in.

P_{TR} = 7.8 kip Lo_H = 38.375in.

$P_D = \omega_{SW}(2L_{OH} + L)$ ω_{SW} = Specimen Self-Weight, kip/ft

Figure 4-1: Determination of specimen shear strength, V_{test}

4.2.2 Evaluation of Serviceability Data

In order to evaluate the serviceability performance of the specimens, two parameters were considered: (1) first cracking load, and (2) progression of maximum diagonal crack width.

The first diagonal cracking load was obtained by visual observation of the test region between load increments. These observations provided a load range in which the first diagonal crack appeared. Visual observations were corroborated through strain gauge data. Strain measurements from skin and transverse reinforcements were analyzed to find the load at which a sudden increase in strain occurred. A sample evaluation of V_{crack} is illustrated in Figure 4-2.

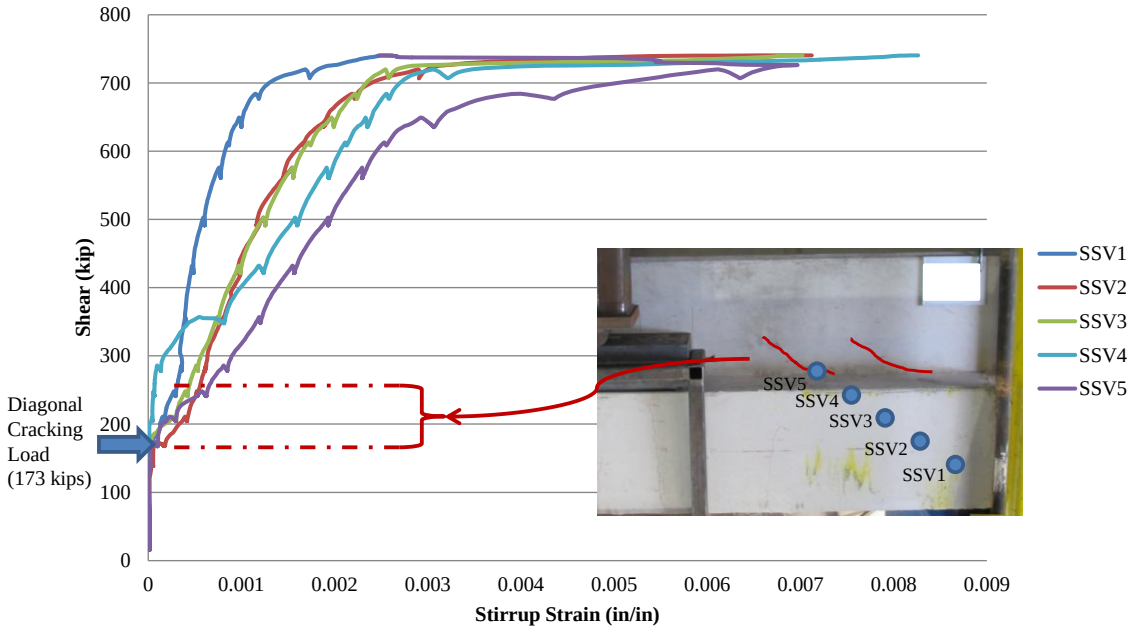

Figure 4-2: Visual and gauge-based determination of V_{crack} (Garber 2011)

The maximum diagonal crack width was located and recorded between each load increment. Measurements were taken on each face of the specimens using crack comparator cards by two students and then averaged to minimize reading errors. A typical crack width progression is shown in Figure 4-3.

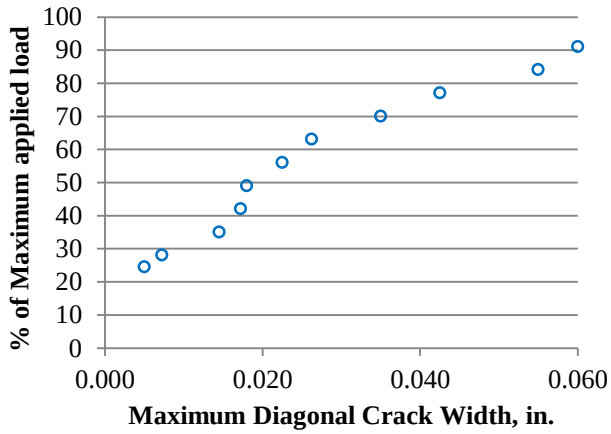

Figure 4-3: Typical crack width progression

4.3 APPLICABILITY OF 45-DEGREE LOAD SPREAD

In this Chapter, test strength results are compared with those estimated by the STM modeling provisions of TxDOT project 5253. To apply the provisions that were developed for rectangular beams to inverted-T beams, a 45-degree load spread under the applied loads was assumed for hanger-tie dimensioning. Therefore, hanger ties were given a width equal to the length of the bearing plate (W) plus twice the depth of the ledge (d_f) for short and long ledges. In cut-off ledges, the hanger tie was assumed to spread only twice the distance from the center of the loading plate to the edge of the ledge, as shown in Figure 4-4. The same assumptions are made in AASHTO Eq. 5.13.2.5.5-3 to calculate the strength of hanger reinforcements.

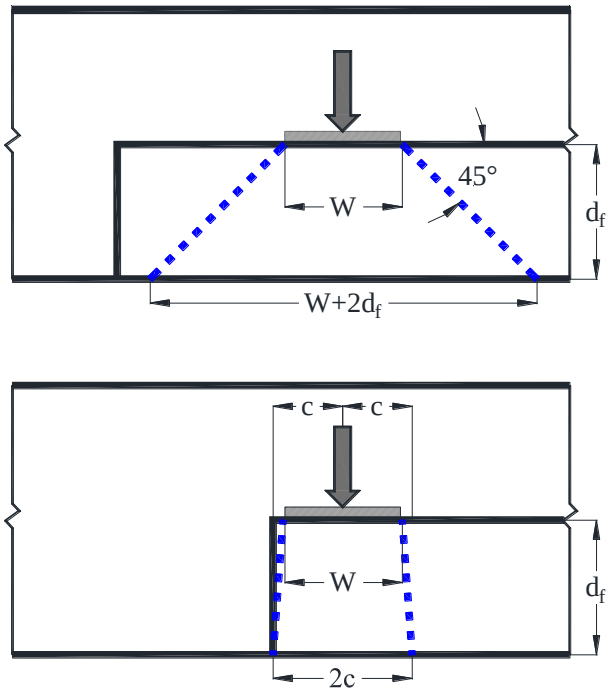

Figure 4-4: 45-degree load spread; (top) short ledge, (bottom) cut-off ledge

The hanger-tie width assumptions were validated by measuring strains in the hanger reinforcements using electrical strain gauges during the tests; as described in Section 3.6.1. Typical measured strains normalized by yielding strains for the hanger reinforcement are shown in Figure 4-5 and Figure 4-6.

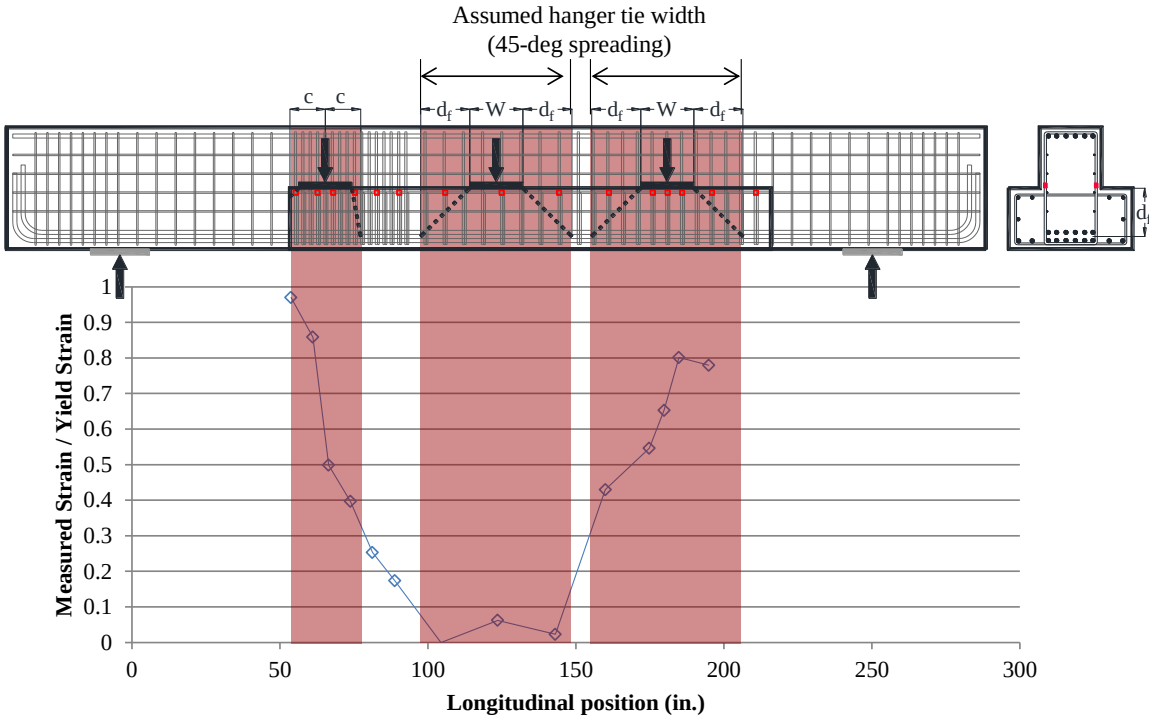

Figure 4-5: Typical hanger strains at failure (specimen 15a: DC3-42-1.85-03); three point load test, short and cut-off ledge

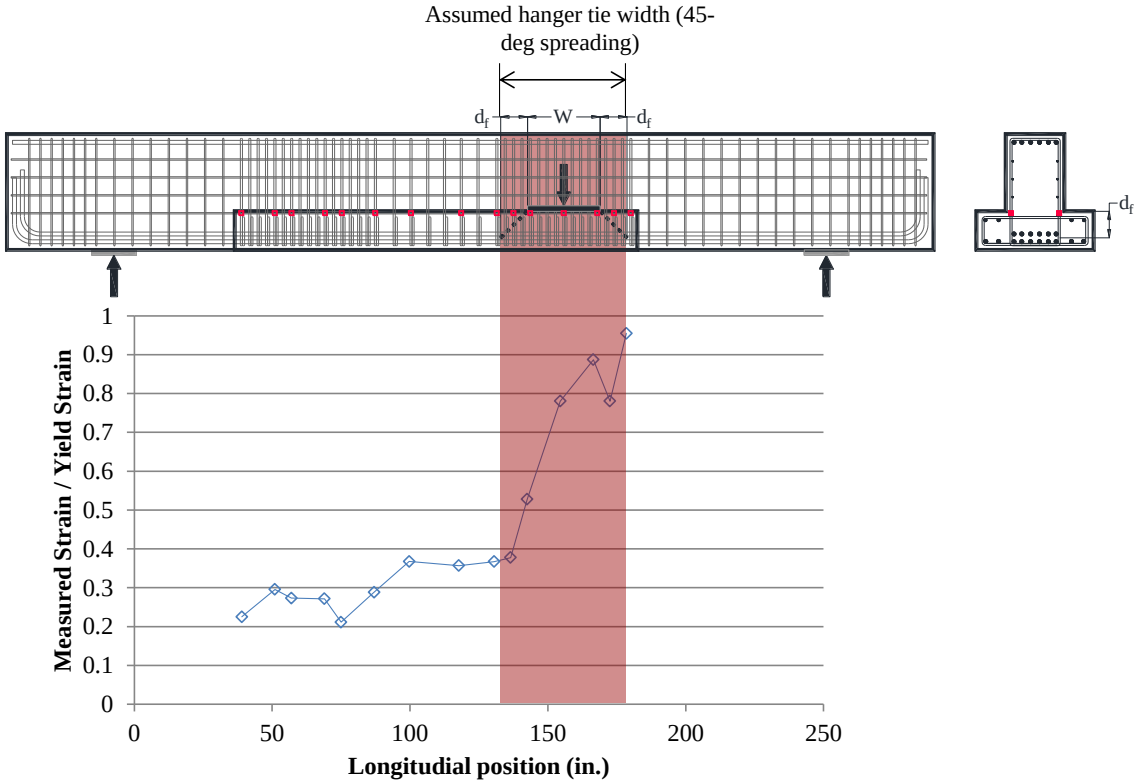

Figure 4-6: Typical hanger strains at failure (specimen 16a: SS1-42-2.50-03); one point load test, shallow ledge

In the above figures, high strains can be seen to concentrate within the assumed load spread length; without reaching yield. Similar strain distributions were observed in most specimens. Strain gauge measurements thus indicate that the 45-degree load spread assumption is reasonable and conservative. The observations noted here are consistent with the preliminary findings reported by Garber (2011). It is therefore recommended to calculate the hanger tie widths as shown in Figure 4-4.

4.4 SERIES I: LEDGE LENGTH

Three different ledge lengths were found in the inspection of the distressed bent caps in the field: (1) 'Cut-off ledges' –ledges that are interrupted right next to the outer most stringer, (2) 'Long ledges' – ledges that run continuously from support to support, and (3) 'Short ledges' –ledges that end between the first two extreme cases allowing for a

45-deg spreading of the force from the loading plate to the bottom of the beam. Section 3.2.3.2 provides background information for the ledge length series.

This series was designed to evaluate the effects of ledge length on strength and serviceability of inverted-T straddle bent caps. The results of Series I will be used to develop design recommendations in regards to ledge length.

4.4.1 Experimental Results

Twenty tests have been conducted to produce eight groups of two or three directly comparable specimens in which every parameter was kept constant except the ledge length. A summary of the experimental results from the ledge length series is provided in

Table 4-2. All variables are defined in Section 4.2 except for V_{pred}, which is the predicted shear capacity using the strut-and-tie modeling provision of TxDOT Project 5253. Note that V_{pred} was evaluated using measured material properties and the procedure outlined in Section 2.5.1.

Table 4-2: Series I experimental results

Test	Specimen	f'_c (psi)	V_{test} (kip)	$\frac{V_{test}}{f'_c b_w d}$	$\frac{V_{test}}{\sqrt{f'_c} b_w d}$	V_{crack} (kip)	$\frac{V_{crack}}{\sqrt{f'_c} b_w d}$	V_{pred} (kip)	$\frac{V_{test}}{V_{pred}}$
01a	DS1-42-1.85-03	5258	712	0.17	12.42	172	2.99	463	1.54
10a	DL1-42-1.85-03	4929	626	0.16	11.28	242	4.36	468	1.34
15a	DC3-42-1.85-03	4568	395	0.11	7.39	152	2.84	370	1.07
15b	DS3-42-1.85-03	4568	454	0.13	8.49	164	3.07	389	1.17
17b	DL3-42-1.85-03 (f)	4202	629	0.19	12.27	276	5.39	359	1.75
06b	SC3-42-1.85-03	5873	483	0.10	7.98	90	1.48	427	1.13
04a	SS3-42-1.85-03	5891	523	0.11	8.62	126	2.08	456	1.15
11a	SL3-42-1.85-03	5037	571	0.14	10.17	172	3.06	409	1.39
02a	DS1-42-1.85-06	5024	621	0.16	11.09	188	3.35	479	1.30
03a	DL1-42-1.85-06	4830	741	0.19	13.48	168	3.06	464	1.60
17a	DC1-42-2.50-03	4035	365	0.11	7.28	70	1.40	250	1.46
01b	DS1-42-2.50-03	5389	406	0.10	6.99	N/A	N/A	202	2.01
10b	DL1-42-2.50-03	4929	510	0.13	9.19	N/A	N/A	235	2.17
18b	SC1-42-2.50-03 (r)	4281	319	0.09	6.18	N/A	N/A	258	1.24
16a	SS1-42-2.50-03	5703	398	0.09	6.67	157	2.63	213	1.87
18a	SL1-42-2.50-03	4281	498	0.15	9.62	167	3.24	269	1.85
06a	SC3-42-2.50-03	5873	329	0.07	5.44	113	1.87	257	1.28
04b	SS3-42-2.50-03	5891	447	0.10	7.38	140	2.31	215	2.08
02b	DS1-42-2.50-06	5088	503	0.13	8.93	N/A	N/A	338	1.49
03b	DL1-42-2.50-06	4986	622	0.16	11.15	N/A	N/A	353	1.76

(f) Flexural failure

(r) Shear friction failure of the web-to-ledge interface

It is important to note that all specimens in this series failed in web shear except DL3-42-1.85-03 and SC1-42-2.50-03, which failed in flexure and shear friction respectively. The value reported for V_{test} is the maximum shear carried at the critical section at the onset of failure, regardless of the failure mode.

4.4.2 Strength Results

Twenty tests are compared in eight groups of two or three directly comparable specimens in which every parameter was kept constant except the ledge length. Comparison of strength results are provided in Figure 4-7 and Figure 4-8. For completeness, in Figure 4-7 V_{test} is normalized by $f'_c b_w d$, and in Figure 4-8 V_{test} is normalized by $\sqrt{f'_c} b_w d$. In each sub-plot of Figure 4-7 and Figure 4-8, results are

compared for specimens in which every parameter was kept constant except the ledge length.

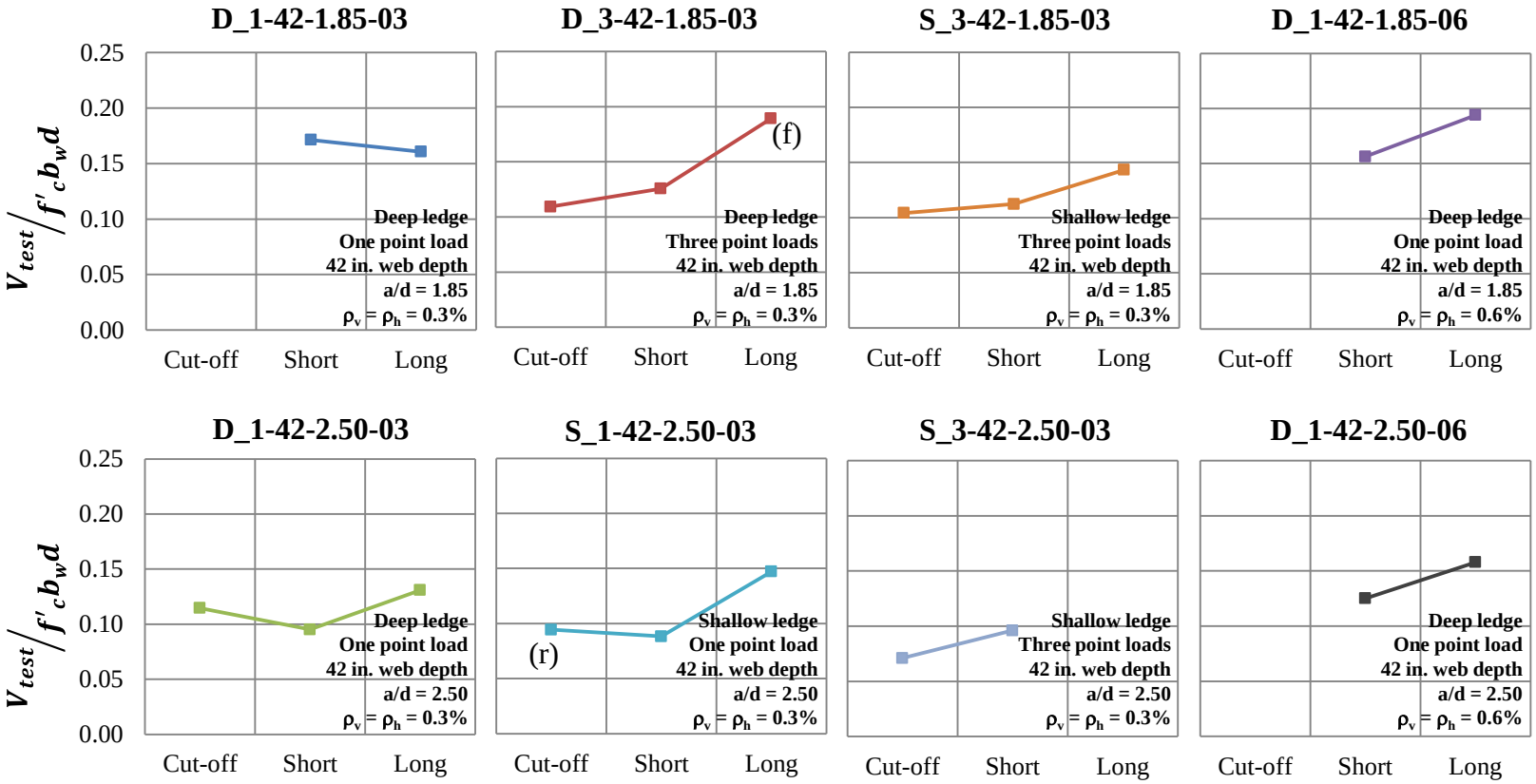

(f) Flexural failure
(r) Shear friction failure of the web-to-ledge interface

Figure 4-7: Series I: Ledge Length: comparisons of V_{test} normalized by $f'_c b_w d$

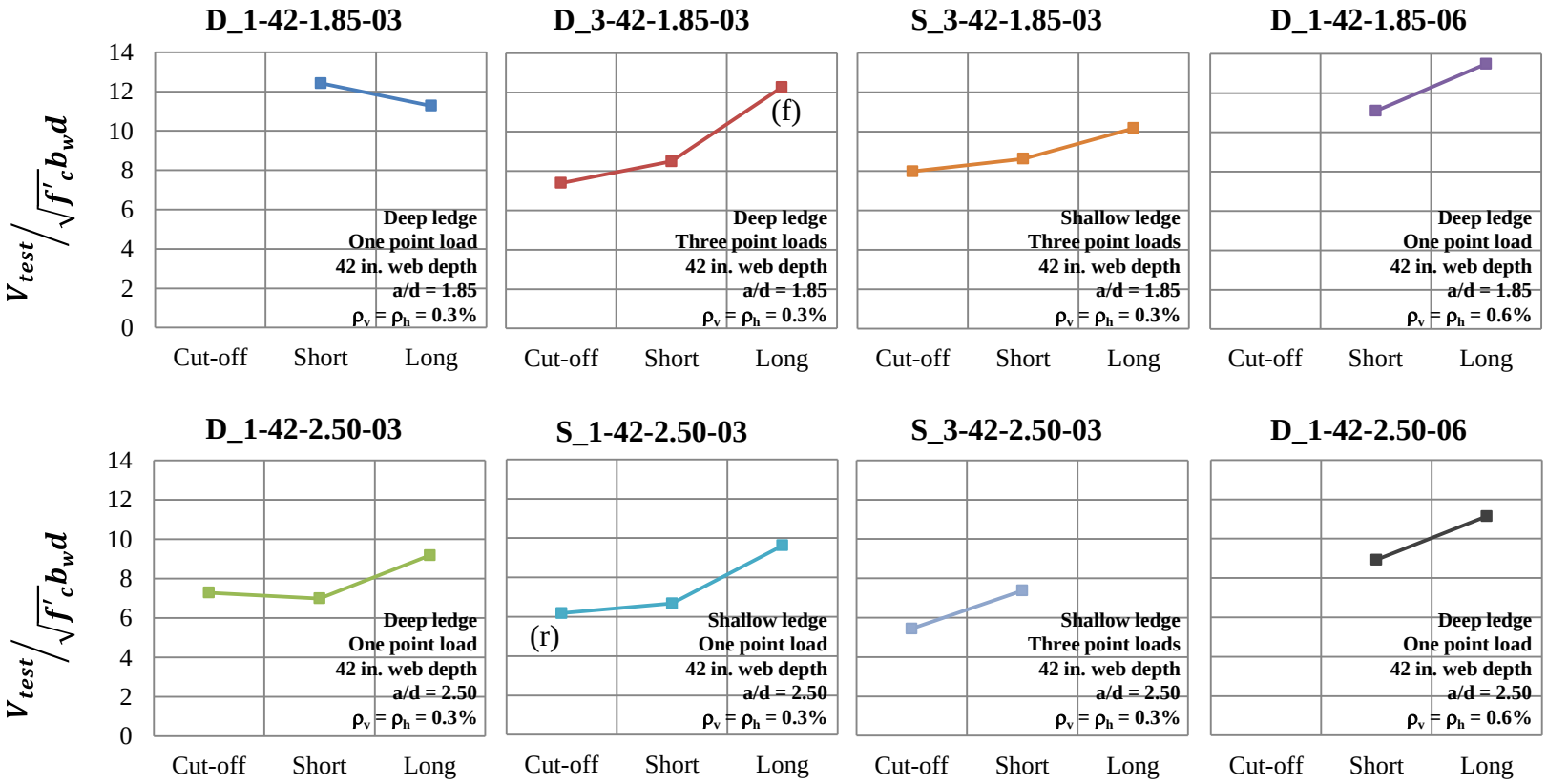

(f) Flexural failure
(r) Shear friction failure of the web-to-ledge interface

Figure 4-8: Series I: Ledge Length: comparisons of V_{test} normalized by $\sqrt{f'_c}\,b_w d$

As can be observed in Figure 4-7 and Figure 4-8, there is a strong trend of increased shear capacity with increasing ledge length. In only one comparison that trend is not observed. The trend holds for both a/d =1.85 and *a/d* = 2.50. The trend also holds for web reinforcement ratios of 0.3% and 0.6% and for deep and shallow ledges.

4.4.3 Serviceability Results

First cracking loads for the ledge length series are presented in Figure 4-9. V_{crack} is normalized by $\sqrt{f'_c}b_w d$ since the first cracking is associated with the tensile strength of the concrete. In each sub-plot of Figure 4-9, results are compared for specimens in which every parameter was kept constant except the ledge length. Fourteen tests are compared in six groups of two or three directly comparable specimens in which every parameter was kept constant except the ledge length. First cracking load could only be obtained for shear spans that were tested first in each beam.

Crack width progressions are presented in Figure 4-10. Twenty specimens are presented in eight groups of two or three directly comparable specimens in which every parameter was kept constant except the ledge length.

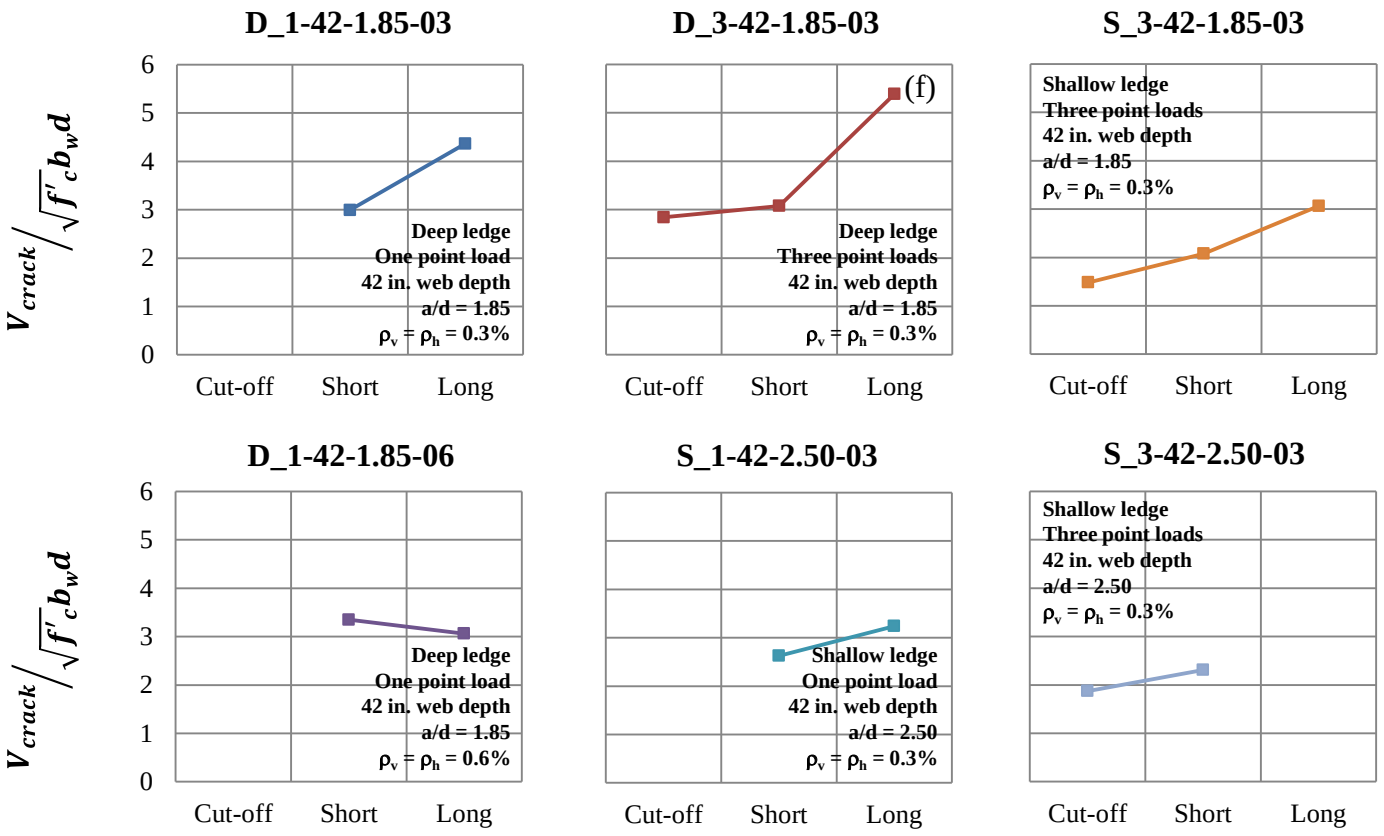

(f) Flexural failure

Figure 4-9: Series I: Ledge Length: comparisons of V_{crack} normalized by $\sqrt{f'_c}b_w d$

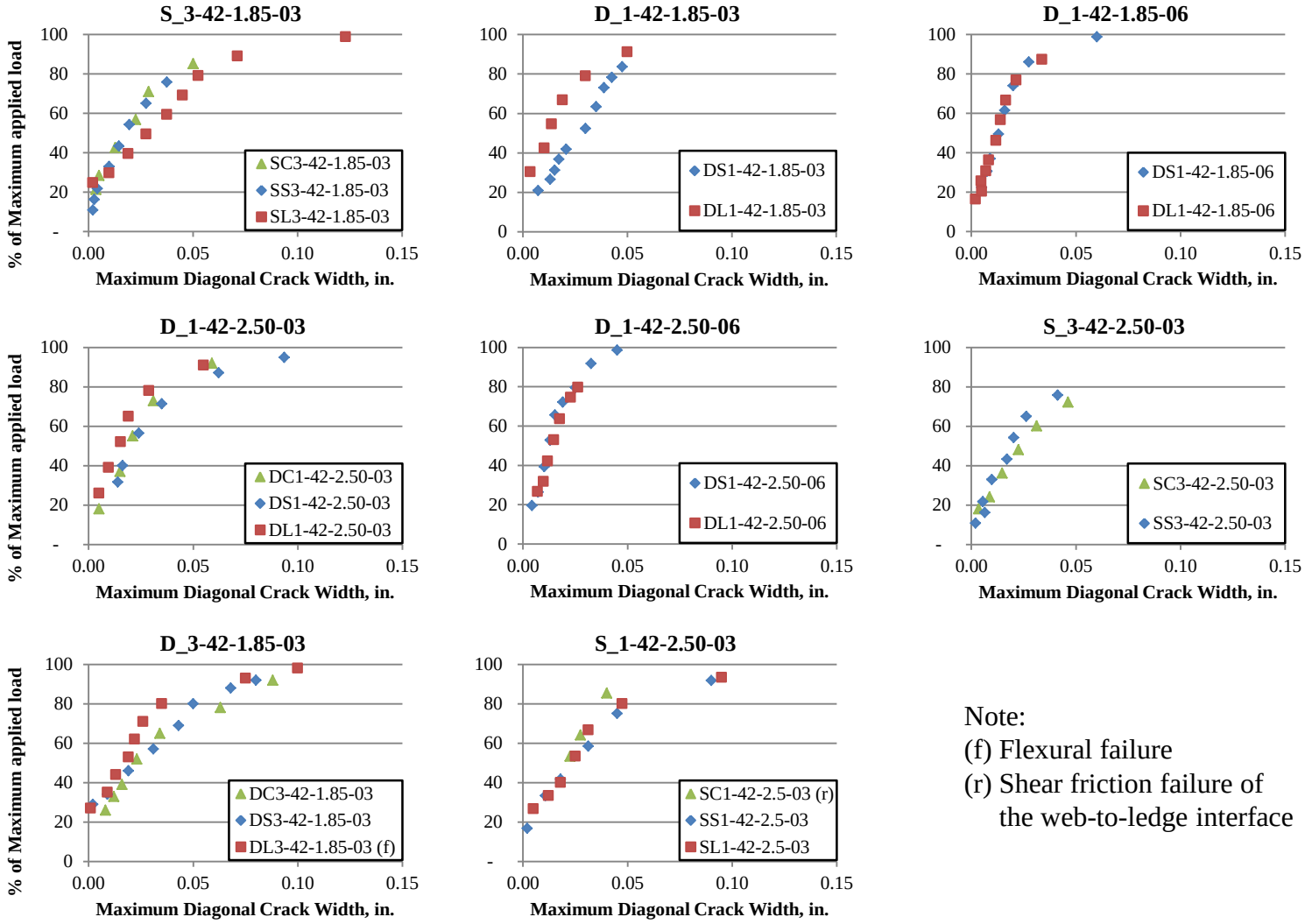

Note:
(f) Flexural failure
(r) Shear friction failure of the web-to-ledge interface

Figure 4-10: Series I: Ledge Length: comparisons of crack width progression

V_{crack} / $b_w d\sqrt{f'_c}$ values varied from 1.40 to 5.39. As can be observed in Figure 4-9, there is a general trend of delayed shear cracking with increasing ledge length. The trend holds for both *a/d* =1.85 and *a/d* = 2.50. The trend also holds for deep and shallow ledges. No clear trend can be distinguished in Figure 4-10 regarding crack width progression. In some cases specimens with longer ledges showed a more accelerated crack widening, whereas in some other cases specimens with cut-off ledges showed a more accelerated crack widening.

4.4.4 TxDOT 5253 STM Design Provisions

Specimens of the experimental program were designed using the strut-and-tie modeling provisions of TxDOT Project 5253. V_{test}/V_{pred} ratios from the twenty specimens of Series I are shown in Figure 4-11 in eight groups of two or three directly comparable specimens.

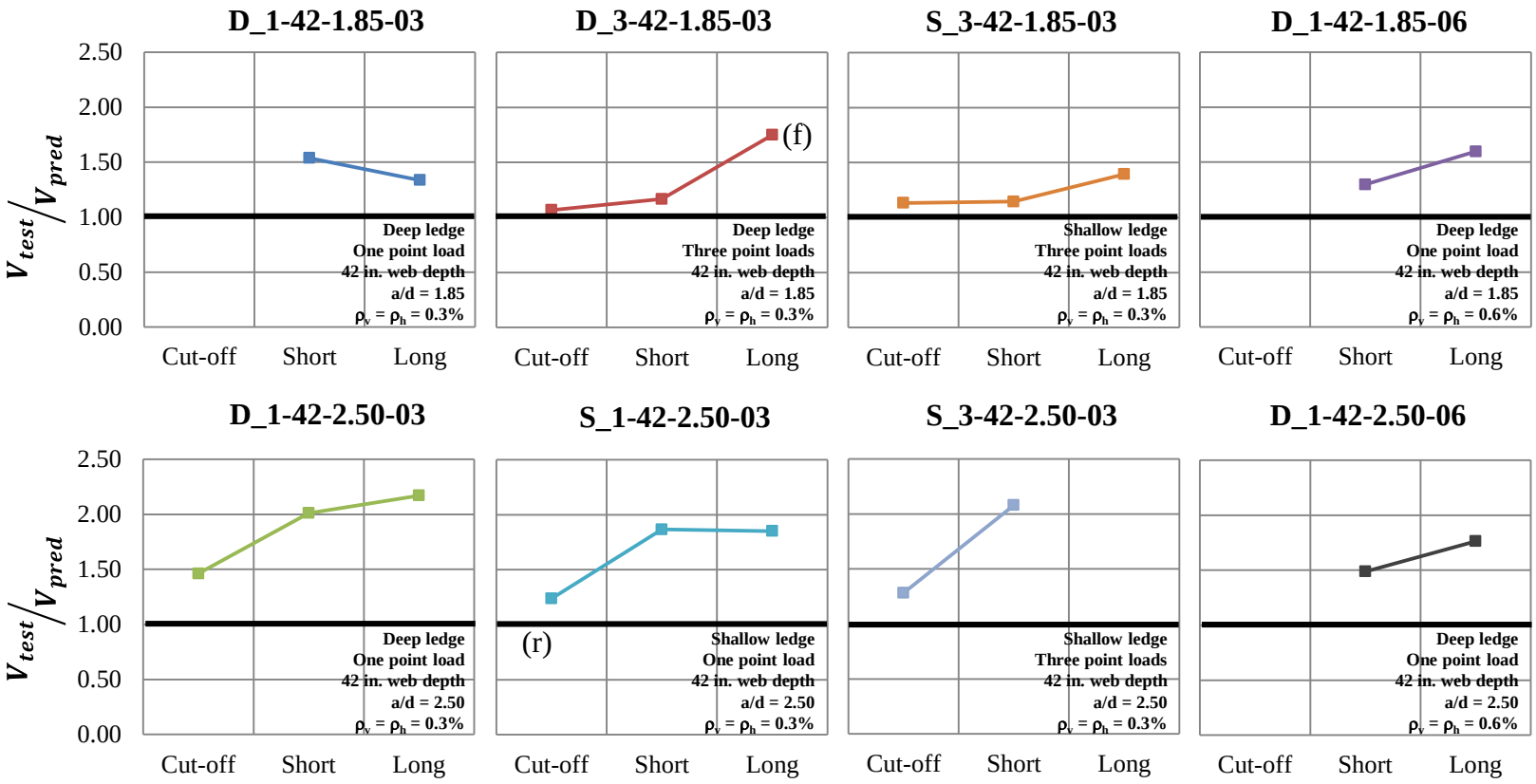

(f) Flexural failure
(r) Shear friction failure of the web-to-ledge interface

Figure 4-11: Series I: Ledge Length: comparisons of V_{test} / V_{pred}

V_{test}/V_{pred} ratios varied between 1.07 and 2.17. It is important to note that all points fall above 1.0, which indicates that the STM provisions of TxDOT Project 5253 produced conservative strength estimates for the twenty inverted-T specimens of the ledge length series. Additionally, there is a clear trend of increased conservatism as the ledge length increases. There are a couple of cases which did not follow this trend, but considering the twenty tests presented in this series, it is evident that longer ledges provide additional strength not captured by the STM provisions.

4.4.5 Summary of Series I: Ledge Length

Direct comparisons have been presented in this section to evaluate the influence of the ledge length in strength, appearance of first diagonal crack, crack width progression and performance of STM design provisions of TxDOT Project 5253.

Results have shown that increasing the ledge length increases strength, delays the appearance of the first diagonal cracking, and increases conservatism of the strength estimations using the STM design provisions of TxDOT Project 5253. Ledge length has no significant effect on crack width progression.

STM design provisions of TxDOT Project 5253 have provided conservative estimates of strength for all twenty specimens evaluated in this series.

4.5 SERIES II: LEDGE DEPTH

This series was designed to evaluate the effects of ledge depth on strength and serviceability of inverted-T straddle bent caps. The results of Series II will be used to develop design recommendations in regard to ledge depth.

4.5.1 Experimental Results

Eighteen tests have been conducted to produce nine pairs of directly comparable specimens in which every parameter was kept constant except the ledge depth. A summary of the experimental results from the ledge depth series is provided in Table 4-3. All variables are defined in Section 4.2, except for V_{pred} which is the predicted shear capacity using the strut-and-tie modeling provision of TxDOT Project 0-5253. Note that

V_{pred} was evaluated using measured material properties and the procedure outlined in Section 2.5.1.

Table 4-3: Series II experimental results

Test	Specimen	f'_c (psi)	V_{test} (kip)	$\frac{V_{test}}{f'_c b_w d}$	$\frac{V_{test}}{\sqrt{f'_c} b_w d}$	V_{crack} (kip)	$\frac{V_{crack}}{\sqrt{f'_c} b_w d}$	V_{pred} (kip)	$\frac{V_{test}}{V_{pred}}$
20a	SC1-42-1.85-03 (le)	4330	451	0.13	8.67	N/A	N/A	443.61	1.02
20b	DC1-42-1.85-03	4303	517	0.15	9.98	127	2.44	460	1.12
16b	SS1-42-1.85-03	5721	583	0.13	9.75	N/A	N/A	503	1.16
01a	DS1-42-1.85-03	5258	712	0.17	12.42	172	2.99	463	1.54
06b	SC3-42-1.85-03	5873	483	0.10	7.98	90	1.48	427	1.13
15a	DC3-42-1.85-03	4568	395	0.11	7.39	152	2.84	370	1.07
04a	SS3-42-1.85-03	5891	523	0.11	8.62	126	2.08	456	1.15
15b	DS3-42-1.85-03	4568	454	0.13	8.49	164	3.07	389	1.17
11a	SL3-42-1.85-03	5037	571	0.14	10.17	172	3.06	409	1.39
17b	DL3-42-1.85-03 (f)	4202	629	0.19	12.27	276	5.39	359	1.75
18b	SC1-42-2.50-03 (r)	4281	319	0.09	6.18	N/A	N/A	258	1.24
17a	DC1-42-2.50-03	4035	365	0.11	7.28	70	1.40	250	1.46
16a	SS1-42-2.50-03	5703	398	0.09	6.67	157	2.63	213	1.87
01b	DS1-42-2.50-03	5389	406	0.10	6.99	N/A	N/A	202	2.01
18a	SL1-42-2.50-03	4281	498	0.15	9.62	167	3.24	269	1.85
10b	DL1-42-2.50-03	4929	510	0.13	9.19	N/A	N/A	235	2.17
04b	SS3-42-2.50-03	5891	447	0.10	7.38	140	2.31	215	2.08
09a	DS3-42-2.50-03	5687	430	0.10	7.21	143	2.40	236	1.82

(f) Flexural failure

(r) Shear friction failure of the web-to-ledge interface

(le) Horizontal ledge tie failure in cross section

It is important to note that all specimens failed in shear, except for the following three specimens: DL3-42-1.85-03 that failed in flexure, and SC1-42-1.85-03 and SC1-42-2.50-03 that experienced local ledge failures. The value reported for V_{test} is the maximum shear carried at the critical section at the onset of failure, regardless of the failure mode.

4.5.2 Strength Results

Direct comparison of strength results are provided in Figure 4-12 and Figure 4-13. Each plot is a direct comparison of two specimens in which every parameter was kept

constant, except the ledge depth. As discussed in Section 4.2.1, in Figure 4-12 V_{test} is normalized by $f'_c b_w d$, and in Figure 4-13 V_{test} is normalized by $\sqrt{f'_c} b_w d$.

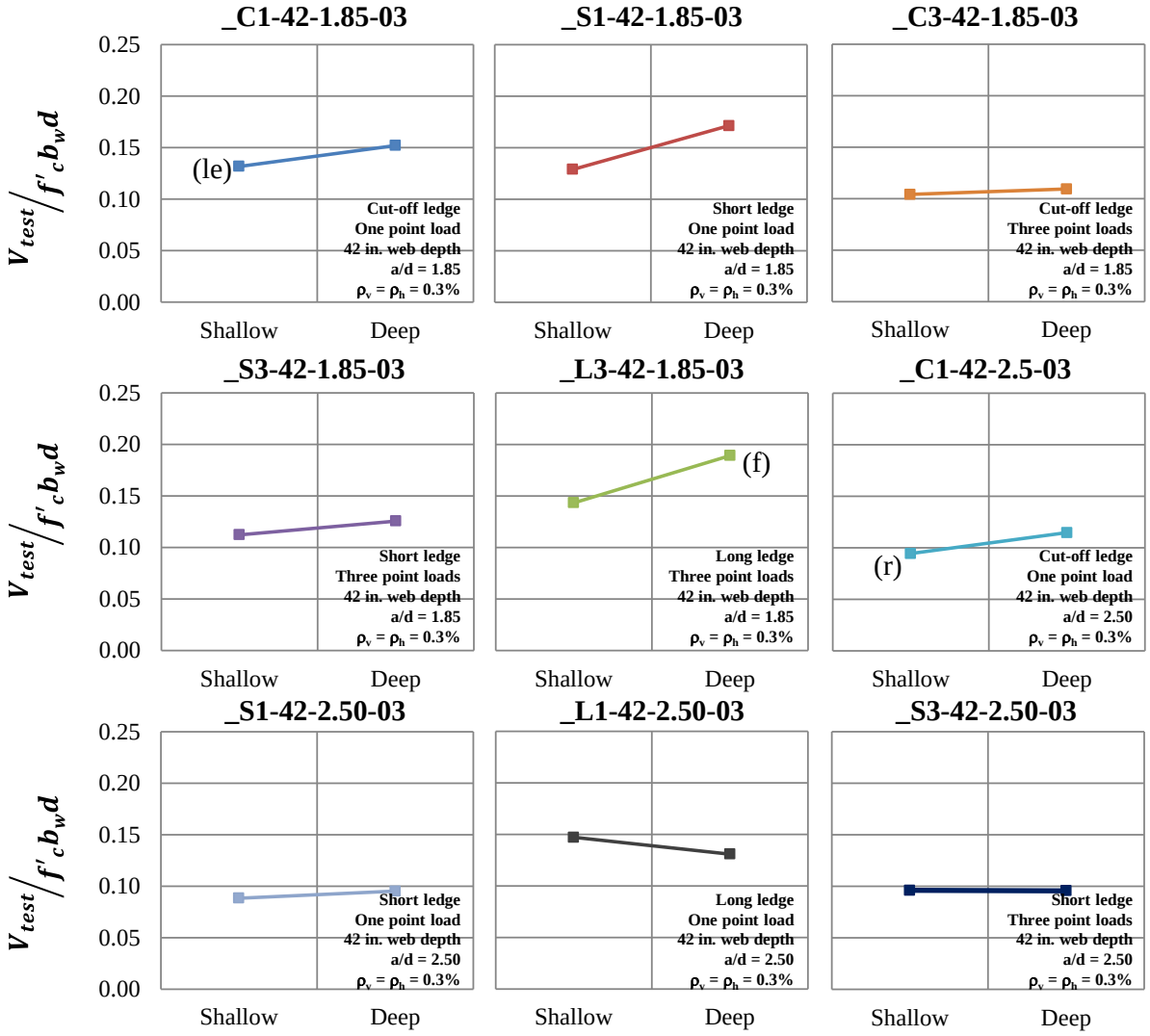

Note:
(f) Flexural failure
(r) Shear friction failure of the web-to-ledge interface
(le) Horizontal ledge tie failure in cross section

Figure 4-12: Series II: Ledge Depth: comparisons of V_{test} normalized by $f'_c\ b_w\ d$

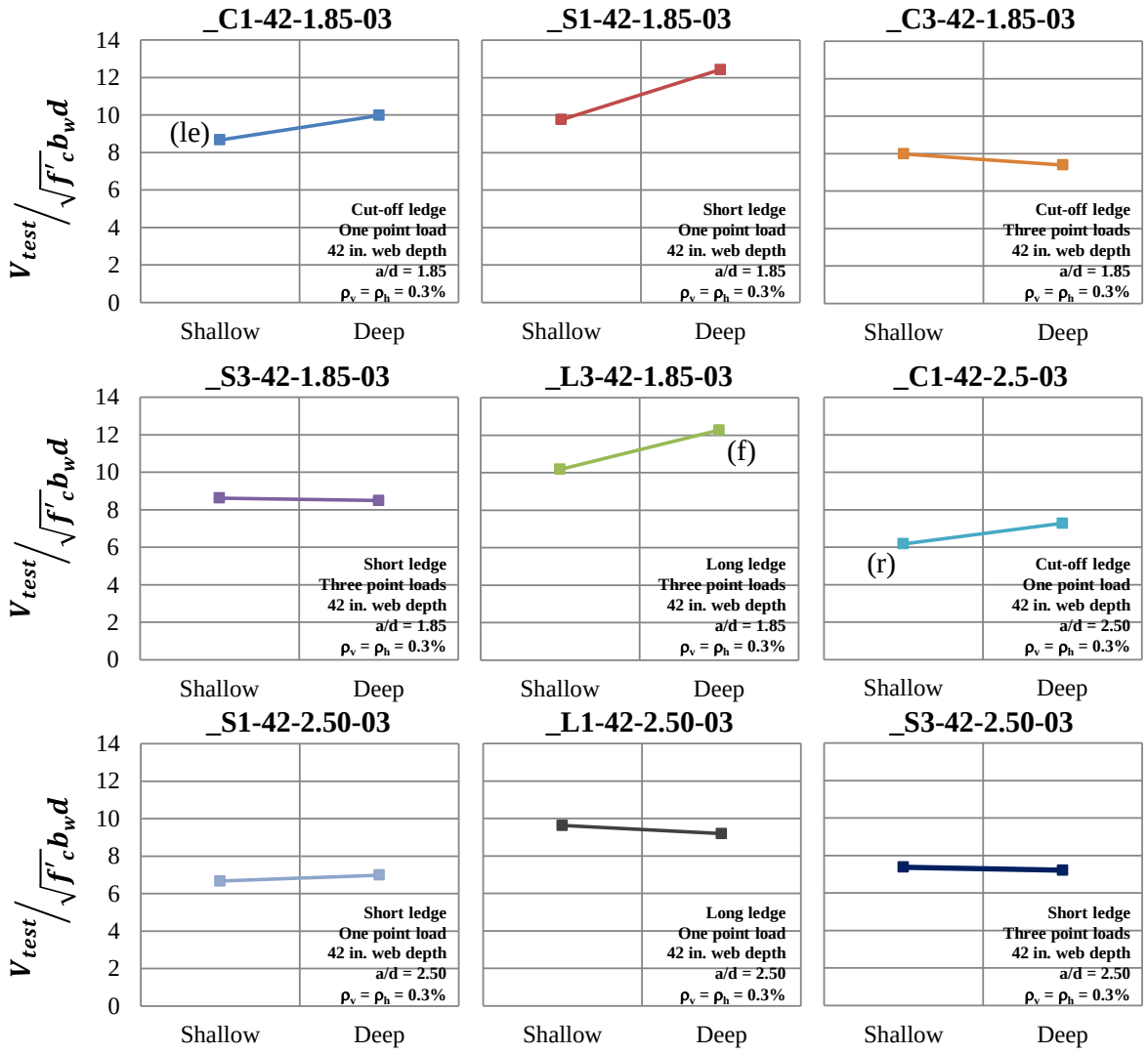

Note:
(f) Flexural failure
(r) Shear friction failure of the web-to-ledge interface
(le) Horizontal ledge tie failure in cross section

Figure 4-13: Series II: Ledge Depth: comparisons of V_{test} normalized by $\sqrt{f'_c}b_w d$

Results shown in Figure 4-12 and Figure 4-13 indicate that the ledge depth has no significant influence on the strength of the specimen. Only in two cases (_S1-42-1.85-03 and _L3-42-1.85-03), specimens with deep ledges exhibited significantly higher strengths than specimens with shallow ledges; considering the inherent variability in shear test results, one can conclude that ledge depth has no significant effect in the strength of the specimens.

4.5.3 Serviceability Results

First cracking loads for the ledge depth series are presented in Figure 4-14. V_{crack} is normalized by $\sqrt{f'_c}b_w d$ since the first cracking is associated with the tensile strength of the concrete. Eight tests are available to be compared in four groups of two directly comparable specimens in which every parameter was kept constant except the ledge depth. First cracking load could only be obtained for shear spans that were tested first in each beam.

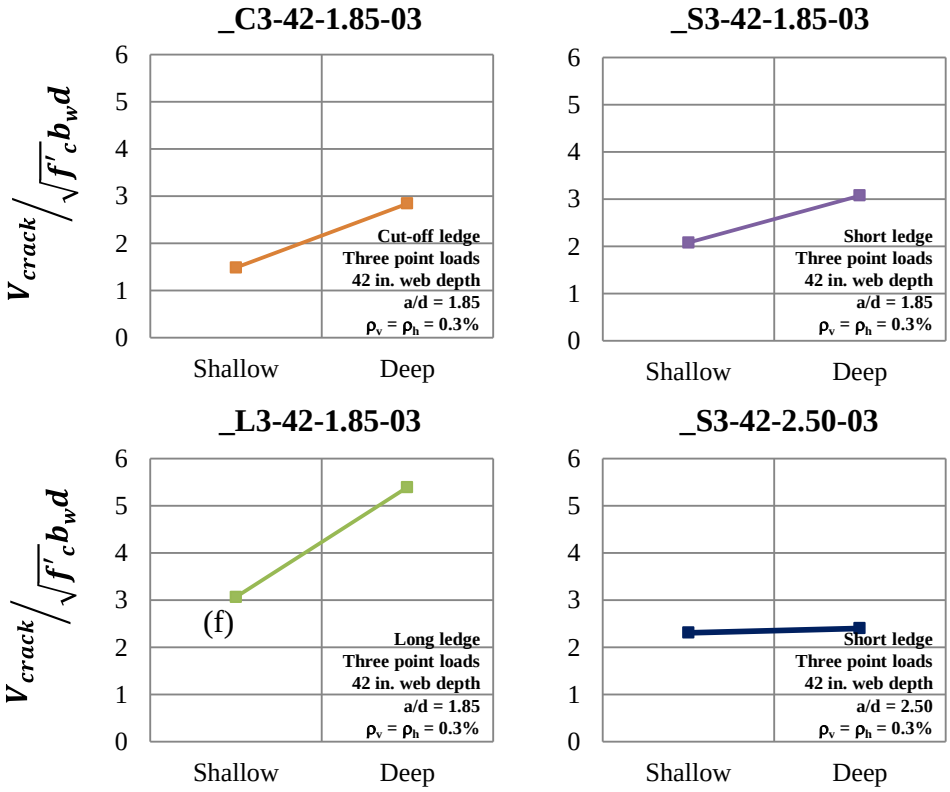

(f) Flexural failure

Figure 4-14: Series II: Ledge Depth: comparisons of V_{crack} normalized by $\sqrt{f'_c}b_w d$

A trend can be observed in Figure 4-14, specimens with shallow ledges experienced first diagonal cracking earlier than comparable specimens with deeper ledges. In other words, increasing the depth of the ledge delays the appearance of the first diagonal cracking.

Crack width progressions are presented in Figure 4-15. Eighteen specimens are presented in nine groups of two directly comparable specimens in which every parameter was kept constant except the ledge depth.

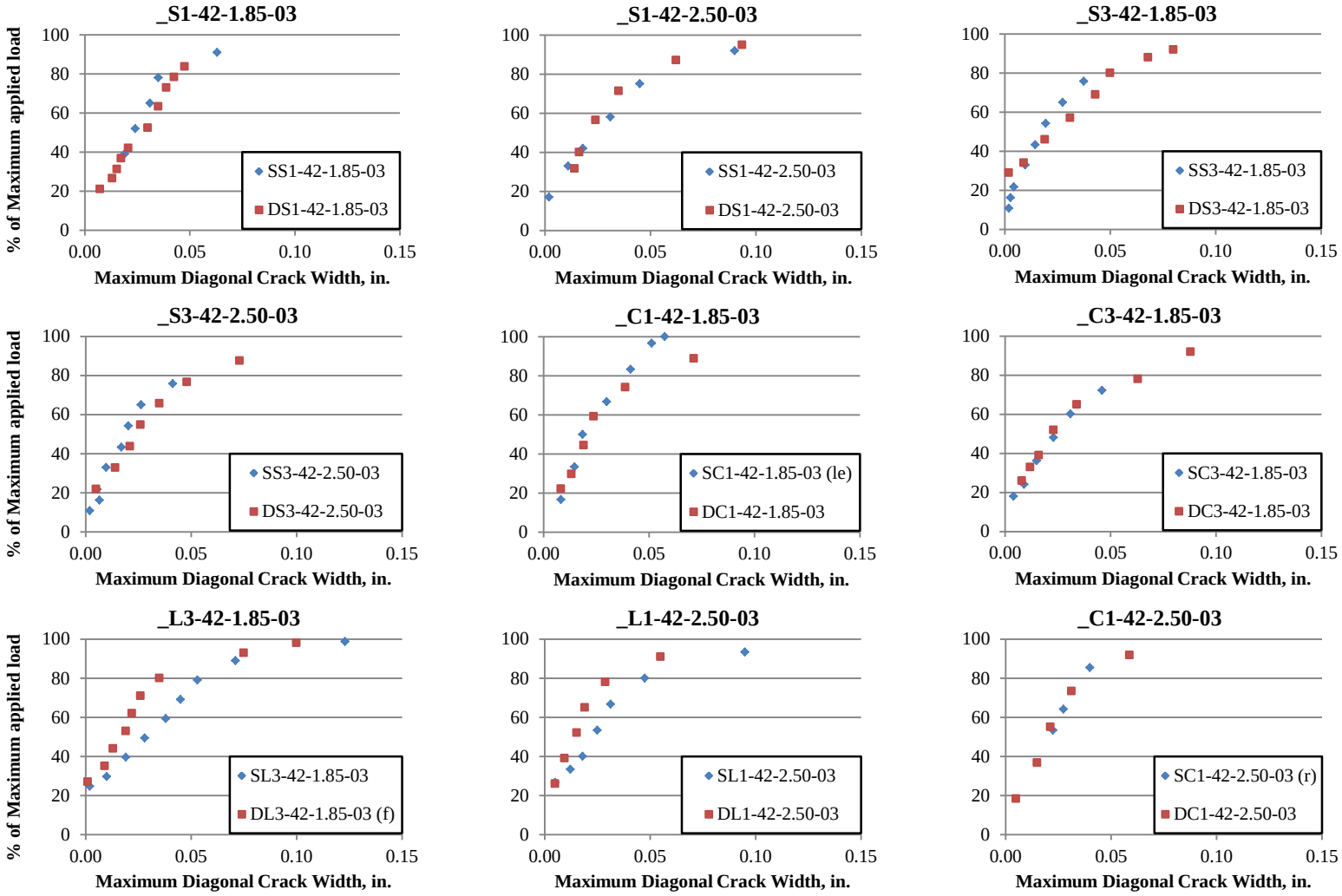

Figure 4-15: Series II: Ledge Depth: comparisons of crack width progression

Regarding crack width progressions, no clear trend can be distinguished in Figure 4-15. In some cases, specimens with deeper ledges showed a more accelerated crack widening, whereas in other cases specimens with shallower ledges showed a more accelerated crack widening. Ultimately, it can be concluded that ledge depth has no significant effect on crack width progression.

4.5.4 TxDOT 5253 STM design provisions

Specimens of the experimental program were designed using the Strut-and-tie modeling provisions of TxDOT Project 5253. V_{test}/V_{pred} ratios from eighteen specimens are shown in Figure 4-16 in nine groups of two directly comparable specimens.

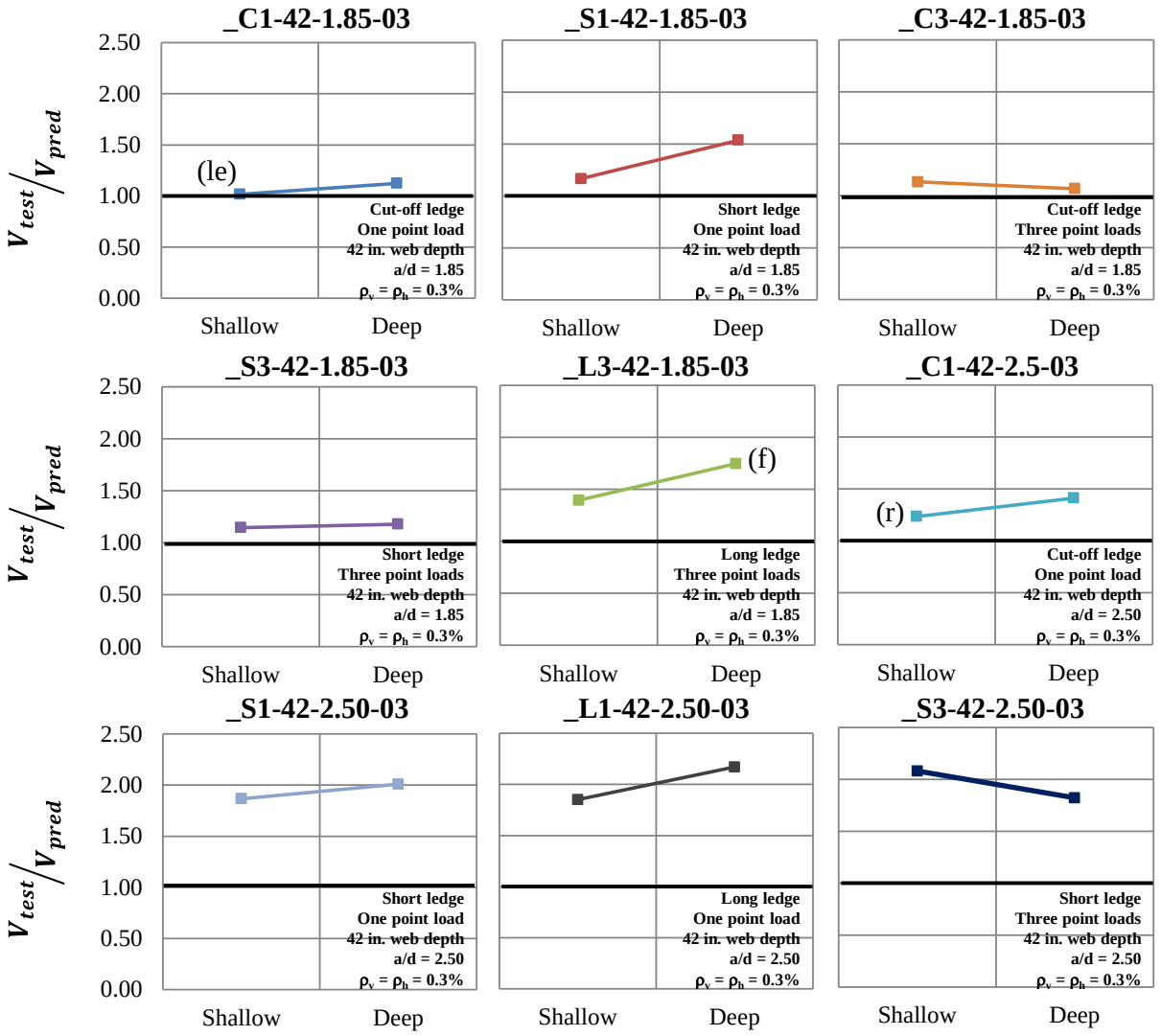

Note:
(f) Flexural failure
(r) Shear friction failure of the web-to-ledge interface
(le) Horizontal ledge tie failure in cross section

Figure 4-16: Series II: Ledge Depth: comparisons V_{test}/V_{pred}

V_{test}/V_{pred} ratios varied between 1.02 and 2.17. It is important to note that all points fall above 1.0, which indicates that the STM provisions of TxDOT Project 5253 produced conservative strength estimates for the eighteen inverted-T specimens of the ledge depth series. Similar conservatism for both shallow and deep ledges can be seen in Figure 4-16. For 70% of the comparisons no significant difference was observed while for the remaining 30% percent an increase in conservatism was observed for deep ledges. The observations indicate that ledge depth has no significant influence in the conservatism of the STM provisions of TxDOT Project 5253 applied to inverted-T specimens.

4.5.5 Summary of Series II: Ledge Depth

Direct comparisons have been presented in this section to evaluate the influence of ledge depth in strength, appearance of first diagonal crack, crack width progression, and performance of STM design provisions of TxDOT Project 5253.

Results have shown that the ledge depth has no significant effect on the strength, crack width progression, or the conservatism of the STM provisions of TxDOT Project 5253. However, it was observed that increasing the ledge depth delays the appearance of the first diagonal cracking.

STM design provisions of TxDOT Project 5253 provided conservative estimates of strength for all eighteen specimens evaluated in this series.

4.6 SERIES IV: NUMBER OF POINT LOADS

This series was designed to evaluate the differences in strength and serviceability between specimens with single and multiple point loads. In this section applicability of the STM provisions from TxDOT Project 5253 to specimens with multiple loading points is verified.

Specimens with a single point load allowed for direct comparisons with compression-chord loaded specimens from TxDOT Project 5253 (Series V), whereas specimens with multiple point loads are more representative of field conditions. Additionally, spreading the load in multiple points reduced the probability of local

failures in the ledges, thus allowing the use of shallower ledges (Series II) and ensuring web shear failures. Another objective of the current series is to investigate the dominant behavior in specimens which may be classified as non-deep beams by AASHTO (2012) and the TxDOT Bridge Design Manual (2011), regardless of having concentrated loads within a distance of 2d from the support (Figure 4-17). This topic covered in more depth in Chapter 5.

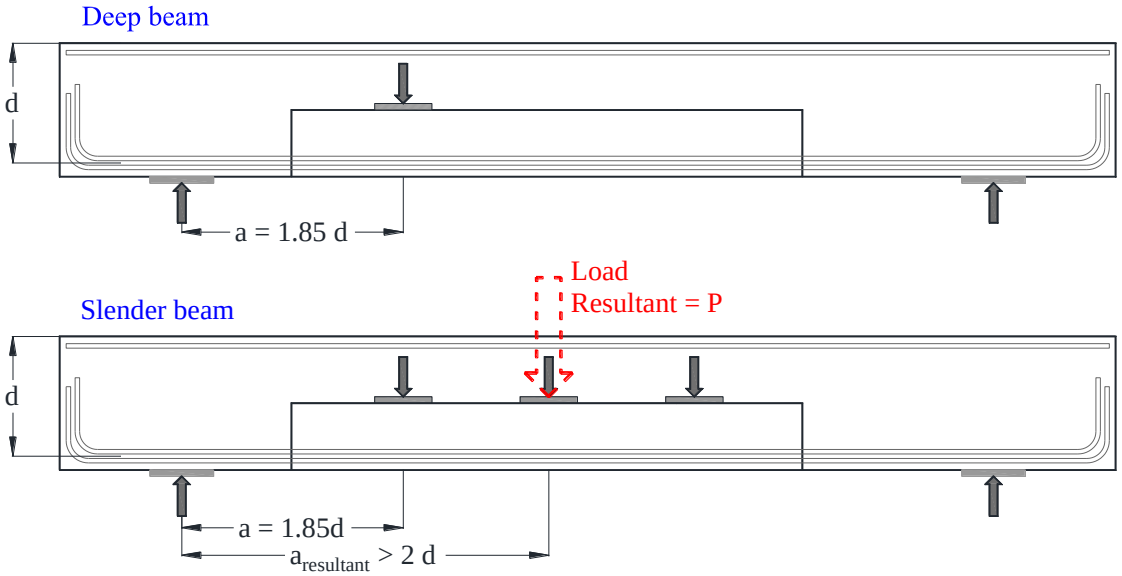

Figure 4-17: Deep and slender beams as classified per AASHTO Art. 5.6.3.1

4.6.1 Experimental Results

Twelve tests have been conducted to produce six pairs of directly comparable specimens in which every parameter was kept constant except the number of point loads. A summary of the experimental results from the number of point loads series is provided in Table 4-4. Note that V_{pred} was evaluated using measured material properties and the procedure outlined in Section 2.5.1.

Table 4-4: Series IV experimental results

Test	Specimen	f'_c (psi)	V_{test} (kip)	$\frac{V_{test}}{f'_c b_w d}$	$\frac{V_{test}}{\sqrt{f'_c} b_w d}$	V_{crack} (kip)	$\frac{V_{crack}}{\sqrt{f'_c} b_w d}$	V_{pred} (kip)	$\frac{V_{test}}{V_{pred}}$
16b	SS1-42-1.85-03	5721	583	0.13	9.75	N/A	N/A	503	1.16
04a	SS3-42-1.85-03	5891	523	0.11	8.62	126	2.08	456	1.15
01a	DS1-42-1.85-03	5258	712	0.17	12.42	172	2.99	463	1.54
15b	DS3-42-1.85-03	4568	454	0.13	8.49	164	3.07	389	1.17
10a	DL1-42-1.85-03	4929	626	0.16	11.28	242	4.36	468	1.34
17b	DL3-42-1.85-03 (f)	4202	629	0.19	12.27	276	5.39	359	1.75
18b	SC1-42-2.50-03 (r)	4281	319	0.09	6.18	N/A	N/A	258	1.24
06a	SC3-42-2.50-03	5873	329	0.07	5.44	113	1.87	257	1.28
16a	SS1-42-2.50-03	5703	398	0.09	6.67	157	2.63	213	1.87
04b	SS3-42-2.50-03	5891	447	0.10	7.38	140	2.31	215	2.08
01b	DS1-42-2.50-03	5389	406	0.10	6.99	N/A	N/A	202	2.01
09a	DS3-42-2.50-03	5687	430	0.10	7.21	143	2.40	236	1.82

(f) Flexural failure

(r) Shear friction failure

It is important to note that all specimens in this series failed in web shear except DL3-42-1.85-03 and SC1-42-2.50-03, which failed in flexure and shear friction respectively. The value reported for V_{test} is the maximum shear carried at the critical section at the onset of failure, regardless of the failure mode.

4.6.2 Strength Results

Comparison of strength results are provided in Figure 4-18 and Figure 4-19. For completeness, in Figure 4-18 V_{test} is normalized by $f'_c b_w d$, and in Figure 4-19 V_{test} is normalized by $\sqrt{f'_c} b_w d$. In each sub-plot of Figure 4-18 and Figure 4-19, results are compared for specimens in which every parameter was kept constant except the number of point loads.

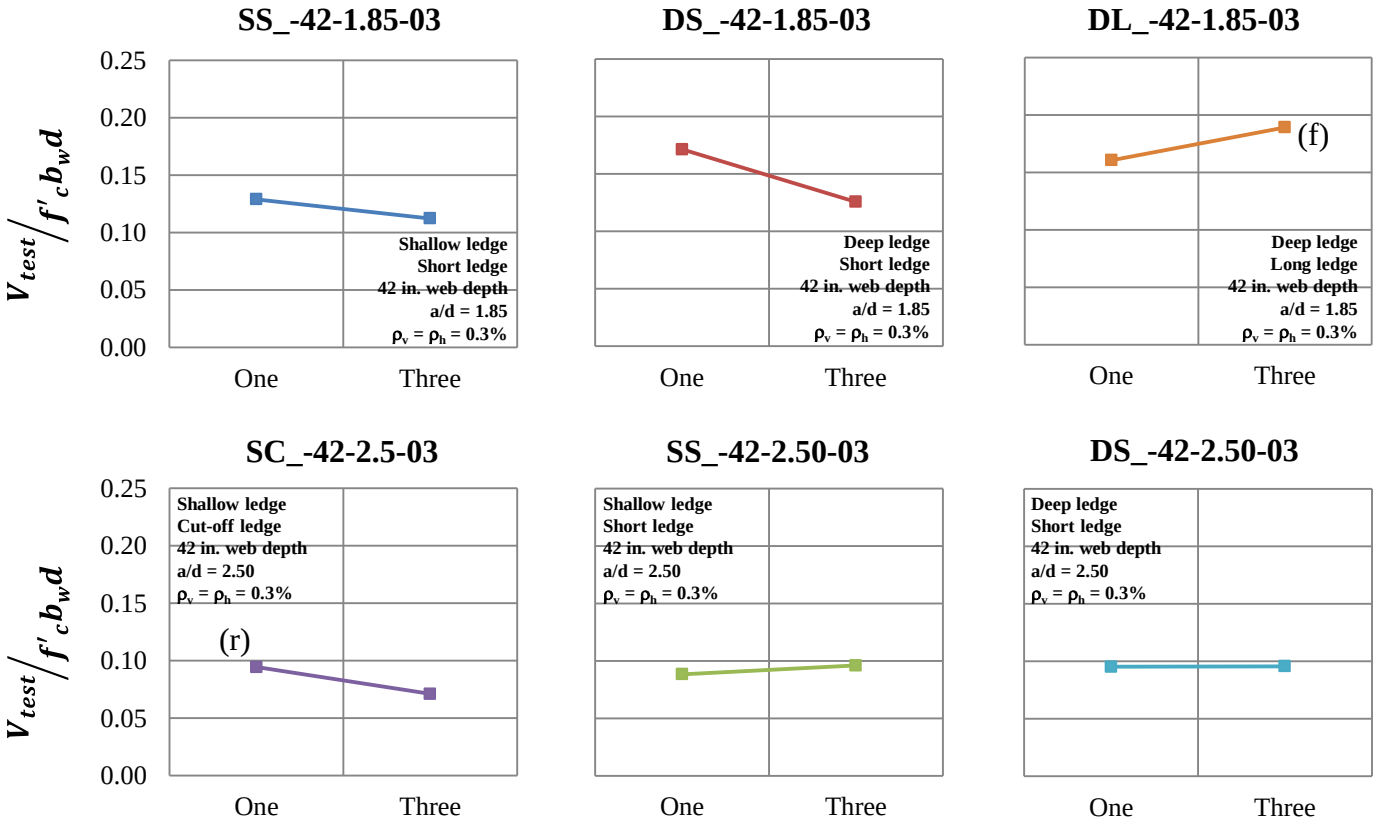

Note:

(f) Flexural failure

(r) Shear friction failure of the web-to-ledge interface

Figure 4-18: Series IV: Number of Point Loads: comparisons of V_{test} normalized by $f'_c b_w d$

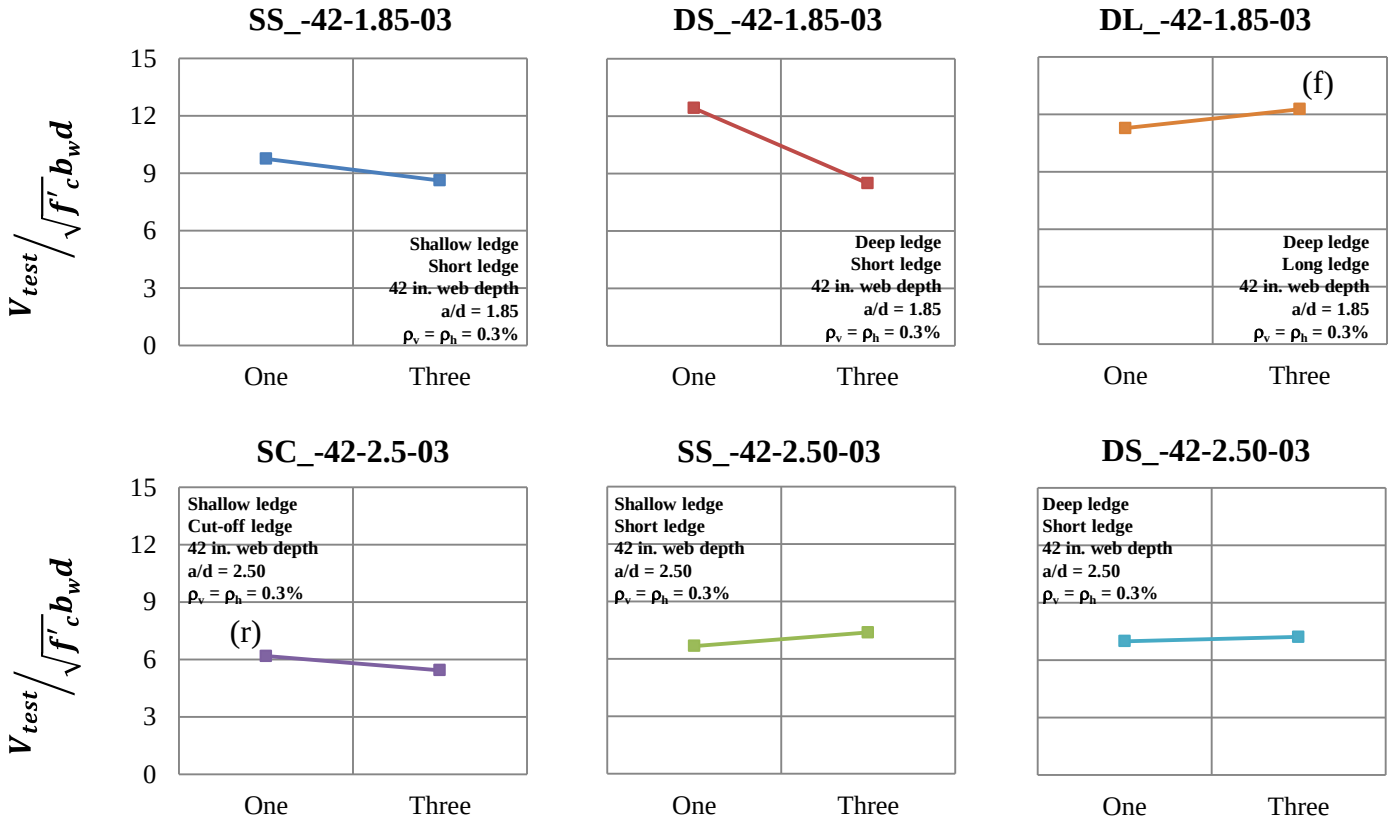

Note:
(f) Flexural failure
(r) Shear friction failure of the web-to-ledge interface

Figure 4-19: Series IV: Number of Point Loads: comparisons of V_{test} normalized by $\sqrt{f'_c}b_w d$

As it can be observed in Figure 4-18 and Figure 4-19, in only two comparisons (DS_-42-1.85-03 and DL_-42-1.85-03) a significant difference between the strength of the two directly comparable specimens is observed. These two comparisons however show contradictory trends. The rest of the comparisons showed similar strengths for specimens with one and three point loads. Results indicate that the number of point loads has no significant effect in the strength of the inverted-T specimens within the range of parameters studied.

4.6.3 Serviceability Results

First cracking loads for the number of point loads series are presented in Figure 4-20. V_{crack} is normalized by $\sqrt{f'_c} b_w d$ since the first cracking is associated with the tensile strength of the concrete. Six tests are available in three pairs of comparable specimens in which every parameter was kept constant except the number of loading points. First cracking load could only be obtained for shear spans that were tested first in each beam.

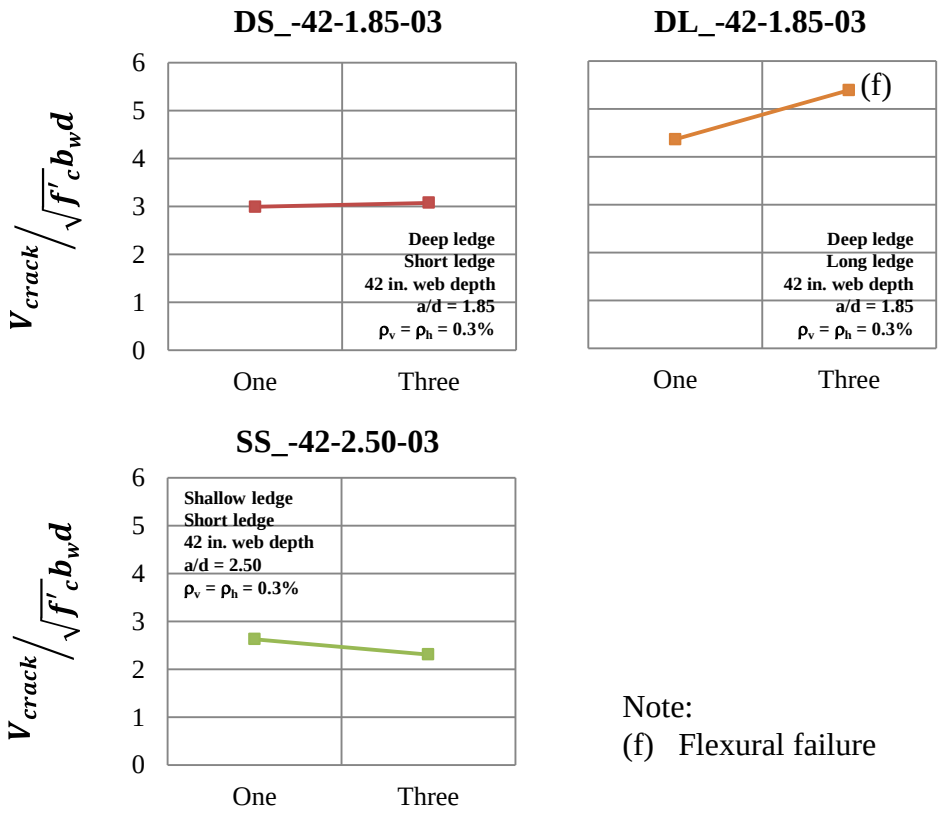

Figure 4-20: Series IV: Number of Point Loads: comparisons of V_{crack} normalized by $\sqrt{f'_c}b_w d$

Results shown in Figure 4-20 do not indicate a clear trend. Two comparisons show similar cracking load for specimens with one and three loading points, whereas one comparison shows an increase in the cracking load for the specimen with multiple loading points. More data would be necessary to reveal a trend, if one exists.

Crack width progressions are presented in Figure 4-21. Twelve specimens are presented in six pairs of directly comparable specimens in which every parameter was kept constant except the number of loading points.

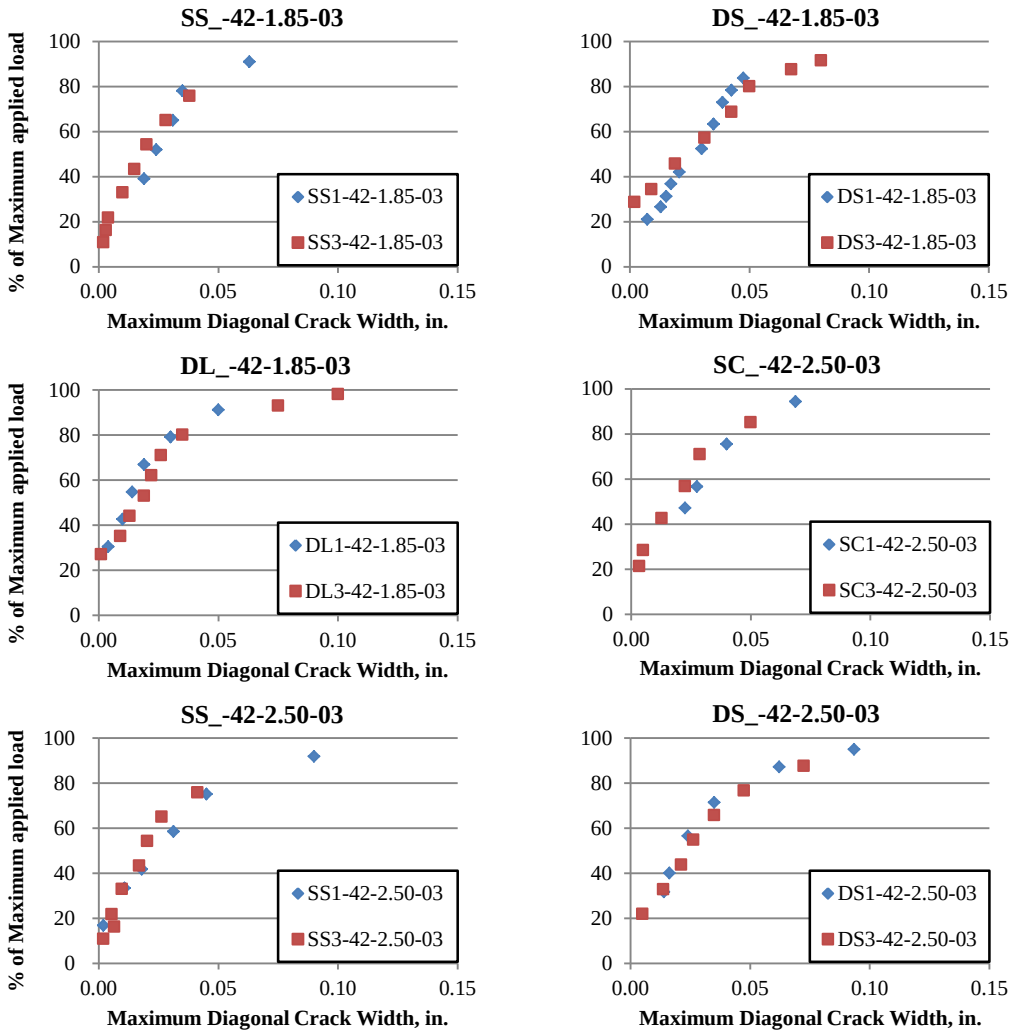

Figure 4-21: Series IV: Number of Point Loads: comparisons of crack width progression

Regarding crack width progressions, similar crack width progressions are observed in Figure 4-21 for both cases. Results show that the number of point loads has no significant effect in the crack width progression.

4.6.4 TxDOT 5253 STM design provisions

Specimens of the experimental program were designed using the Strut-and-tie modeling provisions of TxDOT Project 5253. V_{test}/V_{pred} ratios from twelve specimens are shown in Figure 4-22 in six pairs of directly comparable specimens.

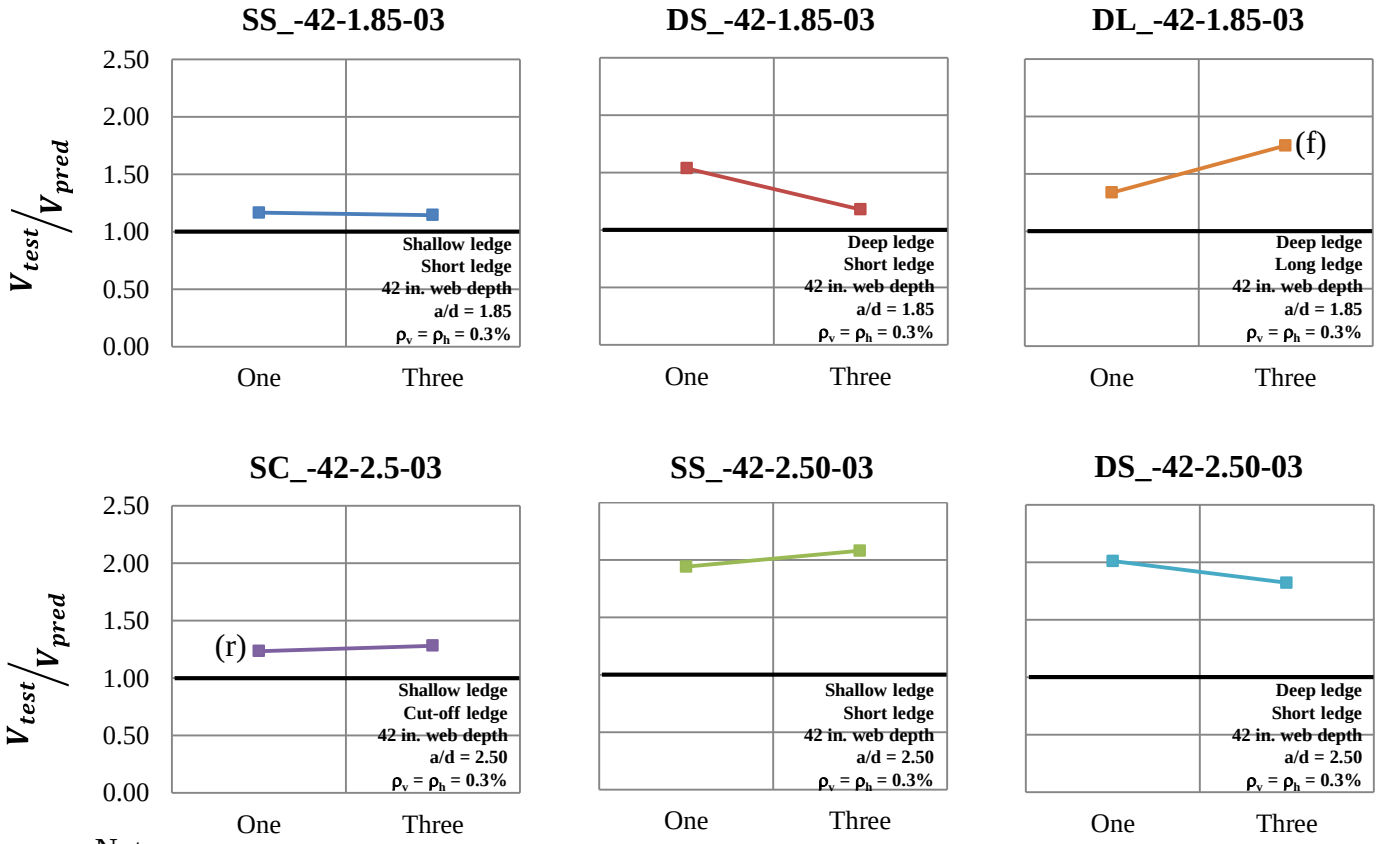

Note:

(f) Flexural failure

(r) Shear friction failure of the web-to-ledge interface

Figure 4-22: Series IV: Number of Point Loads: comparisons V_{test}/V_{pred}

V_{test}/V_{pred} ratios varied between 1.15 and 2.08. It is important to note that all points fall above 1.0, which indicates that the STM provisions of TxDOT Project 5253 produced conservative strength estimates for the twelve inverted-T specimens of the number of point loads series. No clear trend can be observed in the results presented in Figure 4-22; contradictory results can be observed in some cases, whereas in others similar conservatism is observed for comparable specimens with one and three loading points. Ultimately, it can be concluded that the number of loading points has no significant effect in the conservatism of the STM provisions of TxDOT Project 5253 applied to inverted-T specimens. Thus STM provisions are equally conservative and applicable to one- and three-point loaded beams regardless of whether beams are defined as deep or not by any definition of shear span.

4.6.5 Summary of Series IV: Number of Point Loads

Direct comparisons have been presented in this section to evaluate the influence of number of point loads in strength, appearance of first diagonal crack, crack width progression, and performance of STM design provisions of TxDOT Project 5253.

Results have shown that the number of point loads has no significant effect on the strength, crack width progression, or the conservatism of the STM provisions of TxDOT Project 5253. Regarding the appearance of the first diagonal cracking, no trend was observed, but only three pairs of comparable specimens were available for this task. More data is necessary to substantiate that conclusion.

STM design provisions of TxDOT Project 5253 provided conservative estimates of strength for the twelve specimens evaluated in this series. Additionally, it can be concluded that the STM provisions of TxDOT Project 5253 adequately capture the behavior of specimens with single or multiple point loads, regardless of ledge geometry or reinforcement conditions present in the specimens.

4.7 SUMMARY

Experimental results of specimens tested within TxDOT Project 0-6416 were presented. General information regarding the evaluation of strength and serviceability

criteria was presented with discussions on the normalization of strength results, the evaluation of the applied shear force on a specimen, the extraction of the shear force at first inclined cracking, and the assumptions on load spread under the applied ledge loads. Effects of ledge length, ledge depth, and number of point loads on strength and serviceability of the experimental specimens were presented in detail. The accuracy of the STM design provisions of TxDOT Project 5253 was evaluated with respect to capturing the effects of ledge geometry and number of point loads on the strength of inverted-T specimens.

Strain gauge measurements indicated that the 45-degree load spread assumption is reasonable and conservative. Similar strain distributions were observed in most specimens; these findings are consistent with those reported by Garber (2011). It is therefore recommended to calculate the hanger tie widths assuming a 45-degree load spread from the loading plates.

Results showed that increasing the ledge length increased web-shear strength, delayed the appearance of the first diagonal cracking, and increased conservatism of the strength estimations using the STM design provisions of TxDOT Project 5253. Ledge length had no significant effect on crack width progression.

Ledge depth had no significant effect on the strength, crack width progression, or the conservatism of the STM provisions of TxDOT Project 5253. However, it was observed that increasing the ledge depth delayed the appearance of the first diagonal cracking.

Results showed that the number of point loads had no significant effect on strength, crack width progression, or the conservatism of the STM provisions of TxDOT Project 5253; which adequately captured the behavior of specimens with single or multiple point loads, regardless of ledge geometry or reinforcement conditions present in the specimens. Regarding the appearance of the first diagonal cracking, no trend was observed with respect to number of point loads, but only three pairs of comparable specimens were available for this task. More data are necessary to substantiate that conclusion.

STM design provisions of TxDOT Project 5253 provided conservative estimates of strength for all thirty one specimens of the experimental program.

CHAPTER 5
Analysis of Results

5.1 OVERVIEW

In this section results from the experimental program are used to evaluate the accuracy of the following design provisions:

- Sectional shear and special provisions for beam ledges of AASHTO LRFD bridge design specifications 2012
- Sectional shear and special provisions for beam ledges of TxDOT bridge design manual LRFD 2011
- STM provisions of TxDOT project 5253 as implemented in this work for inverted-T beams (Section 2.5.1)

The application of STM for inverted-T specimens is discussed in light of test results. Design recommendations for strength and serviceability are made. An empirical equation is proposed to limit shear stresses in the bent caps under service loads and reduce the probability of diagonal cracking. Web reinforcement ratios are evaluated for crack control under service loads.

5.2 EVALUATION OF DESIGN PROVISIONS

A summary of the V_{test} / V_{pred} results for the three design methods is provided in Table 5-1. Highlighted in the table are values of V_{test} / V_{pred} that are lower than 1.2. Table 5-1 also summarizes the observed failure modes and predicted failure modes for all specimens. From test observations it was difficult to distinguish between node and strut crushing. Both failure modes are termed as direct-strut crushing. Since TxDOT bridge design manual LRFD (2011) provisions follow closely those of AASHTO (2012), both documents produced the same estimates for all tests. Specimens were designed using the STM provisions of TxDOT project 5253.

Table 5-1: V_{test} / V_{pred} results for STM 5253 and AASHTO/TxDOT LRFD provisions

				STM TxDOT 5253			AASHTO/TxDOT LRFD		
Test	Specimen	V_{test}	Observed Failure Mode	V_{pred}	V_{test} / V_{pred}	Design Controlling Element	V_{pred}	V_{test} / V_{pred}	Design Controlling Element
		kips		kips	ratio		kips	ratio	
01a	DS1-42-1.85-03	712	Direct-Strut Crushing	463	1.54	STNI at support	238	2.99	Shear Stirrups
01b	DS1-42-2.50-03	406	Sectional Shear	202	2.01	Intermediate tie	240	1.69	Shear Stirrups
02a	DS1-42-1.85-06	621	Direct-Strut Crushing	479	1.30	STNI at support	362	1.71	Shear Stirrups
02b	DS1-42-2.50-06	503	Sectional Shear	338	1.49	Intermediate tie	363	1.39	Shear Stirrups
03a	DL1-42-1.85-06	741	Direct-Strut Crushing	464	1.60	STNI at support	359	2.07	Shear Stirrups
03b	DL1-42-2.50-06	622	Sectional Shear	353	1.76	Intermediate tie	316	1.97	Shear Friction Steel
04a	SS3-42-1.85-03	523	Direct-Strut Crushing	456	1.15	STNI at support	255	2.05	Shear Stirrups
04b	SS3-42-2.50-03	447	Sectional Shear	215	2.08	Intermediate tie	255	1.75	Shear Stirrups
05b	SS3-42-2.50-06	516	Flexure Failure	415	1.24	Intermediate tie	377	1.37	Shear Stirrups
06a	SC3-42-2.50-03	329	Sectional Shear	257	1.28	Intermediate tie	249	1.33	Shear Stirrups
06b	SC3-42-1.85-03	483	Direct-Strut Crushing	427	1.13	STNI at support	249	1.94	Shear Stirrups
07a	SS1-75-1.85-03	913	Punching Shear	628	1.45	Hanger tie	387	2.36	Shear Friction Steel
08b	SS1-75-2.50-06	688	Punching Shear	474	1.45	Hanger tie	293	2.35	Shear Friction Steel
09a	DS3-42-2.50-03	430	Sectional Shear	236	1.82	Intermediate tie	248	1.74	Shear Stirrups
10a	DL1-42-1.85-03	626	Direct-Strut Crushing	468	1.34	STNI at support	237	2.64	Shear Stirrups
10b	DL1-42-2.50-03	510	Sectional Shear	235	2.17	Intermediate tie	197	2.59	Shear Friction Steel
11a	SL3-42-1.85-03	571	Direct-Strut Crushing	409	1.39	STNI at support	240	2.38	Shear Stirrups
12a	SL3-42-1.85-06	744	Direct-Strut Crushing	424	1.76	STNI at support	381	1.95	Shear Stirrups
14a	SS1-75-1.85-03b	745	Direct-Strut Crushing	361	2.06	STNI at support	358	2.08	Punching Shear
15a	DC3-42-1.85-03	395	Direct-Strut Crushing	370	1.07	STNI at support	231	1.71	Shear Stirrups
15b	DS3-42-1.85-03	454	Direct-Strut Crushing	389	1.17	STNI at support	231	1.96	Shear Stirrups
16a	SS1-42-2.50-03	398	Sectional Shear	213	1.87	Intermediate tie	252	1.58	Shear Stirrups
16b	SS1-42-1.85-03	583	Direct-Strut Crushing	503	1.16	STNI at support	252	2.32	Shear Stirrups
17a	DC1-42-2.50-03	365	Sectional Shear	250	1.46	Intermediate tie	220	1.66	Shear Stirrups
17b	DL3-42-1.85-03	629	Flexure Failure	359	1.75	STNI at support	223	2.82	Shear Stirrups
18a	SL1-42-2.50-03	498	Sectional Shear	269	1.85	Intermediate tie	229	2.18	Shear Stirrups
18b	SC1-42-2.50-03	319	Shear Friction	258	1.24	Intermediate tie	229	1.40	Shear Stirrups
19a	DS1-42-1.85-06/03	539	Direct-Strut Crushing	361	1.49	STNI at support	319	1.69	Shear Stirrups
19b	DS1-42-2.50-06/03	739	Sectional Shear	417	1.77	Intermediate tie	422	1.75	Shear Stirrups
20a	SC1-42-1.85-03	451	Ledge Tie	444	1.02	STNI at comp chord	236	1.91	Shear Stirrups
20b	DC1-42-1.85-03	517	Direct-Strut Crushing	460	1.12	STNI at comp chord	231	2.24	Shear Stirrups

5.2.1 Failure Modes

Web-shear failure was observed in all tests except six in which flexure, punching shear, or ledge tie failures were observed (tests 05b, 07a, 08b, 17b, 18b, and 20a).

For test 05b, a flexural mode of failure was observed. STM and both LRFD provisions predicted web shear failures. However, STM only estimated flexural capacity to be 6% higher than web shear while the LRFD methods estimated flexural capacity to be 13% higher than web shear capacity (from Tables 3-8 to 3-10 in Chapter 3).

Test 07a was originally designed to fail in web-shear based on specified material strengths. However, after updating the design with the measured material strengths hanger reinforcement governed the design, with an over strength in web-shear strength of 10%. Punching shear failure was observed for this specimen. A shear friction failure was predicted by sectional shear provisions, with a 20% over strength for web-shear.

Punching shear failure of the ledge was observed in test 08b. Beam capacity according to STM was governed by two critical elements with approximately the same strength: web-shear and hanger reinforcement. According to sectional shear provisions shear friction failure of the ledge was anticipated, with over strengths of 14% and 19% for web-shear and punching shear respectively.

Test 17b failed in flexure. STM design was controlled by web-shear strength with an over strength of 38% for flexure. Sectional shear design was controlled by web-shear as well, with an over strength of 28% for flexure. It is important to note that the specimen maximum strength was well above the estimated strengths with V_{test}/V_{pred} ratios of 1.75 for the STM provisions and 2.82 for the sectional shear provisions.

Shear friction failure of the ledge was observed in test 18b. STM design was controlled by web shear, with over strengths of 83% and 135% for the ledge tie and strut respectively. No indication of local failure was anticipated in the design phase. It is important to mentions that this specimen had a shallow, cut-off ledge and a single loading point. However, the V_{test}/V_{pred} ratio was still 24% conservative for the STM provisions. Sectional shear design predicted a web-shear failure as well, with the next critical element being punching shear with an over strength of 21%.

Test 20a sustained a local failure in the ledge. This specimen also had a shallow, cut-off ledge and a single loading point. STM design was governed by web shear; however, ledge strut and ledge tie were just 10% stronger than the weakest failure mode. Hanger reinforcement had an over strength of 20%. Sectional shear design was controlled by web-shear with no indications of any other failure mode being close to governing specimen strength.

All observed web shear failures were correctly predicted by the STM provisions of TxDOT project 5253. AASHTO (2012) and TxDOT Bridge Manual (2011) correctly predicted web-shear failures for most tests that failed by web-shear, except for tests 03b, 10b, and 14a for which the predicted failure modes were shear friction, shear friction, and punching shear respectively. For those tests however, the estimated web-shear capacity according to LRFD methods was only slightly larger than that of the estimated weakest failure mode. In fact, web-shear was estimated at only 14%, 20% and 7% higher than the weakest failure modes for tests 03b, 10b, and 14a respectively (from Tables 3-9 and 3-10 in Chapter 3).

In all cases where local ledge failure was observed ledges were shallow and either short or cut-off. The observation indicates that all design methods may not be as conservative when estimating the strength of shallow ledges that are short or cut-off, as they are when estimating other element strengths. The observation also supports findings presented in Chapter 4 that showed a reduction in STM design conservatism as the ledge length diminishes.

In conclusion, the STM provisions, as well as the LRFD provisions, estimated the observed failure modes reasonably well. The STM provisions, however, were able to predict the correct mode of failure for 25 out of the 31 tests as opposed to only 22 out of 31 for the LRFD provisions. For both STM and LRFD, when the observed failure mode was not correctly predicted, the observed failure mode was usually the second weakest predicted mode of failure with an over-strength of less than 20% over the weakest predicted failure mode.

5.2.2 Maximum Strength

Ratios of V_{test} / V_{pred} for the 31 tests of the experimental program are compared in Figure 5-1 for the STM and LRFD design procedures. As can be seen in Figure 5-1, all ratio values fall above 1.0 for all methods, indicating that the three design methods yielded conservative estimations of strength. However, the STM provisions provided more accurate strength estimates than the LRFD methods (Figure 5-1 and Table 5-2). As summarized in Table 5-2, the mean strength-ratio of all tests for the STM provisions is

1.52 as opposed to 1.99 for the LRFD provisions (more than a 30% difference). The standard deviation of the ratios for STM is 0.33 compared to 0.43 for the LRFD methods; which indicates less scatter in the STM strength estimates.

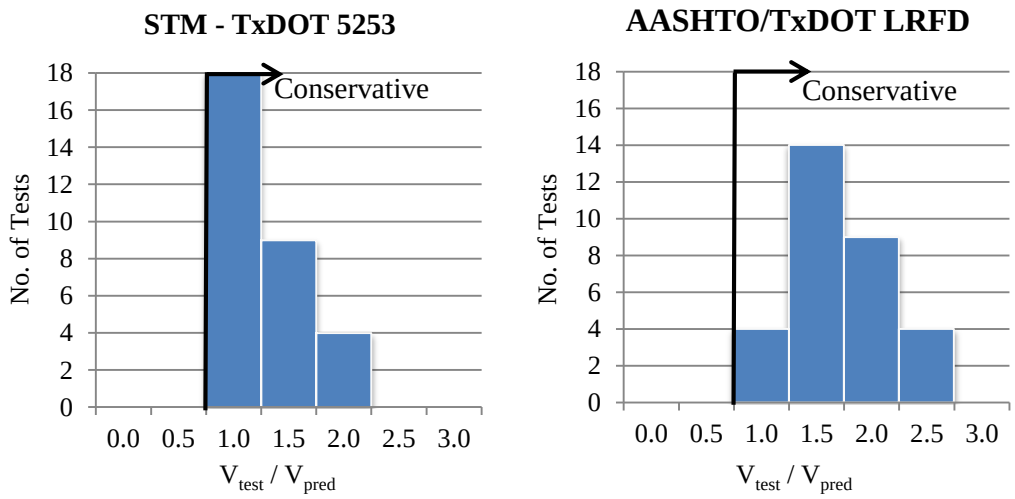

Figure 5-1: Range of experimental / calculated strengths from the experimental program

Table 5-2: Overall accuracy of inverted-T provisions

	Vtest / Vpred	
n = 31	**STM TxDOT 5253**	**AASHTO / TxDOT LRFD**
Min	1.02	1.33
Max	2.17	2.99
Mean	1.52	1.99
Unconservative*	0%	0%
Std deviation	0.33	0.43
COV**	0.22	0.21

n = number of tests under analysis

* Unconservative = percentage of tests for which Experimental / Predicted < 1.0

** COV = Coefficient of Variation = Standard Deviation / Mean

5.2.2.1 Effects of Number of Point Loads

Designs using the AASHTO and TxDOT LRFD codes were calculated using the sectional shear approach as specified in AASHTO Art. 5.8.3.4.1. AASHTO requires specimens in which the distance between the centers of applied load and the supporting reaction is less than about twice the member thickness to be designed using the STM provisions (AASHTO Art. 5.6.3.1). This shear span definition could be interpreted as the distance between the center of the reaction and the resultant of the load; therefore, specimens with a single loading point and *a/d* ratio of 1.85 (as defined in this dissertation) should be designed for web shear using STM provisions, and specimens with three loading points using the sectional shear approach, since for both *a/d* = 1.85 and 2.5, the center of the applied load coincides with that of the center load (Figure 5-2). For these specimens, even though 33% of the load is concentrated within a distance of 2d from the support, sectional shear design could be considered as recommended by AASHTO. If we consider the typical configuration of the inverted-T bent caps in the field, most if not all have multiple loading points, and consequently allowed to be designed using the sectional shear approach by the AASHTO code.

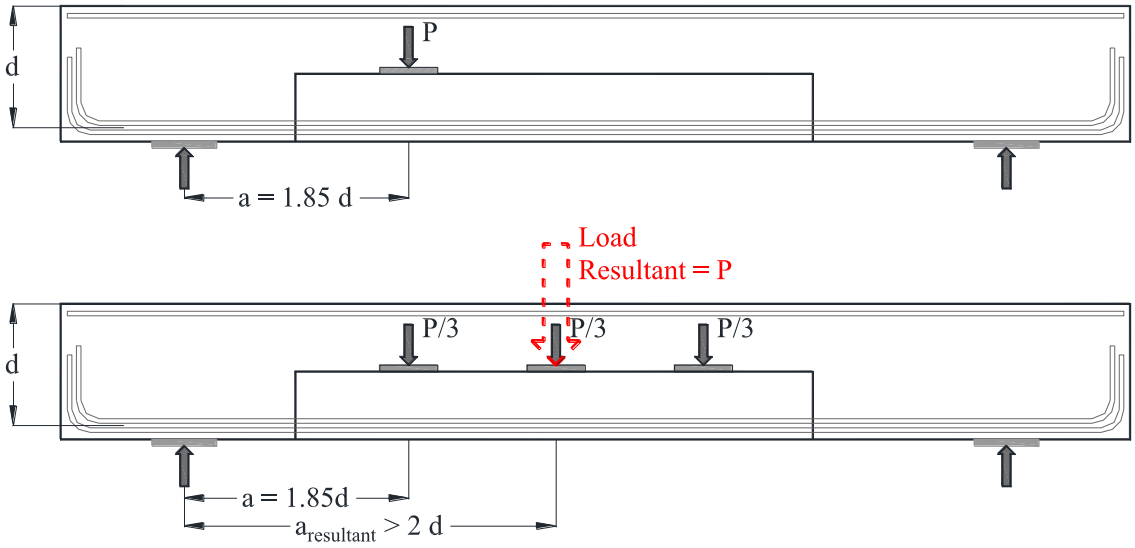

Figure 5-2: AASHTO a/d limit for sectional shear design

Recall that the definition of *a/d* within the context of this dissertation is taken similarly to that of ACI 318-011 as the ratio of the distance from the center of the support to the center of the nearest loading point (a) with respect to the effective depth of the specimen (d) measured from the centroid of web longitudinal tension steel to the extreme compression fiber of the web. ACI 318-11 (Art. 11.7.1) requires deep beam provisions to be applied for "members with $\boldsymbol{l_n}$ not exceeding ***4h*** or regions of beams with concentrated loads within a distance ***2h*** from the support that are loaded on one face and supported on the opposite face so that compression struts can develop between the loads and supports."

Typically, sectional shear design will produce web shear capacities that are smaller or similar to those produced by STM. The AASHTO definition of shear span allows more beams to be designed using sectional shear than the ACI 318-11 definition and should therefore inherently produce overall more conservative shear strength estimates. The validity of both shear span definitions is explored based on test results from this experimental program.

Specimens with *a/d* ratio of 2.50 were designed to fail at the intermediate ties (yielding of the transverse reinforcement in the shear span). For that failure mode, the shear strengths estimated by both STM and LRFD methods are directly dependent on the amount and strength of transverse steel within the shear span. Hence, STM and LRFD are expected to produce similar shear strength results. Most specimens with an *a/d* ratio of 2.50 failed by yielding of the web transverse reinforcement. Thus it is not surprising that both STM and LRFD methods produced similar shear strength estimates, as can be seen in Figure 5-3 and Table 5-3.

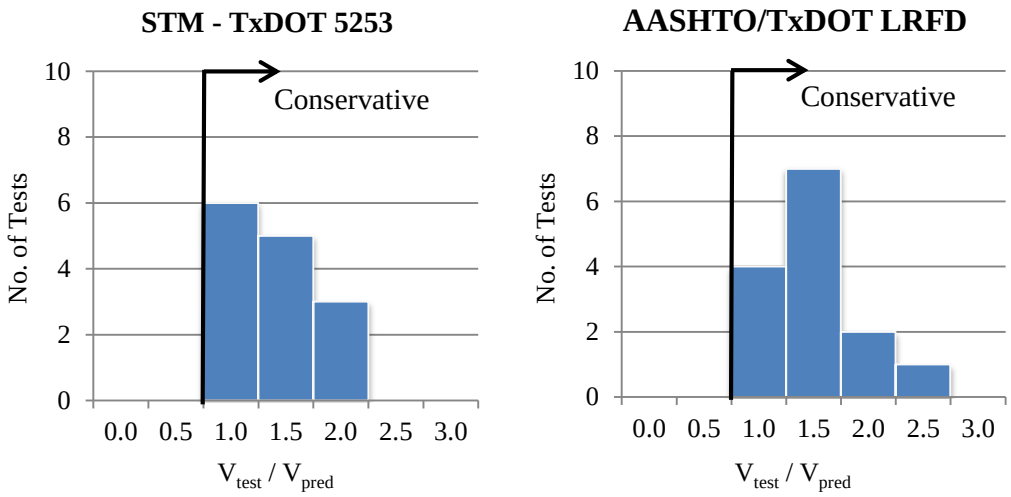

Figure 5-3: Test specimens with a/d ratios of 2.50

Table 5-3: Test specimens with a/d ratios of 2.50

	Vtest / Vpred	
n = 14	**STM TxDOT 5253**	**AASHTO / TxDOT LRFD**
Min	1.24	1.33
Max	2.17	2.59
Mean	1.68	1.77
Unconservative*	0%	0%
Std deviation	0.32	0.38
COV**	0.19	0.22

n = number of tests under analysis

* Unconservative = percentage of tests for which
Experimental / Predicted < 1.0

** COV = Coefficient of Variation = Standard Deviation / Mean

On the other hand, most specimens with *a/d* ratios of 1.85 failed by crushing of the direct strut or STNI (strut-to-node-interface) of this strut. Since sectional design does not account for that failure mode and estimates web shear-strength based on the weaker tie-yielding mode, it was not surprising to find that LRFD sectional design produced very conservative estimates while STM produced more accurate estimates for specimens with *a/d* = 1.85 (Figure 5-4 and Table 5-4).

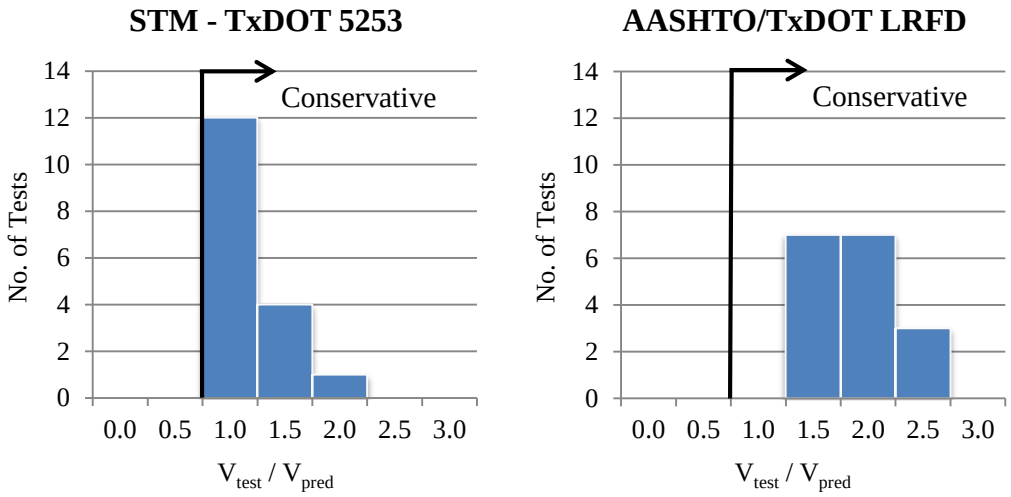

Figure 5-4: Test specimens with a/d ratio of 1.85

Table 5-4: Test specimens with a/d ratio of 1.85

	Vtest / Vpred	
n = 17	**STM TxDOT 5253**	**AASHTO / TxDOT LRFD**
Min	1.02	1.69
Max	2.06	2.99
Mean	1.38	2.17
Unconservative*	0%	0%
Std deviation	0.29	0.38
COV**	0.21	0.18

n = number of tests under analysis

* Unconservative = percentage of tests for which
Experimental / Predicted < 1.0

** COV = Coefficient of Variation = Standard Deviation / Mean

Specimens with an *a/d* ratio of 1.85 (as defined in this project) and three loading points are defined as non-deep by AASHTO and TxDOT LRFD provisions but as deep by ACI 318-11. Therefore sectional design is required by the LRFD methods while STM is required by ACI 318-11 for those specimens. V_{test} / V_{pred} ratios for specimens with an *a/d* ratio of 1.85 and three loading points are presented in Figure 5-5 and summarized in Table 5-5. As can be seen in the figure and table, STM provisions are significantly more

accurate than sectional shear provisions, with mean values of V_{test} / V_{pred} of 1.34 and 2.12 respectively.

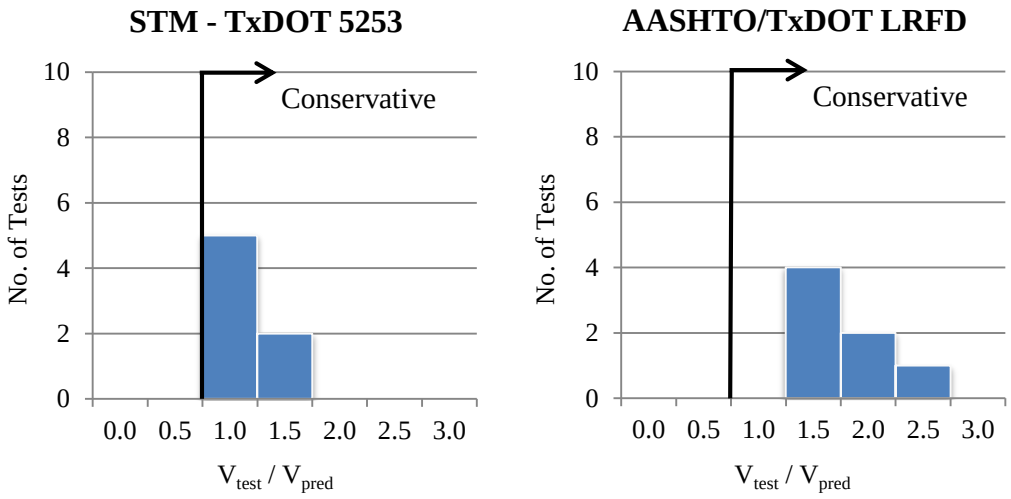

Figure 5-5: Test specimens with a/d ratio of 1.85 and multiple loading points

Table 5-5: Test specimens with a/d ratio of 1.85 and multiple loading points

	Vtest / Vpred	
n = 7	**STM TxDOT 5253**	**AASHTO / TxDOT LRFD**
Min	1.07	1.71
Max	1.76	2.82
Mean	1.34	2.12
Unconservative*	0%	0%
Std deviation	0.30	0.37
COV**	0.22	0.17

n = number of tests under analysis

* Unconservative = percentage of tests for which Experimental / Predicted < 1.0

** COV = Coefficient of Variation = Standard Deviation / Mean

Thus sectional shear provisions, as mandated per AASHTO/TxDOT LRFD, result in over conservative designs for specimens with three point loads and an *a/d* ratio of 1.85 (as defined in this project). Deep beam provisions (or STM) may therefore be more

appropriate for specimens in which at least 33% of the total load is concentrated within a distance of twice the depth of the member from the center of the support (Figure 5-2). The experimental program however only included specimens with one and three concentrated loads. As the number of point loads increases, the percentage of load that is applied within a distance of 2.0d from the support diminishes. It is probable that a smaller percentage of the total load (e.g. 25%, 20%) applied within a distance of 2.0d from the support will be enough to result in deep beam behavior (Figure 5-6). However, further research is required to identify the minimum amount of concentrated load that needs to be applied within a distance of 2.0 *d* from the support for deep beam behavior to dominate.

It is important to note here that the AASHTO and TxDOT LRFD definition of shear span results in conservative web-shear estimates, albeit perhaps too conservative for shorter beams with few point loads. However, since STM is applicable for both sectional-shear and deep-beam cases, defining the shear span according to ACI 318-11 should result in more accurate yet still conservative estimates of shear strength for inverted-T beams.

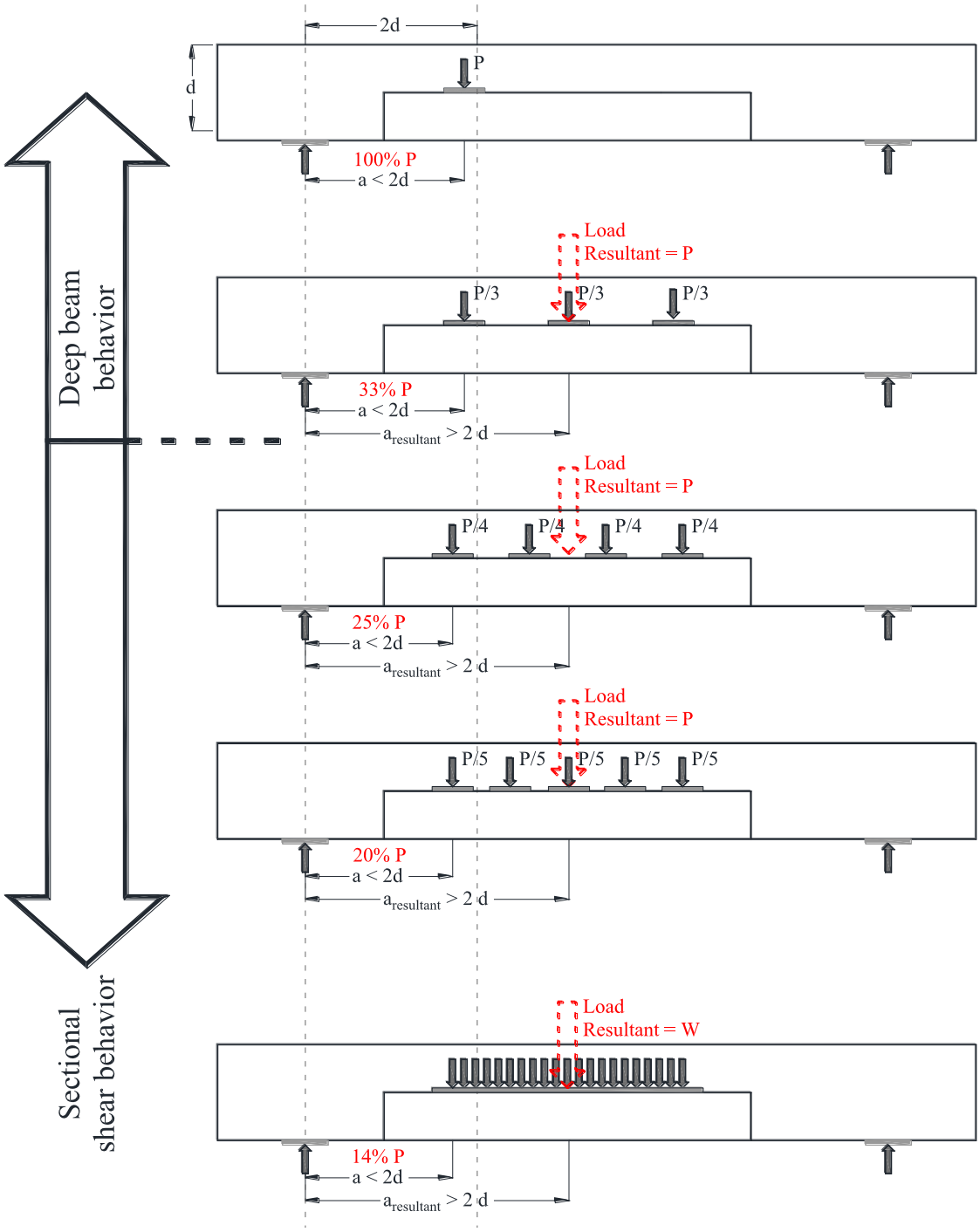

Figure 5-6: Deep beam-sectional shear limit

5.2.2.2 Effects of Ledge Geometry

Strength ratios (V_{test} / V_{pred}) using the STM and LRFD provisions are presented in Figure 5-7, grouping the thirty one tests of the experimental program according to their ledge lengths. As can be observed in the figure, the general averages for the entire experimental program confirm the trend presented in Chapter 4 for directly comparable specimens, in which an increase in conservatism was observed as the ledge length increased. General strength averages for cut-off, short, and long ledges were 1.19, 1.57, 1.70 for STM provisions and 1.74, 1.92, 2.32 for LRFD provisions. The same trend is observed with both set of provisions, but with different degrees of conservatism; conservatism observed in long ledges was 43% higher than that of cut-off ledges for STM provisions, and 33% higher considering the LRFD provisions. It is not surprising to observe that the highest strength ratio (2.17) was found for a long ledge specimen, whereas the lowest (1.02) corresponded to a cut-off ledge specimen; based on STM provisions.

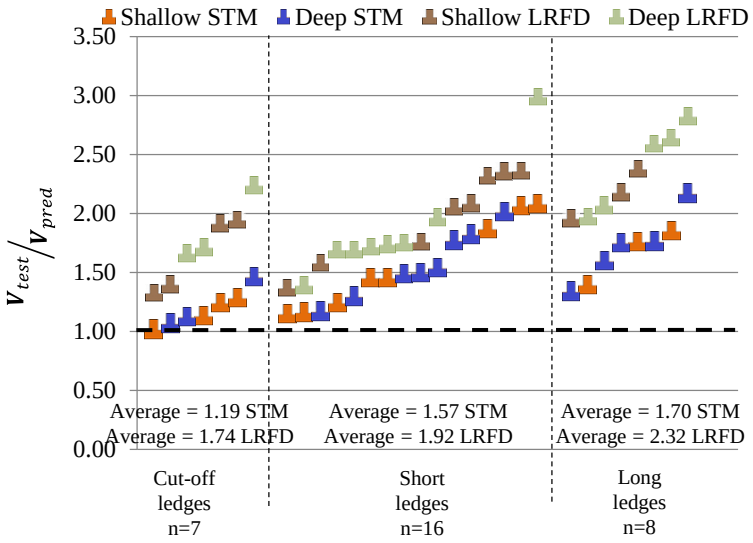

Figure 5-7: STM and LRFD strength predictions for different ledge lengths

Strength ratios of the thirty one tests of the experimental program are grouped according to their ledge depth in Figure 5-8. General averages for deep and shallow ledges are very similar (5% difference using STM and 6% using LRFD), confirming the

trend observed in the direct comparisons of Chapter 4; ledge depth has no significant effect on the conservatism of the STM provisions to estimate web-shear strengths.

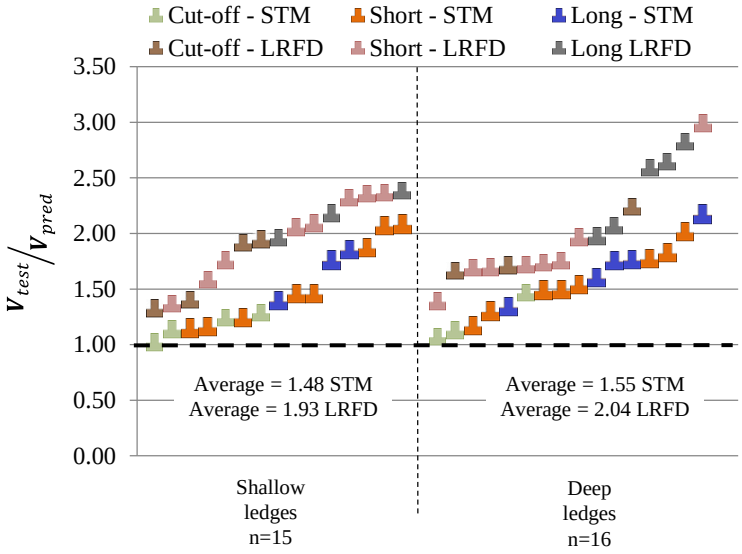

Figure 5-8: STM and LRFD strength predictions for different ledge depths

Results in this section indicate that using cut-off ledges reduces significantly the conservatism of the STM provisions. Although all the strength ratios were conservative, it may be preferable to avoid cut-off ledges in practice, since many uncertainties in the field may further diminish the shear strength of the members and potentially render unsafe conditions. While short and long ledges are suitably treated by STM provisions, it is recommended to use long ledges whenever possible.

Effects of ledge depth on web-shear strength are adequately captured by the strut-and-tie model presented in Chapter 2. It is important to mention that most of the designs of the specimens in the experimental program were controlled by web-shear as ledge failures were not within the scope of this study. Therefore, no data is available to evaluate the effects of further reductions of ledge depth. However, STM provisions mandate a minimum angle of 25 degrees between a strut and a tie; a minimum ledge depth is implicit in this provision. Therefore, no further recommendations are made regarding ledge depths.

5.2.3 Summary

A summary of the comparisons of V_{test} / V_{pred} is provided in Table 5-6. It can be observed from the table that all methods yielded conservative results in all cases. However in every comparison, the most accurate method for estimating web shear-strength is STM; especially for shear span-to-depth ratios of 1.85 (deep beam behavior). Additionally, STM was found to offer a more rational approach to designing inverted-T deep beams, which inherently considers all failure modes for the ledges, web, and bearing points, and can be used for deep and non-deep beams.

Table 5-6: Range of experimental / predicted shear strength results

	n = 31 All specimens		**n = 14 Specimens with a/d = 2.50**		**n = 17 Specimens with a/d = 1.85**		**n = 7 Specimens with a/d = 1.85, and multiple loads**	
V_{test}/V_{pred}	**STM TxDOT 5253**	**AASHTO/ TxDOT LRFD**	**STM TxDOT 5253**	**AASHTO/ TxDOT LRFD**	**STM TxDOT 5253**	**AASHTO/ TxDOT LRFD**	**STM TxDOT 5253**	**AASHTO/ TxDOT LRFD**
Min	1.02	1.33	1.24	1.33	1.02	1.69	1.07	1.71
Max	2.17	2.99	2.17	2.59	2.06	2.99	1.76	2.82
Mean	1.52	1.99	1.68	1.77	1.38	2.17	1.34	2.12
Unconservative*	0%	0%	0%	0%	0%	0%	0%	0%
Std deviation	0.33	0.43	0.32	0.38	0.29	0.38	0.30	0.37
COV**	0.22	0.21	0.19	0.22	0.21	0.18	0.22	0.17

n = number of tests under analysis

* Unconservative = percentage of tests for which Experimental / Predicted < 1.0

** COV = Coefficient of Variation = Standard Deviation / Mean

Regarding ledge geometry, cut-off ledges are not recommended in practice due to the low conservatism observed in strength estimates of specimens with cut-off ledges. The shear strength of specimens with short and long ledge are adequately estimated by all design methods, however long ledges are recommended to be used whenever possible for the higher conservatism in their strength estimations. Additionally, ledge depth must be such that the angle between the horizontal tie and the diagonal strut in the cross sectional STM is not less than 25 degrees.

5.3 SERVICEABILITY EVALUATION

Serviceability criteria for inverted-T bent caps are evaluated in this section. An empirical equation to estimate the load at first diagonal cracking is evaluated, and

reinforcement requirements to adequately control crack widths and distribution are discussed.

5.3.1 First Diagonal Cracking under Service Loads

For durability considerations, it is important to limit diagonal cracking under service loads in reinforced concrete members. In this section, trends between the shear force at first diagonal cracking and pertinent variables are investigated. An empirical equation proposed by TxDOT Project 5253 relating first cracking to the *a/d* ratio and concrete strength is investigated for applicability to inverted-T beams.

Since cracking is expected in reinforced concrete structures for reinforcing steel to be engaged, provisions to completely eliminate cracking under service loads are impractical. However, to extend the lifespan of reinforced concrete structures, it is important to reduce the probability of cracking and minimize crack widths to tolerable levels at service loads.

The main types of cracks in inverted-T beams are depicted in Figure 5-9. The focus of this project is on web-shear cracks and flexure-shear cracks. No difference has been made in this study between these two types of cracks. Flexural and punching shear cracks are not considered in the following discussions.

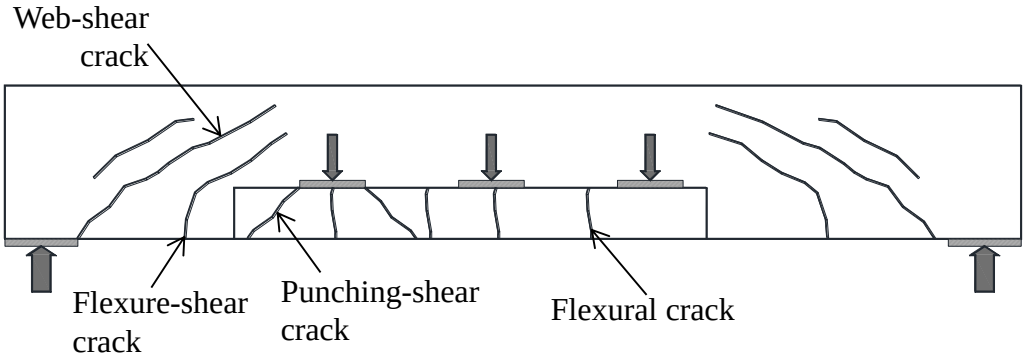

Figure 5-9: Types of cracks in inverted-T deep beams

ACI-ASCE Committee 326 report (1962) identified the major variables that affect the diagonal cracking load of reinforced concrete beams. These variables are: (1) section size ($b_w d$), (2) tensile strength of concrete that is related to $\sqrt{f'_c}$, (3) longitudinal

reinforcement ratio (ρ_l), and (4) moment to shear ratio at the critical section (*M/V*). Since *M/V* is constant in the main shear span of beams loaded with concentrated loads, the shear span-to-depth ratio (*a/d*) can be used in lieu of *M/V*. Trends between the load at first diagonal cracking (V_{cr}) and the variables listed above are investigated for tests in the evaluation database and specimens of the experimental program for which cracking information was available; as listed in Table 5-7 and shown in Figure 5-10 to Figure 5-13.

Table 5-7: Specimens in first diagonal cracking evaluation

Test	Specimen	Vcrack	ρ_v	ρ_h	a/d ratio
01a	DS1-42-1.85-03	172	0.3%	0.3%	1.85
02a	DS1-42-1.85-06	188	0.6%	0.6%	1.85
03a	DL1-42-1.85-06	168	0.6%	0.6%	1.85
04a	SS3-42-1.85-03	126	0.3%	0.3%	1.85
04b	SS3-42-1.85-06 (f)	151	0.6%	0.6%	1.85
5b	SS3-42-2.50-06 (f)	115	0.6%	0.6%	2.50
6a	SC3-42-1.85-03	113	0.3%	0.3%	1.85
6b	SC3-42-2.50-03	90	0.3%	0.3%	2.50
7a	SS1-75-1.20-06 (p)	264	0.6%	0.6%	1.20
8b	SS1-75-2.50-06 (p)	232	0.6%	0.6%	2.50
9a	DS3-42-1.85-03	282	0.3%	0.3%	1.85
10a	DL1-42-1.85-03	242	0.3%	0.3%	1.85
11a	SS3-42-2.50-03	109	0.3%	0.3%	2.50
12a	DC1-42-1.85-06	107	0.6%	0.6%	1.85
14a	SS1-75-1.85-03b	346	0.3%	0.3%	1.85
15a	DC3-42-1.85-03	152	0.3%	0.3%	1.85
15b	DS3-42-1.85-03	164	0.3%	0.3%	1.85
16a	SS1-42-1.85-03	157	0.3%	0.3%	1.85
17a	DC1-42-2.50-03	70	0.6%	0.6%	1.85
18a	SL1-42-2.50-03	167	0.3%	0.3%	2.50
19a	DS1-42-1.85-6/3	64	0.6%	0.3%	1.85
20a	SC1-42-1.85-03 (lt)	127	0.3%	0.3%	1.85

(f) Flexure failure

(p) Punching shear failure

(lt) Ledge tie failure

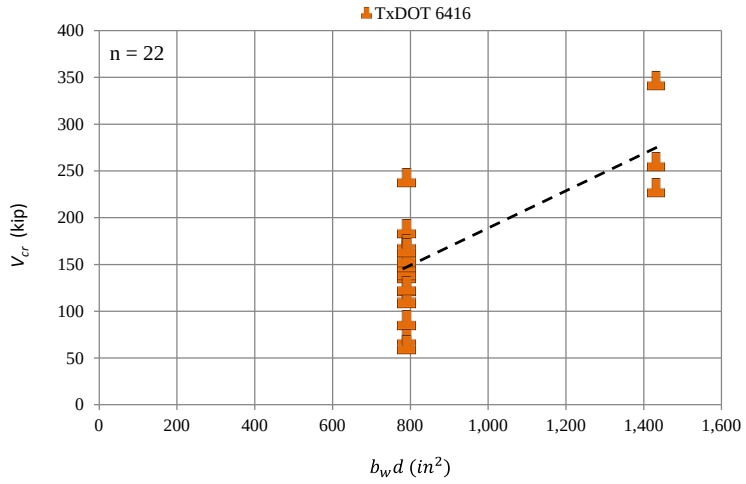

Figure 5-10: Effect of section size on diagonal cracking load of inverted-T beams

As expected, there is an increase in cracking load as the size of a beam section increases, as seen in Figure 5-10. There is however a lot of variability in cracking loads for specimens of a given section size. The scatter could be attributed to other variables.

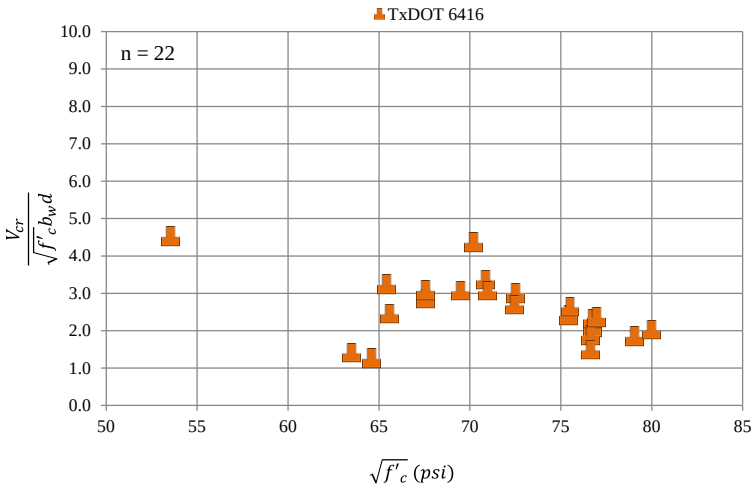

Figure 5-11: Effect of concrete tensile strength on diagonal cracking load of inverted-T beams

In Figure 5-11, the square root of the concrete compressive strength is used as a proxy for the tensile strength of concrete. No clear trend can be observed in Figure 5-11; a larger amount of data would be required to reveal any trend since most of the specimens shown in the figure had very similar concrete strengths. In order to isolate the effect of

the rest of the variables, the cracking load V_{cr} is normalized in the following figures by $b_w d$ and the square root of the concrete compressive strength.

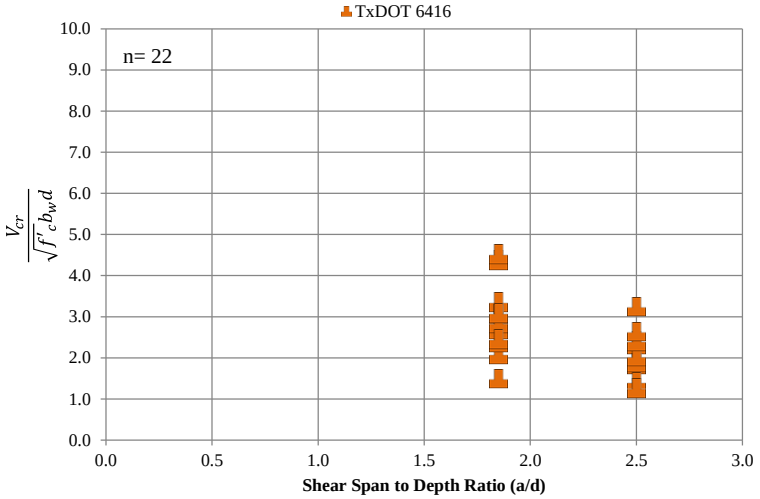

Figure 5-12: Effect of a/d ratio on diagonal cracking load of inverted-T beams

A large scatter is observed in Figure 5-12 for specimens with same *a/d* ratios. No clear trend is observed in the figure but a trend may be obscured by the effects of other variables. A wider range of *a/d* ratios may also help to reveal trends.

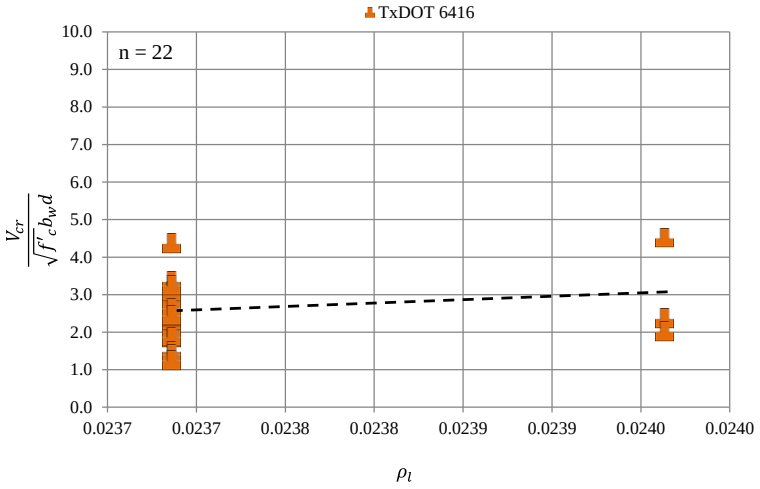

Figure 5-13: Effect of longitudinal reinforcement on diagonal cracking load of inverted-T beams with similar cross-section size

Only two different values of the reinforcement ratio are available in Figure 5-13, leaving not enough data to properly evaluate the effects of this variable.

A key observation form the figures above is that there is significant variability in the results. One constant in the results however is that in all cases $V_{cr} > \sqrt{f'_c} b_w d$ for inverted-T beams, a value that is half of that typically observed in slender rectangular beams ($2\sqrt{f'_c} b_w d$). This reduction in cracking strength seems reasonable considering the tension field induced in the web by the loading conditions. Concrete tensile strength and section size are the variables with more effects on the diagonal cracking load. Shear span-to-depth ratio and longitudinal reinforcement ratio were also found to have an effect on the diagonal cracking load.

An empirical equation incorporating all of these variables except the longitudinal reinforcement ratio was proposed by TxDOT project 5253 to provide a lower bound on the diagonal cracking load of rectangular beams. The equation allows for a serviceability check for which the estimated service loads must remain below the estimated cracking load. The equation was based on data from 59 tests of rectangular deep beams compiled in the aforementioned project.

$$\frac{V_{cr}}{\sqrt{f'_c} b_w d} = 6.5 - 3(a/d) \qquad \textit{(5-1)}$$

but not greater than $5\sqrt{f'_c} b_w d$ nor less than $2\sqrt{f'_c} b_w d$

where:

V_{cr}	=	diagonal cracking load (kip)
a	=	shear span (in.)
d	=	effective depth of the member (in.)
f'_c	=	compressive strength of concrete (psi)
b_w	=	web width of the member (in.)

The cracking load estimated by equation 5-1 is compared with the cracking loads of the 59 rectangular beam tests in Figure 5-14. It can be observed in the figure that the simple equation provides a reasonably conservative estimate on cracking loads for rectangular deep beams.

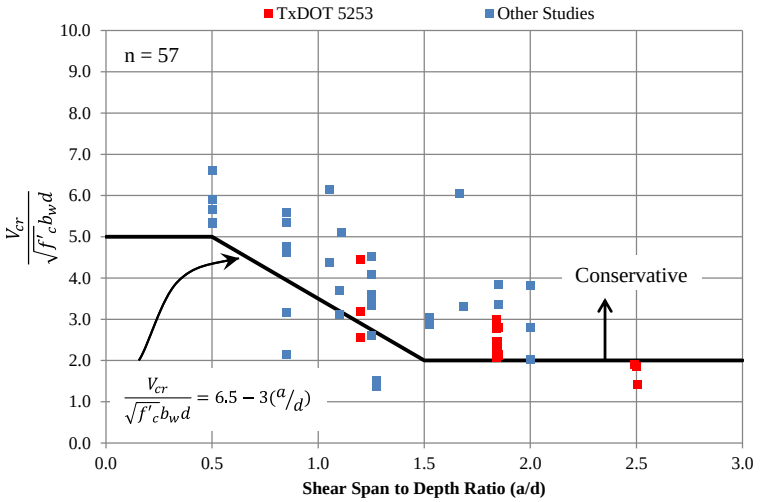

Figure 5-14: Diagonal cracking strength results and prediction for rectangular deep beams (adapted from Bircher, et al 2008).

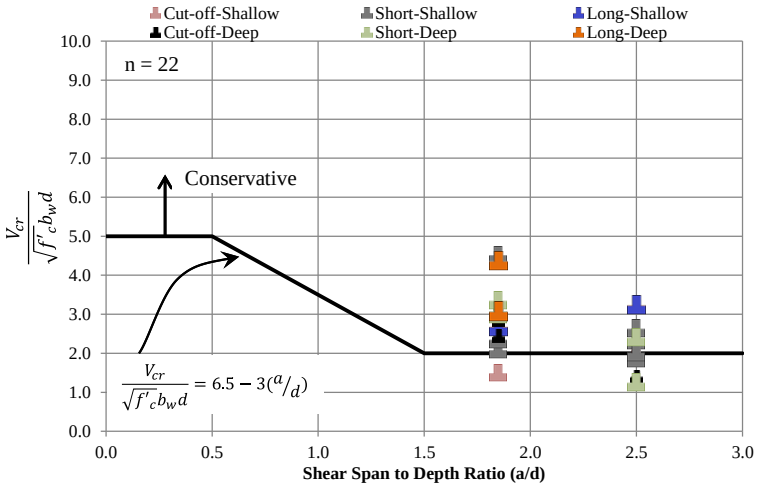

Figure 5-15: Measured diagonal cracking forces for different ledge configurations from the experimental program

The cracking loads of the inverted-T deep beams compiled in this study are shown in Figure 5-15 along with the estimated cracking load using equation 5-1. One should note that the *a/d* ratios shown in the figure above were calculated, as defined in this document, considering the distance between center of the support and the first concentrated load.

Equation 5-1, which was calibrated using rectangular beams, yields reasonably conservative estimates of diagonal cracking loads for inverted-T specimens. However, cracking loads of five specimens, with cut-off and short ledges, fall below their estimated cracking loads.

Ratios of measured diagonal cracking load (Vcr_{test}) to predicted diagonal cracking load (Vcr_{pred}) are plotted versus ledge length and ledge depth in Figure 5-16 and Figure 5-17. Values above 1.0 denote conservative estimations of the diagonal cracking load using equation 5-1.

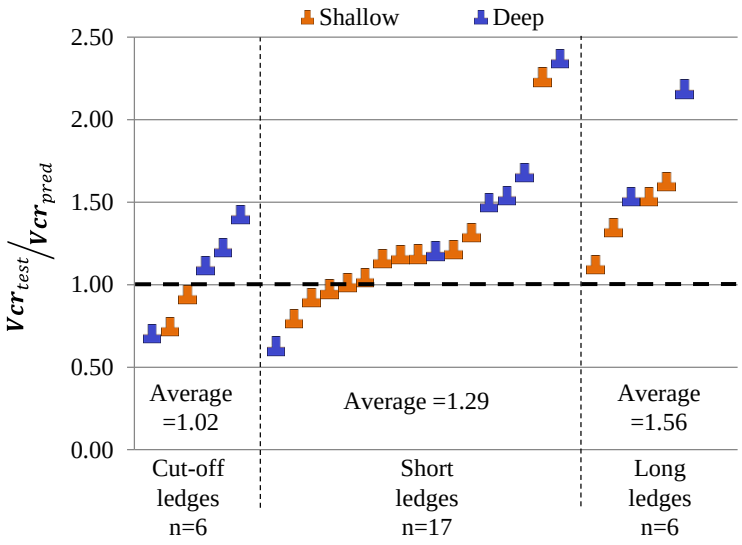

Figure 5-16: Ledge length effect on diagonal cracking load

Six specimens with cut-off ledges are shown in Figure 5-16 with 50% percent of them cracking below their predicted cracking load. The average Vcr_{test}/Vcr_{pred} ratio for the cut-off ledges was 1.02. Seventeen specimens with short ledges are shown in the figure, only four of them (24%) had a cracking ratio below 1.0; most of these had shallow ledges. The average Vcr_{test}/Vcr_{pred} ratio for the specimens with short ledges was 1.29. Six specimens with long ledges are shown in Figure 5-16, all of which cracked after reaching their predicted cracking load. The average Vcr_{test}/Vcr_{pred} ratio for long ledged specimens was 1.56.

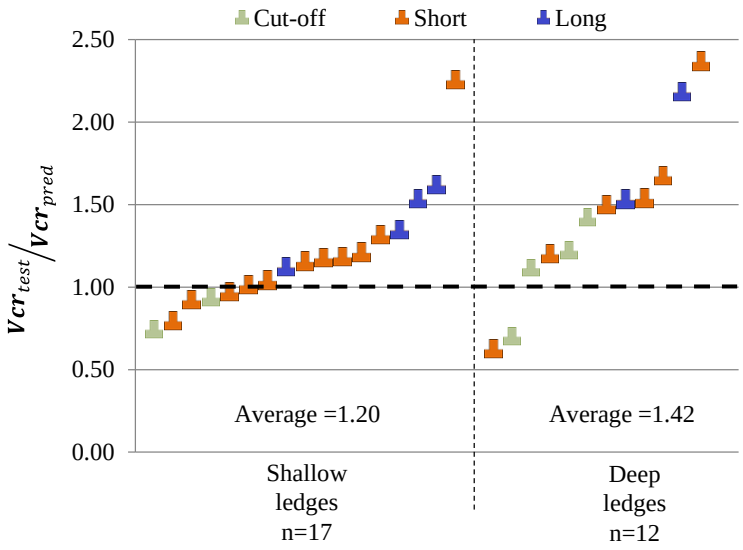

Figure 5-17: Ledge depth effect on diagonal cracking load

Seventeen specimens with shallow ledges are shown in Figure 5-17 with 29% percent of them cracking below their predicted cracking load. The average Vcr_{test}/Vcr_{pred} ratio for the shallow ledges was 1.20. Twelve specimens with deep ledges are shown in the figure; only two of them (17%) fell below 1.0. The average Vcr_{test}/Vcr_{pred} ratio for the deep ledges was 1.42.

It is important to note that the estimates provided by equation 5-1 represent a lower bound on the load at which a beam will crack. Limiting the service demands using equation 5-1 may still result in some bent caps cracking under full service load. At service loads, designers must ensure adequate detailing to maintain the width of the cracks within tolerable limits. Minimum steel requirements for crack width control will be evaluated in the following section.

5.3.2 Crack Width Control

Research on diagonal crack widths is scarce. A detailed study of the available research on the matter was presented by Bircher et al. 2008. In that study, the main factor affecting the widths of diagonal cracks in deep beams was found to be the amount of web reinforcement. The study concluded that a minimum of 0.3% vertical and horizontal web reinforcement ratios should be provided to ensure enough force and crack redistribution

in the concrete. Birrcher et al. 2008 also found that providing web steel above 0.3% has diminishing returns in regards to controlling diagonal crack widths. Additionally, the study determined that longitudinal steel, shear span-to-depth ratio, and cover within a range of 0.2 to 2 in. do not have a significant impact on diagonal crack widths.

The effects of ledge length, ledge depth, and number of point loads on crack width progression were presented in Sections 4.4.3, 4.5.3 and 4.6.3. Neither ledge geometry nor number of point loads were found to affect crack width progression in the specimens tested.

In order to characterize the cracking performance of test specimens at service load levels, a benchmark crack width of 0.016 in. was selected. Maximum crack widths recorded below that threshold were deemed acceptable for long-term serviceability considerations. The selected value is consistent with the tolerable service crack widths listed in ACI 224R-01 and fib-1999 for dry exposure, as well as with TxDOT Project 0-5253. ACI 224R-01 reports that crack width limits are expected to be exceeded by a significant portion of the cracks thus the values are only meant as general guidelines to be used in conjunction with sound engineering judgment. Thus even though bent caps may be exposed to wet and dry cycles, the dry exposure crack limit was deemed acceptable for the evaluation of test specimens for which the actual maximum crack widths were recorded at every loading increment.

Along with the limit on maximum crack width, a service load level corresponding to 33% of the maximum applied load was selected as an approximate service load level for test specimens. This value is consistent with the value used in TxDOT Project 0-5253. Assumptions leading to the 33% value are detailed in Figure 5-18. Maximum diagonal crack width progressions of four typical tests are presented in Figure 5-19 in conjunction with the load and crack width serviceability criteria. In that figure, specimens with crack progression outside of the bottom right quadrant drawn by the selected limits are deemed to have acceptable detailing to limit crack widths at service loads.

φ Nominal Capacity $\approx$ η Service Load

$$\frac{\varphi}{\eta} \approx \frac{\text{Service Load}}{\text{Nominal Capacity}}$$

Assumptions:

1). Load Case: 1.25DL + 1.75LL
2). DL = 75% of Service Load
LL = 25% of Service Load
3). Nominal = 2/3 Experimental

} $\eta = 1.4$

$$2/3 \quad \frac{0.70}{1.4} = 0.33 \approx \frac{\text{Service Loads}}{\text{Experimental Capacity}}$$

φ = strength reduction factor, 0.70
η = load factor
DL = dead load
LL = live load

Figure 5-18: Service load level estimation (Birrcher, et al., 2008)

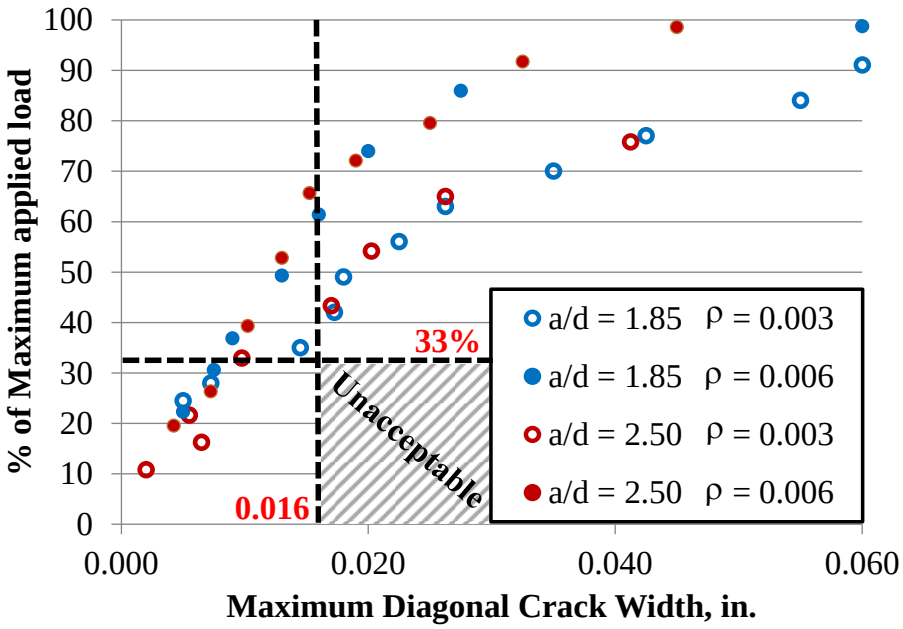

Figure 5-19: Typical crack width progression plot

Crack width progressions from thirty one tests conducted in the experimental program of the current study are evaluated in this section. Details of these specimens are summarized in Table 5-8. Eighteen specimens were tested had an *a/d* ratio of 1.85

(Figure 5-20) and thirteen specimens had an *a/d* ratio of 2.50 (Figure 5-21). All the specimen crack width progressions grouped according to their reinforcement ratios are shown in Figure 5-22 along with the serviceability criteria.

Table 5-8: Crack width evaluation specimens

Test	Specimen	b in.	h in.	d in.	Ledge Depth	Ledge Length	Point Loads	Support Plate in.	Load Plate in.	ρ_v	a/d ratio
01a	DS1-42-1.85-03	21	42	37.6	h/2	Short	1	16 x 20	26 x 9	0.3%	1.85
01b	DS1-42-2.50-03	21	42	37.6	h/2	Short	1	16 x 20	26 x 9	0.3%	2.50
02a	DS1-42-1.85-06	21	42	37.6	h/2	Short	1	16 x 20	26 x 9	0.6%	1.85
02b	DS1-42-2.50-06	21	42	37.6	h/2	Short	1	16 x 20	26 x 9	0.6%	2.50
03a	DL1-42-1.85-06	21	42	37.6	h/2	Long	1	16 x 20	26 x 9	0.6%	1.85
03b	DL1-42-2.50-06	21	42	37.6	h/2	Long	1	16 x 20	26 x 9	0.6%	2.50
04a	SS3-42-1.85-03	21	42	37.6	h/3	Short	3	16 x 20	18 x 9	0.3%	1.85
04b	SS3-42-2.50-03	21	42	37.6	h/3	Short	3	16 x 20	18 x 9	0.3%	2.50
5b	SS3-42-2.50-06 (f)	21	42	37.6	h/3	Short	3	16 x 20	18 x 9	0.6%	2.50
6a	SC3-42-1.85-03	21	42	37.6	h/3	Cut-off	3	16 x 20	18 x 9	0.3%	1.85
6b	SC3-42-2.50-03	21	42	37.6	h/3	Cut-off	3	16 x 20	18 x 9	0.3%	2.50
7a	SS1-75-1.85-03 (p)	21	75	68.2	h/3	Short	1	16 x 20	30 x 10	0.3%	1.85
8b	SS1-75-2.50-06 (p)	21	75	68.2	h/3	Short	1	16 x 20	30 x 10	0.6%	2.50
9a	DS3-42-2.50-03	21	42	37.6	h/2	Short	3	16 x 20	18 x 9	0.3%	2.50
10a	DL1-42-1.85-03	21	42	37.6	h/2	Long	1	16 x 20	26 x 9	0.3%	1.85
10b	DL1-42-2.50-03	21	42	37.6	h/2	Long	1	16 x 20	26 x 9	0.3%	2.50
11a	SL3-42-1.85-03	21	42	37.6	h/3	Long	3	16 x 20	18 x 9	0.3%	1.85
12a	SL3-42-1.85-06	21	42	37.6	h/3	Long	3	16 x 20	18 x 9	0.6%	1.85
14a	SS1-75-1.85-03b	21	75	68.2	h/3	Short	1	16 x 20	30 x 10	0.3%	1.85
15a	DC3-42-1.85-03	21	42	37.6	h/2	Cut-off	3	16 x 20	18 x 9	0.3%	1.85
15b	DS3-42-1.85-03	21	42	37.6	h/2	Short	3	16 x 20	18 x 9	0.3%	1.85
16a	SS1-42-1.85-03	21	42	37.6	h/3	Short	1	16 x 20	26 x 9	0.3%	1.85
16b	SS1-42-2.50-03	21	42	37.6	h/3	Short	1	16 x 20	26 x 9	0.3%	2.50
17a	DC1-42-2.50-03	21	42	37.6	h/2	Cut-off	1	16 x 20	26 x 9	0.6%	1.85
17b	DL3-42-1.85-03 (f)	21	42	37.6	h/2	Long	3	16 x 20	18 x 9	0.3%	1.85
18a	SL1-42-2.50-03	21	42	37.6	h/3	Long	1	16 x 20	26 x 9	0.3%	2.50
18b	SC1-42-2.50-03 (r)	21	42	37.6	h/3	Cut-off	1	16 x 20	26 x 9	0.3%	2.50
19a	DS1-42-1.85-6/3	21	42	37.6	h/2	Short	1	16 x 20	26 x 9	0.6%	1.85
19b	DS1-42-2.50-6/3	21	42	37.6	h/2	Short	1	16 x 20	26 x 9	0.6%	2.50
20a	SC1-42-1.85-03 (le)	21	42	37.6	h/3	Cut-off	1	30 x 21	18 x 9	0.3%	1.85
20b	DC1-42-1.85-03	21	42	37.6	h/2	Cut-off	1	30 x 21	18 x 9	0.3%	1.85

(f) Flexure failure (r) Shear friction failure

(p) Punching shear failure (le) Ledge tie failure

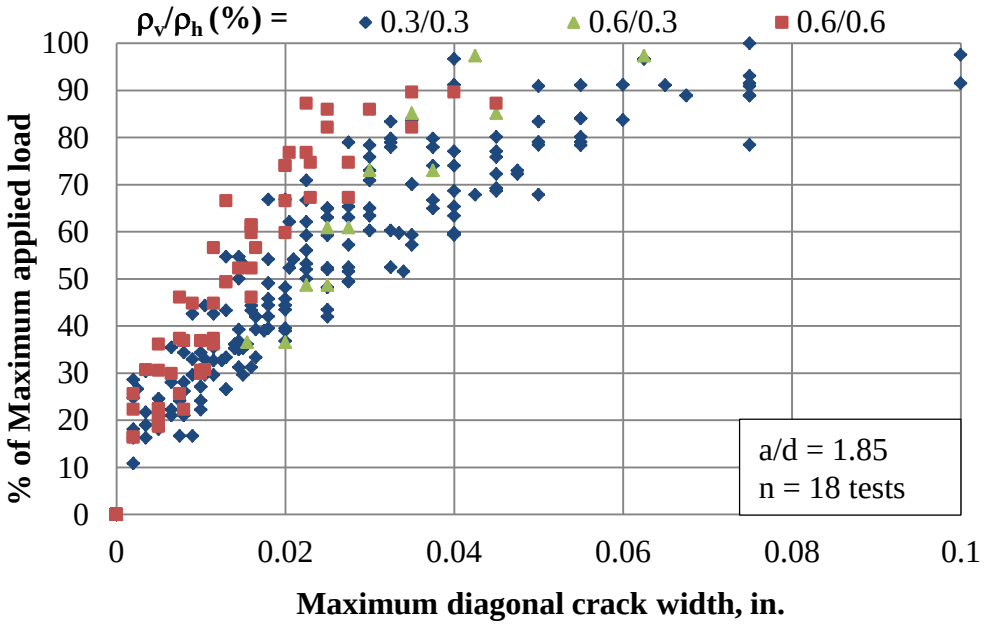

Figure 5-20: Crack width data for specimens with a/d=1.85

A strong correlation between the transverse reinforcement ratio and maximum diagonal crack widths can be seen in Figure 5-20. As expected, specimens with more reinforcement showed narrower cracks at a given load. Specimens with 0.6% vertical reinforcement ratio and 0.3% in the horizontal direction exhibited intermediate crack width progressions between those of specimens with 0.6% and 0.3% reinforcement ratios in both directions. Similar trends were observed for specimens with an *a/d* ratio of 2.50, as shown in Figure 5-21.

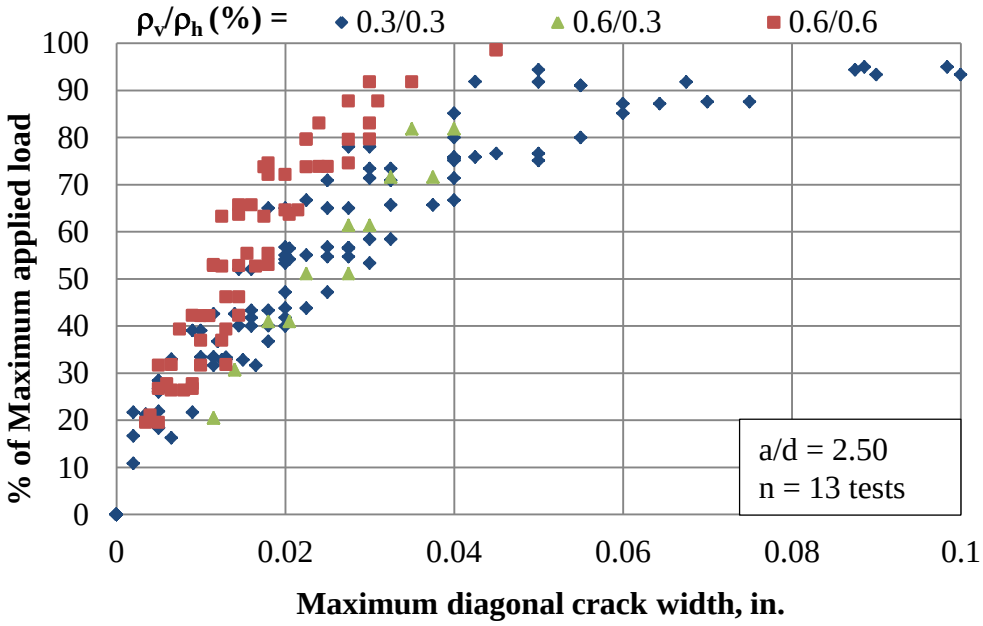

Figure 5-21: Crack width data for specimens with a/d=2.50

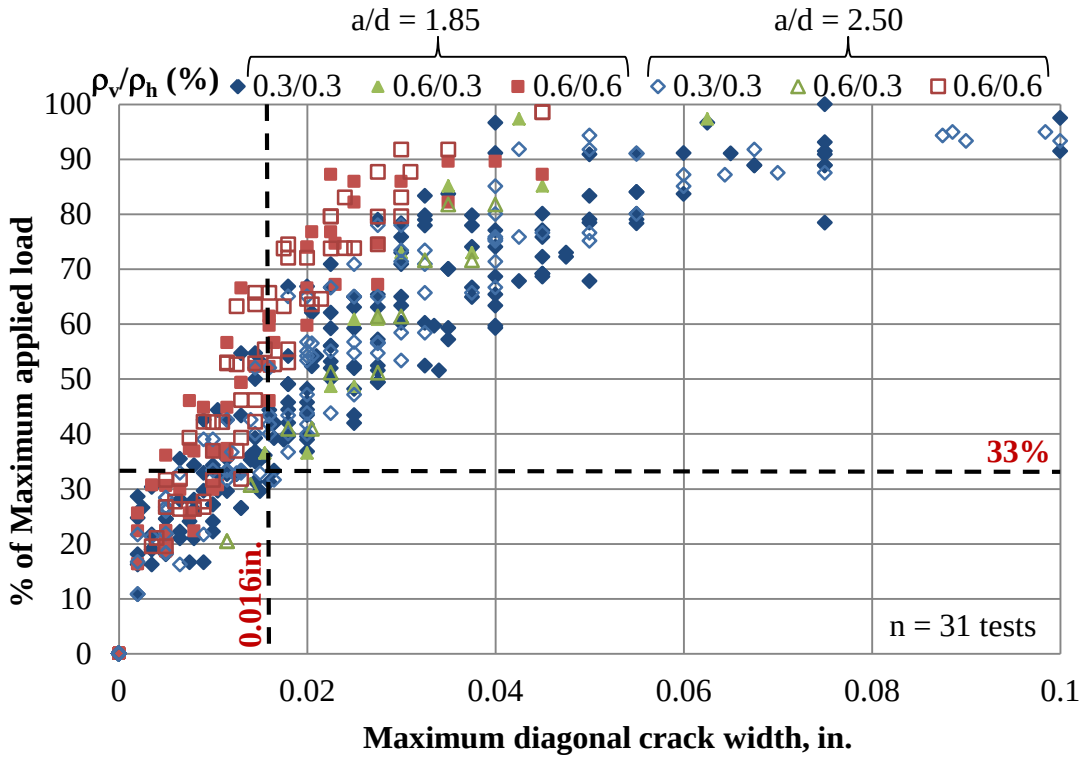

Figure 5-22: Crack width data for all specimens with serviceability criteria

Results shown in Figure 5-22 indicate that providing a minimum web transverse reinforcement ratio of 0.3% distributed evenly in each direction adequately restrains the maximum diagonal crack widths below 0.016 in. up to the assumed service load level. This limit is consistent with the findings of TxDOT project 0-5253 for rectangular deep beams. This limit was recently adopted in the TxDOT bridge design manual (2011) for inverted-T beams.

5.3.3 Summary

Confirming the trends noted in Chapter 4, reducing ledge length and height has a detrimental effect on web shear-cracking as evident by the reduction in the shear force at first diagonal cracking. Since specimens with cut-off ledges showed the worst performance, it is not recommended to use cut-off ledges in the designs of inverted-T beams.

The lower bound equation of first diagonal cracking proposed by project 5253 provides a reasonable lower bound on that cracking load for most inverted-T beams; with the exception of beams with shallow and cut-off ledges. It is therefore not recommended to use the cracking equation for such beams.

Minimum transverse reinforcement ratios of 0.3% evenly distributed in each direction were proven to adequately restrain the maximum diagonal cracks widths below 0.016 in. at service load levels.

5.4 STM APPLICATION FOR INVERTED-T BEAMS

Inverted-T beams are typically under complex states of stress along most of their spans. The disturbed stress regions are induced by changes in the cross section as well as the application of concentrated loads and reactions. Sectional design is not applicable for disturbed regions; however, strut-and-tie modeling is applicable and offers a rational design approach. The application of STM design to inverted-T beams is discussed next in light of the experimental results.

5.4.1 Geometric Layout of Strut-and-Tie Models for Inverted-T Beams

The first step in building a strut-and-tie model is to define the layout of the struts and ties. For inverted-T beams, some assumptions on load spread need to be made to define the geometry of key elements: hanger ties, compression-block struts, intermediate ties in the shear span (if they are present), and ledge tension tie.

When evaluating the strength of test specimens, the widths of the hanger ties were obtained by assuming a 45-degree load-spread angle below the loading plates. The assumption was shown to work reasonably well based on strain measurements in hanger reinforcements (Section 4.3).

The depth of the compression block, as obtained from flexural sectional analysis, was used as the depth of the prismatic compression strut comprising the top- or compression-chord. The contribution of the flexural compression steel to the strength of the strut and nodal interfaces was considered in specimen design. The full yield strength of the compression steel was used (Section 2.4.3, Equation 2-27). Strength estimates were

also performed at the design phase ignoring the effects of the compression steel. In the later strength calculations the compression strut was found to govern beam strength in several cases. However, the observed failure modes for those cases were not of top-chord compression strut failure but matched more closely failure modes predicted by including the strength benefits of the compression steel. Test results therefore indicate that including the strength contribution of compression steel in struts using Equation 2-27 is appropriate.

STM provisions of TxDOT project 5253 implicitly check the strength of the struts by calculating their capacity at the strut-to-node-interface (STNI); considering this point the weakest of a bottle-shape strut. In inverted-T specimens with long ledges, the diagonal struts are bounded by the web width on the upper portion of the web but not in the lower portion of the web where stresses can spread the width of the ledge near the support node (Figure 5-23). In such a case, the weakest point of the strut may shift from the STNI to the location where the thickness of the strut changes from the ledge width to the web width. Therefore, thickness of the STNI at the support may be considered as the smallest of the bearing width and the web thickness.

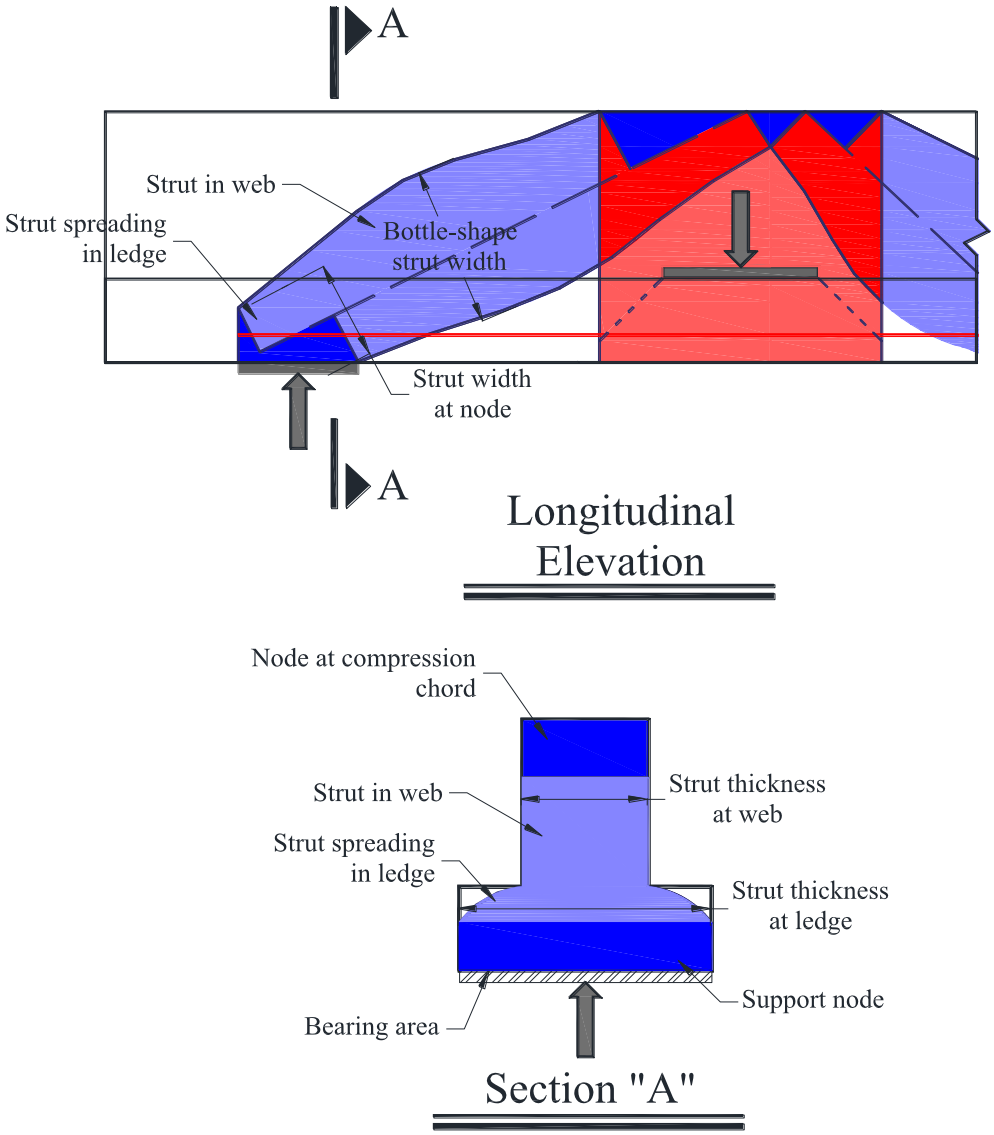

Figure 5-23: Width variation in bottle-shape struts

The width of the intermediate tie in the shear spans of specimens with *a/d* ratios of 2.50 was assumed to be bound by the nearest hanger tie and the intersection of the top surface of the beam and a line extending from the center of the support at a 25-degree angle from the vertical; consistent with the technique proposed by Wight & Parra-Montesinos (2003) as illustrated in Figure 5-24.

Typical strain readings in hanger and transverse steel are presented in Figure 5-24 and Figure 5-25. An abrupt increase in the strains coinciding with the centroid of the

intermediate tie can be observed in Figure 5-24; which validates the assumptions made about the location and width of intermediate ties. A significant difference is observed between strains of the hanger and those of the intermediate tie. The difference can at least partly be attributed to the change in bar size and spacing within the two ties. The hanger tie is comprised of No. 6 bars spaced at 3 in. center-to-center, whereas the intermediate tie is comprised of No. 4 bars spaced at 6.5 in. center-to-center. The observed strains are consistent with the predicted capacities of the STM design in which the controlling element was the intermediate tie while the hanger tie had an estimated capacity/demand ratio of 3.08. Strains at service-load level, estimated as 33% of the maximum applied load, are roughly three times larger at the intermediate tie than at the hanger tie. Strain measurements shown in Figure 5-25 also confirm the hanger and intermediate tie widths assumptions.

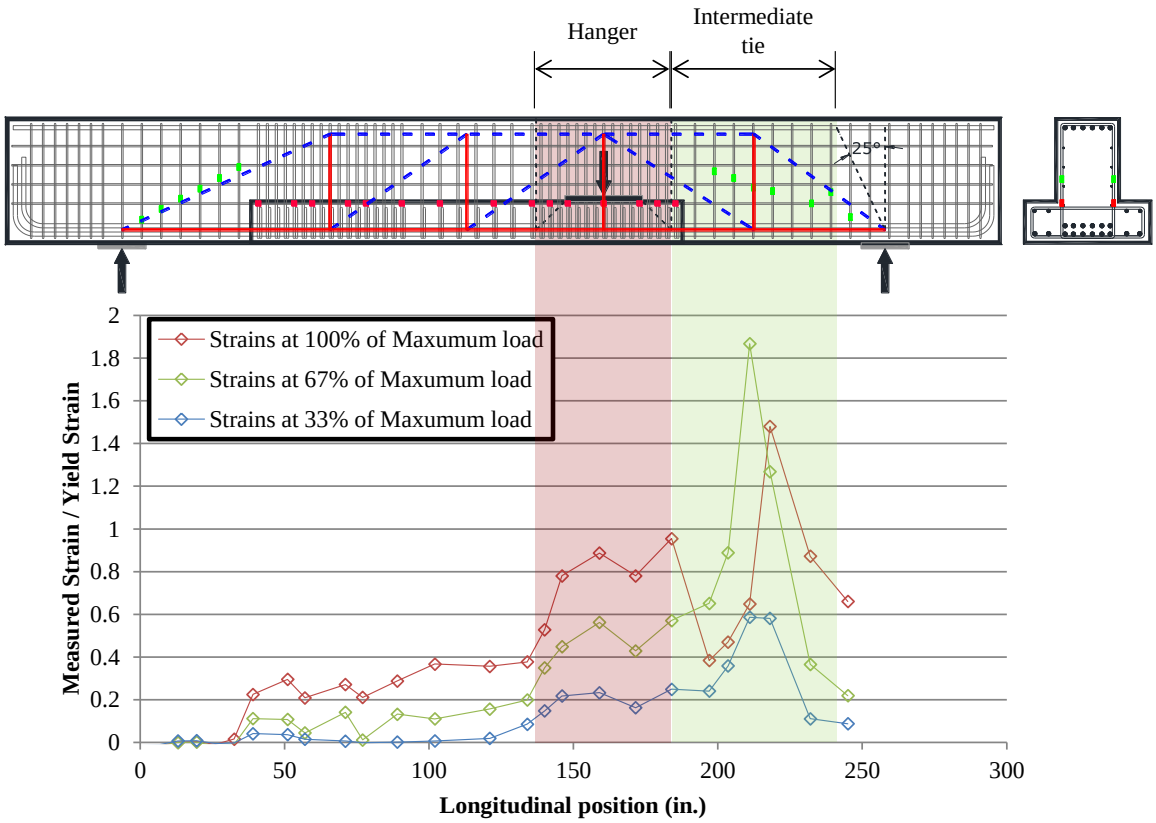

Figure 5-24: Hanger and intermediate tie strains at various loading stages for specimen 16a: SS1-42-2.50-03

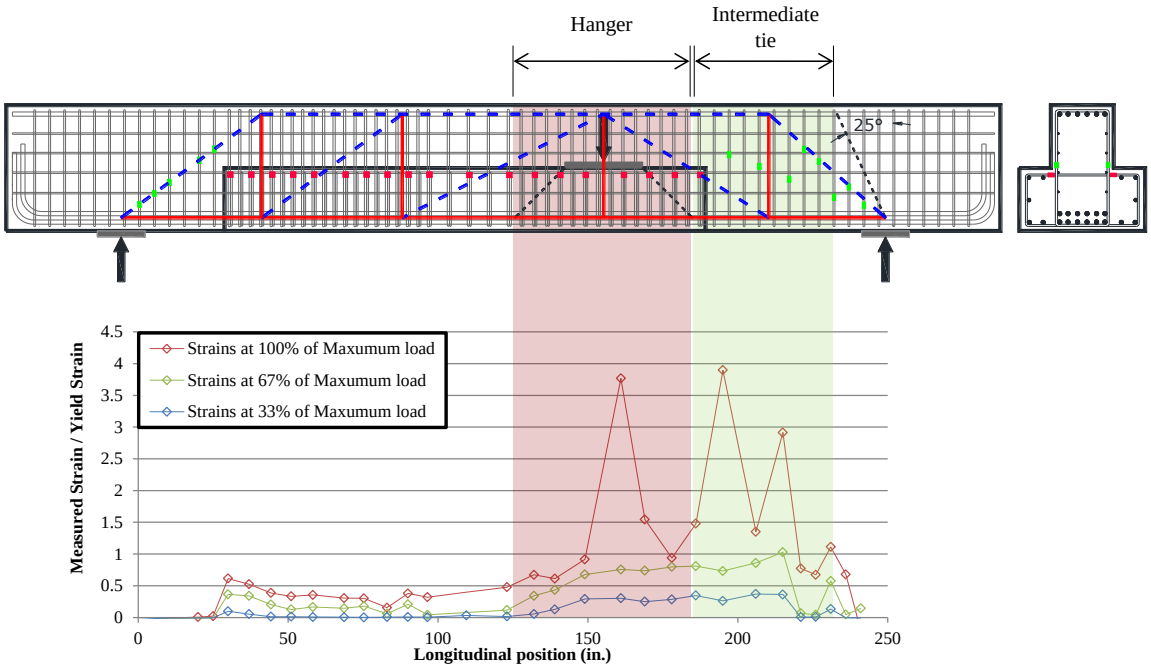

Figure 5-25: Hanger and intermediate tie strains at various loading stages for specimen 19a: DS1-42-2.50-06/03

Tension reinforcement engaged in the flexural bending of the cantilevered ledge is assumed to be effective within a width of ($W + 5a_f$) around the loading plate; as illustrated in Figure 5-26. This assumption was suggested by Ma (1971), adopted in AASHTO LRFD Bridge Design Specifications (2012), and used in this dissertation to design test specimens. Measured strains in the tension reinforcement of the ledge in specimens of the current study corroborate the suggested effective width as seen in Figure 5-26. For cut-off ledges the recommended effective width of the ledge tension reinforcements is 2c around the loading plate; *c* is the distance from the center of the plate to the edge of the ledge (Figure 5-27). Strain measurements also corroborate the suggested effective length in cut-off ledges as seen in Figure 5-27. However, it is still recommended to avoid using cut-off ledges in inverted-T beams due to their poor performance in tests.

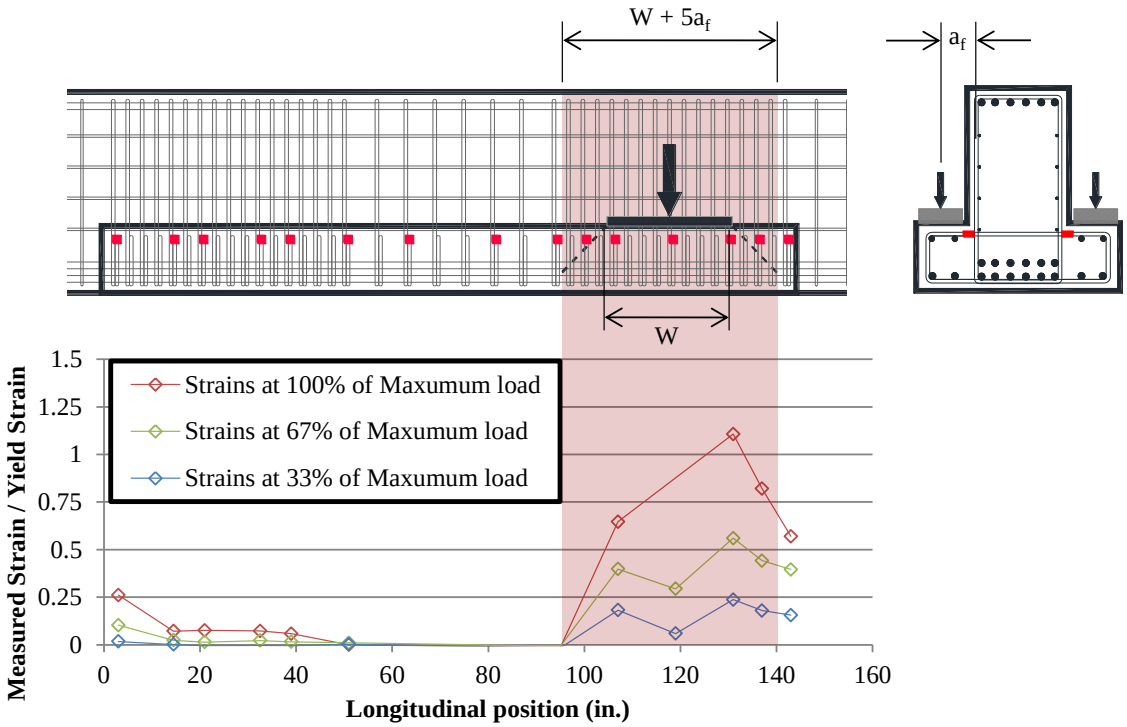

Figure 5-26: Horizontal ledge-tie strains at various loading stages for specimen 16a: SS1-42-2.50-03

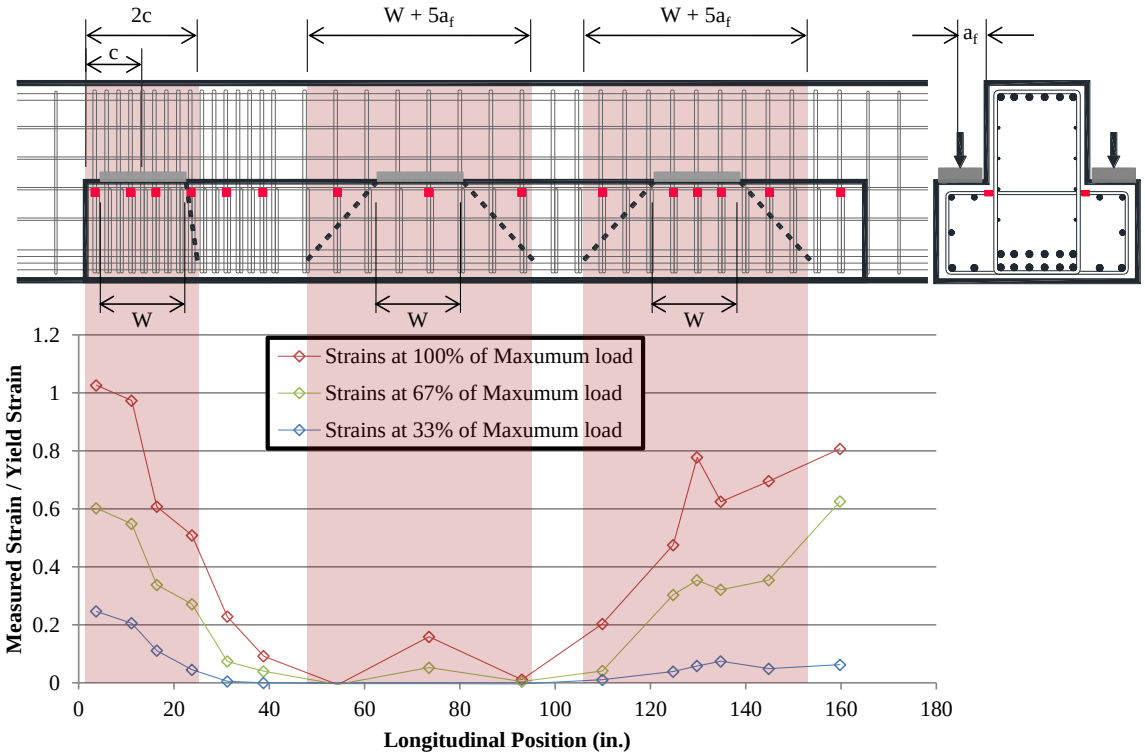

Figure 5-27: Horizontal ledge-tie strains at various loading stages for specimen 15a: DC3-42-1.85-03

5.4.2 Ledge Depth and Cantilever Projection

No limits are directly specified by STM design procedures for ledge depth or cantilever projection of the ledge in the transverse direction. However, as with any STM, the angle between a strut and a tie entering the same node must not be less than 25 degrees to prevent excessive strain in the reinforcement and excessive widening of cracks. Deep ledge specimens from the current study as well as the 75-in deep specimens were designed with the angle between the diagonal strut of the ledge and the hanger tie to be close to 25 degrees (Figure 5-28). Given that ledges with the shallow strut-to-tie angles performed adequately in tests, one can conclude that designing with angles larger than 25 degrees between strut-and-tie is valid in ledge design.

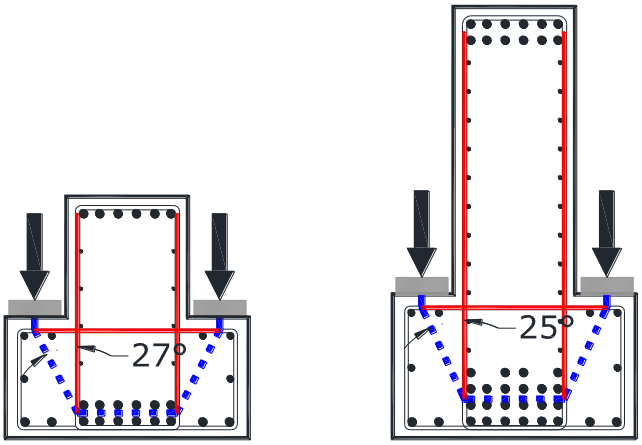

Figure 5-28: Typical cross-sectional models for 42-in. specimens with deep ledges and 75-in. specimens with shallow ledges

5.4.3 STM Conservatism for Long Ledges

Results of the experimental program revealed an increase in strength for longer ledges not captured by the strut-and-tie model. The state of stresses observed at the support of a long-ledge specimen is a more complex problem than that of a short-ledge specimen. Long ledges can provide tri-axial confinement to nodes and struts at the support increasing strength at the support region. This effect is considered in TxDOT 5253 STM provisions using the *m* factor as defined in Equation 2-28 (Figure 5-29).

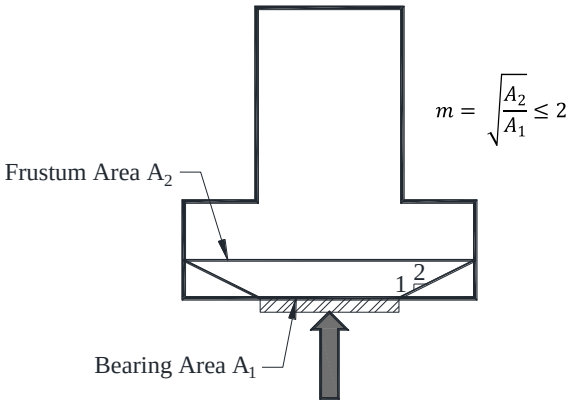

Figure 5-29: Application of frustum area to calculate the confinement factor

However, the confinement provided by long ledges was not considered in the strut-and-tie models of the experimental program since the ledges did not extended past the support plates due to limitations of the test setup, which required the ledges to be discontinued near the center of the reaction plates, as shown in Figure 5-30.

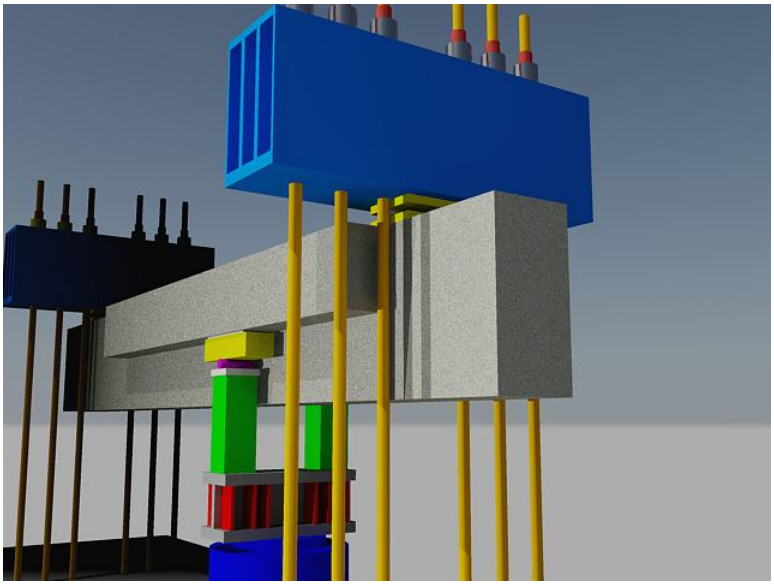

Figure 5-30: Perspective view of test setup with a long-ledge specimen

Designs of five of the eight long-ledged specimens in the experimental program were controlled by the capacity of the strut-to-node interface at the support (the five specimens had a/d = 1.85). The observed increase in conservatism of the strength estimates for these specimens may therefore be attributed in part to the partial confinement of the support region by the ledges; an effect that was neglected in the design due to the discontinuity of the ledges within the nodal region. Strength estimations assuming full confinement at the support region by the ledges are shown in Table 5-9.

Table 5-9: Strength estimations considering the effects of ledge confinement

				Unconfined support			Confined support		
Test	Specimen	V_{test}	Observed Failure Mode	V_{pred}	V_{test} / V_{pred}	Design Controlling Element	V_{pred}	V_{test} / V_{pred}	Design Controlling Element
		kips		kips	ratio		kips	ratio	
03a	DL1-42-1.85-06	741	Direct-Strut Crushing	464	1.60	STNI at support	710	1.04	Tension chord
03b	DL1-42-2.50-06	622	Sectional Shear	353	1.76	Intermediate tie	353	1.76	Intermediate tie
10a	DL1-42-1.85-03	626	Direct-Strut Crushing	468	1.34	STNI at support	555	1.13	Hanger tie
10b	DL1-42-2.50-03	510	Sectional Shear	235	2.17	Intermediate tie	235	2.17	Intermediate tie
11a	SL3-42-1.85-03	571	Direct-Strut Crushing	409	1.39	STNI at support	558	1.02	Tension chord
12a	SL3-42-1.85-06	744	Direct-Strut Crushing	424	1.76	STNI at support	528	1.41	Tension chord
17b	DL3-42-1.85-03	629	Flexure Failure	359	1.75	STNI at support	495	1.27	Tension chord
18a	SL1-42-2.50-03	498	Sectional Shear	269	1.85	Intermediate tie	269	1.85	Intermediate tie

As can be seen in Table 5-9, conservatism for the five long-ledged specimens originally controlled by the STNI at the support (a/d = 1.85) reduced significantly when full confinement of the supports was assumed. The controlling element for specimen 17b coincided with the observed failure mode when confinement was accounted for. It may therefore be acceptable to utilize the benefits of ledges confinement on the struts crossing the ledges. Designs of the remaining three long-ledged specimens (a/d = 2.50) were controlled by the intermediate tie; for these specimens the conservatism remained constant. These specimens observed higher strength and conservatism in strength estimates than those observed in comparable specimens with shorter ledges.

5.5 DESIGN RECOMMENDATIONS

Based on findings presented in this dissertation as part of the TxDOT project 0-6416, recommendations for the design of inverted-T beams are presented.

5.5.1 Ledge Geometry

It is recommended to extend beam ledges beyond the edge of loading plates in the longitudinal direction for a distance at least equal to the ledge depth. Cut-off ledges are not recommended in inverted-T bent caps since they were found to reduce the shear

strength, the diagonal cracking load, and the conservatism of design provisions for the specimens tested.

It is recommended to use long ledges whenever possible. Long ledges increase the strength of the specimens, delay the appearance of diagonal cracking, and increase the conservatism of strength design provisions.

5.5.2 Strength Design

Strut-and-tie modeling as proposed by TxDOT project 5253 and implemented in this work is recommended for the design of all inverted-T bent caps. STM provisions were found to produce more accurate strength estimates (over 30% more accurate overall) than the sectional shear design methods coupled with special ledge design procedures. STM procedures produced much higher accuracy for deep beams and performed on par with sectional design methods for non-deep beams. The proposed STM procedures inherently account for all the different failure modes of interest in inverted-T beams. Thus the procedures provide a single rational and simple design approach for the design of inverted-T beams.

It is recommended to evaluate the shear span of inverted-T beams as the distance between centers of support and the nearest concentrated load; consistent with the definition provided in ACI 318-11 (Art. 11.7.1). Since STM procedures were demonstrated to be equally valid for deep and non-deep beams (by any definition of shear span), such a definition change will improve the accuracy in the design of a portion of the beams that are defined differently by the two competing shear span definitions, while producing comparable accuracy to the sectional design methods for the other portion.

One should note that if STM is used for all inverted-T-beam designs, the definition of shear span becomes a moot point for the differentiation between deep and non-deep beams.

5.5.3 Serviceability

It is recommend to limit shear forces in inverted-T beams to the limits evaluated using Equation 5-1 under un-factored service loads. It is left to the designer to determine what percentage of the live load to include in the service load calculations.

Minimum transverse reinforcement ratios of 0.3% distributed evenly in each direction of the web must be provided to adequately restrain the width of diagonal cracks at service load levels. The minimum transverse reinforcement ratios will also allow for sufficient force redistributions for the struts to reach their full capacity.

5.6 SUMMARY

Data from the experimental program were used to compare the accuracy of the sectional AASHTO and TxDOT design provisions for inverted-T bent caps with that of STM provisions of the TxDOT project 5253 as implemented in this dissertation for inverted-T beams. Strut-and-tie modeling is recommended for the design of all inverted-T beams after producing improved accuracy and reduced unnecessary conservatism compared with sectional shear design methods; especially for deep beams. Additionally, shear span definitions of AASHTO LRFD (2012) and ACI 318-11 were compared, showing that ACI definition results in more accurate strength estimations for inverted-T beams with up to three point loads.

Ledge geometry recommendations were made for inverted-T beam design. Cut-off ledges are not recommended due to reduced conservatism in strength design compared with longer ledges and reduced first-cracking load. Deep and long ledges are recommended whenever possible, due to strength and serviceability benefits observed in the experimental results.

Data from the literature and evaluation database were used to evaluate the main variables influencing the diagonal cracking load. Shear span-to-depth ratio, concrete tensile strength, and section size were shown to be the main variables affecting the diagonal cracking load of inverted-T deep beams. An empirical equation proposed by TxDOT project 5253 was shown to give reasonably conservative estimates of cracking loads for inverted-T beams. It is recommended to introduce a serviceability check in the

design of inverted-T beams to limit shear stresses under service loads to below the estimated diagonal cracking load using the proposed equation. The provision should reduce but not eliminate the probability of inclined cracking under service loads. Minimum transverse steel ratios of 0.3% evenly distributed in each direction of the web are recommended to adequately restrain the diagonal crack widths under service load and to allow for enough force redistribution for struts to reach their full capacity. Finally, the application of STM for inverted-T specimens was discussed in light of test results.

CHAPTER 6
Summary and Conclusions

6.1 SUMMARY

Diagonal web cracking of recently built inverted-T straddle bent caps has been reported with increasing frequency in Texas, triggering concerns about current design procedures for such elements. To address the concerns, the Texas Department of Transportation (TxDOT) funded project 0-6416 with objectives of obtaining a better understanding of the behavior of inverted-T beams and developing strength and serviceability design criteria that will minimize such cracking in the future.

In order to accomplish the objectives mentioned above, the following tasks are addressed in TxDOT project 0-6416. Highlighted are the tasks accomplished within the scope of this dissertation:

1. **Literature review**
2. **Inverted-T database (Section 2.6)**
3. Examination of bent caps in the field
4. Experimental research on strength and serviceability of inverted-T beams
    - i. **Ledge length (Section 4.4)**
    - ii. **Ledge depth (Section 4.5)**
    - iii. Web reinforcement ratio
    - iv. **Number of point loads (Section 4.6)**
    - v. Loaded chord
    - vi. Web depth
5. **Development of design recommendations (Section 5.4)**
6. Proof testing of the proposed design recommendations

Assembly of the inverted-T database, which includes 128 tests from the literature, is presented. Most of the compiled tests were found not to be applicable to the inclined cracking focus of this project or were conducted on beams drastically smaller than the

bent caps in service in Texas. Moreover, very limited serviceability information regarding diagonal crack widths was available in the literature. It was therefore deemed necessary to conduct a comprehensive experimental program of full-scale inverted-T beam specimens to achieve project goals.

Thirty one full-scale tests were conducted with some of the specimens measuring among the largest reinforced concrete deep beams ever tested to determine shear capacity. Strength and serviceability effects of ledge geometry and number of point loads were presented in Sections 4.4, 4.5, and 4.6. Comparisons between the accuracy of STM and sectional LRFD design methods are provided in Section 5.2. Serviceability evaluations pertaining to detailing that controls service load cracking are presented in Section 5.3. Finally, design recommendations for strength and serviceability of inverted-T beams were presented in Section 5.5.

The main focus of the current study was on the shear strength and serviceability of the inverted-T specimens. Torsional effects were not included in the current study, since the cracking patterns observed in the distressed bent caps in service are all consistent with shear issues and no indication of torsional deficiencies were observed in the field inspections.

6.2 CONCLUSIONS

Conclusions of the current study were based on results from the experimental program.

6.2.1 Applicability of 45-Degree Load Spread Under Ledge Loads

The purpose of this task was to validate the 45-degree load spread assumed under the loading plates to calculate the width of the hanger ties. Strain gauge measurements indicated that the 45-degree load spread assumption is reasonable and conservative. It is therefore recommended to calculate the hanger tie widths by assuming a 45-degree spreading of the applied load as shown in Figure 4-4.

6.2.2 Ledge Length Effects

Results have shown that increasing the ledge length increases strength, delays the appearance of the first diagonal cracking, and increases conservatism of the strength estimations. Ledge length has no significant effect on crack width progression.

6.2.3 Ledge Depth Effects

Results have shown that the ledge depth has no significant effect on the strength, crack width progression, or strength-estimate conservatism. However, it was observed that increasing the ledge depth delays the appearance of the first diagonal cracking. Additionally, shallower ledges were more susceptible to local failures.

6.2.4 Number of Point Loads Effects

Results have shown that the number of point loads has no significant effect on the strength, crack width progression, or strength conservatism. Regarding the appearance of the first diagonal cracking, no trend was observed, but only three pairs of comparable specimens were available for this task. More data are necessary to substantiate that conclusion.

6.2.5 Comparison Sectional Shear Provisions vs. STM provisions

Both methods yielded conservative results. However, the most accurate method for estimating web shear-strength is STM; especially for shear span-to-depth ratios of 1.85 (deep beam behavior). Additionally, STM offers a rational approach to designing inverted-T deep beams, which inherently considers all failure modes for the ledges, web, and bearing points, and can be used for deep and non-deep beams. Moreover, it must be mentioned that the application of sectional design for deep beams is fundamentally flawed, since the general assumptions of beam theory do not apply in disturbed regions.

6.3 DESIGN RECOMMENDATIONS

6.3.1 Strength Design

Strut-and-tie modeling as proposed by TxDOT project 5253 and implemented in this work is recommended for the design of all inverted-T bent caps. STM provisions were found to produce more accurate strength estimates than sectional methods.

It is recommended to evaluate the shear span of inverted-T beams as the distance between centers of support and the nearest concentrated load; consistent with the definition provided in ACI 318-11 (Art. 11.7.1).

6.3.2 Serviceability

It is recommend to limit shear forces in inverted-T beams to the limits evaluated using Equation 5-1 under un-factored service loads. It is left to the designer to determine what percentage of the live load to include in the service load calculations.

Minimum transverse reinforcement ratios of 0.3% distributed evenly in each direction of the web must be provided to adequately restrain the width of diagonal cracks at service load levels.

6.3.3 Detailing

It is recommended to extend beam ledges beyond the edge of loading plates in the longitudinal direction for a distance at least equal to the ledge depth. Cut-off ledges are not recommended in inverted-T bent caps since they were found to reduce the shear strength, the diagonal cracking load, and the conservatism of design provisions for the specimens tested.

It is recommended to use long ledges whenever possible. Long ledges increase the strength of the specimens, delay the appearance of diagonal cracking, and increase the conservatism of strength design provisions.

APPENDIX A

Collection Database References

Cussens, A. R., & Besser, I. I. (1985, September). Shear strength of reinforced concrete wall-beams under combined top and bottom loads. *The Structural Engineer, 63B*(3), 50-56.

Fereig, S. M., & Smith, K. N. (1977, May 1). Indirect Loading on Beams with Short Shear Spans. *ACI Journal, 74*(5), 220-222.

Ferguson, P. M. (1956, August 1). Some Implications of Recent Diagonal Tension Tests. *ACI, 53*(8), 157-172.

Fernandez-Gomez, E., Larson, N., Garber, D., Bayrak, O., & Ghannoum, W. (2012). *TxDOT Project 0-6416: Strength and Serviceability Design of Reinforced Concrete Inverted-T Straddle Bent Caps.* The University of Texas at Austin: Center for Transportation Research.

Furlong, R. W., & Mirza, S. A. (1974). *153-1F - Strength and Serviceability of Inverted T-Beam Bent Caps Subject to Combined Flexure, Shear, and Torsion.* Austin: Center for Highway Research, University of Texas at Austin.

Furlong, R. W., Ferguson, P. M., & Ma, J. S. (1971). *113-4 - Shear and anchorage study of reinforcement in inverted-T beam bent cap girders.* Austin TX: Center for highway research at The University of Texas at Austin.

Galal, K., & Sekar, M. (2007, June 1). Rehabilitation of RC inverted-T girders using anchored CFRP sheets. (S. Direct, Ed.) *Composites: Part B - Engineering, 39*(4), 604-617.

Graf, O. , Brenner, E., & Bay, H. (1943). Versuche mit einem wandartigen Trager aus Stahlbeton. *Deutscher Ausschuss fur Stahlbeton, 99*, 41-54.

Leonhardt, F., & Walther, R. (1966). Wandartige Träger. *Deutscher Ausschuss furStahlbeton, 178*.

Schütt, H. (1956, October). Über das Tragvermögen wandartiger Stahlbetonträger. *Beton und Stahlbetonbau, 10*, 220-224.

Smith, K. N., & Fereig, S. M. (1974, January 1). Effect Of Loading And Supporting Condidtions On The Shear Strength Of Deep Beams. *ACI, SP 42,* 441-460.

Tan, K. H., Kong, F. K., & Weng, L. W. (1997, June 3). High strength concrete deep beams subjected to combined top-and bottom-loading. *The Structural Engineer, 75*(11), 191-197.

Taylor, R. (1960, November). Some shear tests on reinforced concrete beams without shear reinforcement. *Magazine of Concrete Research, 12*(36), pp. 145-154.

Zhu, R. R.-H., Dhonde, H., & Hsu, T. T. (2003). *TxDOT Project 0-1854: Crack Control for Ledges in Inverted "T" Bent Caps.* University of Houston.

APPENDIX B

Experimental Specimens Details

B.1 OVERVIEW

Construction details of all the specimens fabricated in the current project are presented in this Appendix.

Beam 01

Beam 01b
DS1-42-2.50-03

Beam 01a
DS1-42-1.85-03

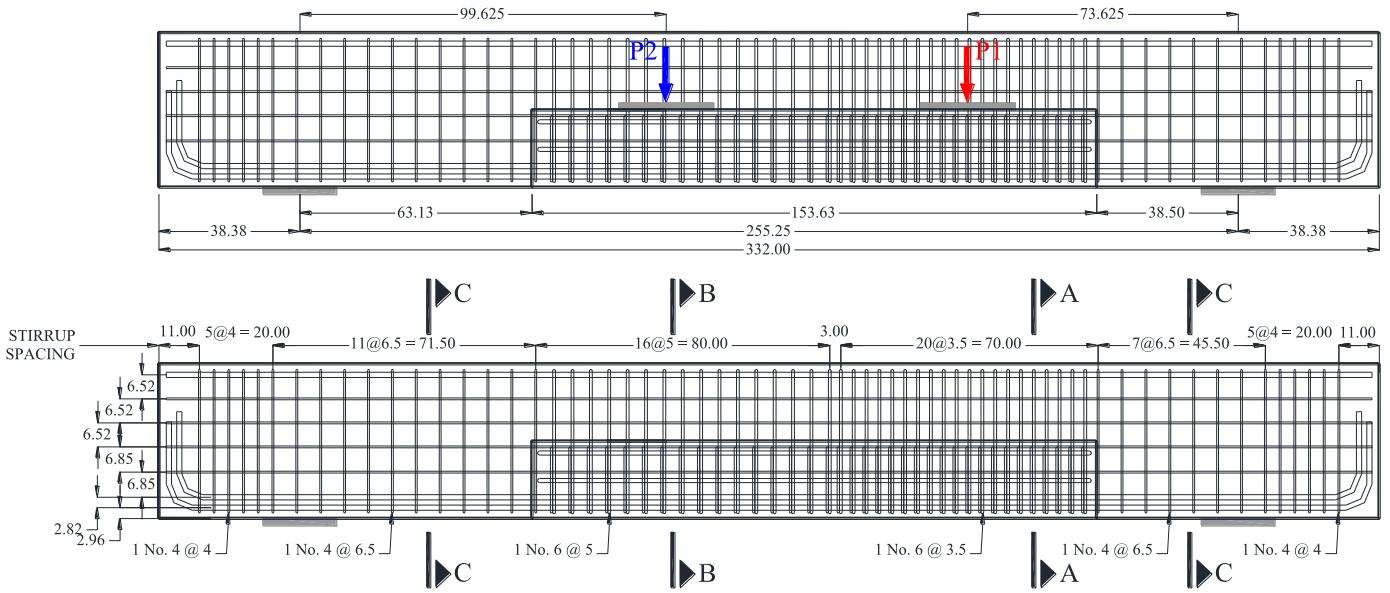

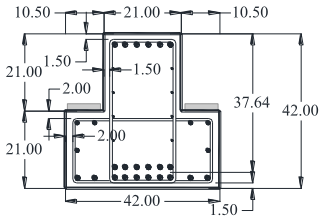

Cross Section

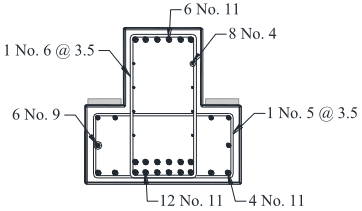

Section A

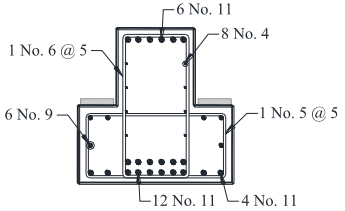

Section B

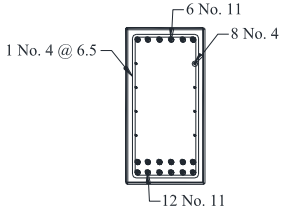

Section C

Beam 02

Beam 02b
DS1-42-2.50-06

Beam 02a
DS1-42-1.85-06

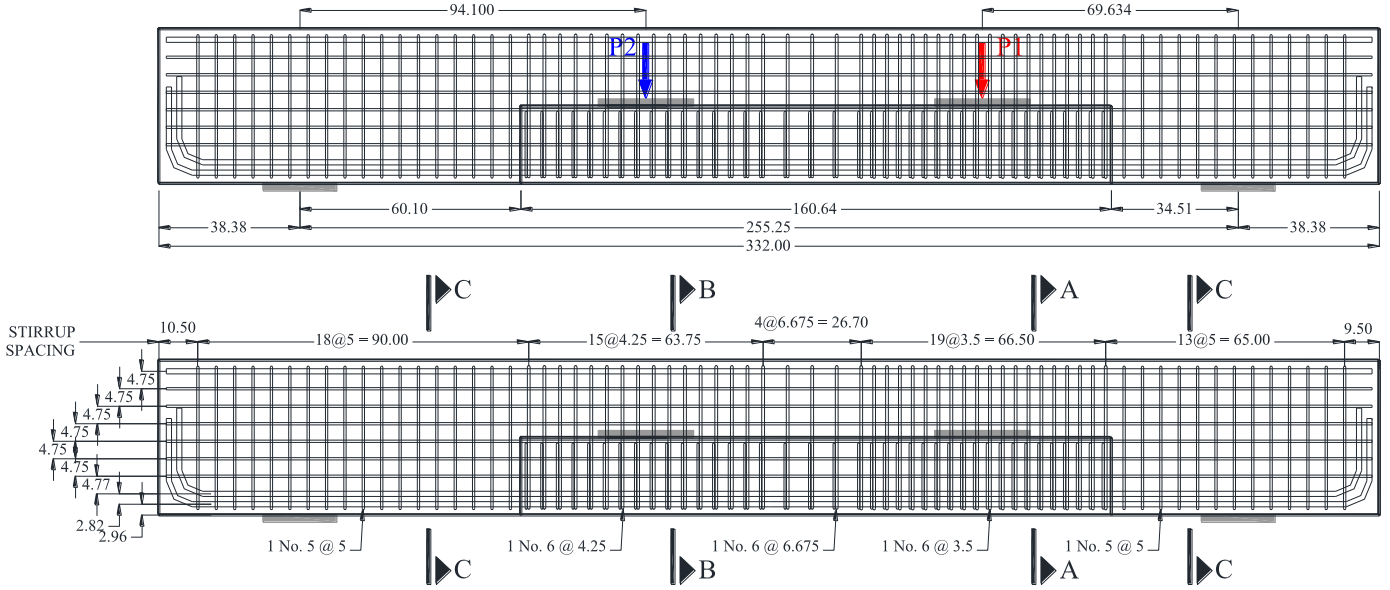

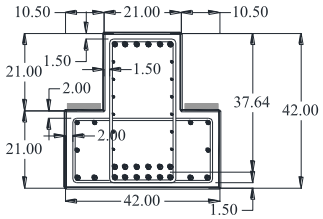

Cross Section

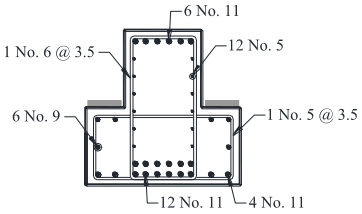

Section A

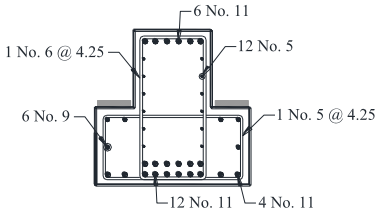

Section B

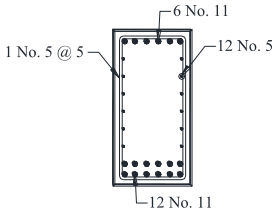

Section C

Beam 03

Beam 03b
DL1-42-2.50-06

Beam 03a
DL1-42-1.85-06

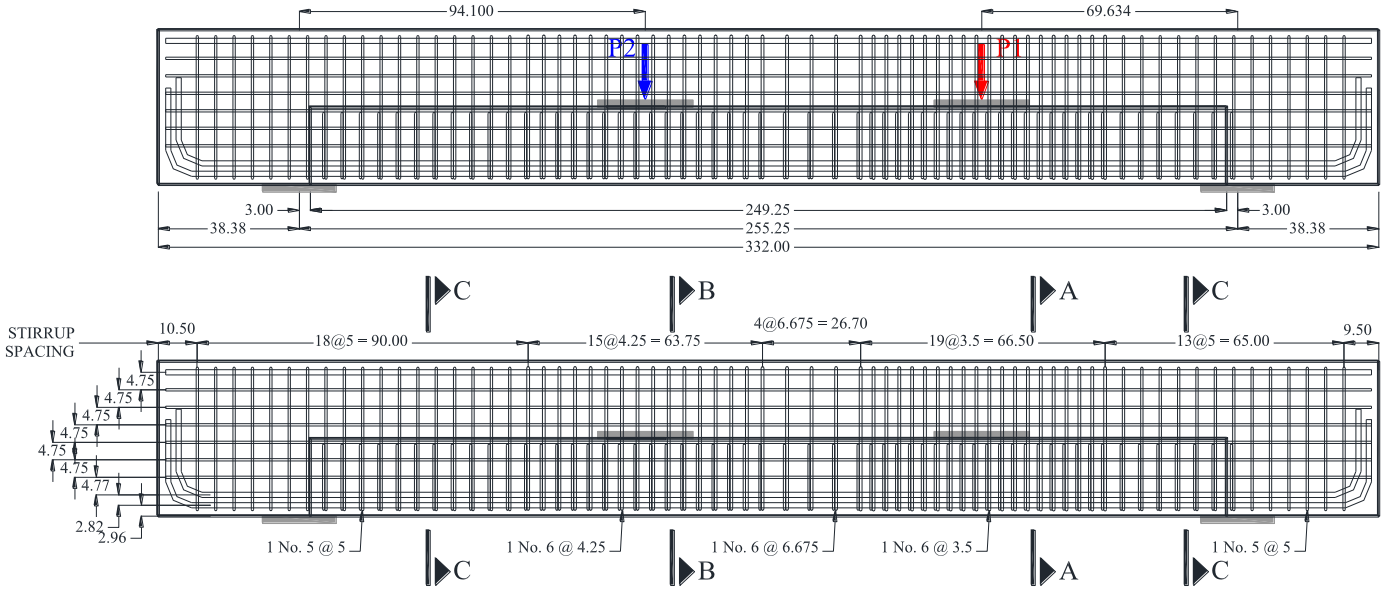

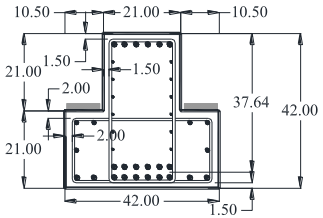

Cross Section

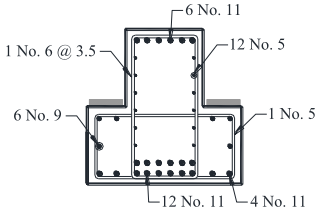

Section A

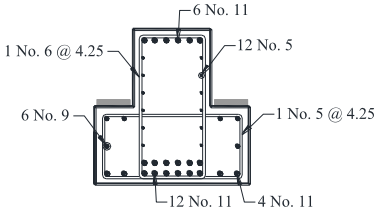

Section B

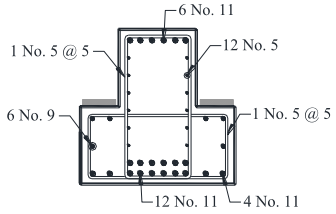

Section C

Beam 04

Beam 04b
SS3-42-2.50-03

Beam 04a
SS3-42-1.85-03

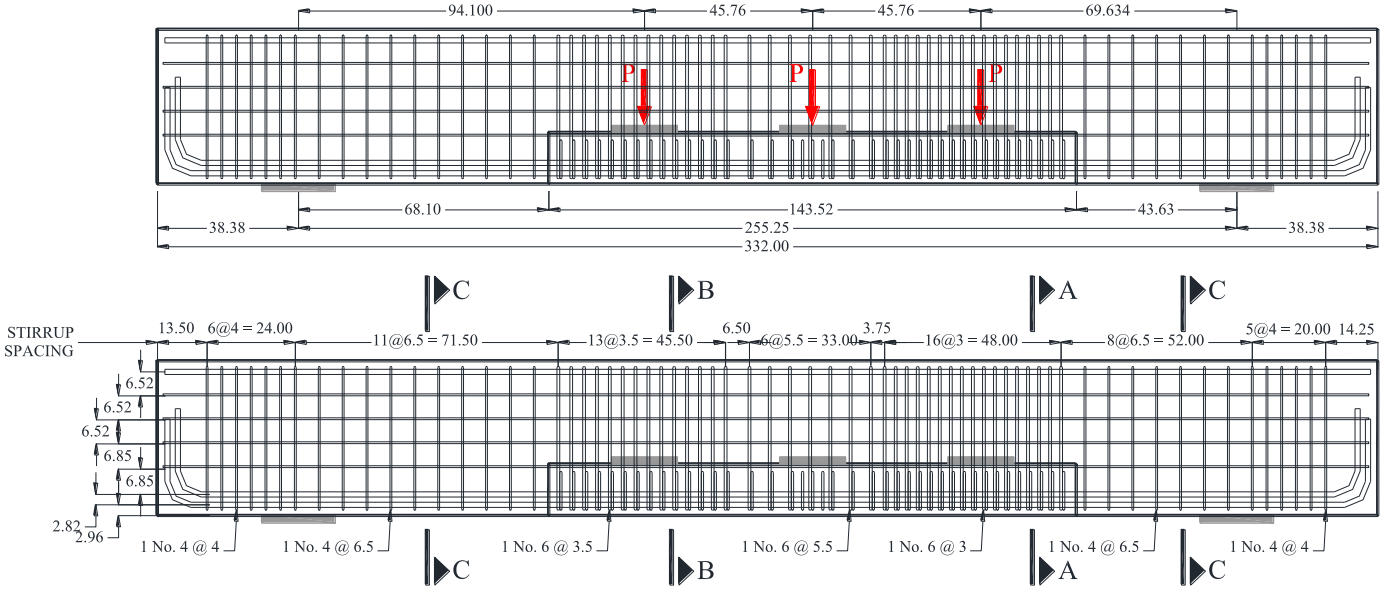

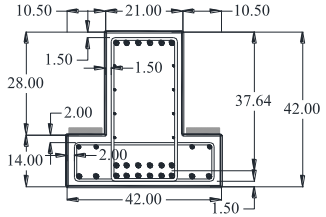

Cross Section

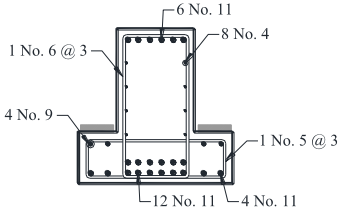

Section A

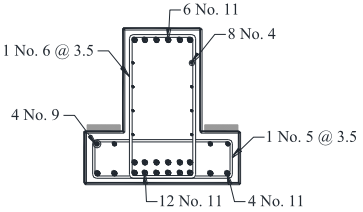

Section B

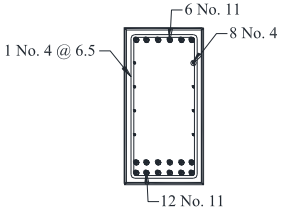

Section C

Beam 05

Beam 05b
SS3-42-2.50-06

Beam 05a
SS3-42-1.85-06
(Not tested)

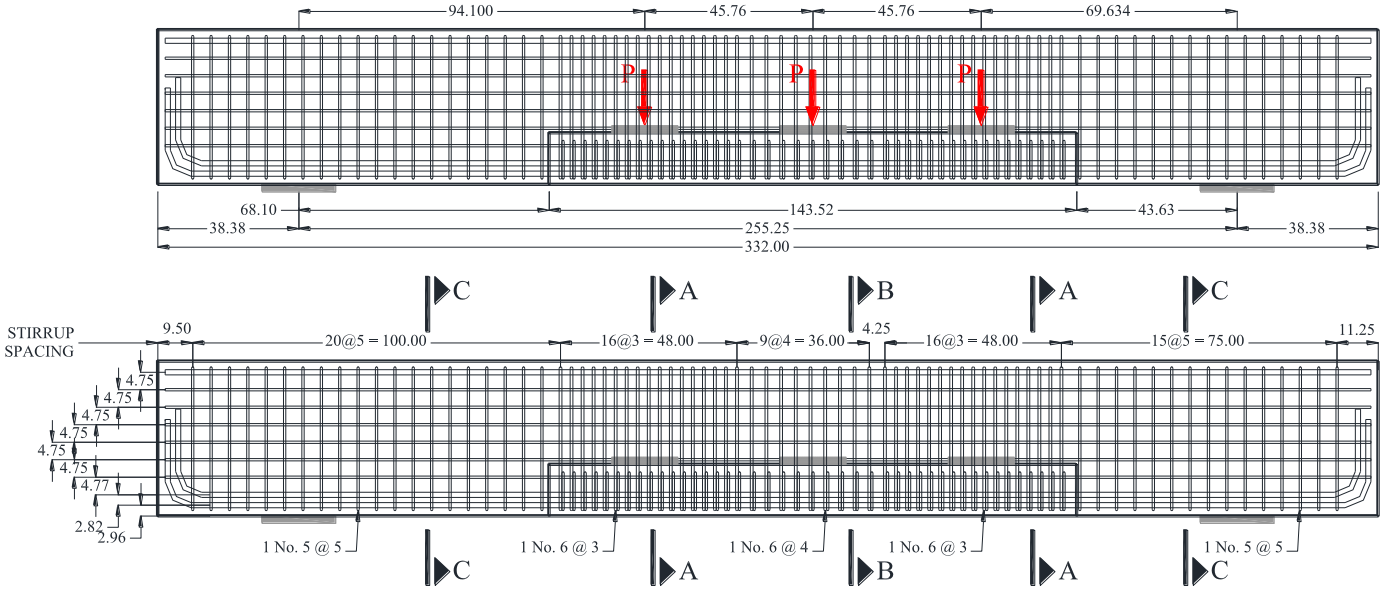

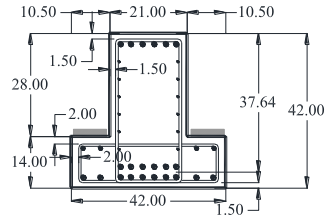

Cross Section

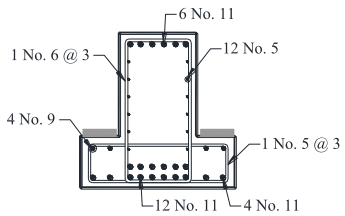

Section A

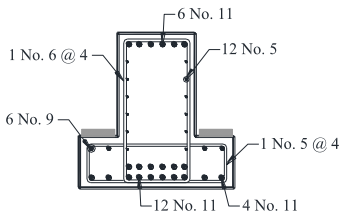

Section B

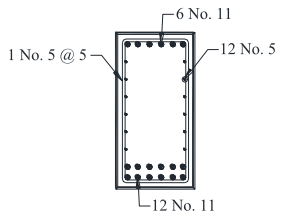

Section C

Beam 06

Beam 06a
SC3-42-2.50-03

Beam 06b
SC3-42-1.85-03

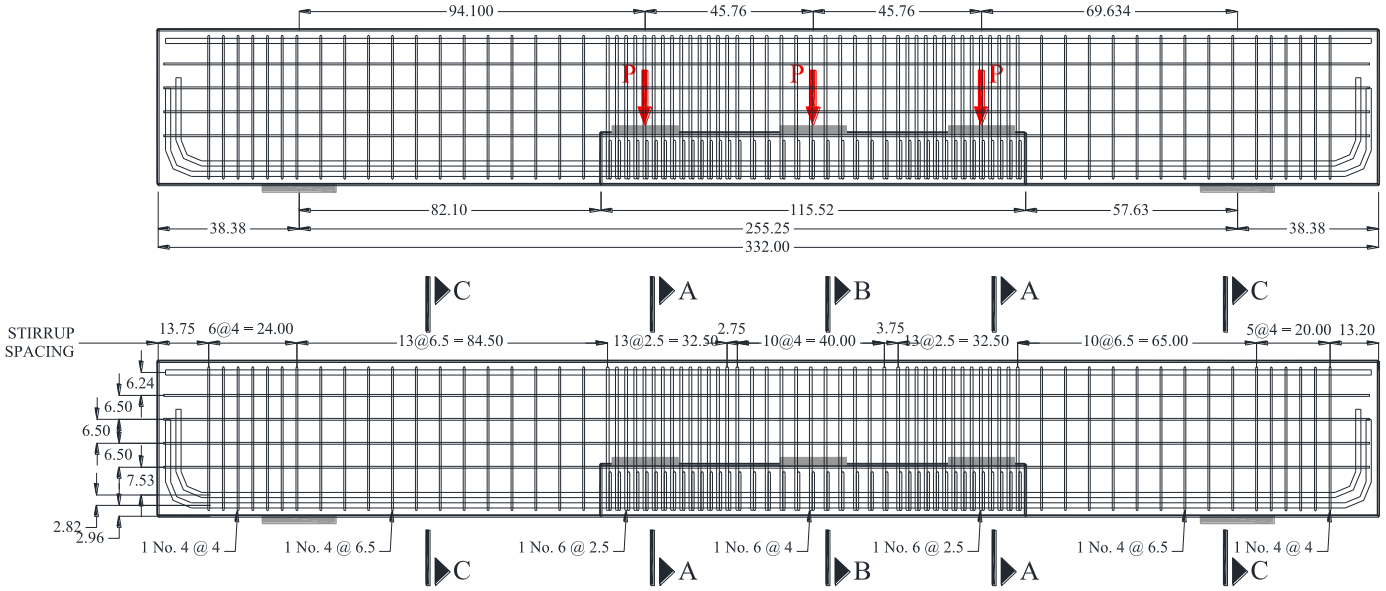

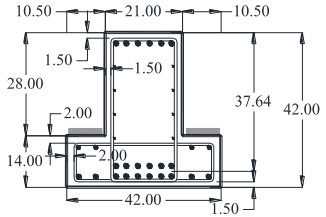

Cross Section

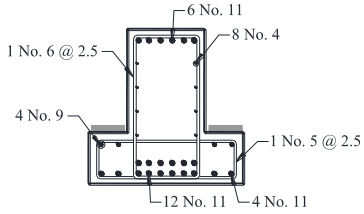

Section A

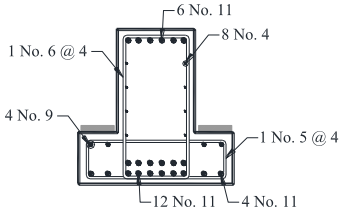

Section B

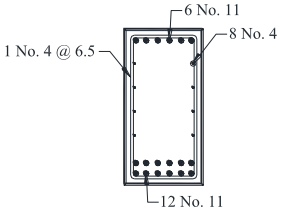

Section C

Beam 07b
SS1-75-1.85-06
(Not Tested)

Beam 07

Beam 07a
SS1-75-1.85-03

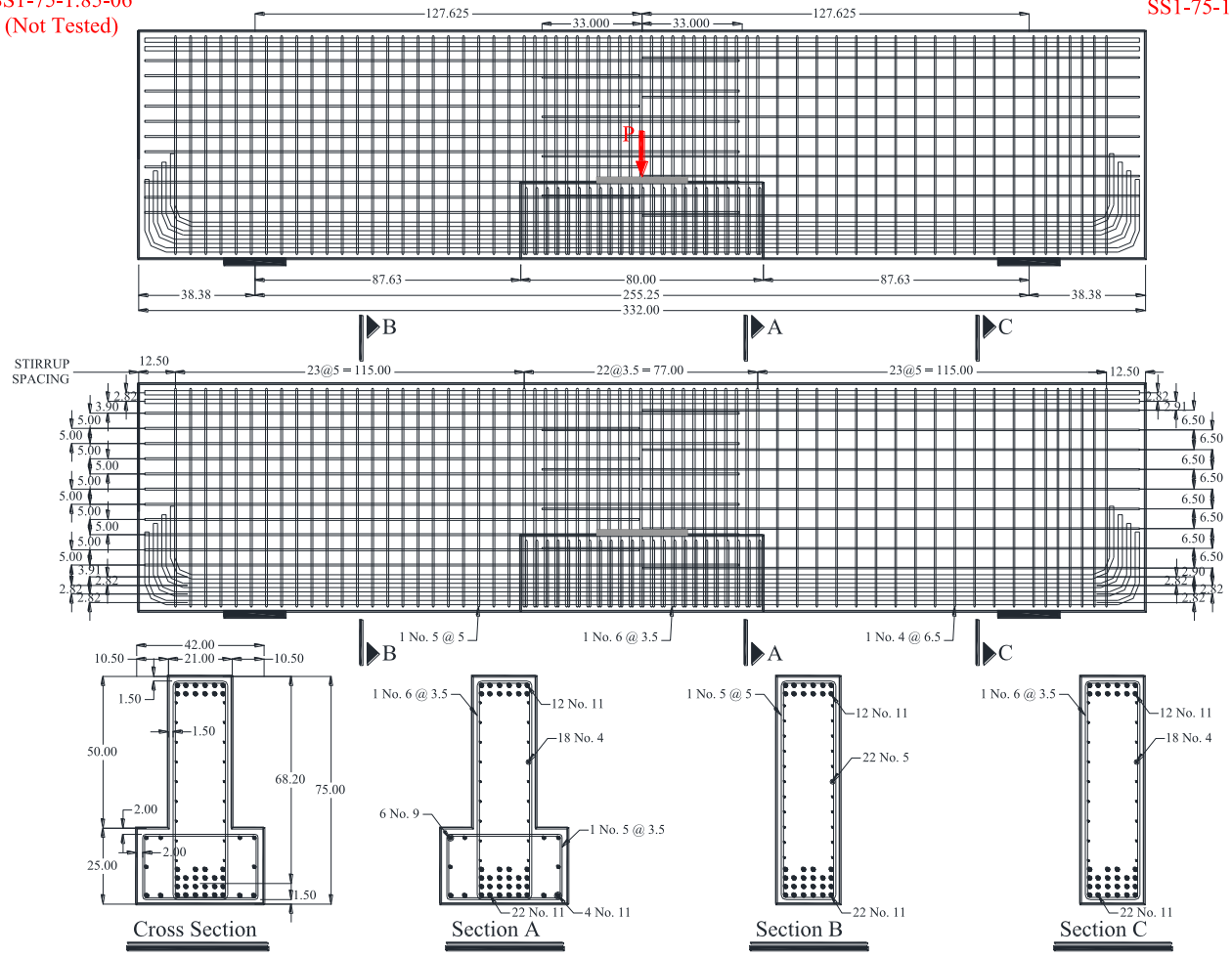

Beam 08

Beam 08b
SS1-75-1.20-06
(Not Tested)

Beam 08a
SS1-75-2.50-06

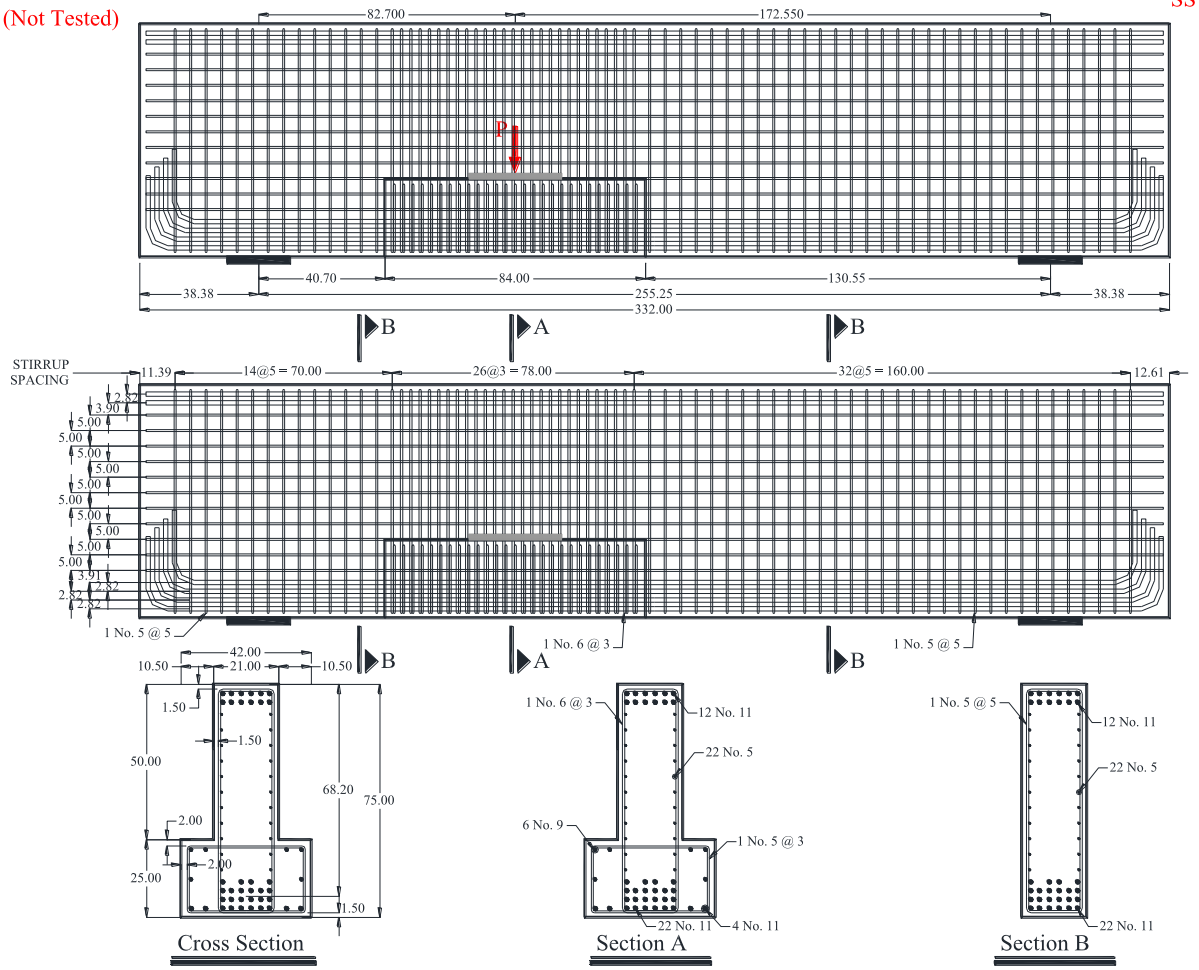

Beam 09

Beam 09a
DS3-42-2.50-03

Beam 09c
DS2-42-1.85-03

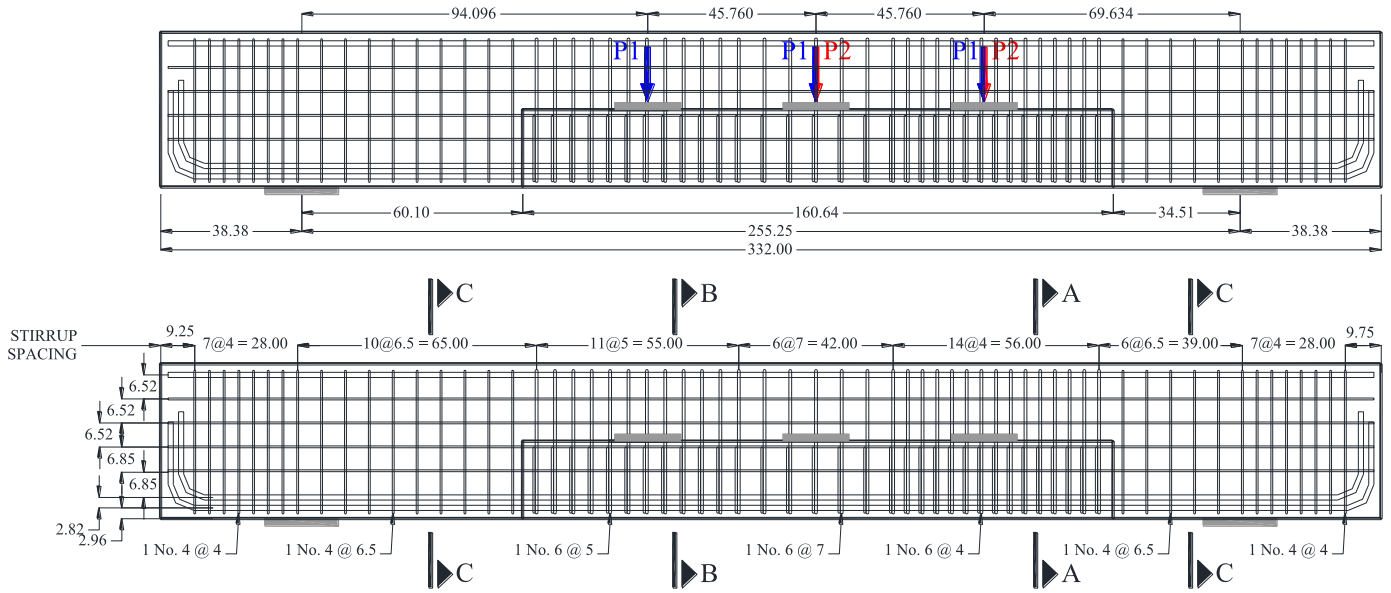

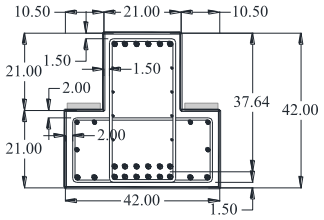

Cross Section

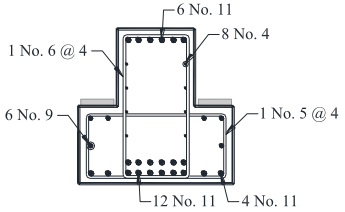

Section A

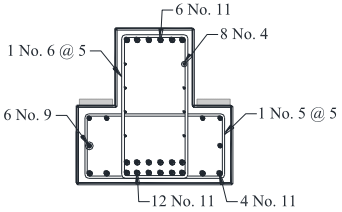

Section B

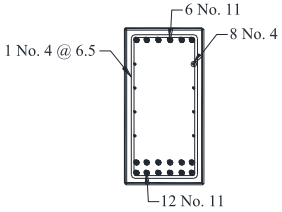

Section C

Beam 10

Beam 10b
DL1-42-2.50-03

Beam 010a
DL1-42-1.85-03

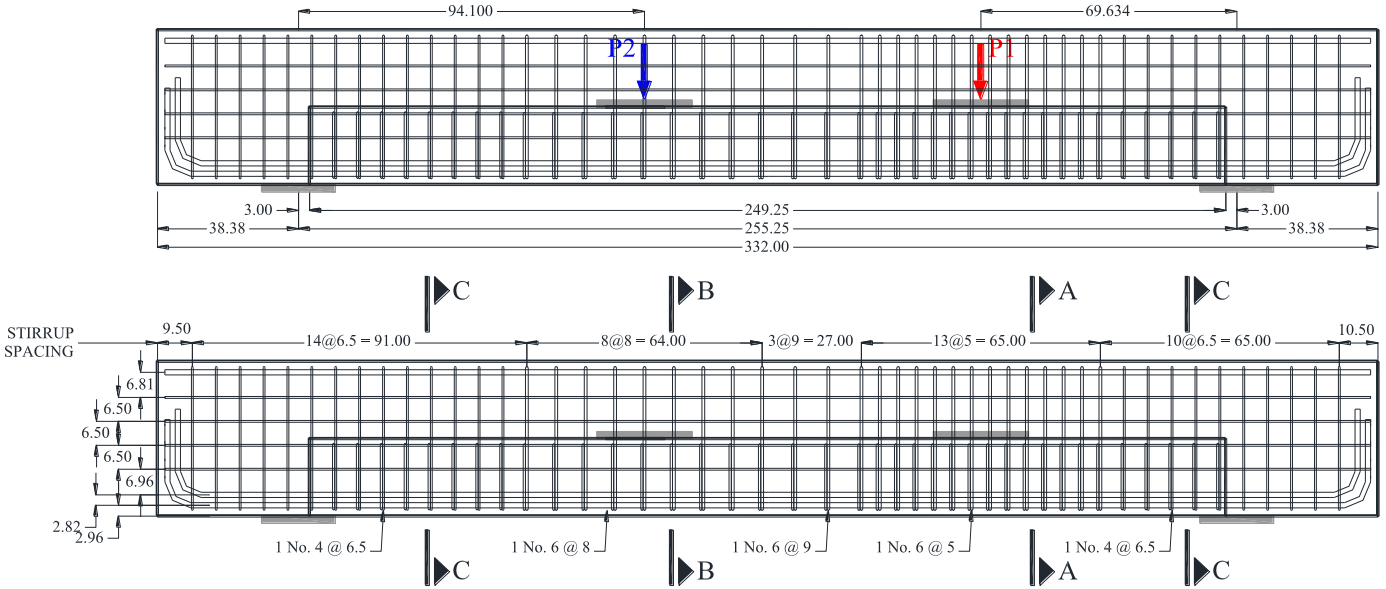

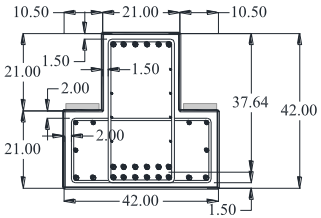

Cross Section

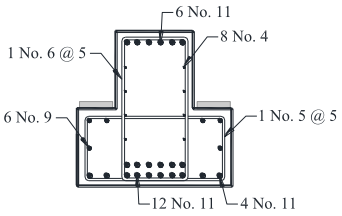

Section A

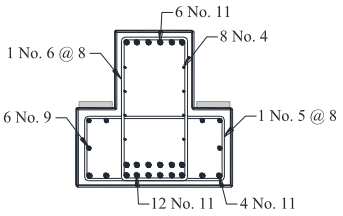

Section B

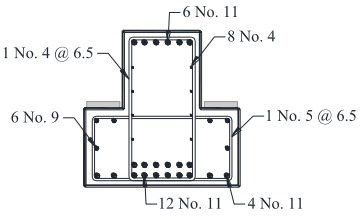

Section C

Beam 11

Beam 11b
SS3-42-2.50-03
(Not tested)

Beam 11a
SL3-42-1.85-03

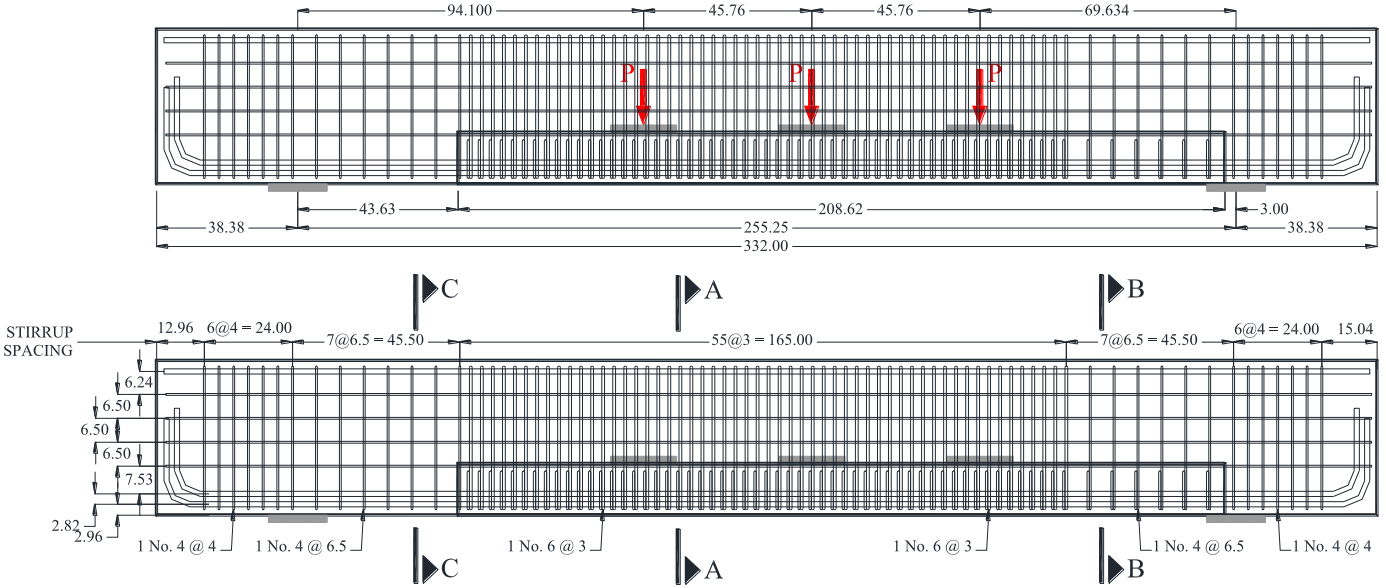

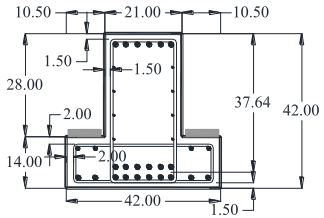

Cross Section

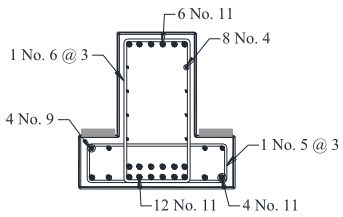

Section A

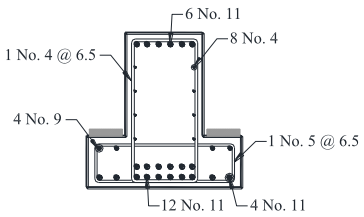

Section B

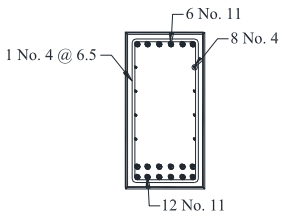

Section C

Beam 12

Beam 12b
SL3-42-2.50-06
(Not tested)

Beam 12a
SL3-42-1.85-06

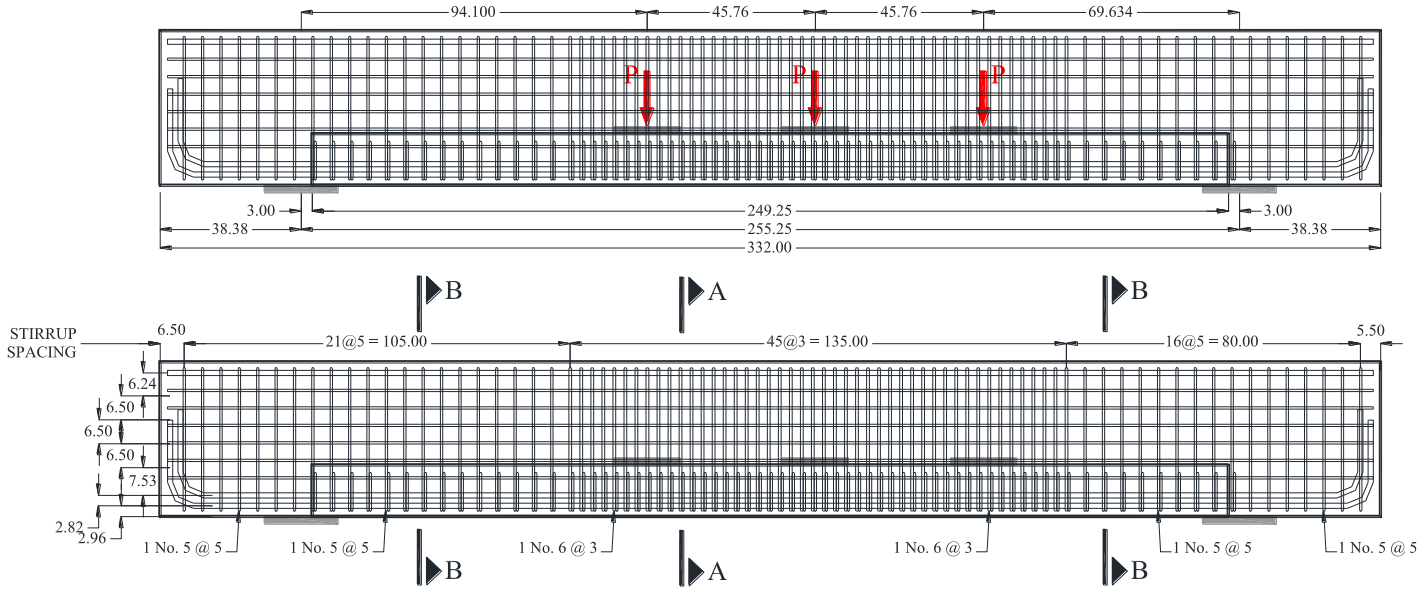

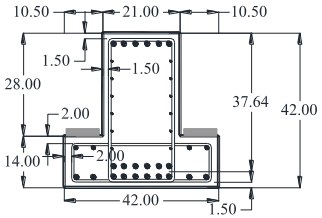

Cross Section

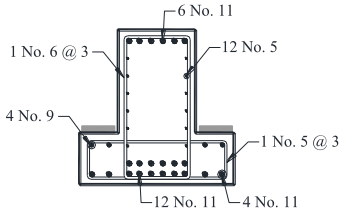

Section A

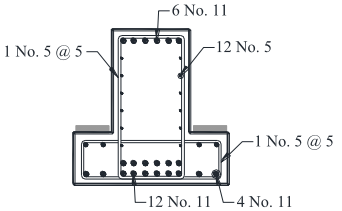

Section B

Beam 13

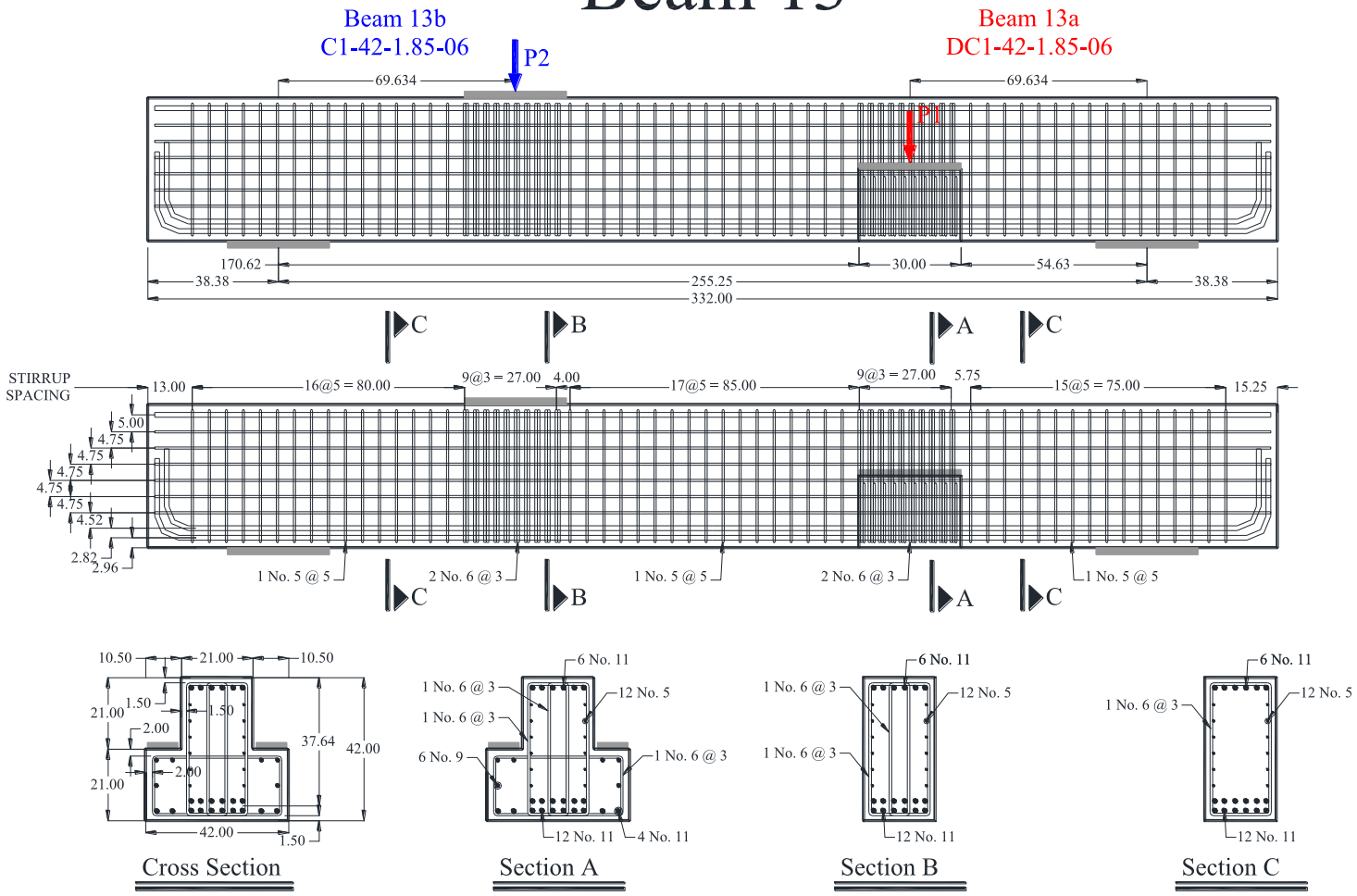
Beam 13b
C1-42-1.85-06
P2
Beam 13a
DC1-42-1.85-06
P1
69.634
69.634
170.62
30.00
54.63
38.38
255.25
38.38
332.00
C
B
A
C
STIRRUP SPACING
13.00
16@5 = 80.00
9@3 = 27.00
4.00
17@5 = 85.00
9@3 = 27.00
5.75
15@5 = 75.00
15.25
5.00
4.75
4.75
4.75
4.75
4.75
4.52
2.82
2.96
1 No. 5 @ 5
2 No. 6 @ 3
1 No. 5 @ 5
2 No. 6 @ 3
1 No. 5 @ 5
C
B
A
C
10.50
21.00
10.50
21.00
1.50
1.50
2.00
37.64
42.00
2.00
21.00
42.00
1.50
Cross Section
6 No. 11
1 No. 6 @ 3
12 No. 5
1 No. 6 @ 3
6 No. 9
1 No. 6 @ 3
12 No. 11
4 No. 11
Section A
6 No. 11
1 No. 6 @ 3
12 No. 5
1 No. 6 @ 3
12 No. 11
Section B
6 No. 11
1 No. 6 @ 3
12 No. 5
12 No. 11
Section C

Beam 14

Beam 14b
SS1-75-1.85-06b
(Not Tested)

Beam 14a
SS1-75-1.85-03b

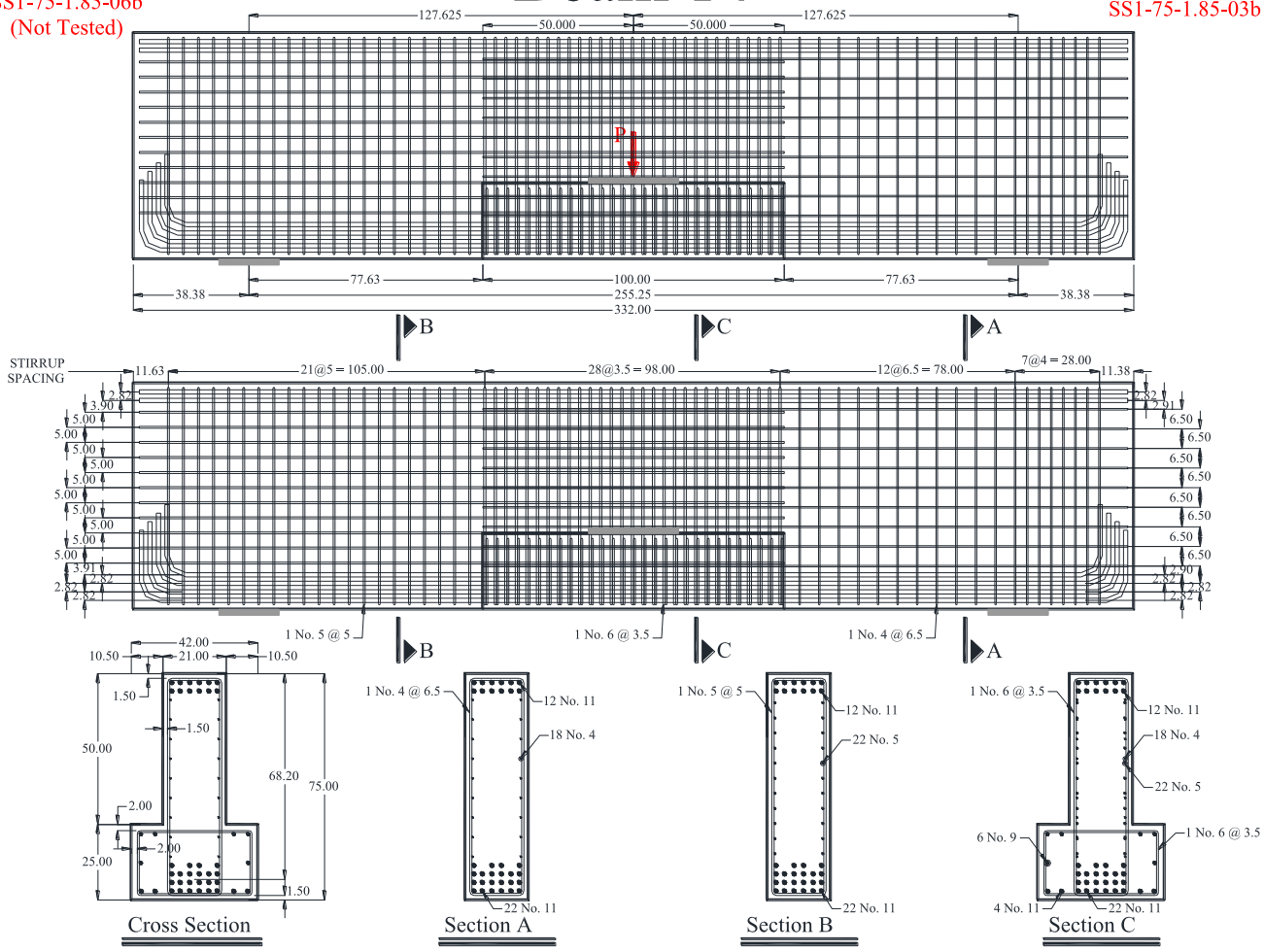

Beam 15

Beam 15b
DS3-42-1.85-03

Beam 15a
DC3-42-1.85-03

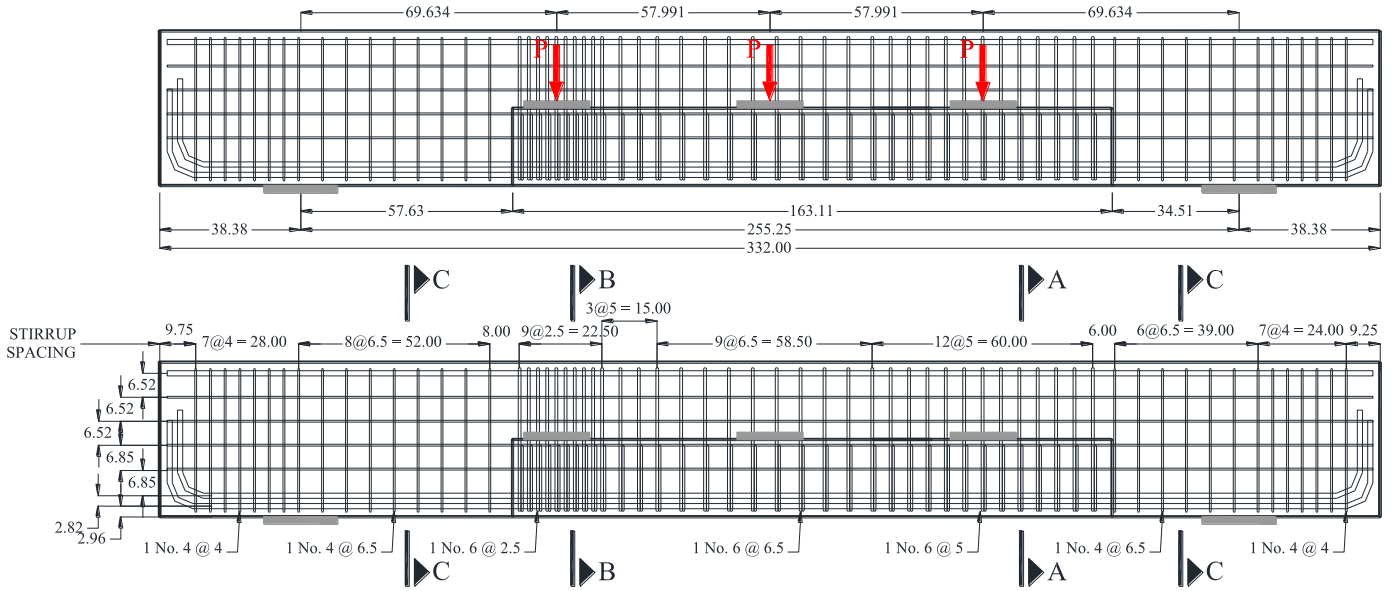

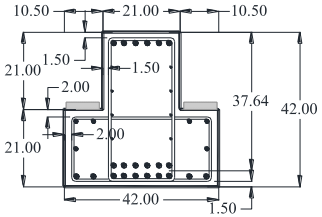

Cross Section

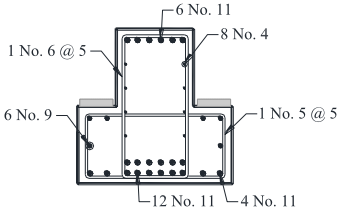

Section A

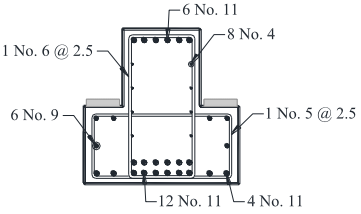

Section B

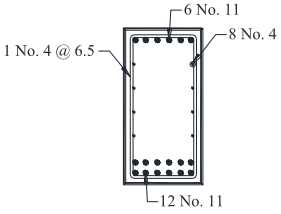

Section C

Beam 16

Beam 16b
SS1-42-1.85-03

Beam 16a
SS1-42-2.50-03

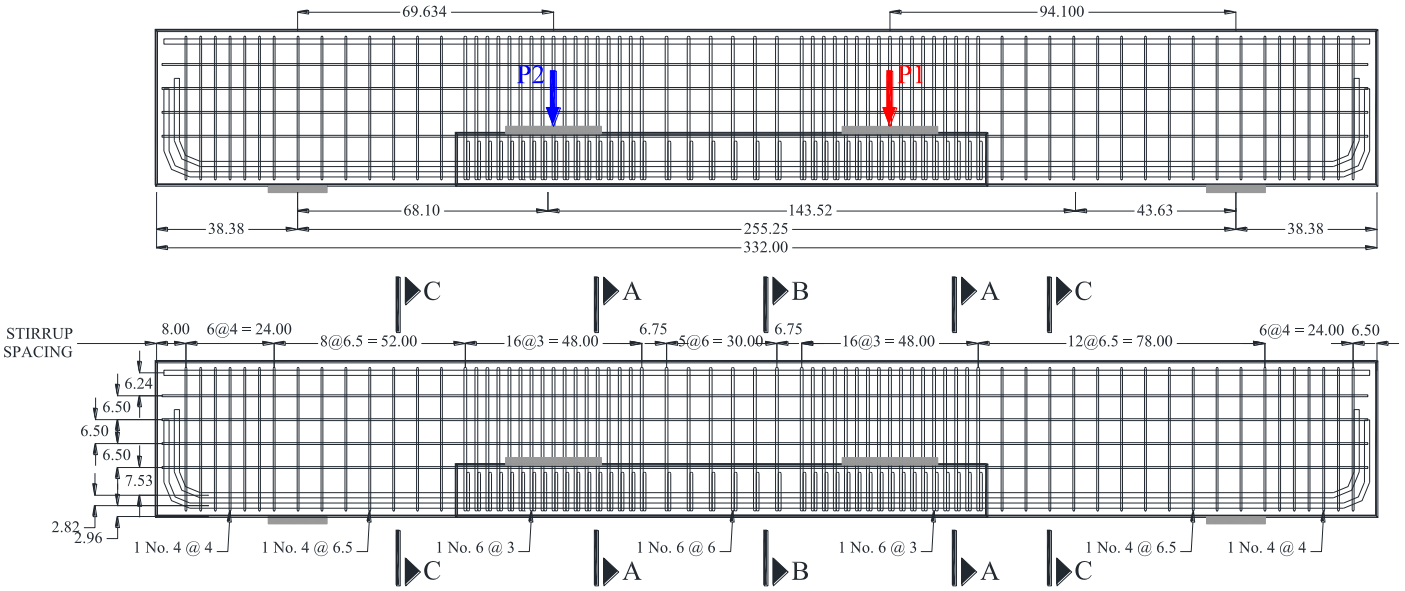

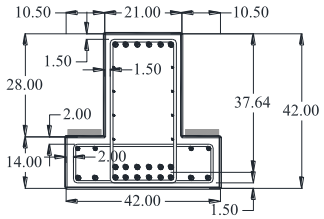

Cross Section

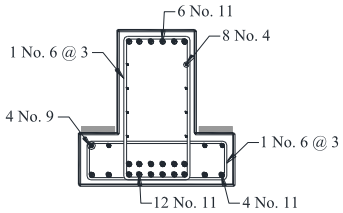

Section A

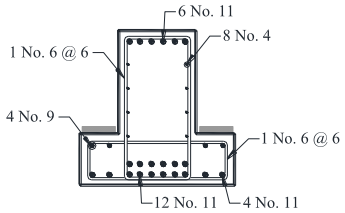

Section B

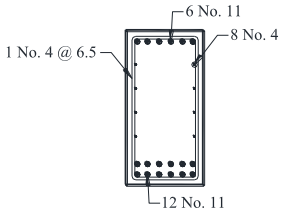

Section C

Beam 17

Beam 17b
DL3-42-1.85-03

Beam 17a
DC1-42-2.50-03

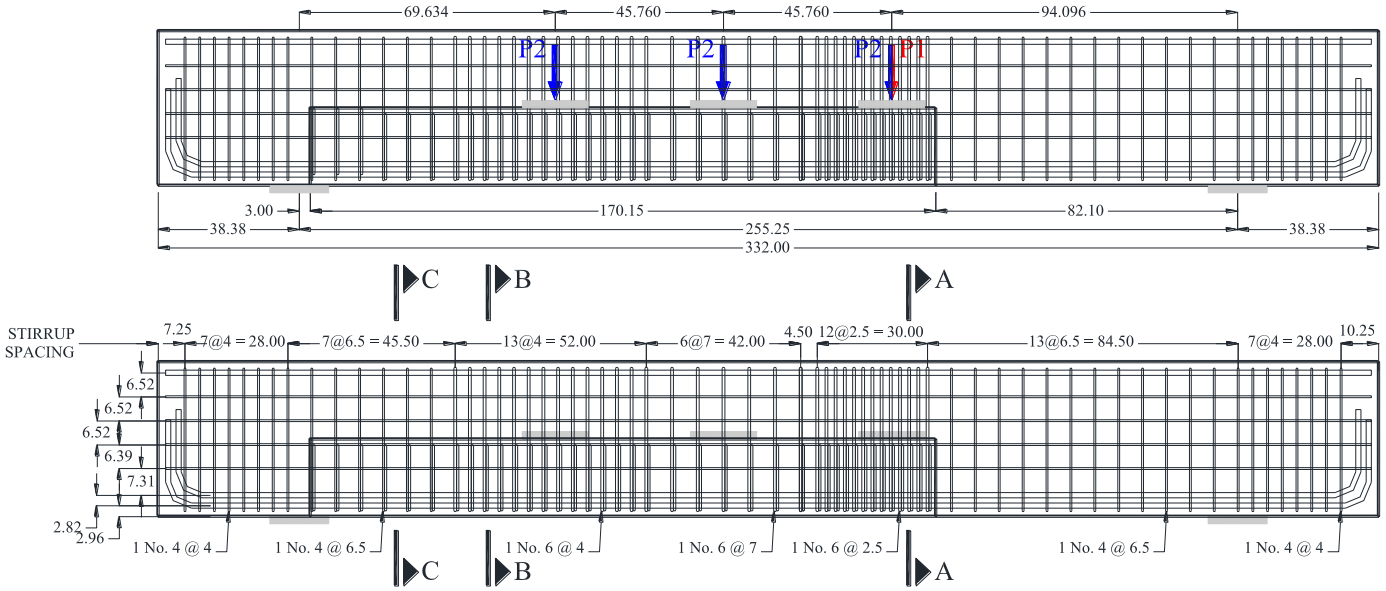

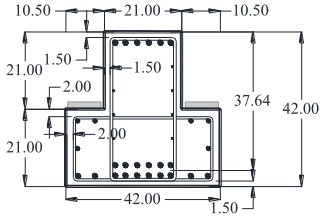

Cross Section

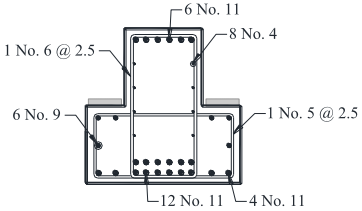

Section A

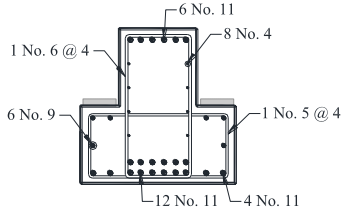

Section B

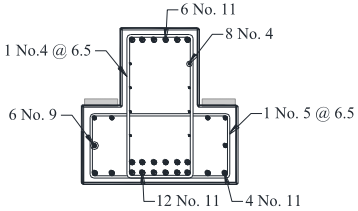

Section C

Beam 18

Beam 18b
SC1-42-2.50-03

Beam 18a
SL1-42-2.50-03

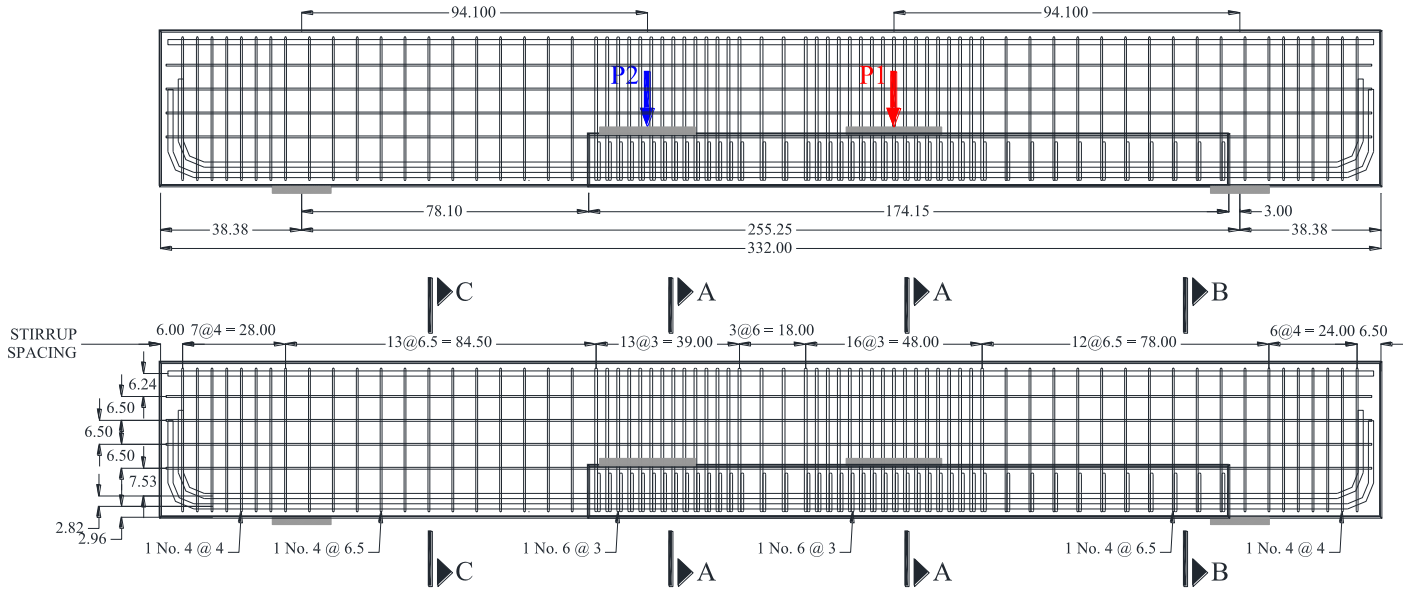

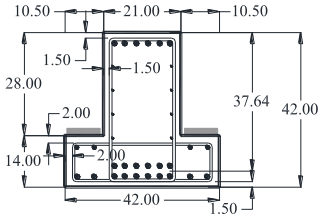

Cross Section

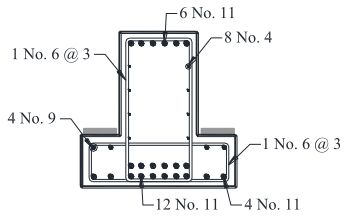

Section A

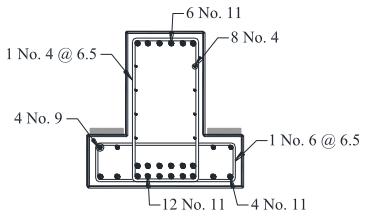

Section B

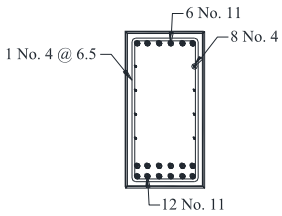

Section C

Beam 19

Beam 19a
DS1-42-2.50-03/06

Beam 19b
DS1-42-1.85-03/06

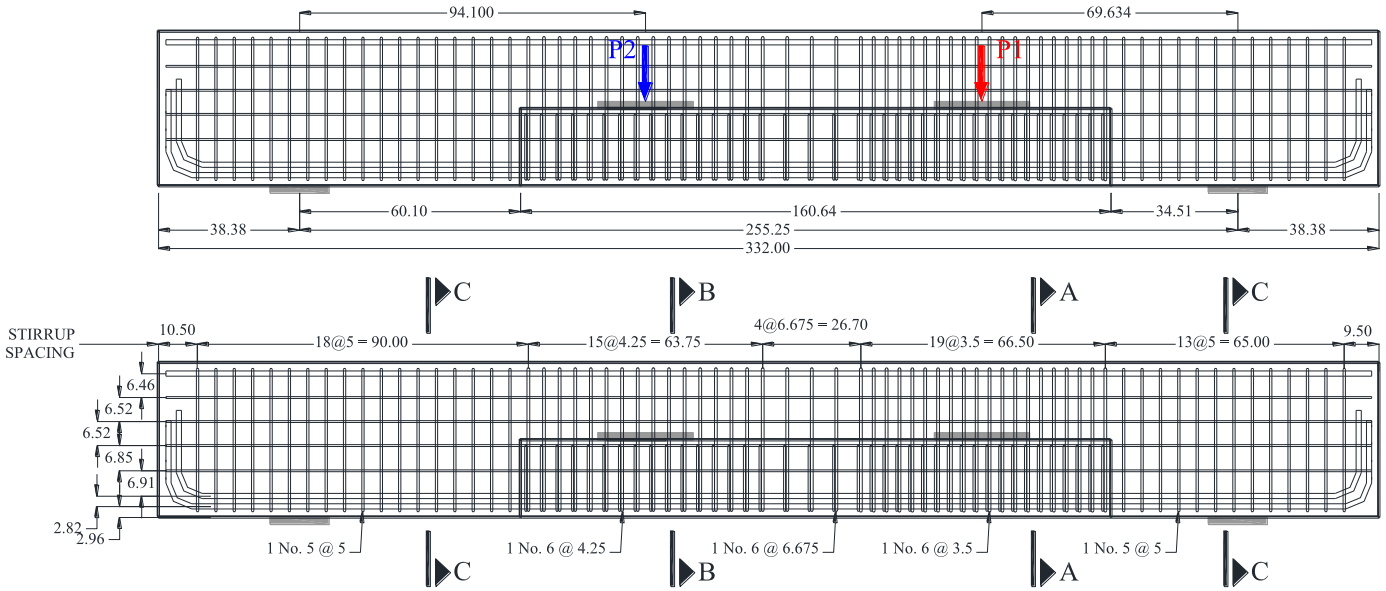

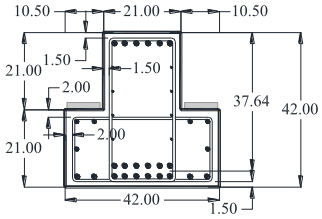

Cross Section

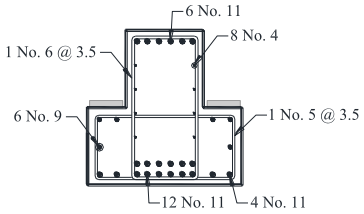

Section A

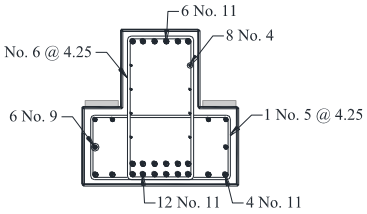

Section B

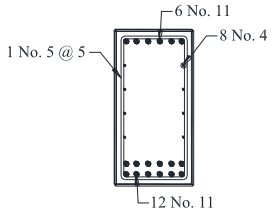

Section C

Beam 20

Beam 20b
DC1-42-1.85-03

Beam 20a
SC1-42-1.85-03

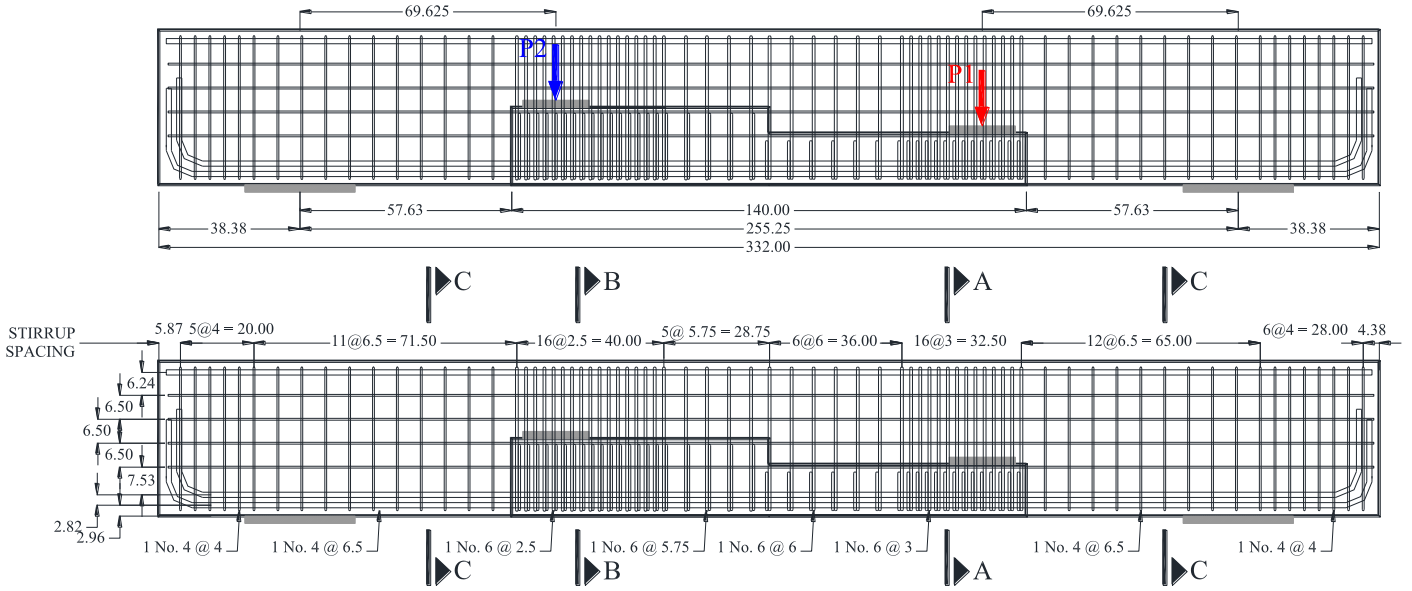

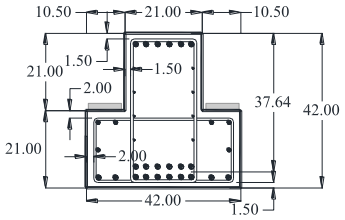

Cross Section

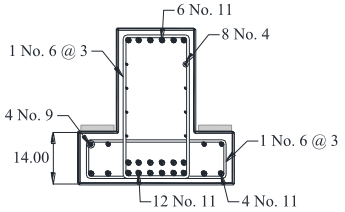

Section A

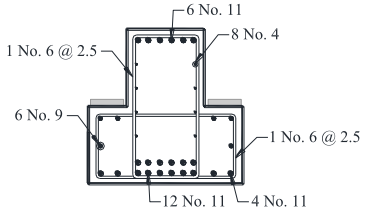

Section B

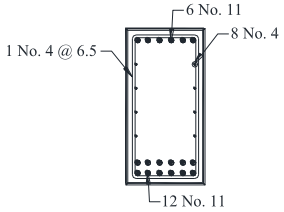

Section C

APPENDIX C
Design Example

C.1 OVERVIEW

A detailed example of the design of one specimens of the experimental program is provided in this appendix using the following provisions:

1. **STM PROVISIONS OF TXDOT PROJECT 5253**
2. **TXDOT BRIDGE DESIGN MANUAL – LRFD (2011)**
3. **ASHTO BRIDGE DESIGN SPECIFICATIONS (2012)**

Beam 01a: DS1-42-1.85-03 - TxDOT 0-5253 STM Design

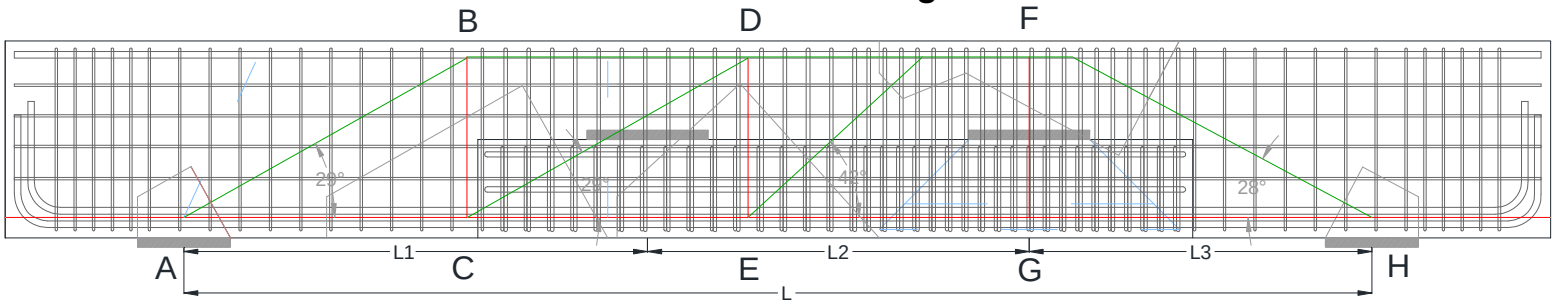

Gross Properties

$L := 255.25\,in$ Length of the beam between supports

$L_1 := 99.625\,in$ Support A to load 1

$L_2 := 82\,in$ Distance Between Loads

$L_3 := 73.625\,in$ Support I to load 2

$b := 21\,in$ Web width

$h_l := 21\,in$ Ledge Height

$w_l := 9\,in$ Load plate width

$l_l := 26\,in$ Load plate length

$w_s := 20\,in$ Support plate width

$l_s := 16\,in$ Support plate length

$d_l := h_l - 1.5\,in - 0.5 d_5 = 19.188\,in$ Top of ledge to comp reinf

$l_{sp} := l_l + 2 \cdot d_l = 64.375\,in$ Load spread

Material Properties

$f'_c := 5.26\,ksi$

$f_{y\_11} := 69.23929\,ksi$ $A_{11} := 1.56\,in^2$ $d_{11} := 1.41\,in$

$f_{y\_6} := 63.71\,ksi$ $A_6 := 0.44\,in^2$ $d_6 := 0.75\,in$

$f_{y\_5} := 62.996\,ksi$ $A_5 := 0.31\,in^2$ $d_5 := 0.625\,in$

$f_{y\_4} := 63.135\,ksi$ $A_4 := 0.20\,in^2$ $d_4 := 0.5\,in$

STM Factors

$\varphi := 1.0$

$\beta_{CCC\_b} := 0.85$

$\beta_{CCT\_b} := 0.7$

$\beta_{TTC} := 0.65$

$$\beta_{CCT\_stn} := \begin{cases} 0.45 & \text{if } \left(0.85 - \frac{f'_c}{20\,ksi}\right) < 0.45 = 0.587 \\ 0.65 & \text{if } \left(0.85 - \frac{f'_c}{20\,ksi}\right) > 0.65 \\ 0.85 - \frac{f'_c}{20\,ksi} & \text{otherwise} \end{cases}$$

Geometric Properties

$A'_s := 6 \cdot A_{11} = 9.36 \cdot in^2$ Compression Steel

$A_s := 12A_{11} = 18.72 \cdot in^2$ Flexure Steel

$w_{flex} := 2 \cdot 4.365in = 8.73 \cdot in$ Flexure Tie Width

$$a := \frac{A_s \cdot f_{y\_11} - A'_s \cdot f_{y\_11}}{0.85 \cdot b \cdot f'_c} = 6.902 \cdot in$$

$$d := 42in - \frac{w_{flex}}{2} = 37.635 \cdot in$$ Top of beam to center of flex

$$h := d - \frac{a}{2} = 34.184 \cdot in$$ Moment arm

$$a_{d2} := \frac{L_3}{d} = 1.956 \qquad a_{d1} := \frac{L_1}{d} = 2.647$$ Shear span-to-depth ratio

$$l_{fe} := l_{sp} \cdot \left(1 - \frac{L_1 + L_2}{L}\right) = 18.568 \cdot in$$

$$l_{fh} := l_{sp} \cdot \left(\frac{L_1 + L_2}{L}\right) = 45.807 \cdot in$$

$$l_h := 0.5l_{fh} + l_{fe} - 0.5l_{sp} = 9.284 \cdot in$$

$$l_e := l_{fh} + 0.5l_{fe} - 0.5l_{sp} = 22.903 \cdot in$$

$$\theta_A := \operatorname{atan}\left(\frac{3 \cdot h}{L_1 + L_2}\right) = 0.514$$

$$\Theta_A := \theta_A \cdot \frac{180}{\pi} = 29.45$$ Angle between Strut AB and Tie AC

$$\theta_C := \operatorname{atan}\left(\frac{3 \cdot h}{L_1 + L_2}\right) = 0.514$$

$$\Theta_C := \theta_C \cdot \frac{180}{\pi} = 29.45$$ Angle between Strut CD and Tie CE

$$\theta_E := \operatorname{atan}\left[\frac{h}{\left(\frac{L_1 + L_2}{3}\right) - l_e}\right] = 0.737$$

$$\Theta_E := \theta_E \cdot \frac{180}{\pi} = 42.246$$ Angle between Strut EG and Tie EF

$$\theta_H := \operatorname{atan}\left(\frac{h}{L_3 - l_h}\right) = 0.488$$

$$\Theta_H := \theta_H \cdot \frac{180}{\pi} = 27.981$$ Angle between Strut FH and Tie GH

Including Ledge Reinforcement:

$A_{s2} := 16 \cdot A_{11} = 24.96 \cdot in^2$

$w_{flex2} := 2 \cdot 3.98125in = 7.963 \cdot in$

$$a_2 := \frac{A_{s2} \cdot f_{y\_11} - A'_s \cdot f_{y\_11}}{0.85 \cdot b \cdot f'_c} = 11.504 \cdot in$$

$$d_2 := 42in - \frac{w_{flex2}}{2} = 38.019 \cdot in$$

$$h_2 := d_2 - \frac{a_2}{2} = 32.267 \cdot in$$

$A_1 := w_s \cdot l_s = 320 \cdot in^2$

$A_2 := \left(w_s \cdot 1.05\right)\left(l_s \cdot 1.05\right) = 352.8 \cdot in^2$

$$m := \sqrt{\frac{A_2}{A_1}} = 1.05$$

Member Capacities

Node

A

$R_A := \varphi \cdot \beta_{CCT\_b} \cdot f'_c \cdot m \cdot w_s \cdot l_s = 1237.152 \cdot kip$

$AB_A := \varphi \cdot \beta_{CCT\_stn} \cdot m \cdot w_s \cdot \left(l_s \cdot \sin\left(\theta_A\right) + w_{flex} \cdot \cos\left(\theta_A\right) \right) \cdot f'_c = 1002.988 \cdot kip$

Node F

$DF_F := \varphi \cdot \beta_{CCT\_stn} \cdot b \cdot a \cdot f'_c + A'_s \cdot f_{y\_11} = 1095.636 \cdot kip$

$EF_F := \varphi \cdot \beta_{CCT\_stn} \cdot b \cdot \left| \left(l_{fe} + a \cdot \tan\left(\theta_E\right) \right) \sin\left(\theta_E\right) - \frac{a}{\cos\left(\theta_E\right)} \right| \cdot f'_c = 478.149 \cdot kip$

$FH_F := \varphi \cdot \beta_{CCT\_stn} \cdot b \cdot \left(l_{fh} \cdot \sin\left(\theta_H\right) + a \cdot \cos\left(\theta_H\right) \right) \cdot f'_c = 1788.759 \cdot kip$

Node H

$FH_H := \varphi \cdot \beta_{CCT\_stn} \cdot m \cdot w_s \cdot \left(l_s \cdot \sin\left(\theta_H\right) + w_{flex} \cdot \cos\left(\theta_H\right) \right) \cdot f'_c = 986.633 \cdot kip$

$R_H := \varphi \cdot \beta_{CCT\_b} \cdot m \cdot f'_c \cdot w_s \cdot l_s = 1237.152 \cdot kip$

Load

$P_L := 2 \cdot \varphi \cdot \beta_{CCT\_b} \cdot f'_c \cdot w_l \cdot l_l = 1723.176 \cdot kip$

Member Forces

$P := FH_H \cdot \sin\left(\theta_H\right) \cdot \left(\frac{L}{L_1 + L_2} \right) = 650.56 \cdot kip$ $P = 651 \cdot kip$ *Design Beam to Fail at Strut-to-Node Interface at Node H*

Node H

$F_{RH} := \left(\frac{L_1 + L_2}{L} \right) P = 462.913 \cdot kip$ $\frac{R_H}{F_{RH}} = 2.673$

$$F_{FH} := \frac{F_{RH}}{\sin(\theta_H)} = 986.633 \cdot kip \qquad \frac{FH_H}{F_{FH}} = 1 \qquad \frac{FH_F}{F_{FH}} = 1.813 \qquad F_{GH} := F_{FH} \cdot \cos(\theta_H) = 871.296 \cdot kip$$

Node A

$$F_{RA} := \left(\frac{L_3}{L}\right) P = 187.65 \cdot kip \qquad \frac{R_A}{F_{RA}} = 6.593$$

$$F_{AB} := \frac{F_{RA}}{\sin(\theta_A)} = 381.658 \cdot kip \qquad \frac{AB_A}{F_{AB}} = 2.628 \qquad F_{AC} := F_{AB} \cdot \cos(\theta_A) = 332.341 \cdot kip$$

Node B

$$F_{BD} := F_{AB} \cdot \cos(\theta_A) = 332.341 \cdot kip \qquad \frac{DF_F}{F_{BD}} = 3.297 \qquad F_{BC} := F_{AB} \cdot \sin(\theta_A) = 187.65 \cdot kip$$

Node C

$$F_{CD} := \frac{F_{BC}}{\sin(\theta_C)} = 381.658 \cdot kip \qquad F_{CE} := F_{CD} \cdot \cos(\theta_C) + F_{AC} = 664.681 \cdot kip$$

Node D

$$F_{DF} := F_{CD} \cdot \cos(\theta_C) + F_{BD} = 664.681 \cdot kip \qquad \frac{DF_F}{F_{DF}} = 1.648 \qquad F_{DE} := F_{CD} \cdot \sin(\theta_C) = 187.65 \cdot kip$$

Node E

$$F_{EF} := \frac{F_{DE}}{\sin(\theta_E)} = 279.109 \cdot kip \qquad \frac{EF_F}{F_{EF}} = 1.713 \qquad F_{EG} := F_{EF} \cdot \cos(\theta_E) + F_{CE} = 871.296 \cdot kip$$

Node F

$$F_{FG} := F_{EF} \cdot \sin(\theta_E) + F_{FH} \cdot \sin(\theta_H) = 650.563 \cdot kip$$

Checks

$$F_{RH} + F_{RA} - P = 0 \cdot kip \qquad F_{EG} - F_{GH} = -0 \cdot kip \qquad F_{DF} + F_{EF} \cdot \cos(\theta_E) - F_{FH} \cdot \cos(\theta_H) = -0 \cdot kip$$

Tie Requirements

Flexural Reinforcement- #11 bars

$F_{flex} := \max(F_{AC}, F_{CE}, F_{EG}, F_{GH}) = 871.296 \cdot kip$

$T_{flex} := A_s \cdot f_{y\_11} = 1296.16 \cdot kip$

$\frac{T_{flex}}{F_{flex}} = 1.488$

Hanger Bars- #6 stirrups

$T_{FG} := 38 \cdot A_6 \cdot f_{y\_6} = 1065.231 \cdot kip$

$\frac{T_{FG}}{F_{FG}} = 1.637$

Tie BC- #4 stirrups and #6 hangers

$T_{BC} := 16A_4 \cdot f_{y\_4} + 10A_6 \cdot f_{y\_6} = 482.356 \cdot kip$

$\frac{T_{BC}}{F_{BC}} = 2.571$

Tie DE- #6 hangers

$T_{DE} := 20A_6 \cdot f_{y\_6} = 560.648 \cdot kip$

$\frac{T_{DE}}{F_{DE}} = 2.988$

Cross Section Model

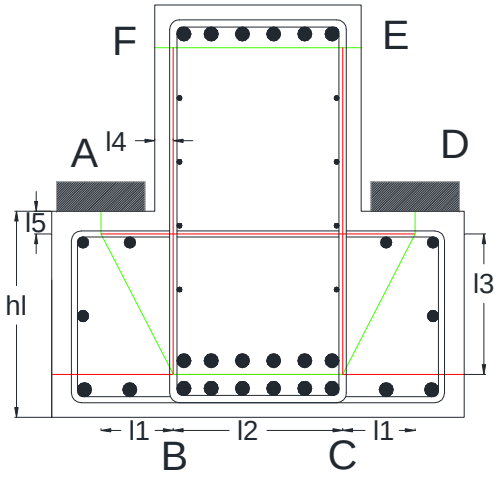

Truss Geometry

$l_4 := \left(1.5 + \frac{3}{8}\right)in$

$l_1 := l_4 + 1in + 0.5w_l = 7.375 \cdot in$

$l_3 := h_l - 0.5w_{flex} - l_5 = 14.322 \cdot in$

$l_n := l_{sp} - w_{flex}$

$\theta := \operatorname{atan}\left(\frac{l_3}{l_1}\right) = 1.095$

$l_2 := b - 2l_4 = 17.25 \cdot in$

$l_5 := \left(2 + \frac{5}{16}\right)in = 2.313 \cdot in$

$a_f := 5.5in$

$l_{ledge} := l_l + 5 \cdot a_f = 53.5 \cdot in$

$\Theta := \theta \cdot \frac{180}{\pi} = 62.755$

Truss Capacities

Node a

$R_a := \varphi \cdot \beta_{CCT\_b} \cdot f'_c \cdot w_l \cdot l_l = 861.588 \cdot kip$

$ab_a := \varphi \cdot \beta_{CCT\_stn} \cdot l_l \cdot \left(w_l \cdot \sin(\theta) + 2l_5 \cdot \cos(\theta)\right) \cdot f'_c = 812.32 \cdot kip$

Node b

$ab_b := \varphi \cdot \beta_{CCT\_stn} \cdot l_{sp} \cdot \left(w_{flex} \cdot \cos(\theta) + 2l_4 \cdot \sin(\theta)\right) \cdot f'_c = 1457.057 \cdot kip$

$bc_b := \varphi \cdot \beta_{CCT\_stn} \cdot l_n \cdot w_{flex} \cdot f'_c = 1499.907 \cdot kip$

Truss Forces

$T_{Ra} := \frac{P}{2} = 325.282 \cdot kip$

$\frac{R_a}{T_{Ra}} = 2.649$

$T_{ab} := \frac{T_{Ra}}{\sin(\theta)} = 365.873 \cdot kip$

$\frac{ab_a}{T_{ab}} = 2.22$

$T_{dc} := T_{ab} = 365.873 \cdot kip$

$T_{bc} := T_{ab} \cdot \cos(\theta) = 167.495 \cdot kip$

$\frac{bc_b}{T_{bc}} = 8.955$

$T_{ad} := T_{ab} \cdot \cos(\theta) = 167.495 \cdot kip$

$T_{bf} := T_{ab} \cdot \sin(\theta) = 325.282 \cdot kip$

$T_{ce} := 0.5F_{FG} = 325.282 \cdot kip$

$T_{bf} - T_{ce} = \blacksquare \cdot kip$

Tie Requirements

Tie ad- #5 bars

$Tie_{ad} := 15 \cdot A_5 \cdot f_{y\_5} = 292.931 \cdot kip$

$\frac{Tie_{ad}}{T_{ad}} = 1.749$

Bars in ledge spread length

Tie bf- #6 bars

Checked in elevation STM

Hanger Reinforcement:

$s_{bar\_S} := 3.5in$ $n_{legs} := 2$

$a_v := 5.5in$ Distance between Load and Face of web

$c := 35.125in$ Distance between Load and end of ledge

$S := L_2 = 82 \cdot in$ Distance between Loads

$fy := f_{y\_6} = 63.71 \cdot ksi$

$b_v := b = 21 \cdot in$

$W := l_l = 26 \cdot in$

$A_{hr} := A_6 \cdot n_{legs} = 0.88 \cdot in^2$

$$A_{hr\_min} := 0.0316 \frac{kip^{0.5}}{in} \cdot \sqrt{f'_c} \cdot \frac{b_v \cdot s_{bar\_S}}{fy} = 0.084 \cdot in^2$$

$$Min_{hr\_SteelCheck} := \begin{cases} \text{"OK"} & \text{if } A_{hr\_min} \le A_{hr} \\ \text{"NG"} & \text{otherwise} \end{cases}$$

$Min_{hr\_SteelCheck} = \text{"OK"}$

Service Limit State *AASHTO LRFD 5.13.2.5.5*

Interior Beams

$$V_{all\_1} := \frac{A_{hr} \cdot \left(\frac{2}{3} fy\right)}{s_{bar\_S}} \cdot \left(W + 3a_v\right) = 454 \cdot kip$$

$$V_{all\_2} := \frac{A_{hr} \cdot \left(\frac{2}{3} fy\right)}{s_{bar\_S}} \cdot (S) = 876 \cdot kip$$

$$Vn_{int\_serv} := \min\left(V_{all\_1}, V_{all\_2}\right) = 454 \cdot kip$$

$$Vn_{hr\_serv} := \min\left(Vn_{int\_serv}, Vn_{ext\_serv}\right) = 454 \cdot kip$$

$Vn_{hr\_serv} = 454 \cdot kip$

Exterior Beams

$$V_{all\_3} := \frac{A_{hr} \cdot \left(\frac{2}{3} fy\right)}{s_{bar\_S}} \cdot \left(\frac{W + 3a_v}{2} + c\right) = 602 \cdot kip$$

$$V_{all\_4} := \frac{A_{hr} \cdot \left(\frac{2}{3} fy\right)}{s_{bar\_S}} \cdot \left(\frac{S}{2} + c\right) = 813 \cdot kip$$

$$Vn_{ext\_serv} := \min\left(V_{all\_3}, V_{all\_4}\right) = 602 \cdot kip$$

Strength Limit State *AASHTO LRFD 5.13.2.5.5*

$b_f := 42in$ Flange width

$d_f := d_l = 19.188\,in$

Interior Beams

$$V_{n\_1} := \frac{A_{hr}\cdot fy}{s_{bar\ S}}\cdot S = 1314\cdot kip$$

$$V_{n\_2} := 0.063\,\frac{kip^{0.5}}{in}\sqrt{f'_c}\cdot b_f\cdot d_f + \frac{A_{hr}\cdot fy}{s_{bar\_S}}\cdot\left(W + 2d_f\right) = 1148\cdot kip$$

$$Vn_{int\_strength} := \min\left(V_{n\_1}, V_{n\_2}\right) = 1148\cdot kip$$

Exterior Beams

$$V_{n\_3} := \frac{A_{hr}\cdot fy}{s_{bar\ S}}\cdot\left(\frac{S}{2} + c\right) = 1219\cdot kip$$

$$V_{n\_4} := 0.063\,\frac{kip^{0.5}}{in}\sqrt{f'_c}\cdot b_f\cdot d_f + \frac{A_{hr}\cdot fy}{s_{bar\_S}}\cdot\left(\frac{W + 2d_f}{2} + c\right)$$

$V_{n\_4} = 1194.686\cdot kip$

$$Vn_{ext\_strength} := \min\left(V_{n\_1}, V_{n\_2}, V_{n\_3}, V_{n\_4}\right) = 1148\cdot kip$$

$$Vn_{hr\_stre} := \min\left(Vn_{int\_strength}, Vn_{ext\_strength}\right) = 1148\cdot kip$$

$Vn_{hr\_stre} = 1148\cdot kip$

Stirrups: Nominal Shear Resistance:

AASHTO LRFD 5.8.3.3

Find dv:

$A_s := 12A_{11} = 18.72\cdot in^2$ $A'_s := 6\cdot A_{11} = 9.36\cdot in^2$

$H := 42in$

$d := H - 4.365in = 37.635\,in$

$d' := 2.955in$ top cover + 1/2 bar

$A_{stirrup} := 0.2in^2$

$Legs := 2$

$s_{stirrup} := 6.5in$

$\beta := 2$

$\theta := 45deg$

$\alpha := 90deg$

$fy_v := f_{y\_4} = 63.135\cdot ksi$

As per AASHTO 5.8.3.4.1 - Simpliefied procedure for Nonprestressed Sections

Angle of stirrups to long axis

$$\beta_1 := \begin{cases} 0.85 & \text{if } f'_c \le 4ksi \\ 0.65 & \text{if } f'_c \ge 8\cdot ksi \\ 0.85 - \frac{0.05}{ksi}\cdot\left(f'_c - 4ksi\right) & \text{otherwise} \end{cases} = 0.787$$

$$A_v := A_{stirrup} \cdot Legs = 0.4 \cdot in^2$$

$$a := \frac{A_s \cdot f_{y\_11} - A'_s \cdot f_{y\_11}}{0.85 \cdot f'_c \cdot b} = 6.902 \cdot in$$

$$Mn := A'_s \cdot f_{y\_11} \cdot (d - d') + \left(0.85 \cdot f'_c \cdot b \cdot a\right) \cdot \left(d - \frac{a}{2}\right) = 3719.101 \cdot kip \cdot ft$$

$$dv1 := \frac{Mn}{A_s \cdot f_{y\_11}} = 34.432\,in \qquad dv2 := 0.9d = 33.872\,in$$

$$dv3 := 0.72H = 30.24\,in$$

$$d_v := \max(dv1, dv2, dv3) = 34.432\,in$$

$$V_c := 0.0316 \frac{kip^{0.5}}{in} \cdot \beta \cdot \sqrt{f'_c} \cdot b_v \cdot d_v = 104.807 \cdot kip$$

$$V_s := \frac{A_v \cdot fy_v \cdot d_v \cdot (\cot(\theta) + \cot(\alpha)) \cdot \sin(\alpha)}{s_{stirrup}} = 133.776 \cdot kip$$

$$Vn1 := V_c + V_s = 238.583 \cdot kip$$

$$Vn2 := 0.25 f'_c \cdot b_v \cdot d_v = 950.836 \cdot kip$$

$$Vn_{stirrup} := \min(Vn1, Vn2) = 239 \cdot kip$$

$$A_{v\_min1} := 0.0316 \cdot \frac{kip^{0.5}}{in} \cdot \sqrt{f'_c} \frac{b_v \, s_{stirrup}}{fy} = 0.155 \cdot in^2$$

$$A_{vMinCheck1} := \begin{cases} \text{"OK"} & \text{if } A_{v\_min1} \le A_v \\ \text{"NG"} & \text{otherwise} \end{cases}$$

$$A_{vMinCheck1} = \text{"OK"}$$

$$A_{vminCheck2} := \begin{cases} \text{"OK"} & \text{if } \frac{A_v}{b \cdot s_{stirrup}} \ge 0.003 \\ \text{"NG"} & \text{otherwise} \end{cases}$$

$$A_{vminCheck\_2} := \text{"OK"}$$

Maximum Spacing of Transverse Reinforcement: *AASHTO LRFD 5.8.2.7*

Shear Stress

$$v_u := \frac{Vn_{stirrup}}{b_v \cdot d_v} = 0.33 \cdot ksi$$

$$v_{lim} := 0.125 \cdot f'_c = 0.657 \cdot ksi$$

$$s_{stirrup\_Max1} := \begin{cases} \min(0.8 d_v, 24in) & \text{if } v_u < v_{lim} \\ \min(0.4 d_v, 12in) & \text{if } v_u \geq v_{lim} \end{cases} = 24\,in$$

$$s_{stirrup\_Max} := \min(s_{stirrup\_Max1}, 12in) = 12\,in$$

$$s_{stirrup\_Check} := \begin{cases} \text{"NG"} & \text{if } s_{stirrup\_Max} < s_{stirrup} \\ \text{"OK"} & \text{if } s_{stirrup\_Max} > s_{stirrup} \end{cases}$$

$$s_{stirrup\_Check} = \text{"OK"}$$

Skin Reinforcement: *AASHTO LRFD 5.7.3.4*

$$A_{bar\_T} := A_{stirrup} = 0.2\,in^2$$

$NoTBarsStem := 4$ Number of Bars per face

$$A_{sk\_Req1} := 0.012 \frac{in}{ft} \cdot (d - 30in) = 0.092 \cdot \frac{in^2}{ft}$$

$$A_{sk\_max} := \frac{A_s}{4} \div \frac{d}{2} = 2.984 \cdot \frac{in^2}{ft}$$

$$A_{sk\_Req} := \min(A_{sk\_Req1}, A_{sk\_max}) = 0.092 \cdot \frac{in^2}{ft}$$

$$A_{sk\_prov} := \frac{A_{bar\_T} \cdot NoTBarsStem}{d} = 0.255 \cdot \frac{in^2}{ft}$$

$$A_{sk\_provCheck} := \begin{cases} \text{"OK"} & \text{if } A_{sk\_prov} > A_{sk\_Req} \\ \text{"NG"} & \text{if } A_{sk\_prov} < A_{sk\_Req} \end{cases}$$

$$A_{sk\_provCheck} = \text{"OK"}$$

Check Punching Shear: *AASHTO LRFD 5.13.2.5.4*

with modifications from the TxDOT LRFD Bridge Design Manual

Determine if the Shear Cones Intersect

Longidutinal:

$$Overlap_{l\_Check} := \begin{cases} \text{"OK"} & \text{if } S \geq 2d_f + w_l \\ \text{"NG - Cones Overlap"} & \text{otherwise} \end{cases}$$

$Overlap_{l\_Check} = \text{"OK"}$

Transversal:

$$Overlap_{t\_Check} := \begin{cases} \text{"OK"} & \text{if } 0.5 \cdot b + a_v \geq d_f + 0.5l_l \\ \text{"NG - Cones Overlap"} & \text{otherwise} \end{cases}$$

$Overlap_{t\_Check} = \text{"NG - Cones Overlap"}$

---> Need to check combined surface areas

$$V_{PC\_Int} := 0.125ksi^{.5} \cdot \sqrt{f'_c} \cdot \left(l_l \cdot b + \sqrt{2d_f^{\,2}} \cdot b_f \cdot 2 \right) = 810 \cdot kip$$

$$V_{PC\_Ext1} := 0.125ksi^{.5} \cdot \sqrt{f'_c} \cdot \left[\left(c + \frac{l_l}{2} \right) \cdot b + \sqrt{2d_f^{\,2}} \cdot b_f \right] = 616 \cdot kip$$

$V_{PC\_Ext} := V_{PC\_Int}$

$V_{PC\_Ext} = 810 \cdot kip$

Check Shear Friction (Concrete):

AASHTO LRFD 5.13.2.5.2

$d_e := 18.6875in$ Distance from bottom of ledge to tension reinforcement

Distribution Width for Shear:

AASHTO LRFD 5.13.2.5.2

Exterior Beams:

$$b_s := \min\left(l_l + 4a_v, S, 2c\right) = 48\,in$$

$A_{cv} := d_e \cdot b_s = 897\,in^2$

$$Vn_{c\_vf} := \min\left(0.2f'_c \cdot A_{cv}, 0.8ksi \cdot A_{cv}\right) = 718 \cdot kip$$

$Vn_{c\_vf} = 718 \cdot kip$

Bearing at loading points:

AASHTO LRFD 5.7.5

$A_l := w_l \cdot l_l = 234 \cdot in^2$

$Vn_b := 0.85 \cdot f'_c \cdot A_l = 1046 \cdot kip$

Ledge Reinforcement:

$s_{le} := 3.5in$ Spacing ledge

$As_{le} := 0.31in^2$ Area of ledge bars

$a_f := 7.375in$ Distance from load to hanger

Distribution Width for Shear:
AASHTO LRFD 5.13.2.5.2

Interior Beams:

$b_{s\_Int} := \min(l_l + 4a_v, S) = 48\,in$

Exterior Beams:

$b_{s\_Ext} := \min(l_l + 4a_v, S, 2c) = 48\,in$

Distribution Width for Bending and Axial Loads: *AASHTO LRFD 5.13.2.5.3*

Exterior Beams:

$b_{m\_Ext} := \min(l_l + 5a_f, S, 2c) = 62.875\,in$

Shear Friction: *AASHTO LRFD 5.8.4.1*

$\mu := 1.4$ Friction coefficient *AASHTO LRFD 5.8.4.3*

$c_1 := 0ksi$ Cohesion coefficient for corbels and ledges

$P_c := 0kip$ Axial compression

$f_{y\_ledge} := f_{y\_5} = 63\cdot ksi$

$f_{y\_le} := \min(f_{y\_ledge}, 60ksi) = 60\cdot ksi$

Minimum reiforcement: *AASHTO LRFD 5.8.4.4-1*

Exterior Beams:

$A_{vf\_Ext} := \frac{b_{s\_Ext}}{s_{le}}\cdot As_{le} = 4.251\,in^2$ $\quad a_{vf} := \frac{A_{vf\_Ext}}{b_{s\_Ext}} = 1.063\cdot\frac{in^2}{ft}$

$a_{vf\_min} := \frac{0.05ksi\cdot d_e}{f_{y\_le}} = 0.187\cdot\frac{in^2}{ft}$

$A_{vf\_min} := a_{vf\_min}\cdot b_{s\_Ext} = 0.748\,in^2$

$A_{vf\_minCheck} := \begin{cases} \text{"OK"} & \text{if } A_{vf\_Ext} \geq A_{vf\_min} \\ \text{"NG"} & \text{otherwise} \end{cases}$ $\quad A_{vf\_minCheck} = \text{"OK"}$

$A_{cv\_Ext} := d_e\cdot b_{s\_Ext} = 897\,in^2$

$Vn_{vf\_Ext} := c_1\cdot A_{cv\_Ext} + \mu\cdot(A_{vf\_Ext}\cdot f_{y\_le} + P_c)$ $\quad Vn_{vf\_Ext} = 357\cdot kip$

Ledge Flexure/Axial Reinforcement: *AASHTO LRFD 5.13.2.4.1, 5.13.2.4.2*

$Vu_{le} := 661kip$ (Per side)

$Nu_{le} := 0.2Vu_{le} = 132.2 \cdot kip$

$Mu_{le} := Vu_{le} \cdot a_v + Nu_{le} \cdot \left(h_l + 1in - d_e\right) = 4073 \cdot kip \cdot in$

$a_{n\_Min} := 0.04 \frac{f'_c}{f_{y\_ledge}} d_e = 0.749 \cdot \frac{in^2}{ft}$

$A_{n\_req} := \frac{Nu_{le}}{f_{y\_ledge}} = 2.099\,in^2$ $\quad a_n := \frac{A_{n\_req}}{b_{m\ Ext}} = 0.401 \cdot \frac{in^2}{ft}$

$A_{le} := \frac{b_{m\_Ext}}{s_{le}} \cdot As_{le} = 5.569\,in^2$ $\quad a_{le} := \frac{As_{le}}{s_{le}} = 1.063 \cdot \frac{in^2}{ft}$

$A_{sf} := A_{le} - A_{n\_req} = 3.47\,in^2$ $\quad a_{sf} := \frac{A_{sf}}{b_{m\_Ext}} = 0.662 \cdot \frac{in^2}{ft}$

$c_{le} := \frac{A_{sf} \cdot f_{y\_ledge}}{0.85 \cdot f'_c \cdot \beta_1 \cdot b_{m\_Ext}} = 0.988\,in$

$a_{ledge} := c_{le} \cdot \beta_1 = 0.778\,in$

$Mn_{le} := A_{sf} \cdot f_{y\_ledge} \cdot \left(d_e - \frac{a_{le}}{2}\right) = 4076 \cdot kip \cdot in$

$Vn_{le} := 2 \cdot Vu_{le} = 1322\,kip$

$\frac{Mn_{le}}{Mu_{le}} = 1$

$A_{leCheck1} := \begin{cases} \text{"OK"} & \text{if } a_{le} \geq a_{n\_Min} \\ \text{"NG"} & \text{otherwise} \end{cases} = \text{"OK"}$

$A_{leCheck2} := \begin{cases} \text{"OK"} & \text{if } a_{le} \geq \left(a_n + a_{sf}\right) \\ \text{"NG"} & \text{otherwise} \end{cases} = \text{"OK"}$

$A_{leCheck3} := \begin{cases} \text{"OK"} & \text{if } a_{le} \geq \left(\frac{2a_{vf}}{3}\right) \\ \text{"NG"} & \text{otherwise} \end{cases} = \text{"OK"}$

$A_{leCheck4} := \begin{cases} \text{"OK"} & \text{if } a_n \geq 0.5 \cdot \left(a_{le} - a_n\right) \\ \text{"NG"} & \text{otherwise} \end{cases} = \text{"OK"}$

$A_{leCheck} := \begin{cases} \text{"OK"} & \text{if } \left(A_{leCheck1} = \text{"OK"} \wedge A_{leCheck2} = \text{"OK"} \wedge A_{leCheck3} = \text{"OK"} \wedge A_{leCheck4} = \text{"OK"}\right) \\ \text{"NG"} & \text{otherwise} \end{cases} = \text{"OK"}$

$A_{leCheck} = \text{"OK"}$

Flexural Reinforcement

$b_{stem} := b = 21\,in$ width of stem

$d_{stem} := H - h_l = 21\,in$ depth of stem

$b_f = 42\,in$ width of bottom flange

$b_{ledge} := 10.5in$ width of ledge

$d_{ledge} := h_l = 21\,in$ depth of ledge

$h_{cap} := H = 42\,in$ height of cap

$\varphi_f := 0.9$

$d_{s\_pos} := h_{cap} - 4.365in = 37.635\,in$ $d_{s\_neg} := h_{cap} - 2.25in - 0.5d_{11} = 39.045\cdot in$

$A_s := 12A_{11} = 18.72\cdot in^2$ $A'_s := 6\cdot A_{11} = 9.36\cdot in^2$

$d' := h_{cap} - d_{s\_neg} = 2.955\,in$

$a := \frac{A_s\cdot f_{y\_11} - A'_s\cdot f_{y\_11}}{0.85\cdot f'_c\cdot b_{stem}} = 6.902\cdot in$ $M_n := A'_s\cdot f_{y\_11}\cdot(d - d') + \left(0.85\cdot f'_c\cdot b_{stem}\cdot a\right)\cdot\left(d - \frac{a}{2}\right) = 3719\cdot kip\cdot ft$ $M_r := \varphi_f\cdot M_n = 3347\cdot kip\cdot ft$

$P_{flx} := \frac{L}{L_1 + L_2}\cdot\frac{M_n}{L - L_1 - L_2}$ $P_{flx} = 852\,kip$

$A_g := d_{ledge}\cdot b_f + d_{stem}\cdot b_{stem} = 1323\cdot in^2$ $ybar := \frac{d_{ledge}\cdot b_f\cdot\left(0.5d_{ledge}\right) + d_{stem}\cdot b_{stem}\cdot\left(d_{ledge} + 0.5d_{stem}\right)}{A_g} = 17.5\,in$

$I_g := \frac{b_f\cdot d_{ledge}^3}{12} + b_f\cdot d_{ledge}\cdot\left(ybar - 0.5d_{ledge}\right)^2 + \frac{b_{stem}\cdot d_{stem}^3}{12} + b_{stem}\cdot d_{stem}\cdot\left[ybar - \left(d_{ledge} + 0.5d_{stem}\right)\right]^2 = 178274.25\,in^4$

$f_r := 0.24\sqrt{f'_c\cdot ksi} = 0.55\,ksi$ modulus of rupture $y_t := h_{cap} - ybar = 24.5\cdot in$ $S_{mod} := \frac{I_g}{y_t} = 7276.5\cdot in^3$

$M_{cr} := S_{mod}\cdot f_r = 334\cdot kip\cdot ft$ $M_{cr1} := 1.2M_{cr} = 401\cdot kip\cdot ft$ $M_{cr2} := 1.33\cdot M_n = 4946\cdot kip\cdot ft$ $M_f := \min\left(M_{cr1}, M_{cr2}\right) = 401\cdot kip\cdot ft$

$Mr_{check} := \begin{cases} \text{"OK"} & \text{if } M_r \geq M_f \\ \text{"NG"} & \text{otherwise} \end{cases}$ $Mr_{check} = \text{"OK"}$

Vu_{xx} Summary:

$P_{min} := 335\,kip$

			Ratios:
$Vn_{hr\_serv} = 453.858\,kip$	$P_1 := \frac{Vn_{hr\_serv}}{0.33} = 1375\,kip$	Hanger service	$\frac{P_1}{P_{min}} = 4.11$
$Vn_{hr\_stre} = 1147.632\,kip$	$P_2 := Vn_{hr\_stre} = 1148\,kip$	Hanger strength	$\frac{P_2}{P_{min}} = 3.43$
$Vn_{stirrup} = 238.583\,kip$	$P_3 := Vn_{stirrup}\cdot\left(\frac{L}{L_1 + L_2}\right) = 335\,kip$	Transverse reinforcement	$\frac{P_3}{P_{min}} = 1.00$
$Vn_{vf\_Ext} = 357.12\,kip$	$P_4 := Vn_{vf\_Ext}\cdot 2 = 714\,kip$	Shear friction, ledge reinf	$\frac{P_4}{P_{min}} = 2.13$
$V_{PC\_Ext} = 809.984\,kip$	$P_5 := V_{PC\_Ext} = 810\,kip$	Punching shear	$\frac{P_5}{P_{min}} = 2.42$
$Vn_b = 1046.214\,kip$	$P_6 := Vn_b\cdot 2 = 2092\,kip$	Bearing at load pts	$\frac{P_6}{P_{min}} = 6.25$
$Vn_{c\_vf} = 717.6\,kip$	$P_7 := Vn_{c\_vf}\cdot 2 = 1435\,kip$	Shear friction, ledge concrete	$\frac{P_7}{P_{min}} = 4.28$
$Vn_{le} = 1322\,kip$	$P_8 := Vn_{le} = 1322\,kip$	Ledge reinf; flexure, axial	$\frac{P_8}{P_{min}} = 3.95$
	$P_9 := P_{flx} = 852\,kip$	Flexure	$\frac{P_9}{P_{min}} = 2.54$

Controling element: Stirrups in Shear span

$P_u := \min(P_1, P_2, P_3, P_4, P_5, P_6, P_7, P_8, P_9) = 335\,kip$

$V_u := P_u\cdot\left(\frac{L_1 + L_2}{L}\right) = 239\,kip$

$P_u = 335\,kip$

AASHTO LRFD Bridge Design Specifications

Same design as per TxDOT Specifications, except for the following:

Hanger Reinforcement:

Service Limit State *AASHTO LRFD 5.13.2.5.5*

Interior Beams

$$V_{all\_1} := \frac{A_{hr}\cdot(0.5fy)}{s_{bar\_S}}\cdot\left(W + 3a_v\right) = 340\cdot kip$$

$$V_{all\_2} := \frac{A_{hr}\cdot(0.5fy)}{s_{bar\_S}}\cdot(S) = 657\cdot kip$$

$$Vn_{int\_serv} := \min\left(V_{all\_1}, V_{all\_2}\right) = 340\cdot kip$$

Exterior Beams

$$V_{all\_3} := \frac{A_{hr}\cdot(0.5fy)}{s_{bar\_S}}\cdot\left(\frac{W + 3a_v}{2} + c\right) = 452\cdot kip$$

$$V_{all\_4} := \frac{A_{hr}\cdot(0.5fy)}{s_{bar\_S}}\cdot\left(\frac{S}{2} + c\right) = 610\cdot kip$$

$$Vn_{ext\_serv} := \min\left(V_{all\_3}, V_{all\_4}\right) = 452\cdot kip$$

$$Vn_{hr\_serv} := \min\left(Vn_{int\_serv}, Vn_{ext\_serv}\right) = 340\cdot kip$$

$$Vn_{hr\_serv} = 340\cdot kip$$

Stirrup Reinforcement:

Maximum Spacing of Transverse Reinforcement: *AASHTO LRFD 5.8.2.7*

Shear Stress

$$v_u := \frac{Vn_{stirrup}}{b_v\cdot d_v} = 0.33\cdot ksi$$

$$v_{lim} := 0.125\cdot f'_c = 0.657\cdot ksi$$

$$s_{stirrup\_Max} := \begin{cases} \min\left(0.8d_v, 24in\right) & \text{if } v_u < v_{lim} \\ \min\left(0.4d_v, 12in\right) & \text{if } v_u \geq v_{lim} \end{cases} = 24\,in$$

$$s_{stirrup\_Max} = 24\,in$$

$$s_{stirrup\_Check} := \begin{cases} \text{"NG"} & \text{if } s_{stirrup\_Max} < s_{stirrup} \\ \text{"OK"} & \text{if } s_{stirrup\_Max} > s_{stirrup} \end{cases}$$

$$s_{stirrup\_Check} = \text{"OK"}$$

Check Punching Shear: *AASHTO LRFD 5.13.2.5.4*

Same result, since pyramids overla and conbined surface areas are being considered.

Vu_{xx} Summary:

$P_{min} := 335\,kip$

			Ratios:
$Vn_{hr\_serv} = 340.393\,kip$	$P_1 := \frac{Vn_{hr\_serv}}{0.33} = 1031\,kip$	Hanger service	$\frac{P_1}{P_{min}} = 3.08$
$Vn_{hr\_stre} = 1147.632\,kip$	$P_2 := Vn_{hr\_stre} = 1148\,kip$	Hanger strength	$\frac{P_2}{P_{min}} = 3.43$
$Vn_{stirrup} = 238.583\,kip$	$P_3 := Vn_{stirrup}\cdot\left(\frac{L}{L_1 + L_2}\right) = 335\,kip$	Transverse reinforcement	$\frac{P_3}{P_{min}} = 1.00$
$Vn_{vf\_Ext} = 357.12\,kip$	$P_4 := Vn_{vf\_Ext}\cdot 2 = 714\,kip$	Shear friction, ledge reinf	$\frac{P_4}{P_{min}} = 2.13$
$V_{PC\_Ext} = 809.984\,kip$	$P_5 := V_{PC\_Ext} = 810\,kip$	Punching shear	$\frac{P_5}{P_{min}} = 2.42$
$Vn_b = 1046.214\,kip$	$P_6 := Vn_b\cdot 2 = 2092\,kip$	Bearing at load pts	$\frac{P_6}{P_{min}} = 6.25$
$Vn_{c\_vf} = 717.6\,kip$	$P_7 := Vn_{c\_vf}\cdot 2 = 1435\,kip$	Shear friction, ledge concrete	$\frac{P_7}{P_{min}} = 4.28$
$Vn_{le} = 1322\,kip$	$P_8 := Vn_{le} = 1322\,kip$	Ledge reinf; flexure, axial	$\frac{P_8}{P_{min}} = 3.95$
	$P_9 := P_{flx} = 852\,kip$	Flexure	$\frac{P_9}{P_{min}} = 2.54$

Controling element: Stirrups in Shear span

$P_u := \min(P_1, P_2, P_3, P_4, P_5, P_6, P_7, P_8, P_9) = 335\,kip$

$V_u := P_u\cdot\left(\frac{L_1 + L_2}{L}\right) = 239\,kip$

$P_u = 335\,kip$

APPENDIX D

Tests summary

D.1 OVERVIEW

A brief summary of each test is presented in this appendix. Basic information provided includes: force deformation plot, crack width progression, photograph after testing, and key notes.

D.2 SPECIMEN 01A: DS1-42-1.85-03

Specimen 01a failed in web shear. Crushing of the direct strut occurred after applying a total load of 954 kips; which resulted in a shear load of 712 kips at the critical section including self-weight of the specimen and test setup. The specimen after failure is shown in Figure D-1. The load-deflection relation at the loading point and the maximum diagonal crack width progression are presented in Figure D-2.

Figure D-1: Specimen after failure

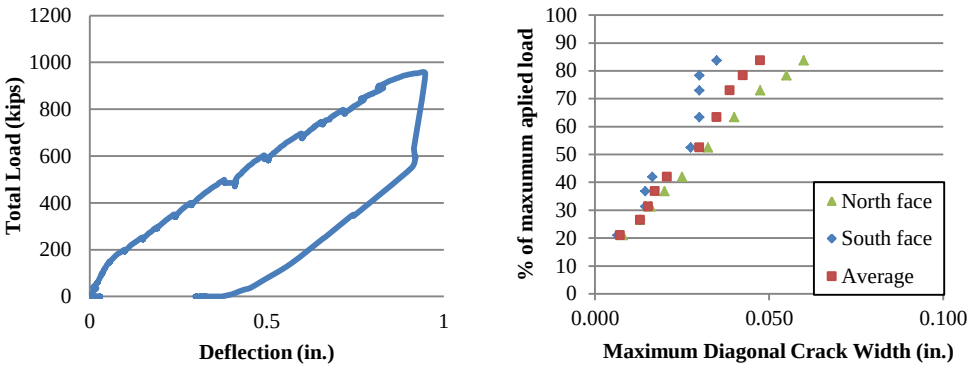

Figure D-2: Load-deflection at loading point (left), crack width progression (right)

D.3 SPECIMEN 01B: DS1-42-2.50-03

Specimen 01b failed in web shear. S-shape cracking consistent with sectional shear was observed at failure after applying a total load of 633 kips; which resulted in a shear load of 406 kips at the critical section including self-weight of the specimen and test setup. The specimen after failure is shown in Figure D-3. The load-deflection relation at the loading point and the maximum diagonal crack width progression are presented in Figure D-4.

Figure D-3: Specimen after failure

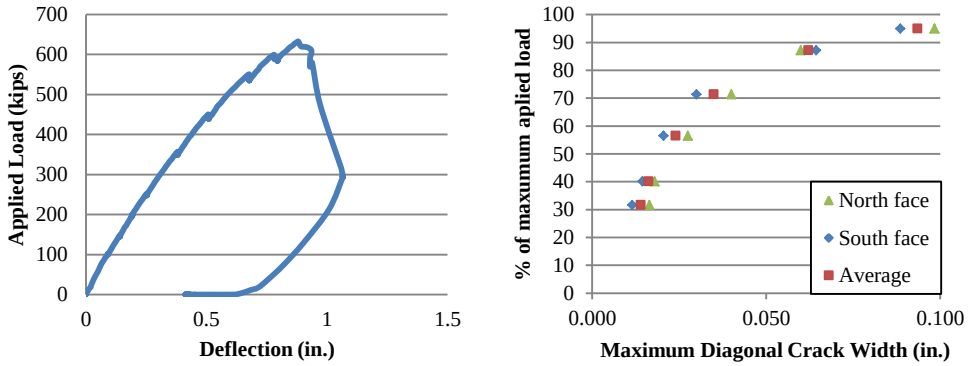

Figure D-4: Load-deflection at loading point (left), crack width progression (right)

D.4 SPECIMEN 02A: DS1-42-1.85-06

Specimen 02a failed in web shear. Crushing of the direct strut occurred after applying a total load of 816 kips; which resulted in a shear load of 621 kips at the critical section including self-weight of the specimen and test setup. The specimen after failure is shown in Figure D-5. The load-deflection relation at the loading point and the maximum diagonal crack width progression are presented in Figure D-6.

Figure D-5: Specimen after failure

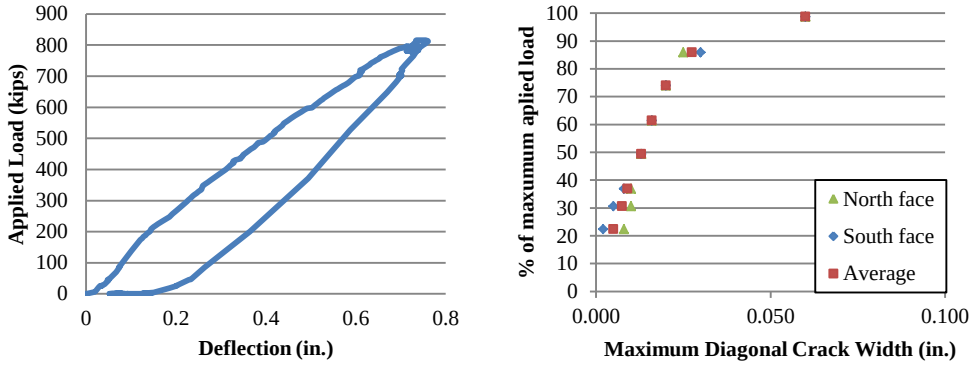

Figure D-6: Load-deflection at loading point (left), crack width progression (right)

D.5 SPECIMEN 02B: DS1-42-2.50-06

Specimen 02b failed in web shear. S-shape cracking consistent with sectional shear was observed at failure after applying a total load of 766 kips; which resulted in a shear load of 503 kips at the critical section including self-weight of the specimen and test setup. The specimen after failure is shown in Figure D-7. The load-deflection relation at the loading point and the maximum diagonal crack width progression are presented in Figure D-8.

Figure D-7: Specimen after failure

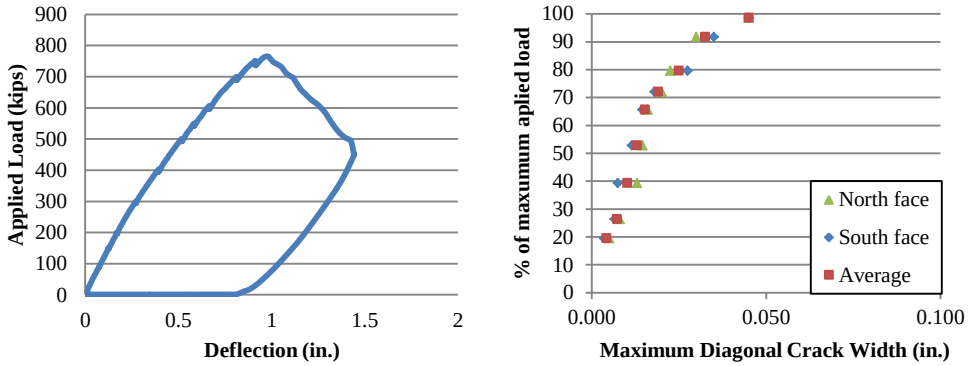

Figure D-8: Load-deflection at loading point (left), crack width progression (right)

D.6 SPECIMEN 03A: DL1-42-1.85-06

Specimen 03a failed in web shear. Crushing of the direct strut occurred after applying a total load of 977 kips; which resulted in a shear load of 741 kips at the critical section including self-weight of the specimen and test setup. The specimen after failure is shown in Figure D-9. The load-deflection relation at the loading point and the maximum diagonal crack width progression are presented in Figure D-10.

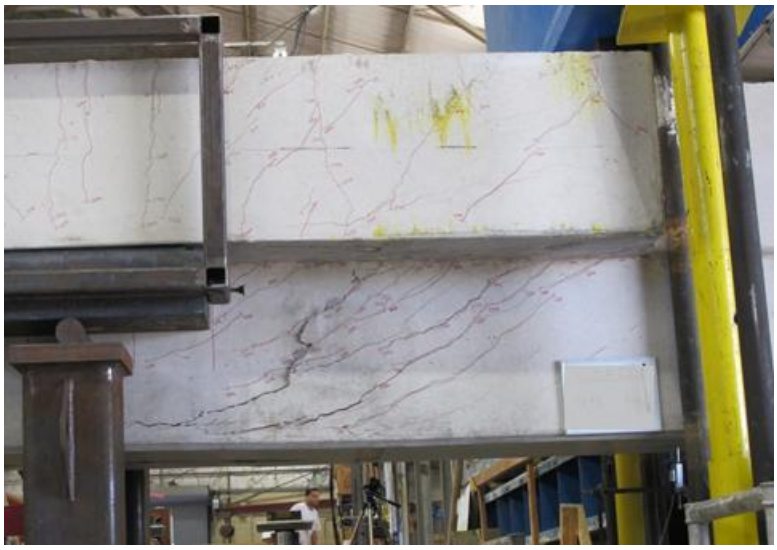

Figure D-9: Specimen after failure

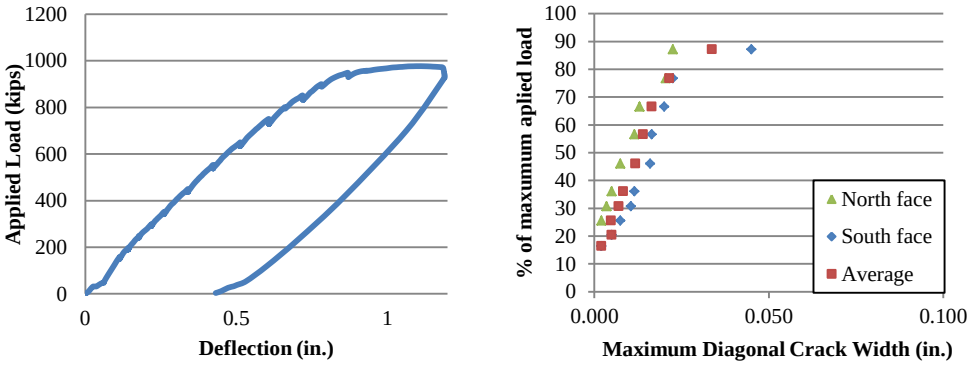

Figure D-10: Load-deflection at loading point (left), crack width progression (right)

D.7 SPECIMEN 03B: DL1-42-2.50-06

Specimen 03b failed in web shear. Diagonal tension cracks, consistent with sectional shear, were observed at failure after applying a total load of 943 kips; which resulted in a shear load of 622 kips at the critical section including self-weight of the specimen and test setup. The specimen after failure is shown in Figure D-11. The load-deflection relation at the loading point and the maximum diagonal crack width progression are presented in Figure D-12.

Figure D-11: Specimen after failure

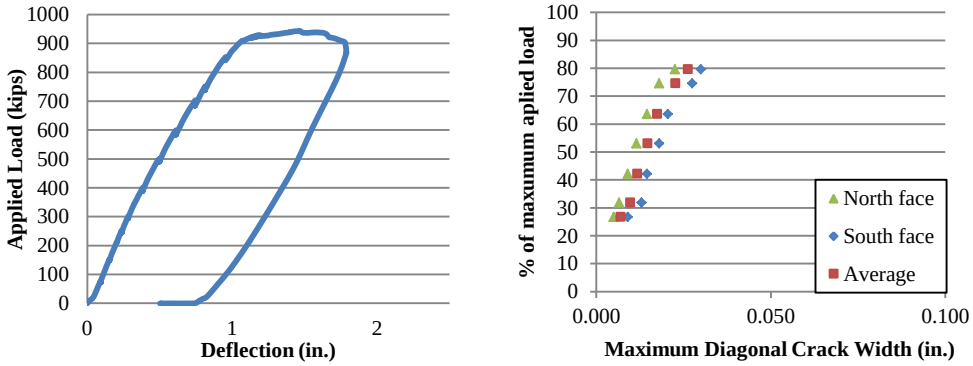

Figure D-12: Load-deflection at loading point (left), crack width progression (right)

D.8 SPECIMEN 04A: SS3-42-1.85-03

Specimen 04a failed in web shear. Crushing of the direct strut occurred after applying a total load of 922 kips; which resulted in a shear load of 523 kips at the critical section including self-weight of the specimen and test setup. The specimen after failure is shown in Figure D-13. The load-deflection relation at the loading point nearest to the critical section and the maximum diagonal crack width progression are presented in Figure D-14.

Figure D-13: Specimen after failure

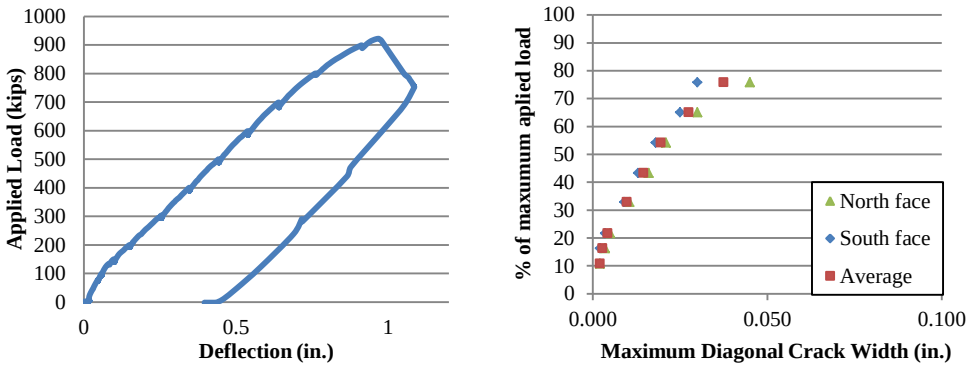

Figure D-14: Load-deflection at the loading point nearest to the critical section (left), crack width progression (right)

D.9 SPECIMEN 04B: SS3-42-2.50-03

Specimen 04b failed in web shear. S-shape cracking consistent with sectional shear was observed at failure after applying a total load of 964 kips; which resulted in a shear load of 447 kips at the critical section including self-weight of the specimen and test setup. The specimen after failure is shown in Figure D-15. The load-deflection relation at the loading point nearest to the critical section and the maximum diagonal crack width progression are presented in Figure D-16.

Figure D-15: Specimen after failure

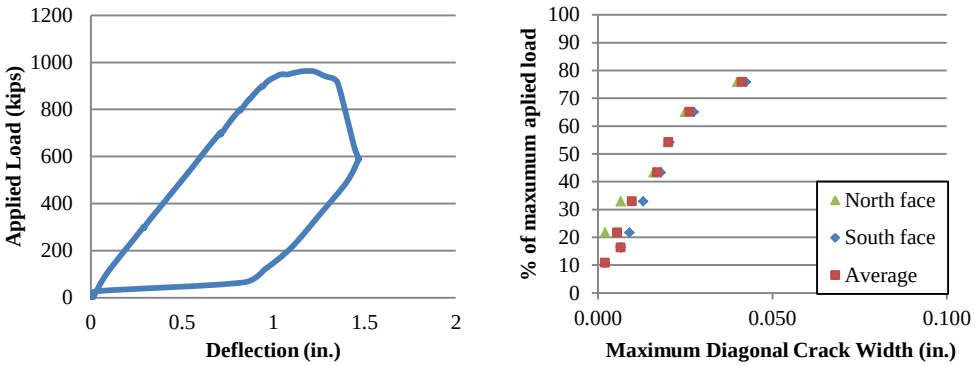

Figure D-16: Load-deflection at the loading point nearest to the critical section (left), crack width progression (right)

D.10 SPECIMEN 05B: SS3-42-2.50-06

Specimen 05b failed in flexure. Crushing at the compression chord was observed at failure after applying a total load of 1084 kips; which resulted in a shear load of 516 kips at the critical section including self-weight of the specimen and test setup. The specimen after failure is shown in Figure D-17. The load-deflection relation at the center point load location and the maximum diagonal crack width progression are presented in Figure D-18.

Figure D-17: Specimen after failure

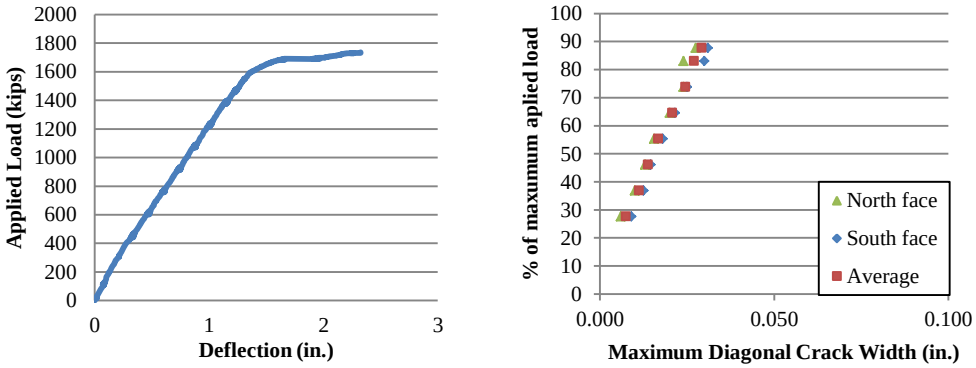

Figure D-18: Load-deflection at center point load (left), crack width progression (right)

D.11 SPECIMEN 06A: SC3-42-2.50-03

Specimen 06a failed in web shear. S-shape cracking consistent with sectional shear was observed at failure after applying a total load of 705 kips; which resulted in a shear load of 329 kips at the critical section including self-weight of the specimen and test setup. The specimen after failure is shown in Figure D-19. The load-deflection relation at the loading point nearest to the critical section and the maximum diagonal crack width progression are presented in Figure D-20.

Figure D-19: Specimen after failure

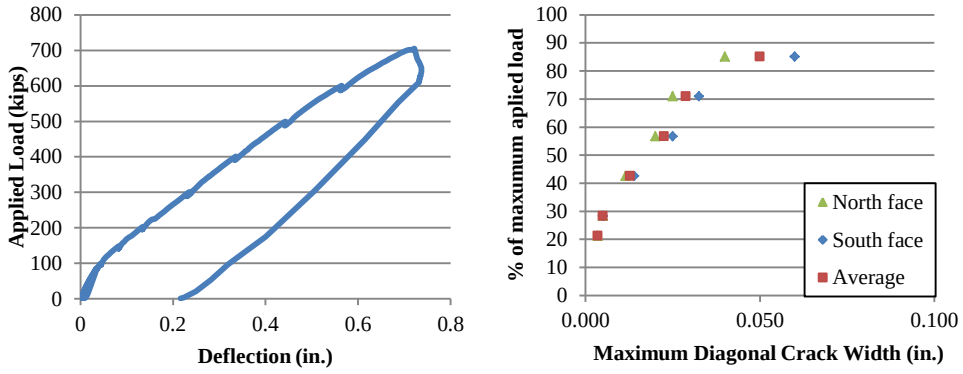

Figure D-20: Load-deflection at the loading point nearest to the critical section (left), crack width progression (right)

D.12 SPECIMEN 06B: SC3-42-1.85-03

Specimen 06b failed in web shear. Crushing of the direct strut occurred after applying a total load of 830 kips; which resulted in a shear load of 483 kips at the critical section including self-weight of the specimen and test setup. The specimen after failure is shown in Figure D-21. The load-deflection relation at the loading point nearest to the critical section and the maximum diagonal crack width progression are presented in Figure D-22.

Figure D-21: Specimen after failure

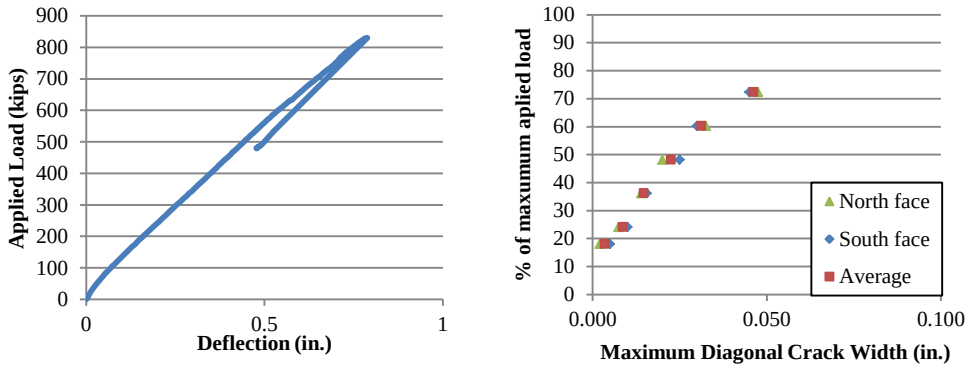

Figure D-22: Load-deflection at the loading point nearest to the critical section (left), crack width progression (right)

D.13 SPECIMEN 07A: SS1-75-1.85-03

Specimen 07a failed in punching shear of the ledge after applying a total load of 1776 kips; which resulted in a shear load of 913 kips at the critical section including self-weight of the specimen and test setup. The specimen after failure is shown in Figure D-23. The load-deflection relation at the loading point and the maximum diagonal crack width progression are presented in Figure D-24.

Figure D-23: Specimen after failure

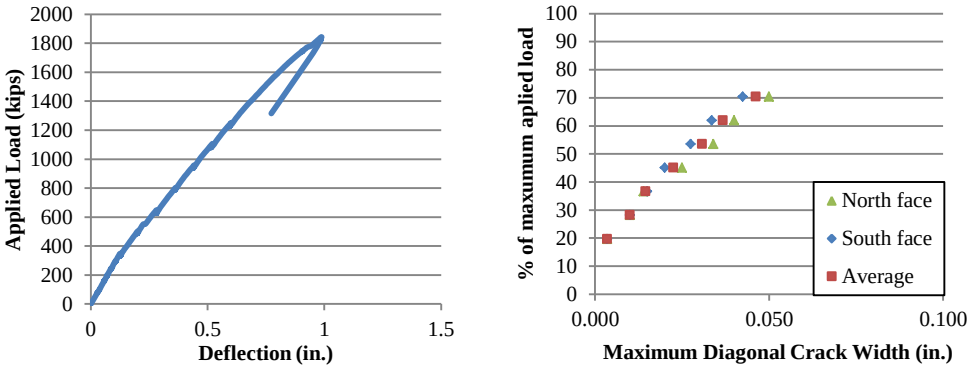

Figure D-24: Load-deflection at loading point (left), crack width progression (right)

D.14 SPECIMEN 08B: SS1-75-2.50-06

Specimen 07a failed in punching shear of the ledge after applying a total load of 2103 kips; which resulted in a shear load of 688 kips at the critical section including self-weight of the specimen and test setup. The specimen after failure is shown in Figure D-25. The load-deflection relation at the loading point and the maximum diagonal crack width progression are presented in Figure D-26.

Figure D-25: Specimen after failure

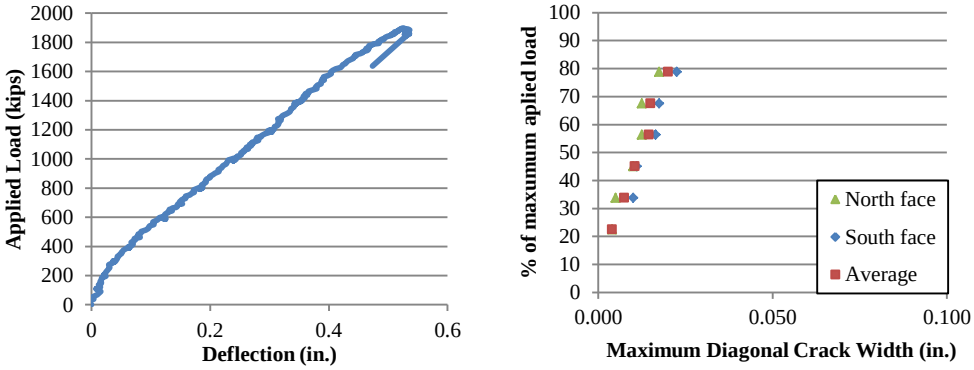

Figure D-26: Load-deflection at loading point (left), crack width progression (right)

D.15 SPECIMEN 09A: DS3-42-2.50-03

Specimen 09a failed in web shear. S-shape cracking consistent with sectional shear was observed at failure after applying a total load of 914 kips; which resulted in a shear load of 430 kips at the critical section including self-weight of the specimen and the test setup. The specimen after failure is shown in Figure D-27. The load-deflection relation at the center point load location and the maximum diagonal crack width progression are presented in Figure D-28.

Figure D-27: Specimen after failure

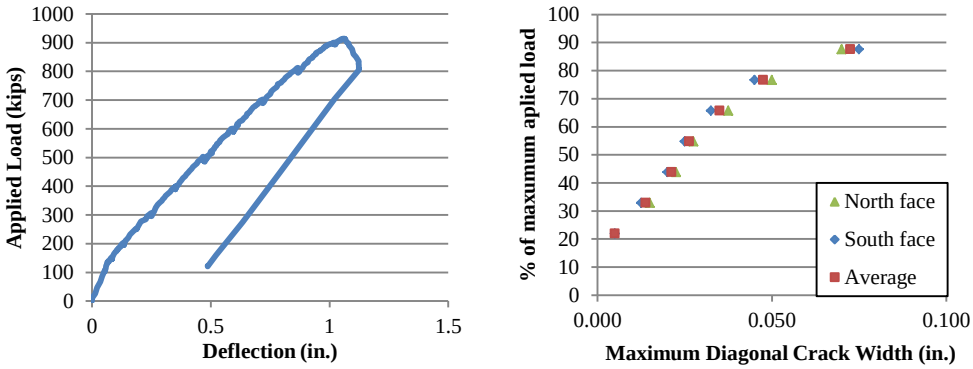

Figure D-28: Load-deflection at center point load (left), crack width progression (right)

D.16 SPECIMEN 10A: DL1-42-1.85-03

Specimen 10a failed in web shear. Crushing of the direct strut occurred after applying a total load of 824 kips; which resulted in a shear load of 626 kips at the critical section including self-weight of the specimen and test setup. The specimen after failure is shown in Figure D-29. The load-deflection relation at the loading point and the maximum diagonal crack width progression are presented in Figure D-30.

Figure D-29: Specimen after failure

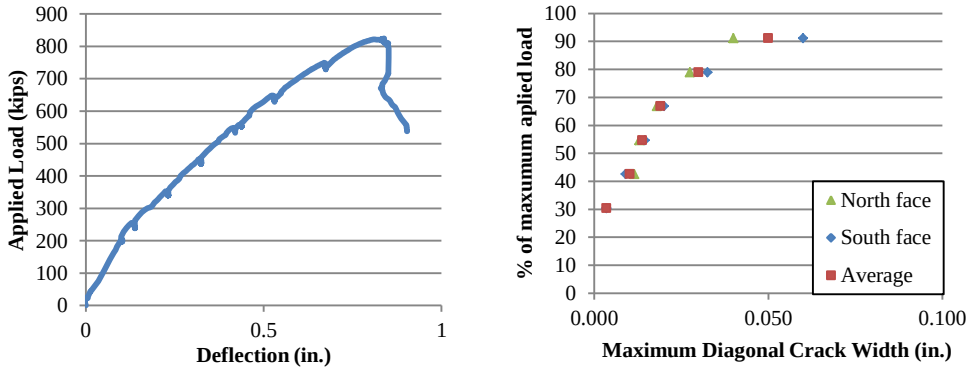

Figure D-30: Load-deflection at loading point (left), crack width progression (right)

D.17 SPECIMEN 10B: DL1-42-2.50-03

Specimen 10b failed in web shear, diagonal tension cracks consistent with sectional shear were observed at failure after applying a total load of 769 kips; which resulted in a shear load of 510 kips at the critical section including self-weight of the specimen and test setup. The specimen after failure is shown in Figure D-31. The load-deflection relation at the loading point and the maximum diagonal crack width progression are presented in Figure D-32.

Figure D-31: Specimen after failure

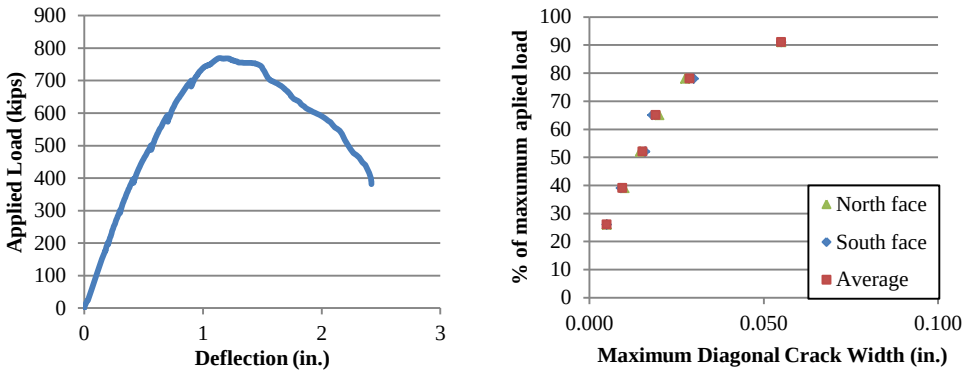

Figure D-32: Load-deflection at loading point (left), crack width progression (right)

D.18 SPECIMEN 11A: SL3-42-1.85-03

Specimen 11a failed in web shear. Crushing of the direct strut occurred after applying a total load of 1011 kips; which resulted in a shear load of 571 kips at the critical section including self-weight of the specimen and test setup. The specimen after failure is shown in Figure D-33. The load-deflection relation at the loading point nearest to the critical section and the maximum diagonal crack width progression are presented in Figure D-34.

Figure D-33: Specimen after failure

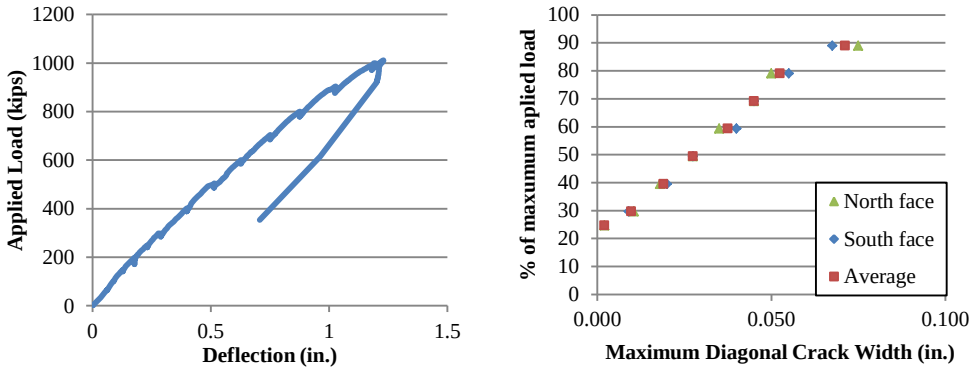

Figure D-34: Load-deflection at the loading point nearest to the critical section (left), crack width progression (right)

D.19 SPECIMEN 12A: SL3-42-1.85-06

Specimen 12a failed in web shear. Crushing of the direct strut occurred after applying a total load of 1338 kips; which resulted in a shear load of 744 kips at the critical section including self-weight of the specimen and test setup. Yielding of the longitudinal steel was observed before the shear failure occurred. The specimen after failure is shown in Figure D-35. The load-deflection relation at the loading point nearest to the critical section and the maximum diagonal crack width progression are presented in Figure D-36.

Figure D-35: Specimen after failure

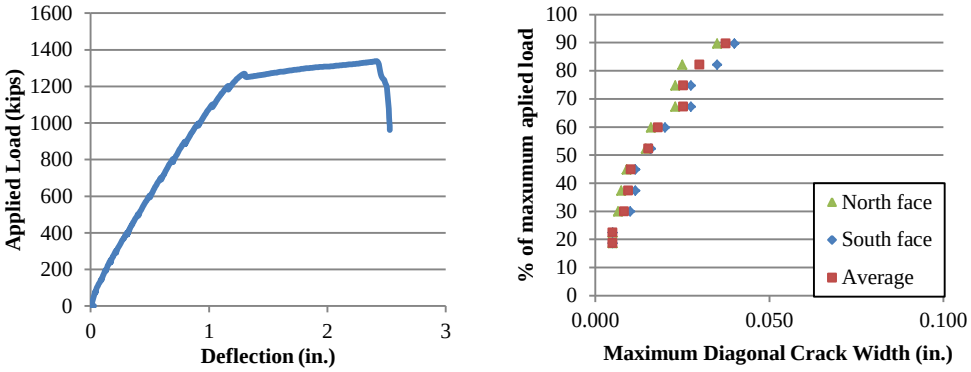

Figure D-36: Load-deflection at the loading point nearest to the critical section (left), crack width progression (right)

D.20 SPECIMEN 14A: SS1-75-1.85-03B

Specimen 14a failed in web shear. Crushing of the direct strut occurred after applying a total load of 1427 kips; which resulted in a shear load of 745 kips at the critical section including self-weight of the specimen and test setup. The specimen after failure is shown in Figure D-37. The load-deflection relation at the loading point and the maximum diagonal crack width progression are presented in Figure D-38.

Figure D-37: Specimen after failure

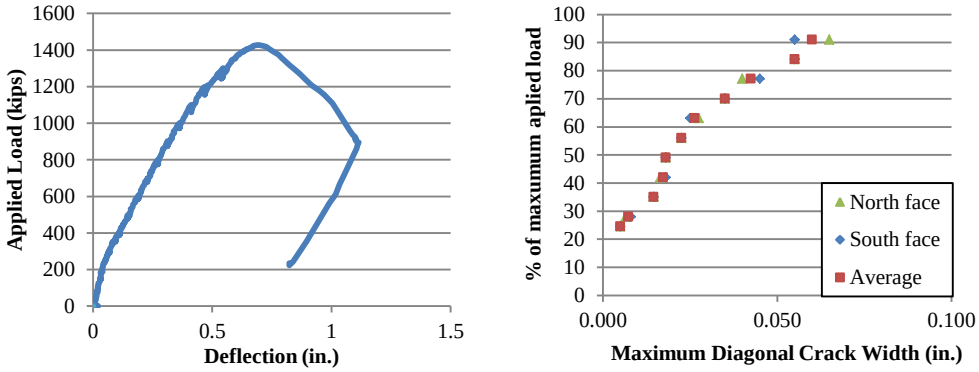

Figure D-38: Load-deflection at loading point (left), crack width progression (right)

D.21 SPECIMEN 15A: DC3-42-1.85-03

Specimen 15a failed in web shear. Crushing of the direct strut occurred after applying a total load of 765 kips; which resulted in a shear load of 395 kips at the critical section including self-weight of the specimen and test setup. The specimen after failure is shown in Figure D-39. The load-deflection relation at the loading point nearest to the critical section and the maximum diagonal crack width progression are presented in Figure D-40.

Figure D-39: Specimen after failure

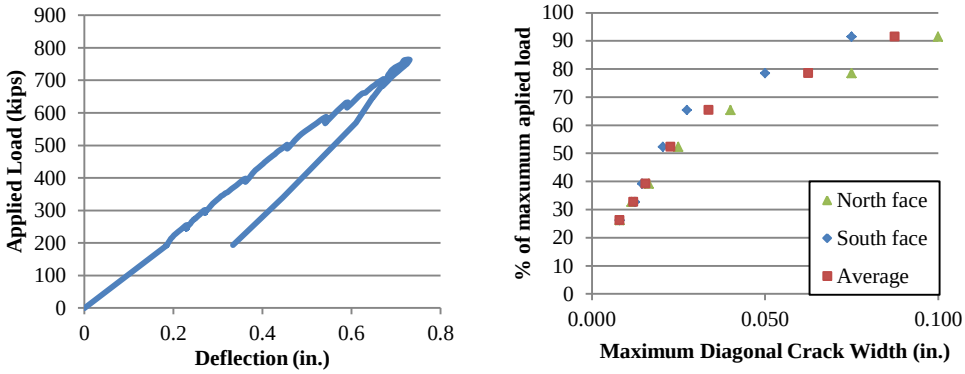

Figure D-40: Load-deflection at the loading point nearest to the critical section (left), crack width progression (right)

D.22 SPECIMEN 15B: DS3-42-1.85-03

Specimen 15b failed in web shear. Crushing of the direct strut occurred after applying a total load of 875 kips; which resulted in a shear load of 454 kips at the critical section including self-weight of the specimen and test setup. The specimen after failure is shown in Figure D-41. The load-deflection relation at the loading point nearest to the critical section and the maximum diagonal crack width progression are presented in Figure D-42.

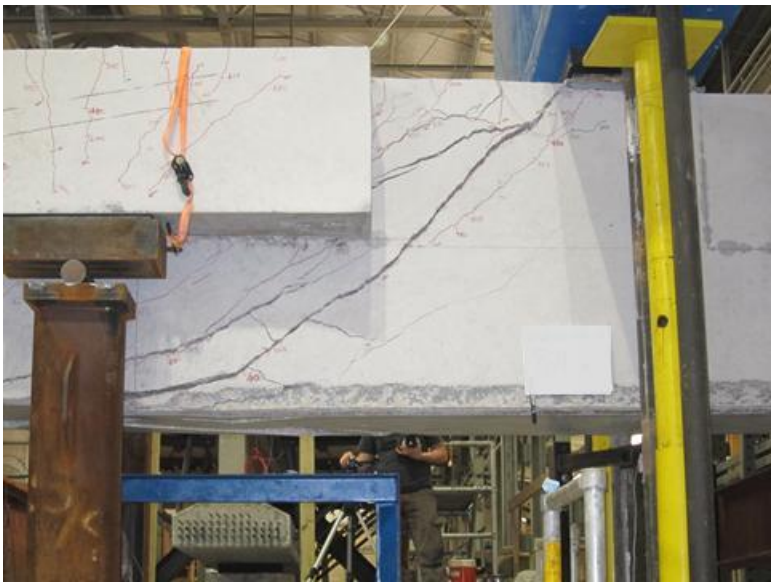

Figure D-41: Specimen after failure

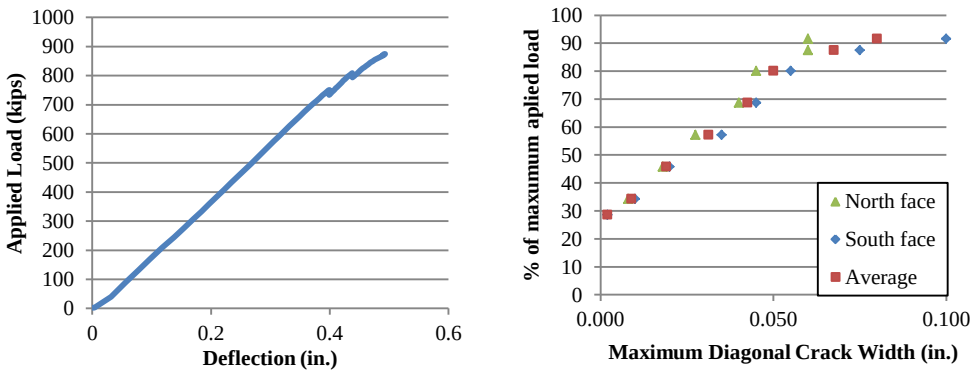

Figure D-42: Load-deflection at the loading point nearest to the critical section (left), crack width progression (right)

D.23 SPECIMEN 16A: SS1-42-2.50-03

Specimen 16a failed in web shear. Diagonal tension cracks, consistent with sectional shear, were observed at failure after applying a total load of 600 kips; which resulted in a shear load of 398 kips at the critical section including self-weight of the specimen and test setup. The specimen after failure is shown in Figure D-43. The load-deflection relation at the loading point and the maximum diagonal crack width progression are presented in Figure D-44.

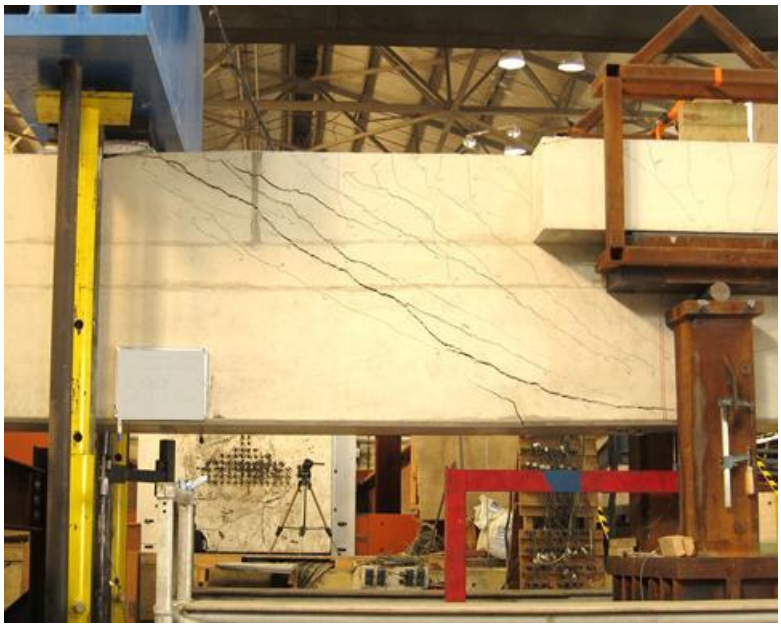

Figure D-43: Specimen after failure

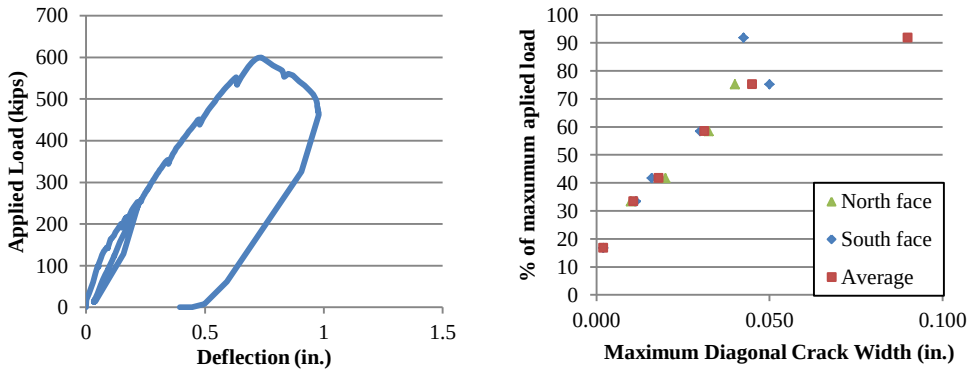

Figure D-44: Load-deflection at loading point (left), crack width progression (right)

D.24 SPECIMEN 16B: SS1-42-1.85-03

Specimen 16b failed in web shear. Crushing of the direct strut occurred after applying a total load of 767 kips; which resulted in a shear load of 583 kips at the critical section including self-weight of the specimen and test setup. The specimen after failure is shown in Figure D-45. The load-deflection relation at the loading point and the maximum diagonal crack width progression are presented in Figure D-46.

Figure D-45: Specimen after failure

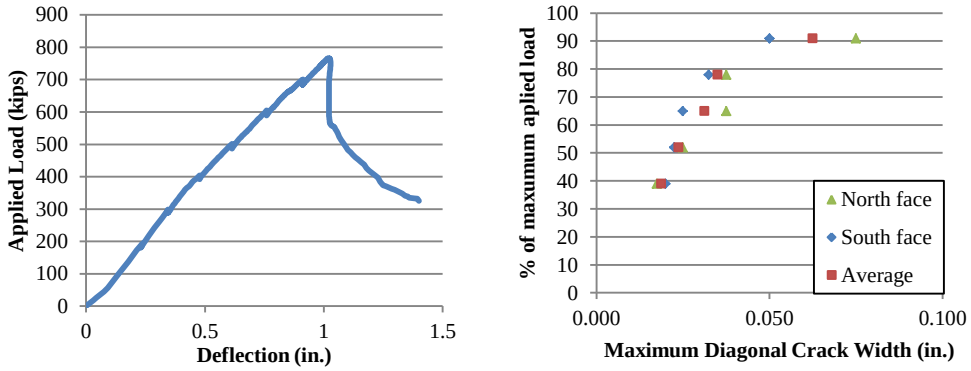

Figure D-46: Load-deflection at loading point (left), crack width progression (right)

D.25 SPECIMEN 17A: DC1-42-2.50-03

Specimen 17a failed in web shear, diagonal tension cracks consistent with sectional shear were observed at failure after applying a total load of 544 kips; which resulted in a shear load of 365 kips at the critical section including self-weight of the specimen and test setup. The specimen after failure is shown in Figure D-47. The load-deflection relation at the loading point and the maximum diagonal crack width progression are presented in Figure D-48.

Figure D-47: Specimen after failure

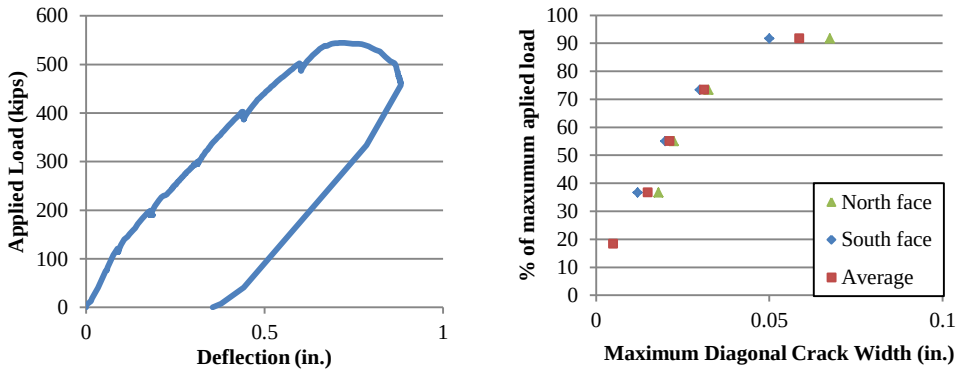

Figure D-48: Load-deflection at loading point (left), crack width progression (right)

D.26 SPECIMEN 17B: DL3-42-1.85-03

Specimen 17b failed in flexure, crushing of the compression chord at the loading point on the opposite end of the beam occurred after applying a total load of 1129 kips; which resulted in a shear load of 629 kips at the critical section including self-weight of the specimen and test setup. Large deformations were observed due to yielding of the longitudinal steel before the failure occurred. The specimen after failure is shown in Figure D-49. The load-deflection relation at the loading point nearest to the critical section and the maximum diagonal crack width progression are presented in Figure D-50; deformations were not recorded beyond 1.75 inches since they exceeded the capacity of the instrumentation at this location.

Figure D-49: Specimen after failure

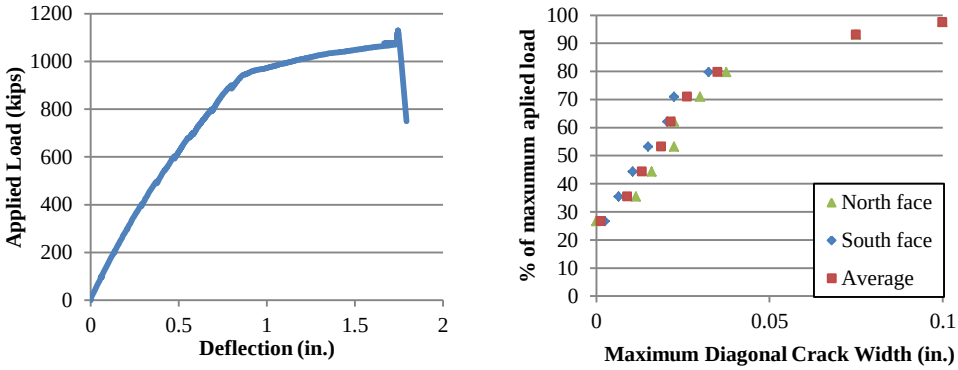

Figure D-50: Load-deflection at the loading point nearest to the critical section (left), crack width progression (right)

D.27 SPECIMEN 18A: SL1-42-2.50-03

Specimen 18a failed in web shear. Diagonal tension cracks, consistent with sectional shear, were observed at failure after applying a total load of 749 kips; which resulted in a shear load of 498 kips at the critical section including self-weight of the specimen and test setup. The specimen after failure is shown in Figure D-51. The load-deflection relation at the loading point and the maximum diagonal crack width progression are presented in Figure D-52.

Figure D-51: Specimen after failure

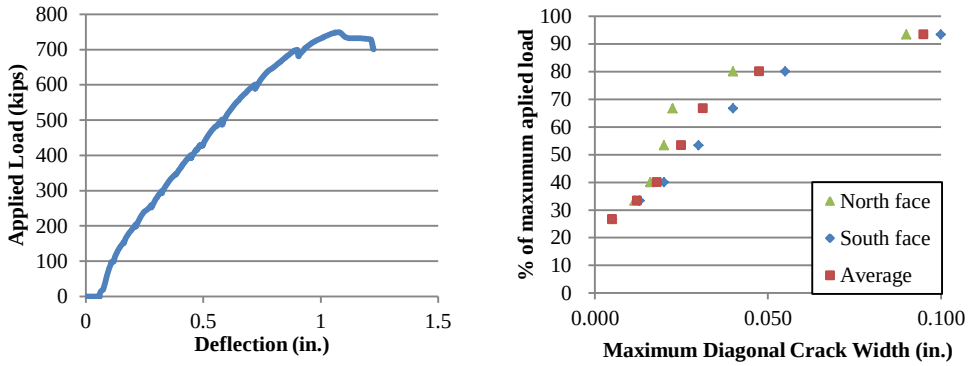

Figure D-52: Load-deflection at loading point (left), crack width progression (right)

D.28 SPECIMEN 18B: SC1-42-2.50-03

Specimen 18b failed in shear friction of the ledge after applying a total load of 469 kips; which resulted in a shear load of 319 kips at the critical section including self-weight of the specimen and test setup. The specimen after failure is shown in Figure D-53. The load-deflection relation at the loading point and the maximum diagonal crack width progression are presented in Figure D-54.

Figure D-53: Specimen after failure

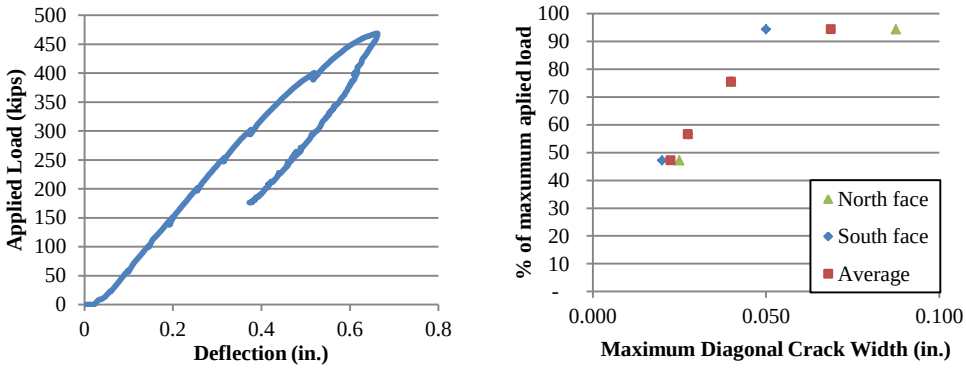

Figure D-54: Load-deflection at loading point (left), crack width progression (right)

D.29 SPECIMEN 19A: DS1-42-2.50-06/03

Specimen 19a failed in web shear. S-shape cracking consistent with sectional shear was observed at failure after applying a total load of 822 kips; which resulted in a shear load of 539 kips at the critical section including self-weight of the specimen and test setup. The specimen after failure is shown in Figure D-55. The load-deflection relation at the loading point and the maximum diagonal crack width progression are presented in Figure D-56.

Figure D-55: Specimen after failure

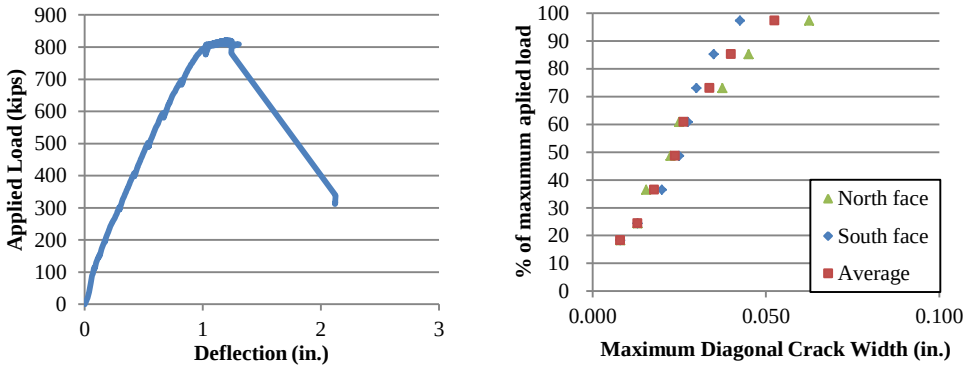

Figure D-56: Load-deflection at loading point (left), crack width progression (right)

D.30 SPECIMEN 19B: DS1-42-1.85-06/03

Specimen 19b failed in web shear. Crushing of the direct strut occurred after applying a total load of 978 kips; which resulted in a shear load of 739 kips at the critical section including self-weight of the specimen and test setup. The specimen after failure is shown in Figure D-57. The load-deflection relation at the loading point and the maximum diagonal crack width progression are presented in Figure D-58.

Figure D-57: Specimen after failure

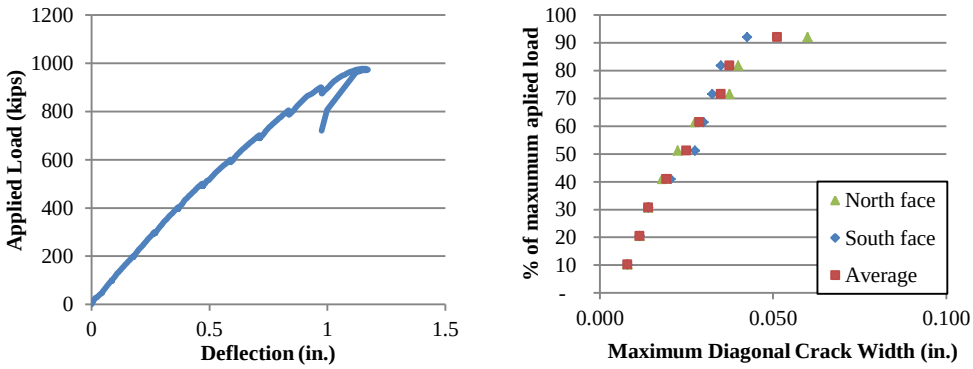

Figure D-58: Load-deflection at loading point (left), crack width progression (right)

D.31 SPECIMEN 20A: SC1-42-1.85-03

Specimen 20a observed local failure of the ledge. The horizontal tie in the cross-sectional STM model yielded before the failure occurred after applying a total load of 583 kips; which resulted in a shear load of 451 kips at the critical section including self-weight of the specimen and test setup. The specimen after failure is shown in Figure D-59. The load-deflection relation at the loading point and the maximum diagonal crack width progression are presented in Figure D-60.

Figure D-59: Specimen after failure

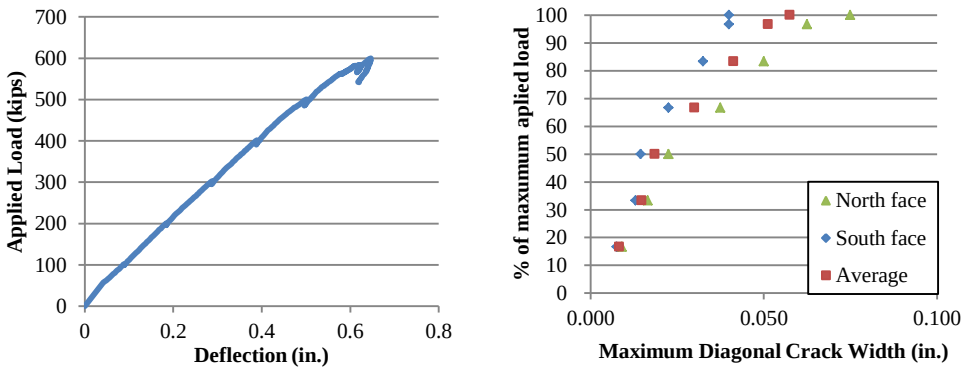

Figure D-60: Load-deflection at loading point (left), crack width progression (right)

D.32 SPECIMEN 20B: DC1-42-1.85-03

Specimen 20b failed in web shear. Crushing of the direct strut occurred after applying a total load of 657 kips; which resulted in a shear load of 517 kips at the critical section including self-weight of the specimen and test setup. The specimen after failure is shown in Figure D-61. The load-deflection relation at the loading point and the maximum diagonal crack width progression are presented in Figure D-62.

Figure D-61: Specimen after failure

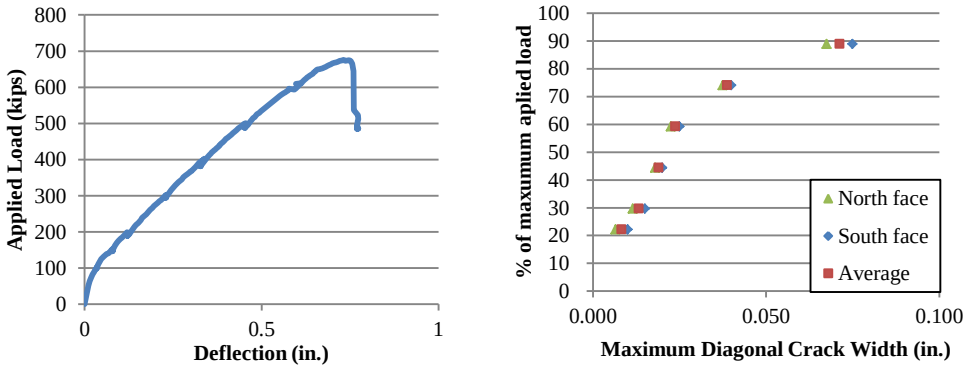

Figure D-62: Load-deflection at loading point (left), crack width progression (right)

REFERENCES

AASHTO. (2012). *LRFD Bridge Design Specifications.*

ACI 224R-01/08. (2008). *Control of Cracking in Concrete Structures.* Farmington Hills, MI: American Concrete Institute.

ACI-ASCE Committee 326. (1962). Shear and Diagonal Tension. *ACI Journal, 59*(1).

Birrcher, D., Tuchscherer, R., Huizinga, M., Bayrak, O., Wood, S., & Jirsa, J. (2009). *Strength and Serviceability Design of Reinforced Concrete Deep Beams.* Austin, TX: Center for Transportation Research, The University of Texas at Austin.

Cussens, A. R., & Besser, I. I. (1985, September). Shear strength of reinforced concrete wall-beams under combined top and bottom loads. *The Structural Engineer, 63B*(3), 50-56.

Fereig, S. M., & Smith, K. N. (1977, May 1). Indirect Loading on Beams with Short Shear Spans. *ACI Journal, 74*(5), 220-222.

Ferguson, P. M. (1956). Some Implications of Recent Diagonal Tension Tests. *Journal of the American Concrete Institute, 53*(8), 157-172.

Fernández-Gómez, E., Larson, N., Garber, D., Ghannoum, W., & Bayrak, O. (2011). Strength and Serviceability of Reinforced Concrete Inverted-T Straddle Bent Caps. *PCI/NBC Proceedings.*

Furlong, R. W., & Mirza, S. A. (1974). *153-1F - Strength and Serviceability of Inverted T-Beam Bent Caps Subject to Combined Flexure, Shear, and Torsion.* Austin: Center for Highway Research, University of Texas at Austin.

Furlong, R. W., Ferguson, P. M., & Ma, J. S. (1971). *113-4 - Shear and anchorage study of reinforcement in inverted-T beam bent cap girders.* Austin TX: Center for highway research at The University of Texas at Austin.

Galal, K., & Sekar, M. (2007, June 1). Rehabilitation of RC inverted-T girders using anchored CFRP sheets. (S. Direct, Ed.) *Composites: Part B - Engineering, 39*(4), 604-617.

Garber, D. B. (2011). *Shear Cracking in Inverted-T Straddle Bents.* Austin: University of Texas at Austin.

Graf, O., Brenner, E., & Bay, H. (1943). Versuche mit einem wandartigen Trager aus Stahlbeton. *Deutscher Ausschuss fur Stahlbeton, 99*, 41-54.

Huizinga, M. R. (2007). *Strength and Serviceability Performance of Large-Scale Deep Beams: Effect of Transverse Reinforcement.* Austin, TX: The University of Texas at Austin.

Leonhardt, F., & Walther, R. (1966). Wandartige Träger. *Deutscher Ausschuss furStahlbeton, 178*.

Ma, J. S. (1971). *PhD Dissertation: Behavior of reinforced concrete inverted T-beams.* Austin, TX: University of Texas at Austin.

Schütt, H. (1956, October). Über das Tragvermögen wandartiger Stahlbetonträger. *Beton und Stahlbetonbau, 10*, 220-224.

Smith, K. N., & Fereig, S. M. (1974, January 1). Effect Of Loading And Supporting Condidtions On The Shear Strength Of Deep Beams. *ACI, SP 42*, 441-460.

Tan, K. H., Kong, F. K., & Weng, L. W. (1997, June 3). High strength concrete deep beams subjected to combined top-and bottom-loading. *The Structural Engineer, 75*(11), 191-197.

Taylor, R. (1960, November). Some shear tests on reinforced concrete beams without shear reinforcement. *Magazine of Concrete Research, 12*(36), pp. 145-154.

TxDOT. (2011). *Bridge Design Manual - LRFD.*

Wight, J. K., & Parra-Montesinos, G. J. (2003, May). Strut-and-Tie Model for Deep Beam Design: A Practical Excersice Using Appendix A of the 2002 ACI Building Code. *Concrete International, 25*(5), 63-70.

Williams, C. S. (2011). *Masters Thesis: Strut-and-Tie Model Design Examples for Bridges.* Austin, TX: The University of Texas at Austin.

Zhu, R. R.-H., Dhonde, H., & Hsu, T. T. (2003). *TxDOT Project 0-1854: Crack Control for Ledges in Inverted "T" Bent Caps.* University of Houston.

Vita

Eulalio Fernández Gómez was born in Chihuahua, Chih, Mexico on April 2, 1981. He graduated from the Universidad Autónoma de Chihuahua with the degree of Bachelor of Civil Engineering in June, 2004. During the following years he was employed as a Structural Engineer in a consulting firm in the city of Chihuahua. In August, 2007, he entered the Graduate School at The University of Texas at Austin where he received a Marster's of Science in Engineering in 2009. Eulalio completed his Ph.D. in August, 2012.

Permanent address: efernandez@utexas.edu

This dissertation was typed by the author.